Available online at www.sciencedirect.com
SCIENCE DIRECT®
Physics Reports 407 (2005) 205–376
PHYSICS REPORTS
www.elsevier.com/locate/physrep

NJL-model analysis of dense quark matter

Michael Buballa*

Institut für Kernphysik, Technische Universität Darmstadt, Schlossgartenstr. 9, D-64289 Darmstadt, Germany

Accepted 15 November 2004
Editor W. Weise
Available online 20 January 2005

Abstract

Investigations of deconfined quark matter within NJL-type models are reviewed, focusing on the regime of low temperatures and "moderate" densities, which is not accessible by perturbative QCD. Central issue is the interplay between chiral symmetry restoration and the formation of color superconducting phases. In order to lay a solid ground for this analysis, we begin with a rather detailed discussion of two- and three-flavor NJL models and their phase structure, neglecting the possibility of diquark pairing in a first step. An important aspect of this part is a comparison with the MIT bag model. The NJL model is also applied to investigate the possibility of absolutely stable strange quark matter. In the next step the formalism is extended to include diquark condensates. We discuss the role and mutual influence of several conventional and less conventional quark–antiquark and diquark condensates. As a particularly interesting example, we analyze a spin-1 diquark condensate as a possible pairing channel for those quarks which are left over from the standard spin-0 condensate. For three-flavor systems, we find that a self-consistent calculation of the strange quark mass, together with the diquark condensates, is crucial for a realistic description of the 2SC–CFL phase transition. We also study the effect of neutrality constraints which are of relevance for compact stars. Both, homogeneous and mixed, neutral phases are constructed. Although neutrality constraints generally tend to disfavor the 2SC phase we find that this phase is again stabilized by the large values of the dynamical strange quark mass which follow from the self-consistent treatment. Finally, we combine our solutions with existing hadronic equations of state to investigate the existence of quark matter cores in neutron stars.

PACS: 12.39.−Ki; 12.38.AW; 11.30.Qc; 25.75.Nq; 26.60.+c

Keywords: Dense quark matter; QCD phase diagram; Color superconductivity; Compact stars

* Tel.: +49 6151 16 3272; fax: +49 6151 16 6076.
E-mail address: michael.buballa@physik.tu-darmstadt.de (M. Buballa).

0370-1573/$ - see front matter © 2004 Published by Elsevier B.V.
doi:10.1016/j.physrep.2004.11.004

Contents

1. Introduction

Exploring the phase structure of quantum chromodynamics (QCD) is certainly one of the most exciting topics in the field of strong interaction physics. Already in the 1970s, rather soon after it had become

clear that hadrons consist of confined quarks and gluons, it was argued that the latter should become deconfined at high temperature or density when the hadrons strongly overlap and loose their individuality [1,2]. In this picture, there are thus two distinct phases, the "hadronic phase" where quarks and gluons are confined, and the so-called quark–gluon plasma (QGP) where they are deconfined. This scenario is illustrated in the upper left panel of Fig. 1.1 by a schematic phase diagram in the plane of (quark number) chemical potential and temperature. A diagram of this type has essentially been drawn already in Ref. [2] and can be found, e.g., in Refs. [3,4].

In nature, the QGP surely existed in the early universe, a few microseconds after the Big Bang when the temperature was very high. It is less clear whether deconfined quark matter also exists in the relatively cold but dense centers of neutron stars. Experimentally, the creation and identification of the QGP is the ultimate goal of ultra-relativistic heavy-ion collisions. First, indications of success have been reported in press releases at CERN (SPS) [5] and BNL (RHIC) [6], although the interpretation of the data is still under debate. There is little doubt that the QGP will be created at the Large Hadron Collider (LHC), which is currently being built at CERN.

At least on a schematic level, the phase diagram shown in the upper left panel of Fig. 1.1 remained the standard picture for about two decades. In particular, the possibility of having more than one deconfined phase was not taken into account. Although Cooper pairing in cold, dense quark matter ("color superconductivity") had been mentioned already in 1975 [1] and had further been worked out in

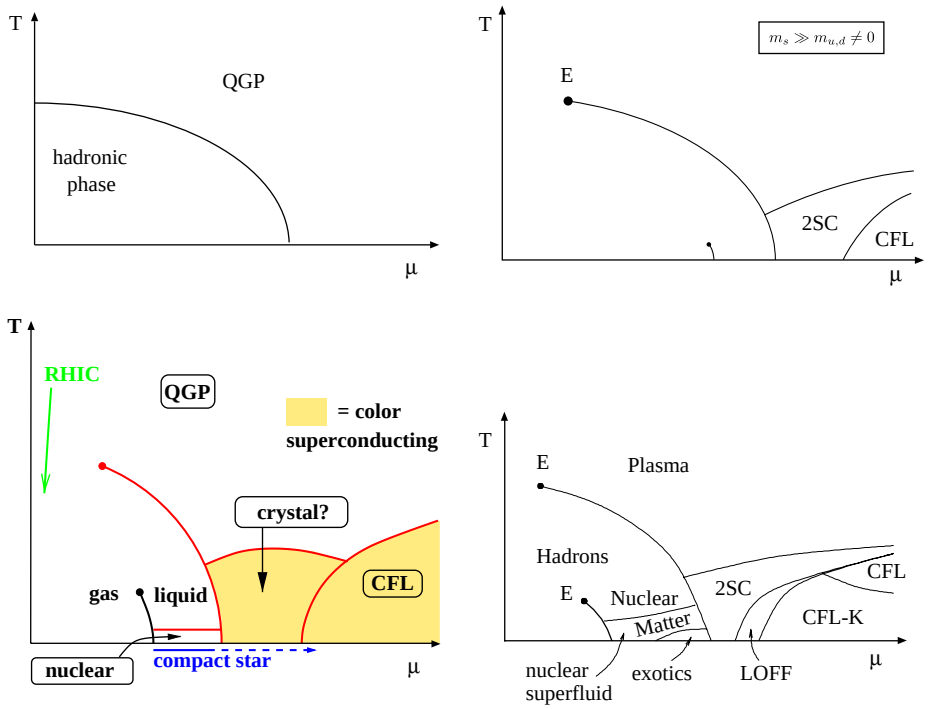

Fig. 1.1. Schematic QCD phase diagrams in the chemical potential–temperature plane. Upper left: generic phase diagram of the "pre-color superconductivity era", see, e.g., Refs. [3,4]. The other diagrams are taken from the literature. Upper right: Rajagopal [16a]. Lower left: with permission from Alford (2003) [22]. Lower right: with permission from Schäfer (2003) [14].

Refs. [7–9], the relevance of this idea for the QCD phase diagram was widely ignored until the end of the 1990s. At that time, new approaches to color superconductivity revealed that the related gaps in the fermion spectrum could be of the order of 100 MeV [10,11], much larger than expected earlier. Since larger gaps are related to larger critical temperatures, this would imply a sizeable extension of the color superconducting region into the temperature direction. Hence, in addition to the two standard phases, there should be a non-negligible region in the QCD phase diagram where strongly interacting matter is a color superconductor. (For reviews on color superconductivity, see Refs. [12–15].)

Once color superconductivity was on the agenda, the door was open for many new possibilities. This is illustrated by the remaining three phase diagrams of Fig. 1.1, which are taken from the literature. It is expected that at large chemical potentials up, down, and strange quarks are paired in a so-called color–flavor locked (CFL) condensate [16]. However, this might become unfavorable at lower densities, where the strange quarks are suppressed by their mass. It is thus possible that in some intermediate regime there is a second color superconducting phase (2SC) where only up and down quarks are paired. This scenario is depicted in the upper right diagram of Fig. 1.1, taken from Ref. [16a]. More recently, further phases, like three-flavor color superconductors with condensed kaons (CFL-K) [17–19] or crystalline color superconductors ("LOFF phase") [20,21] have been suggested, which might partially (lower right diagram [14]) or even completely (lower left diagram [22]) replace the 2SC phase.

Fig. 1.1, which is only an incomplete compilation of recent suggestions, illustrates the potential richness of the phase structure, which has not been appreciated for a long time. At the same time, it makes obvious that the issue is not at all settled. Note that all phase diagrams shown in the figure are only "schematic", i.e., educated guesses, based on certain theoretical results or arguments. In this situation, and since exact results from QCD are rather limited, model calculations may provide a useful tool to test the robustness of these ideas and to develop new ones.

In the present report we discuss the phase diagram and related issues which result from studies with Nambu–Jona-Lasinio (NJL) type models. These are schematic models with point-like quark–(anti-)quark vertices, but no gluons. As a consequence, NJL-type models have several well-known shortcomings, most important, they do not have the confinement property of QCD. This is certainly a major drawback in the hadronic phase, where constituent quarks are not the proper quasi-particle degrees of freedom. At high temperatures, confinement becomes less relevant but obviously a realistic description of the quark–*gluon* plasma requires explicit gluon degrees of freedom. On the other hand, the use of NJL-type models seems to be justified—at least on a schematic level—to study cold deconfined quark matter where both, confinement and gluon degrees of freedom, are of minor importance.

In any case, every model calculation should be confronted with the "facts", as far as available. To that end, we briefly list the main features of QCD in Section 1.1 and summarize what is currently known about the QCD phase diagram in Section 1.2. The present work will then be outlined in more details in Section 1.3.

1.1. Basics of QCD

Quantum chromodynamics is defined by the Lagrangian [23,24]

$$\mathscr{L}_{\mathrm{QCD}} = \bar{q}(\mathrm{i}\gamma^{\mu} D_{\mu} - \hat{m})q - \tfrac{1}{4} G^{a\mu\nu} G^{a}{}_{\mu\nu} \,, \tag{1.1}$$

where q denotes a quark field with six flavor (u, d, s, c, b, t) and three color degrees of freedom, and $\hat{m} = \mathrm{diag}_f(m_u, m_d, \ldots)$ is the corresponding mass matrix in flavor space. The covariant derivative

$$D_\mu = \partial_\mu - \mathrm{i}g\,\frac{\lambda^a}{2}\,A^a_\mu \tag{1.2}$$

is related to the gluon field A^a_μ, and

$$G^a{}_{\mu\nu} = \partial_\mu A^a_\nu - \partial_\nu A^a_\mu + g f^{abc} A^b_\mu A^c_\nu \tag{1.3}$$

is the gluon field strength tensor. λ^a and f^{abc} denote the generators of $SU(3)$ (Gell–Mann matrices) and the corresponding antisymmetric structure constants, respectively. g is the QCD coupling constant.

The QCD Lagrangian is by construction symmetric under $SU(3)$ gauge transformations in color space. Because of the non-Abelian character of the gauge group, underlined by the presence of the f^{abc} term in Eq. (1.3), the theory has several non-trivial features which are not present in Abelian gauge theories, like quantum electrodynamics:

- $\mathscr{L}_{\mathrm{QCD}}$ contains gluonic self-couplings (three- and four-gluon vertices), i.e., gluons carry color.
- QCD is an asymptotically free theory [25,26], i.e., the coupling becomes weak at short distances or, equivalently, large Euclidean momenta Q. To one-loop order,

$$\alpha_s(Q^2) \equiv \frac{g^2(Q^2)}{4\pi} = \frac{4\pi}{(11 - \frac{2}{3}N_f)\ln(Q^2/\Lambda^2_{\mathrm{QCD}})}\ , \tag{1.4}$$

  where N_f is the number of relevant flavors and Λ_{QCD} is the QCD scale parameter which can be determined, e.g., by fitting Eq. (1.4) (or improved versions thereof) to experimental data at large Q^2. In this way, one finds $\Lambda_{\mathrm{QCD}} \simeq 200\,\mathrm{MeV}$ for five flavors in the $\overline{MS}$ scheme.
  Eq. (1.4) is the fundamental basis for the perturbative treatment of QCD in the high-momentum regime. For instance at $Q^2 = M_Z^2$ one finds $\alpha_s \simeq 0.12$. (For a recent overview, see Ref. [27].)
- In turn, Eq. (1.4) implies that the coupling becomes strong at low momenta. In particular, perturbative QCD is not applicable to describe hadrons with masses below $\sim 2\,\mathrm{GeV}$. This may or may not be related to the phenomenon of "confinement", i.e., to the empirical fact that colored objects, like quarks and gluons, do not exist as physical degrees of freedom in vacuum. There are interesting attempts to relate confinement to particular topological objects in the QCD vacuum, like monopoles or vortices, but it is fair to say that confinement is not yet fully understood (see, e.g., Refs. [28,29] and references therein).

Another important feature of $\mathscr{L}_{\mathrm{QCD}}$ is its (approximate) chiral symmetry, i.e., its symmetry under global $SU(N_f)_L \times SU(N_f)_R$ transformations. This is equivalent to be invariant under global vector and axial-vector $SU(N_f)$ transformations,

$$SU(N_f)_V: \quad q \to \exp(\mathrm{i}\theta^V_a \tau_a) q, \qquad SU(N_f)_A: \quad q \to \exp(\mathrm{i}\theta^A_a \gamma_5 \tau_a) q\ , \tag{1.5}$$

where τ_a are the generators of flavor $SU(N_f)$. These symmetries would be exact in the limit of N_f massless flavors. (For $SU(N_f)_V$ it is sufficient to have N_f *degenerate* flavors.) In reality all quarks have non-vanishing masses. Still, chiral symmetry is a useful concept in the up/down sector ($N_f = 2$) and even, although with larger deviations, when strange quarks are included as well ($N_f = 3$). The sector of

heavy quarks (charm, bottom, top) is governed by the opposite limit, corresponding to an expansion in inverse quark masses, but this will not be of further interest for us.

The $SU(N_f)_V$ is also an (approximate) symmetry of the QCD vacuum, reflected by the existence of nearly degenerate $SU(N_f)$ multiplets in the hadron spectrum. If this was also true for the axial symmetry each hadron should have an approximately degenerate "chiral partner" of opposite parity. Since this is not the case, one concludes that chiral symmetry is spontaneously broken in vacuum. This is closely related to the existence of a non-vanishing quark condensate $\langle\bar{q}q\rangle$, which is not invariant under $SU(N_f)_A$ and therefore often deals as an order parameter for spontaneous chiral symmetry breaking.[1]

Another hint for the spontaneously broken chiral symmetry is the low mass of the pion which comes about quite naturally if the pions are interpreted as the corresponding Goldstone bosons in the two-flavor case. If chiral symmetry was exact on the Lagrangian level ("chiral limit") they would be massless, while the small but finite pion mass reflects the explicit symmetry breaking through the up and down quark masses. In the analogous way, the pseudoscalar meson octet corresponds to the Goldstone bosons in the three-flavor case. The Goldstone bosons obey several low-energy theorems which provide the basis for chiral perturbation theory (χPT) [30–32]. Unlike ordinary perturbation theory, χPT corresponds to an expansion in quark masses and momenta and can be applied in regions where α_s is large.

Since the perturbative vacuum is chirally symmetric for massless quarks, one expects that chiral symmetry gets restored at high temperature. This would also be the case at high density if the matter was in a trivial rather than in a color superconducting state (see footnote 1). The "partial restoration" of chiral symmetry, i.e., the in-medium reduction of $|\langle\bar{q}q\rangle|$ at small temperatures or densities can be studied within χPT. For two flavors one finds to leading order in temperature and density [33,34]

$$\frac{\langle\bar{q}q\rangle_{T,\rho_B}}{\langle\bar{q}q\rangle_{0,0}} = 1 - \frac{T^2}{8f_\pi^2} - \frac{\sigma_{\pi N}}{f_\pi^2 m_\pi^2}\,\rho_B + \cdots\ , \tag{1.6}$$

where $f_\pi = 92.4\,\mathrm{MeV}$ is the pion decay constant and $\sigma_{\pi N} \simeq 45\,\mathrm{MeV}$ is the pion–nucleon sigma term. The two correction terms on the r.h.s. describe the effect of thermally excited non-interacting pions and of nucleons, respectively. (Interaction effects are of higher order.) To be precise, the T^2 behavior is only correct in the chiral limit, i.e., for massless pions, which are otherwise exponentially suppressed. Since in the hadronic phase the physical pion mass can never be assumed to be small against the temperature, Eq. (1.6) is more of theoretical rather than practical interest. Systematic mass corrections are of course possible [33]. It remains at least qualitatively correct that pions, being the lightest hadrons, dominate the low-temperature behavior.

On the classical level, $\mathscr{L}_{\mathrm{QCD}}$ is also invariant under global

$$U_A(1): \quad q \to \exp(\mathrm{i}\alpha\gamma_5)q\ , \tag{1.7}$$

in the limit of massless quarks. This symmetry is, however, broken on the quantum level and therefore not a real symmetry of QCD [35]. Most prominently, this is reflected by the relatively heavy η' meson which should be much lighter (lighter than the η-meson) if it was a Goldstone boson of a spontaneously broken symmetry.

In this context instantons play a crucial role. These are semiclassical objects which originate in the fact that the classical Yang–Mills action gives rise to an infinite number of topologically distinct degenerate

[1] Note, however, that $\langle\bar{q}q\rangle = 0$ does not necessarily mean that chiral symmetry is restored since it could still be broken by other condensates. This is for instance the case for three massless flavors in the CFL phase, see Section 5.1.2.

vacuum solutions. Instantons correspond to tunneling events between these vacua. When quarks are included, the instantons mediate an interaction which is $SU(N_f)_L \times SU(N_f)_R$ symmetric, but explicitly breaks the $U_A(1)$ symmetry ("'t Hooft interaction") [35]. In particular it is repulsive in the η'-channel.

In the instanton liquid model [36], the gauge field contribution to the QCD partition function is replaced by an ensemble of instantons, characterized be a certain size and density distribution in Euclidean space. It turned out that hadronic correlators obtained in this way agree remarkably well with the "exact" solutions on the lattice (see Ref. [37] for review).

1.2. The QCD phase diagram

We have pointed out that the phase diagrams presented in Fig. 1.1 are schematic conjectures, which are constrained only by a relatively small number of safe theoretical or empirical facts. Before discussing them in more detail, we should note that in general we are not restricted to a single chemical potential, but there is a chemical potential for each conserved quantity. Hence, the QCD phase diagram has in general more dimensions than shown in Fig. 1.1. If we talk about one chemical potential only, we thus have to specify under which conditions this is fixed. For instance, it is often simply assumed that the chemical potential is the same for all quark species. On the other hand, in a neutron star we should consider neutral matter in beta equilibrium whereas in heavy-ion collisions we should conserve isospin and strangeness. This means, the different sources of information we are going to discuss below describe different phase diagrams (or different slices of the complete multi-dimensional phase diagram) as far as they correspond to different physical situations. Moreover, the results are often obtained in or extrapolated to certain unphysical limits, like vanishing or unrealistically large quark masses or the neglect of electromagnetism.

Direct empirical information about the phase structure of strongly interacting matter is basically restricted to two points at zero temperature, both belonging to the "hadronic phase" where quarks and gluons are confined and chiral symmetry is spontaneously broken. The first one corresponds to the vacuum, i.e., $\mu = 0$, the second to nuclear matter at saturation density (baryon density $\rho_B = \rho_0 \simeq 0.17\,\mathrm{fm}^{-3}$), which can be inferred from systematics of atomic nuclei.[2] Since the binding energy of nuclear matter is about $E_\mathrm{b} \simeq 16\,\mathrm{MeV}$ per nucleon, it follows a baryon number chemical potential of $\mu_B = m_N - E_\mathrm{b} \simeq 923\,\mathrm{MeV}$, corresponding to a quark number chemical potential $\mu = \mu_B/3 \simeq 308\,\mathrm{MeV}$. Unless there exists a so-far unknown exotic state which is bound more strongly (like absolutely stable strange quark matter [39,40]), this point marks the onset of dense matter, i.e., the entire regime at $T = 0$ and $\mu < 308\,\mathrm{MeV}$ belongs to the vacuum.[3] The onset point is also part of a first-orderphase boundary which separates a hadron gas at lower chemical potentials from a hadronic liquid at higher chemical potentials if one moves to finite temperature. This phase boundary is expected to end in a critical endpoint, which one tries to identify within multifragmentation experiments. Preliminary results seem to indicate a corresponding critical temperature of about 15 MeV [42]. Of course both, the gas and the liquid are part of the hadronic phase.

---

[2] The numbers quoted in Ref. [38] are a binding energy of $(16 \pm 1)\,\mathrm{MeV}$ per nucleon and a Fermi momentum of $k_F = (1.35 \pm 0.05)\,\mathrm{fm}^{-1}$.

[3] The authors of Ref. [41] distinguish between "QCD", which is a theoretical object with strong interactions only, and "QCD+", which corresponds to the real world with electromagnetic effects included. In this terminology, our discussion refers to QCD. In QCD+ the ground state of matter is solid iron, i.e., a crystal of iron nuclei and electrons. Here the onset takes place at $\mu_B \simeq 930\,\mathrm{MeV}$ and the density is about 13 orders of magnitude smaller than in symmetric nuclear matter.

They have been mentioned for completeness but are not subject of this report. There might be further hadronic phases, e.g., due to the onset of hyperons or to superfluidity.[4]

Obtaining empirical information about the QGP is the general aim of ultra-relativistic heavy-ion collisions. As mentioned earlier, there are some indications that this phase has indeed been reached at SPS [5] and at RHIC [6]. There are also claims that the chemical freeze-out points, which are determined in a thermal-model fit to the measured particle ratios, must be very close to the phase boundary [43]. However, since the system cannot be investigated under static conditions but only integrating along a trajectory in the phase diagram, an interpretation of the results without theoretical guidance is obviously very difficult.

There is also only little hope that information about color superconducting phases can be obtained from ultra-relativistic heavy-ion collisions, which are more suited to study high temperatures rather than high densities. For instance, at chemical freeze-out one finds $T \simeq 125\,\mathrm{MeV}$ and $\mu_B \simeq 540\,\mathrm{MeV}$ at AGS and $T \simeq 165\,\mathrm{MeV}$ and $\mu_B \simeq 275\,\mathrm{MeV}$ for Pb–Pb collisions at SPS [44]. Even though the CBM project at the future GSI machine is designed to reach higher densities [45], it is very unlikely that the corresponding temperatures are low enough to allow for diquark condensation. Of course, no final statement can be made as long as reliable predictions for the related critical temperatures are missing.

On the theoretical side, most of our present knowledge about the QCD phase structure comes from ab initio Monte Carlo calculations on the lattice (see Refs. [46,47] for recent reviews). For a long time, these were restricted to zero chemical potential, i.e., to the temperature axis of the phase diagram, and only recently some progress has been made in handling non-zero chemical potentials. Before summarizing the main results, let us mention that 20 years ago, the chiral phase transition at finite temperature has been analyzed on a more general basis, applying universality arguments related to the symmetries of the problem [48]. It was found that the order of the phase transition depends on the number of light flavors: If the strange quark is heavy, the phase transition is second order for massless up and down quarks and becomes a smooth cross-over if up and down have non-vanishing masses. On the other hand, if m_s is small enough the phase transition becomes first order. The question which scenario corresponds to the physical quark masses cannot be decided on symmetry arguments but must be worked out quantitatively. In principle, this can be done on the lattice. In practice, there is the problem that it is not yet possible to perform lattice calculations with realistic up and down quark masses. The calculations are therefore performed with relatively large masses and have to be extrapolated down to the physical values. Although this imposes some uncertainty, the result is that the transition at $\mu = 0$ is most likely a cross-over [46,47].

While there is thus no real phase transition, the cross-over is sufficiently rapid that the definition of a transition temperature makes sense. This can be defined as the maximum of the chiral susceptibility, which is proportional to the slope of the quark condensate. One finds a transition temperature of about 170 MeV. It is remarkable that the susceptibility related to the Polyakov loop—which deals as order parameter of the deconfinement transition—peaks at the same temperature, i.e., chiral and deconfinement transition coincide. It is usually expected that this is a general feature which also holds at finite chemical potential, but this is not clear.

When extrapolated to the chiral limit, the critical temperature is found to be $(173 \pm 8)\,\mathrm{MeV}$ for two flavors and $(154 \pm 8)\,\mathrm{MeV}$ for three flavors [49]. This is considerably lower than in the pure $SU(3)$

[4] We are using the word "phase" in a rather lose sense. If there is a first-order phase boundary which ends in a critical endpoint one can obviously go around this point without meeting a singularity. Hence, in a strict sense, both sides of the "phase boundary" belong to the same phase. However, from a practical point of view it often makes sense to be less strict, since the properties of matter sometimes change rather drastically *across* the boundary (see, e.g., liquid water and vapor).

gauge theory without quarks where $T_c = (269 \pm 1)$ MeV [46,47]. According to the symmetry arguments mentioned above, the phase transition in the two-flavor case is expected to belong to the $O(4)$ universality class, thus having $O(4)$ critical exponents. Present lattice results seem to be consistent with this, but they are not yet precise enough to rule out other possibilities.

The extension of lattice analyses to (real) non-zero chemical potentials is complicated by the fact that in this case the fermion determinant in the QCD partition function becomes complex. As a consequence the standard statistical weight for the importance sampling is no longer positive definite which spoils the convergence of the procedure. Quite recently, several methods have been developed which allow to circumvent this problem, at least for not too large chemical potentials ($\mu/T \lesssim 1$). One possibility is to perform a Taylor expansion in terms of μ/T and to evaluate the corresponding coefficients at $\mu = 0$ [50,51]. The second method is a reweighting technique where the ratio of the fermion determinants at $\mu \neq 0$ and at $\mu = 0$ is taken as a part of the operator which is then averaged over an ensemble produced at $\mu = 0$ [52–54]. The third way is to perform a calculation at imaginary chemical potentials [55–57]. In this case the fermion determinant remains real and the ensemble averaging can be done in the standard way. The results are then parametrized in terms of simple functions and analytically continued to real chemical potentials.

These methods have been applied to study the behavior of the phase boundary for non-zero μ. From the Taylor expansion one finds for the curvature of the phase boundary at $\mu = 0$ [50], $T_c(\mathrm{d}^2 T_c/\mathrm{d}\mu^2)|_{\mu=0} = -0.14 \pm 0.06$, i.e., $T_c(\mu) \simeq T_c(0) - (0.07 \pm 0.03)\mu^2/T_c(0)$. Within error bars this result is consistent with the two other methods. However, all these calculations have been performed with relatively large quark masses, and the curvature is expected to become larger for smaller masses.

Another important result is the lattice determination of a critical endpoint [51,53,54]. We have seen that at $\mu = 0$ the phase transition should be second order for two massless flavors and most likely is a rapid cross-over for realistic quark masses. On the other hand, it has been argued some time ago that at low temperatures and large chemical potentials the phase transition is probably first order. Hence, for two massless flavors there should be a "tricritical point", where the second-order phase boundary turns into a first-order one [41,58,59]. Similarly, for realistic quark masses one expects a first-order phase boundary at large μ, which ends in a (second-order) critical endpoint, as indicated in the three last phase diagrams in Fig. 1.1.

It has been suggested that this point could possibly be detected in heavy-ion experiments through event-by-event fluctuations in the multiplicities N_π and mean transverse momenta p_T^π of charged pions. These fluctuations should arise as a result of critical fluctuations in the vicinity of the endpoint [60,61]. To that end N_π and p_T^π should be measured as a function of a control parameter x which determines the trajectory of the evolving system in the phase diagram. This parameter could be, e.g., the beam energy or the centrality of the collision. If for some value of x the trajectory comes very close to the critical point this should show up as a maximum in the above event-by-event fluctuations. In this case the system is expected to freeze out close to the critical point because of critical slowing down. For a more detailed discussion of possible signatures under realistic conditions (including finite size and finite time effects), see Ref. [61].

On the lattice, the position of the endpoint has been determined first by Fodor and Katz, employing the reweighting method [53]. The result was $T = (160 \pm 3.5)$ MeV and $\mu_B = 3\mu = (725 \pm 35)$ MeV. However, these calculation suffered from the fact that they have been performed on a rather small lattice with relatively large up and down quark masses. More recently, the authors have performed an improved calculation on a larger lattice and with physical quark masses, shifting the endpoint to $T = (162 \pm 2)$ MeV

and $\mu_B = (360 \pm 40)$ MeV. This result is consistent with estimates using the Taylor expansion method, indicating a critical endpoint at $\mu/T \sim 1$, i.e., $\mu_B \sim 3T$ [51].

The techniques described above do not allow to study the expected transition to color superconducting phases at large chemical potentials but low temperatures. So far, the only controlled way to investigate these phases is a weak-coupling expansion, which becomes possible at very large densities because of asymptotic freedom. These analyses show that strongly interacting matter at asymptotic densities is indeed a color superconductor, which for three flavors is in the CFL phase [62,63]. Unfortunately, the weak-coupling expansion breaks down at densities several orders of magnitude higher than what is of "practical" relevance [64], e.g., for the interior of compact stars, and it can, of course, not be applied to study the hadron–quark phase transition itself.

1.3. Scope and outline of this report

The above discussion has shown that the detailed phase structure of strongly interacting matter at (not asymptotically) high density and low temperature is largely unknown. In particular, there is practically no exact information about the density region just above the hadron–quark phase transition which might be relevant for the interiors of compact stars.

In this situation models may play an important role in developing and testing new ideas on a semi-quantitative basis and checking the robustness of older ones. Since models are simpler than the fundamental theory (QCD)—otherwise they are useless—they often allow for studying more complex situations than accessible by the latter. The price for this is, of course, a reduced predictive power due to dependencies on model parameters or certain approximation schemes. The results should therefore always be confronted with model-independent statements or empirical facts, as far as available. In turn, models can help to interprete the latter where no other theory is available. Also, "model-independent results" are often derived by an expansion in parameters which are assumed to be small. Thus, although mathematically rigorous, they do not necessarily describe the real physical situation. Here models can give hints about the validity of these assumptions or even uncover further assumptions which are hidden.

An example which will be one of the central points in this report is the effect of the strange quark mass M_s on the phase structure. Starting from the idealized case of three massless flavors, this is often studied within an expansion in terms of M_s/μ, assuming that the strange quark mass is much smaller than the chemical potential. Obviously, this can always be done for large enough values of μ, but the expansion eventually breaks down, when μ becomes of the order of M_s. However, the crucial point is that M_s itself should be considered to be a μ-dependent effective ("constituent") quark mass. This does not only imply that the expansion breaks down earlier than one might naively expect (because M_s can be considerably larger than the perturbative quark mass m_s which is listed in the particle data book), but also that effects due to the μ dependence of M_s are missed completely. In particular, there can be strong discontinuities in M_s across first-order phase boundaries which, of course, cannot be described by a Taylor expansion.

In the present work we investigate this kind of questions within models of the Nambu–Jona-Lasinio type, i.e., schematic quark models with simple four-fermion (sometimes six-fermion) interactions. Historically, the NJL model [65,66] has been introduced to describe spontaneous chiral symmetry breaking in vacuum *in analogy* to the BCS mechanism for superconductivity [67] and has later been extended to study its restoration at non-vanishing temperatures or densities. On the other hand, NJL-type models are straightforwardly used in the original BCS sense to calculate color superconducting pairing gaps. In fact, the renewed interest in color superconductivity was caused by analyses in such models [10,11]. For

the obvious next step, namely considering chiral quark condensates and diquark condensates simultaneously and studying their competition and mutual influence, NJL-type models are therefore the natural choice [68]. Going further, the relatively simple interaction allows to attack quite involved problems. For instance, in order to describe the transition from two- to three-flavor color superconductors including dynamical mass effects, we have to allow for six different condensates which can be all different if we consider beta equilibrated matter.

The details of the results of these investigations are of course model dependent. In particular, it is not clear whether the model parameters, which are usually fitted to vacuum properties, can still be applied at large densities. In fact, it seems to be quite natural that the four-point couplings are μ and T dependent quantities, just like the effective quark masses we compute. Nevertheless, at least qualitatively, our analysis can give important hints which of the so-far neglected effects could be important and which are indeed negligible. In the first place it should therefore be viewed in conjunction with and relative to other approaches.

There are few exceptions, where we make definite predictions for—in principle—observable quantities, like absolutely stable strange quark matter or quark matter cores in neutron stars. Here, although we try to estimate the robustness of the results with respect to the parameters, we are forced to assume that these are at least not *completely* different from the vacuum fit. In these cases the arguments could be turned around: If at some stage the predictions turn out to be wrong, this would mean that the model parameters must change drastically.

The focus of the present report is an NJL-model study of the phase diagram at large densities, with special emphasis on color superconducting phases and their properties. We begin, however, with a rather detailed discussion of the model and its phase structure *without* taking into account diquark pairing. Besides defining the basic concepts of the model, this is done because we think that in order to understand the influence of color superconductivity one should know how the model behaves without. In particular, some detailed knowledge about the mechanism of the chiral phase transition in the model will be helpful when this is combined with the pairing transition. This pre-discussion will also allow us to point out the main limitations of the model. Many of them, like artifacts of missing confinement or of the mean-field treatment, are not restricted to the NJL model, and this discussion could also be useful for other approaches.

The remainder of this report is organized as follows.

In Chapter 2 we review the thermal properties of the NJL model, concentrating on color non-superconducting quark matter with two flavors. Besides setting up the formalism, a central aspect will be a comparison with the MIT bag model, which is often used to describe dense matter. In Chapter 3 the model is extended to three quark flavors. As a first application, we investigate the possibility of absolutely stable strange quark matter.

Color superconducting phases are included in Chapters 4–7. In Chapter 4 we again restrict ourselves to two-flavor systems. We begin with a general overview about the basic concepts of color superconductivity and briefly discuss other approaches. We then extend our formalism to include diquark pairing and discuss the role and mutual influence of several conventional and less conventional quark–antiquark and diquark condensates. A point of particular interest will be the discussion of a spin-1 diquark condensate as a possible pairing channel for those quarks which are left over from the standard spin-0 condensate. Next, in Chapter 5 we consider color superconductivity in a three-flavor system. Central issue will be the description of the 2SC–CFL phase transition, taking into account μ- and T-dependent constituent quark masses together with the diquark condensates. For simplicity, we consider a single chemical potential

for all quarks. This restriction is relaxed in Chapter 6, where we construct neutral quark matter in beta equilibrium which is of possible relevance for compact stars. To that end we have to introduce up to four independent chemical potentials. Both, homogeneous and mixed neutral phases are discussed. In Chapter 7 we use the resulting homogeneous quark matter equation of state to investigate the possibility of a quark matter core in neutron stars. In order to model the hadronic phase we take existing hadronic equations of state from the literature. Finally, in Chapter 8 we summarize what we have done and, more important, what remains to be done.

2. NJL-model description of color non-superconducting two-flavor quark matter

In this chapter we give a general introduction to the use of Nambu–Jona-Lasinio (NJL) type models for analyzing quark matter at non-zero density or temperature. To that end, we concentrate on the—technically simpler—two-flavor version of the model and neglect the possibility of color superconducting phases. The NJL model will be introduced in Section 2.2 where we briefly summarize its vacuum properties, before the analysis is extended to hot and dense matter in Section 2.3. Of course, this is not meant to be exhaustive, and the interested reader is referred to Refs. [69–72] for reviews. Here, our main intention is to lay a solid ground for our later investigations, including a critical discussion of the limits of the model.

A central aspect of the present chapter will be a comparison with the MIT bag model, which is the most frequently used model to describe quark–gluon matter at large temperature or density. Originally, both models have been developed to analyze hadron properties. Focusing on two different aspects of QCD, they are almost complementary: Whereas the MIT bag model is based on a phenomenological realization of confinement, the main characteristics of the NJL model is chiral symmetry and its spontaneous breakdown in vacuum. On the other hand the NJL model does not confine and the MIT bag model violates chiral symmetry. Nevertheless, the models behave quite similarly when they are employed to calculate the equation of state of deconfined quark matter at high density. In this regime the essential feature of both models is the existence of a non-vanishing vacuum pressure ("bag constant") whereas confinement and chiral symmetry are of course less important in the deconfined, chirally restored regime.[5] In the MIT bag model the bag constant is an external parameter, while in the NJL model it is dynamically generated. In order to work out this correspondence in some detail, we begin with a brief summary of the basic features of the MIT bag model.

2.1. MIT bag model

The MIT bag model has been suggested in the mid-seventies as a microscopic model for hadrons [73–75]. At that time, QCD had already been formulated and the MIT bag model was one of the first quark models where the notions of confinement and asymptotic freedom have been implemented in a constitutive way.[6]

[5] In fact, the MIT bag model is chirally symmetric in the thermodynamic limit, because chiral symmetry is broken only at the bag surface.

[6] Strictly speaking, rather than on asymptotic freedom, the model was based on the experimental fact of Bjorken scaling. Since QCD was not yet generally accepted, at least at the beginning [73], the model was presented in a more general way, referring to QCD only as one of several possibilities.

In the MIT bag model, hadrons consist of free (or only weakly interacting) quarks which are confined to a finite region of space: the "bag". The confinement is not a dynamical result of the underlying theory, but put in by hand, imposing the appropriate boundary conditions.[7] The bag is stabilized by a term of the form $g^{\mu\nu}B$ which is added to the energy-momentum tensor *inside* the bag. Recalling the energy-momentum tensor of a perfect fluid in its rest frame,

$$T^{\mu\nu}_{\text{fluid}} = \text{diag}(\epsilon, p, p, p) \ , \tag{2.1}$$

the bag constant B is immediately interpreted as positive contribution to the energy density ϵ and a negative contribution to the pressure p inside the bag. Equivalently, we may attribute a term $-g^{\mu\nu}B$ to the region *outside* the bag. This leads to the picture of a non-trivial vacuum with a negative energy density $\epsilon_{\text{vac}} = -B$ and a positive pressure $p_{\text{vac}} = +B$. The stability of the hadron then results from balancing this positive vacuum pressure with the pressure caused by the quarks inside the bag.

The MIT bag model says nothing about the origin of the non-trivial vacuum, but treats B as a free parameter. Evaluating the energy-momentum tensor in QCD, one finds

$$B_{\text{QCD}} = -\frac{1}{4}\langle T^{\mu}_{\mu}\rangle = \frac{11-\frac{2}{3}N_f}{32}\,\frac{\alpha_s}{\pi}\,\langle G^{\mu\nu}_a G_{a\mu\nu}\rangle - \frac{1}{4}\sum_f m_f\langle\bar{q}_f q_f\rangle \ , \tag{2.2}$$

which is dominated by the contribution of the gluon condensate (first term on the r.h.s.). In the second term q_f denotes a quark with flavor f, and m_f is the corresponding current quark mass. Employing the QCD sum-rule result of Ref. [76], Shuryak obtained $B_{\text{QCD}} \approx 455\,\text{MeV/fm}^3$ [77], while a modern value of the gluon condensate would yield a somewhat larger result. In any case, as we will see below, this is much larger than the values of B one obtains in a typical bag model fit.

2.1.1. Hadron properties

Assuming a static spherical bag of radius R, the mass of a hadron in the MIT bag model is given by the sum [75]

$$E_{\text{BM}} = \frac{4\pi}{3}BR^3 - \frac{z_0}{R} + \frac{1}{R}\sum_q x_q + E_{\text{pert}} \ . \tag{2.3}$$

The first term on the r.h.s. corresponds to the volume energy, required to replace the non-trivial vacuum by the trivial one inside the bag. The second term was introduced in Ref. [75] to parametrize the finite part of the zero-point energy of the bag. The constant z_0 was treated as a free parameter, whose theoretical determination was left for future work. In a later analysis, however, it turned out that not all singularities arising from the zero-point energy could be absorbed in a renormalization of the model parameters, like the bag constant [78] (also see [79] for a recent discussion). Therefore the definition of the finite part is ambiguous and z_0 remained an undetermined fitting parameter in the literature. The third term in Eq. (2.3) is the (rest + kinetic) energy of the quarks. For massless quarks in the lowest $j = \frac{1}{2}$ state one finds $x_q = 2.04$ as solutions of the eigenvalue problem. Finally, E_{pert} corresponds to perturbative corrections due to lowest-order gluon exchange. This term gives rise, e.g., to the $N - \Delta$ mass splitting.

[7] However, if the quarks are coupled to a non-Abelian gauge field, one finds the non-trivial result that the boundary conditions can only be fulfilled if the system is a color singlet [73].

Table 2.1
Bag-model parameters obtained from fits to light hadron spectra

Fit	m_u (MeV)	m_s (MeV)	B (MeV/fm^3)	z_0	α_s	m_π (MeV)	R_N (fm)
[75]	0	279	57.5	1.84	2.2	280	1.0
[75]	108	353	31.8	1.95	3.0	175	1.1
[86]	0	288	351.7	0.00	<1 (running)	(Tachyonic)	0.6
[87]	5	354	44.7	1.17	0	Not given	1.0
[87]	5	356	161.5	2.04	0	Not given	0.6

Quark masses $m_u = m_d$ and m_s, bag constant B, parameter for the zero-point energy z_0, and strong coupling constant α_s. In the last two columns we list the resulting pion mass and the bag radius of the nucleon. The first two lines correspond to the original fit of the MIT group [75], while the other fits have been performed later within partially modified models (see text).

Eq. (2.3) contains the following parameters: The bag constant B, the parameter z_0, the quark masses (entering x_q), and the strong coupling constant α_s (entering E_{pert}). The bag radius R is not a parameter but is separately fixed for each hadron to minimize its mass. The parameters of the original fit [75] are listed in Table 2.1 (first two lines). They have been adjusted to fit the masses of the nucleon, the Δ, the Ω^-, and the ω-meson. The light quark masses ($m_u = m_d$) have not been fitted, but have been set to zero (fit A) and to 108 MeV (fit B) to test the sensitivity of the fit to its variation. With these parameters the authors of Ref. [75] obtained a good overall fit of the light hadron spectra (baryon octet and decuplet, and vector meson nonet), magnetic moments, and charge radii.

There are, however, a couple of well-known problems: Since chiral symmetry is explicitly broken on the bag surface and the $U_A(1)$ anomaly is not included, the pion mass comes out too large, whereas the η' is too light. Also, the values of α_s needed to reproduce the $N-\Delta$ mass splitting are extremely large and obviously inconsistent with the idea that the corrections are perturbative. Finally, the nucleon radii of 1.0–1.1 fm, as shown in Table 2.1, would mean that the bags overlap with each other in a nucleus, which is clearly inconsistent with the success of meson-exchange models.

Some of these problems are related to each other. For instance, in the so-called chiral bag models, where chiral symmetry is restored by coupling external pion fields (introduced as elementary fields) to the bag surface [80], the bag radii can be considerably smaller than in the MIT bag ("little bag" [81] $R_N \sim 0.3$ fm, "cloudy bag" [82] $R_N \sim 0.8$ fm). This also leads to smaller values of α_s needed to fit the $N-\Delta$ mass splitting [81,82]. In the chiral bag models the nucleon mass is the sum of the bag contribution and a self-energy contribution from the pion cloud. Since the latter is negative, the former can be (much) larger than the physical nucleon mass. This is the reason why the radii can be smaller than in the MIT fit. In fact, many observables are quite insensitive to the bag radius, which can even be taken to be zero ("Cheshire cat principle", for review see, e.g., Ref. [83]).

Eq. (2.3) contains effects of spurious c.m. motion, which can approximately be projected out if one replaces E_{BM} by the mass $M_{\text{BM}} = (E_{\text{BM}}^2 - \sum_q (x_q/R)^2)^{1/2}$ [84–86]. This correction has not been performed in the original MIT fit [75] but is standard in modern bag model calculations. It has the appreciable effect that the bag radius is reduced by about 30% and might also remove some of the other problems discussed above. In fact, instead of a too large pion mass, the authors of Ref. [86] obtain m_π^2 slightly negative, and reasonable values for R_N and α_s, once c.m. corrections are included (third line of Table 2.1). Note, however, that this model also differs from the original MIT bag model in the treatment of the perturbative corrections, bringing in additional parameters, while the parameter z_0 was

not employed in the fit. On the other hand, the authors of Ref. [87] did not include perturbative corrections and restricted their fit to the baryon octet. They also considered ρ and ω mesons, but to that end they introduced independent zero-point energies as additional parameters. In this way the (baryonic) zero-point energy was left undetermined and could be employed to vary the bag radius at will (cf. last two lines of Table 2.1).

For the thermodynamic description of hot or dense quark–gluon matter, many problems discussed above are not of direct relevance (see next section). We have mentioned them, however, because they have a strong effect on the parameter fit, and thereby *indirectly* on the thermodynamics. In this context, the most important parameter is the bag constant. As obvious from Table 2.1, the fitted values of B vary by more than a factor of six, although they are all smaller than the value derived from the gluon condensate, Eq. (2.2). From a modern point of view it is also remarkable that the strange quark mass m_s in all fits listed in the table is considerably larger than today accepted values of its "current quark mass" (see Table 3.1). Later we will see that similar masses appear in NJL-model quark matter at comparable densities.

2.1.2. Thermodynamics

When we consider a large number of quarks and gluons in a large MIT bag we can replace the exact solutions of the boundary problem by plane waves, while zero-point energy and c.m. correction terms drop out. Hence the energy density $\epsilon = E_{\rm BM}/V$ at temperature T and a set of chemical potentials $\{\mu_f\}$ reduces to

$$\epsilon(T,\{\mu_f\}) = B + \epsilon_{\rm free}(T,\{\mu_f\}) + \epsilon_{\rm pert}(T,\{\mu_f\}) \ , \tag{2.4}$$

where $\epsilon_{\rm free}$ is the energy density of a free relativistic gas of quarks, antiquarks, and gluons, while $\epsilon_{\rm pert}$ corresponds to perturbative corrections. Equivalently, we can write for the pressure

$$p(T,\{\mu_f\}) = -B + p_{\rm free}(T,\{\mu_f\}) + p_{\rm pert}(T,\{\mu_f\}) \ . \tag{2.5}$$

Here the earlier mentioned role of B as a negative pressure inside the bag relative to the non-trivial vacuum is obvious. The free part is given by

$$\begin{aligned} p_{\rm free}(T,\{\mu_f\}) = 6T \sum_f \int \frac{{\rm d}^3p}{(2\pi)^3} \Bigg\{ &\ln\left[1+\exp\left(-\frac{1}{T}(E_{p,f}-\mu_f)\right)\right] \\ &+ \ln\left[1+\exp\left(-\frac{1}{T}(E_{p,f}+\mu_f)\right)\right]\Bigg\} \\ &- 16T \int \frac{{\rm d}^3p}{(2\pi)^3} \ln\left[1-\exp\left(-\frac{p}{T}\right)\right] \ , \end{aligned} \tag{2.6}$$

where the second integral corresponds to the gluons (2 spin and 8 color degrees of freedom) and the first integral corresponds to the quarks and antiquarks (2 spin and 3 color degrees of freedom and a sum over flavors). $E_{p,f} = (p^2 + m_f^2)^{1/2}$ is the on-shell energy of a quark of flavor f with three-momentum p.

In the following, we consider the case of two massless quark flavors with a common chemical potential μ. The integrals in Eq. (2.6) are then readily evaluated and the bag model pressure becomes

$$p(T,\mu) = -B + 37\,\frac{\pi^2}{90}\,T^4 + \mu^2 T^2 + \frac{\mu^4}{2\pi^2} \ , \tag{2.7}$$

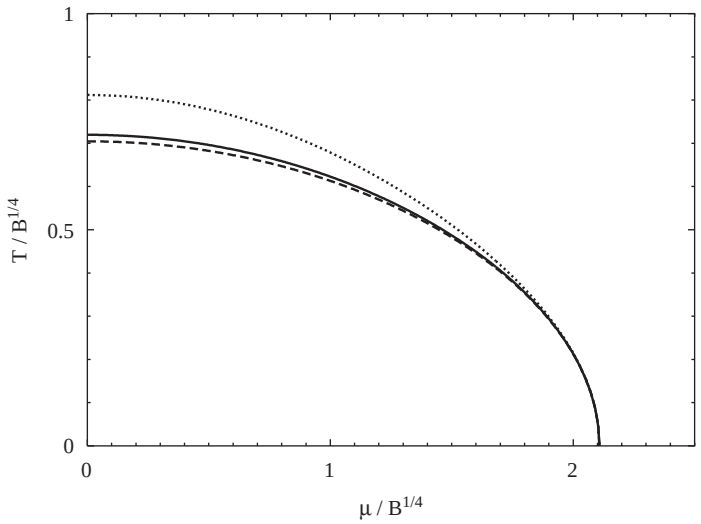

Fig. 2.1. Lines of zero pressure in a two-flavor bag model with non-interacting massless quarks and gluons (dashed) and with quarks only (dotted). The solid line indicates the phase boundary, separating the "hadronic phase", described by a gas of non-interacting massless pions, from the quark–gluon phase.

where we have neglected the perturbative contribution. The famous factor $37 = 16 + 21$ in front of the T^4 term is the sum of the 16 gluonic degrees of freedom and the product of the 24 quark and antiquark degrees of freedom with a factor $\frac{7}{8}$ due to Fermi statistics.

In order to be stable, the pressure in the quark–gluon phase must not be negative. For $\mu = 0$ this leads to a minimum temperature

$$T_0 = \left(\frac{90}{37\pi^2}\, B\right)^{1/4} , \tag{2.8}$$

while for $T = 0$ we obtain a minimum chemical potential

$$\mu_0 = (2\pi^2\, B)^{1/4} . \tag{2.9}$$

It is interesting that T_0 has already been derived by the MIT group in their first paper about the bag model [73]. There T_0 was identified with the "limiting temperature" of a highly excited hadron, i.e., the temperature a hadronic bag must not exceed in order to remain stable. Thus, although formally equivalent to the above derivation of T_0, the perspective is rather opposite.

For arbitrary chemical potentials smaller than μ_0 one can easily solve for the temperature $T(\mu)$ for which the pressure vanishes. The result is displayed in Fig. 2.1 (dashed line). For later purposes we also show the corresponding curve one obtains with quark degrees of freedom only (dotted). In this case the factor 37 in Eq. (2.7) is replaced by 21. Accordingly the minimum temperature is enhanced by a factor $(\frac{37}{21})^{1/4} = 1.15$, while the minimum chemical potential remains unchanged.

Eq. (2.7) is the most simple example for a bag-model description of the quark–gluon plasma. In order to construct a phase transition, we also need an equation of state for the hadronic phase. Usually, the latter is not described within the bag model as well but taken from models with hadronic degrees of

freedom. As a prototype, we consider a gas of non-interacting massless pions, which should dominate the low-temperature $\mu = 0$-regime. The resulting phase boundary, i.e., the line where p becomes equal to the pressure of the pion gas, is indicated by the solid line in Fig. 2.1. Since the pions have an isospin degeneracy of three, the pressure difference is given by Eq. (2.7), but with 37 replaced by $37 - 3 = 34$. Hence, the critical temperature at $\mu = 0$ is given by $T_c = (\frac{37}{34})^{1/4} T_0 = 1.02 T_0$.

So far we have not set the absolute scale in our phase diagram. Taking the bag constant from the original MIT fit, $B = 57.5\,\mathrm{MeV/fm^3}$ ($B^{1/4} = 145\,\mathrm{MeV}$) [75], we obtain $T_c = 104\,\mathrm{MeV}$, whereas in order to get the lattice value, $T_c \simeq 170\,\mathrm{MeV}$, we need a seven times larger bag constant $B \simeq 400\,\mathrm{MeV/fm^3}$ ($B^{1/4} \simeq 235\,\mathrm{MeV}$). For μ_0, which in the present model is the critical chemical potential for the phase transition at $T = 0$, this variation of B leads to values roughly ranging from 300 to 500 MeV.

For several reasons, however, it is clear that a model of this type is too simplistic:

- Since mesons are not sensitive to the (quark number) chemical potential they do not influence the phase transition in the large-μ low-T regime. Thus, for a more realistic description, we need baryonic degrees of freedom. In the above example, it would be most natural to add the contribution of a free nucleon gas to the hadronic phase. It is a well-known fact, however, that this would lead to the unphysical situation that the hadronic phase "wins" at large chemical potentials. This is obvious from the contribution of a fermion of type i to the pressure at $T = 0$,

$$p_i(T = 0, \mu_i) = \frac{g_i}{24\pi^2}\,\mu_i^4 + \cdots\,, \tag{2.10}$$

  where the ellipsis indicates corrections due to the fermion mass which can be neglected at very large chemical potentials. Here g_i is a degeneracy factor which is three times larger for quarks than for nucleons because of color. On the other hand, since nucleons consist of three valence quarks, their chemical potential is three times larger than the quark number chemical potential. Altogether, this means $p_q : p_N = 1 : 27$, which leads to the above-mentioned unphysical result.
- As we have seen, the phase transition at $\mu = 0$ is a result of the larger number of quark–gluon degrees of freedom (37) compared with the hadronic ones (3 for the pion gas), i.e., the larger coefficient of the T^4-term. This necessarily means, that the phase transition is first order with a latent heat per volume

$$\frac{\Delta Q}{V} = (37 - 3)\,\frac{4\pi^2}{90}\,T_c^4\,. \tag{2.11}$$

  This is in strong contrast to the universality arguments mentioned in the Introduction, according to which we would expect a second-order phase transition in QCD with two massless flavors [48]. It is possible to reduce ΔQ by introducing additional hadrons, but obviously it is very difficult to get $\Delta Q = 0$ without inhibiting the phase transition.

It is quite plausible that these problems can be traced back to the hybrid nature of the above model, i.e., the fact that the hadronic and the quark–gluon degrees of freedom are not derived from the same Lagrangian. In a more consistent picture one should start from a gas of hadronic bags to describe the hadronic phase. Since the bags have finite sizes which can only be reduced at the expense of energy, it is obvious that the system will not stay in the hadronic phase up to arbitrarily large densities. In the most naive picture the bags would simply unite to form a uniform phase when the average quark number density exceeds the density inside a single bag. (In fact, it is more difficult to prevent the bags from forming one large bag already at low densities. For this one would need to introduce a negative surface tension or

some repulsive force between separate bags.) In this way also the connection between the chiral and the deconfinement phase transition appears quite natural if one attributes the non-trivial vacuum outside the bags to the spontaneous breakdown of chiral symmetry, which is restored inside the bags. We will come back to this point of view in Section 2.3.3.

While qualitatively the picture drawn in the previous paragraph looks quite attractive, its quantitative realization is of course very difficult. An interesting step in this direction is the quark–meson coupling model where nuclear matter and even finite nuclei are described by MIT bags which interact by exchange of (elementary) scalar and vector mesons [87–90]. A somewhat "cheaper" alternative is to employ hybrid models with finite volume corrections on the hadronic side (see, e.g., Ref. [91]).

2.1.3. Equation of state at zero temperature

Since we are mostly interested in quark matter at low temperature we would like to discuss a few more details of the bag model equation of state in the zero temperature limit. This will also provide a basis for our later comparison with the NJL model.

For $T = 0$, Eq. (2.6) simplifies, and the total pressure is given by

$$p(\{\mu_f\}) = -B + \frac{3}{\pi^2} \sum_f \int_0^{p_{\rm F}^f} {\rm d}p\, p^2 (\mu_f - E_{p,f}) + p_{\rm pert}(\{\mu_f\}) \ , \tag{2.12}$$

where $p_{\rm F}^f = \theta(\mu_f - m_f)(\mu_f^2 - m_f^2)^{1/2}$ denotes the Fermi momentum of flavor f. For simplicity, we have dropped the temperature argument.

In the following, we concentrate again on the case of a uniform chemical potential μ for two massless flavors. Neglecting the perturbative term and applying standard thermodynamic relations, we obtain for the pressure, energy density, and quark number density

$$p(\mu) = -B + \frac{\mu^4}{2\pi^2}, \quad \epsilon(\mu) = B + \frac{3\mu^4}{2\pi^2}, \quad n(\mu) = \frac{2\mu^3}{\pi^2} \ . \tag{2.13}$$

This is simply a free gas behavior, modified by the bag constant. From these expressions we immediately get for the function $\epsilon(p)$, which, e.g., determines the mass–radius relation of neutron stars,

$$\epsilon(p) = 3p + 4B \ . \tag{2.14}$$

Another quantity of interest, which follows from Eq. (2.13), is the energy per particle E/N as a function of density,

$$\frac{E}{N}(n) = \frac{\epsilon}{n}(n) = \frac{B}{n} + \frac{3}{4}\left(\frac{\pi^2}{2} n\right)^{1/3} \ . \tag{2.15}$$

For later convenience, we rephrase this as the energy per baryon number A in terms of the baryon number density $\rho_B = n/3$,

$$\frac{E}{A}(\rho_B) = \frac{\epsilon}{\rho_B}(\rho_B) = \frac{B}{\rho_B} + \frac{9}{4}\left(\frac{3\pi^2}{2} \rho_B\right)^{1/3} \ . \tag{2.16}$$

This function is plotted in Fig. 2.2 (solid line). Its general structure is easily understood if we recall that $\rho_B = A/V$. Thus the first term on the r.h.s. is just the volume energy of the MIT bag, while the second

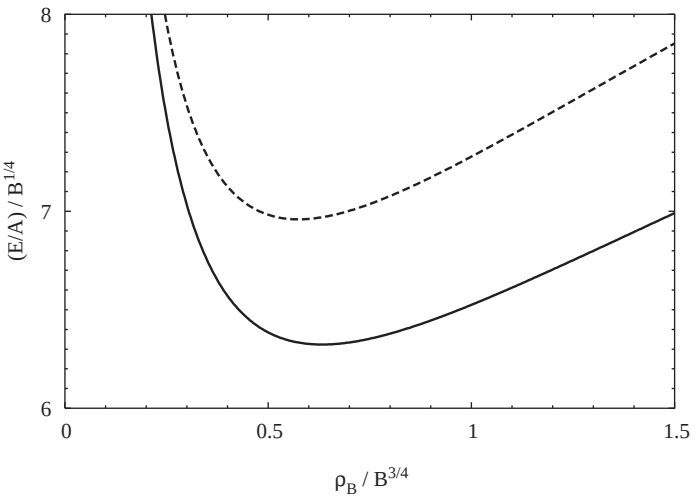

Fig. 2.2. Energy per baryon number E/A in the bag model as a function of baryon number density ρ_B. Solid line: $\alpha_s = 0$. Dashed line: $\alpha_s = 0.5$.

term reflects the $1/R$ behavior of the quark energy in Eq. (2.3). Of course, the coefficient of the latter depends on the number of occupied states and therefore it is different in the thermodynamic limit from the case of a single hadron.

Because of the interplay of the two terms, E/A diverges for both, $\rho_B \to 0$ and $\rho_B \to \infty$, and has a minimum at

$$\left(\frac{E}{A}\right)_{\min} = 3(2\pi^2 B)^{1/4} \equiv 3\mu_0 \quad \text{at } \rho_B = \frac{1}{3}\left(\frac{2}{\pi^2}\right)^{1/4}(4B)^{3/4} =: \rho^* \ . \tag{2.17}$$

Note that this is just the point where the pressure vanishes, reflecting the general thermodynamic relation

$$\frac{\partial}{\partial \rho_B}\left(\frac{\epsilon}{\rho_B}\right) = \frac{p}{\rho_B^2} \ . \tag{2.18}$$

The physical meaning of this relation becomes clear if we consider a finite lump of quark matter (large enough that the thermodynamic treatment is valid). For $\rho_B < \rho^*$ (i.e., $\mu < \mu_0$), the pressure is negative and the lump shrinks, thereby increasing the density. On the other hand, for $\rho_B > \rho^*$ ($\mu > \mu_0$), the pressure is positive and the lump tends to expand, unless this is prevented by external forces. Hence, the only stable point is $\rho_B = \rho^*$, where the pressure vanishes. In a canonical (instead of grand canonical) treatment, which would be more appropriate for this example with fixed particle number, this stability becomes manifest as a minimum in the energy. (Recall that $T = 0$ and hence the Helmholtz free energy $F = E - TS = E$.)

The absolute scale of Fig. 2.2 is again set by the value of the bag constant. As discussed above, varying B between the two "extreme" values, $B = 57.5\,\text{MeV/fm}^3$ from the original MIT fit and $B = 400\,\text{MeV/fm}^3$ from fitting $T_c \simeq 170\,\text{MeV}$ within the simple hybrid model, leads to values of μ_0 between about 300 and 500 MeV. This corresponds to $(E/A)_{\min}$ ranging from about 900 MeV at $\rho_B = 1.4\rho_0$ to 1500 MeV at $\rho_B = 6.5\rho_0$. Of course, values for $(E/A)_{\min}$ lower than the energy per nucleon in atomic nuclei must be

excluded, since otherwise nuclei should be able to decay into a large bag of deconfined quarks. We will come back to this in Section 3.3.

Finally, we discuss briefly the influence of perturbative corrections, which we have neglected so far. To order α_s the free-gas terms in Eq. (2.13) are scaled by a factor [92],

$$p(\mu) = -B + \gamma\,\frac{\mu^4}{2\pi^2}, \quad \epsilon(\mu) = B + \gamma\,\frac{3\mu^4}{2\pi^2}, \quad n(\mu) = \gamma\,\frac{2\mu^3}{\pi^2}, \quad \gamma := \left(1 - 2\,\frac{\alpha_s}{\pi}\right) . \tag{2.19}$$

Obviously, this correction makes only sense for $\alpha_s \ll \pi/2$. This demonstrates again that the value of the original MIT fit, $\alpha_s = 2.2$, is completely out of range for a perturbative treatment. Note that it would even change the sign of the free-gas terms.

As a consequence of the correction, the chemical potential μ_0 at which the pressure vanishes and thus $(E/A)_{\min}$ are enhanced by a factor $\gamma^{-1/4}$, whereas the corresponding baryon number density ρ^* is reduced by a factor $\gamma^{1/4}$. Accordingly, the minimum of E/A is shifted to a larger value at a lower density. This is illustrated by the dashed line in Fig. 2.2, which corresponds to $\alpha_s = 0.5$. On the other hand, the relation between ϵ and p, Eq. (2.14), remains unaffected by the correction.

2.2. Nambu–Jona-Lasinio model in vacuum

As pointed out earlier, the Nambu–Jona-Lasinio (NJL) model is to some extent complementary to the MIT bag model. Historically, it goes back to two papers by Nambu and Jona-Lasinio in 1961 [65,66], i.e., to a time when QCD and even quarks were still unknown. In its original version, the NJL model was therefore a model of interacting *nucleons*, and obviously, confinement—the main physics input of the MIT bag model—was not an issue. On the other hand, even in the pre-QCD era there were already indications for the existence of a (partially) conserved axial vector current (PCAC), i.e., chiral symmetry. Since (approximate) chiral symmetry implies (almost) massless fermions on the Lagrangian level, the problem was to find a mechanism which explains the large nucleon mass without destroying the symmetry. It was the pioneering idea of Nambu and Jona-Lasinio that the mass gap in the Dirac spectrum of the nucleon can be generated quite analogously to the energy gap of a superconductor in BCS theory, which has been developed a few years earlier [67]. To that end they introduced a Lagrangian for a nucleon field ψ with a point-like, chirally symmetric four-fermion interaction [66],

$$\mathscr{L} = \bar{\psi}(\mathrm{i}\partial\!\!\!/ - m)\psi + G\{(\bar{\psi}\psi)^2 + (\bar{\psi}\mathrm{i}\gamma_5\vec{\tau}\psi)^2\} . \tag{2.20}$$

Here m is a small bare mass of the nucleon, $\vec{\tau}$ is a Pauli matrix acting in isospin space, and G a dimensionful coupling constant. As we will discuss in more detail in Section 2.2.1, the self-energy induced by the interaction generates an effective mass M which can be considerably larger than m and stays large, even when m is taken to zero ("chiral limit"). At the same time there are light collective nucleon–antinucleon excitations which become massless in the chiral limit: The pion emerges as the Goldstone boson of the spontaneously broken chiral symmetry. In fact, this discovery was an important milestone on the way to the general derivation of the Goldstone theorem in the same year [93].

After the development of QCD, the NJL model was reinterpreted as a schematic quark model [94–96]. At that point, of course, the lack of confinement became a problem, severely limiting the applicability of the model. On the other hand, there are many situations where chiral symmetry is the relevant feature of QCD, confinement being less important. The most prominent example is again the Goldstone nature of

the pion. In this aspect the NJL model is superior to the MIT bag, which, as we have seen, fails to explain the low pion mass.

End of the nineties, a third era of the NJL model began when the model was employed to study color superconducting phases in deconfined quark matter. There, by definition, lack of confinement is again of minor relevance. As outlined in the Introduction, color superconductivity will be discussed in great detail in Chapter 4 and thereafter.

After the reinterpretation of the NJL model as a quark model, many authors kept the original form of the Lagrangian, Eq. (2.20), with ψ now being a quark field with two flavor and three color degrees of freedom. However, this choice is not unique and we can write down many other chirally symmetric interaction terms. For instance, from a modern point of view, local four-point interactions between quarks in a two-flavor system can be thought of to be abstracted from instanton-induced interactions [35]. In this case the interaction Lagrangian should have the form

$$\mathscr{L}_{\text{inst}} = G\{(\bar{q}q)^2 - (\bar{q}\vec{\tau}q)^2 - (\bar{q}\mathrm{i}\gamma_5 q)^2 + (\bar{q}\mathrm{i}\gamma_5\vec{\tau}q)^2\} \ . \tag{2.21}$$

Here and in the following we denote quark fields by q. In general, we will call all these models "NJL-type models" (or just "NJL models") as long as they describe quarks interacting via four-point vertices (or sometimes higher n-point vertices).

2.2.1. Constituent quarks and mesons

In this section we briefly review the vacuum properties of quarks and mesons described within the NJL model. For simplicity, we restrict this discussion to the standard NJL-Lagrangian, Eq. (2.20), for quarks with two flavor and three color degrees of freedom. Most of this can easily be generalized to other NJL-type Lagrangians with two degenerate flavors. The discussion of the three-flavor case, which has some additional features, is deferred to the next chapter.

In most publications (including the original papers by Nambu and Jona-Lasinio [65,66]) the quark self-energy which arises from the interaction term has been calculated within Hartree or Hartree–Fock approximation. The corresponding Dyson equation is depicted in Fig. 2.3. Since in this approximation the self-energy is local, it only gives rise to a constant shift in the quark mass,

$$M = m + 2\mathrm{i}G \int \frac{\mathrm{d}^4 p}{(2\pi)^4} \operatorname{Tr} S(p) \ . \tag{2.22}$$

Here $S(p) = (\not{p} - M + \mathrm{i}\varepsilon)^{-1}$ is the *dressed* quark propagator, underlining the non-perturbative character of the approximation. The trace is to be taken in color, flavor, and Dirac space. One finds

$$M = m + 8N_f N_c G\mathrm{i} \int \frac{\mathrm{d}^4 p}{(2\pi)^4} \frac{M}{p^2 - M^2 + \mathrm{i}\varepsilon}, \tag{2.23}$$

where $N_f = 2$ and $N_c = 3$ are the number of flavors and colors, respectively. For a sufficiently strong coupling G, this allows for a non-trivial solution $M \neq m$, even in the chiral limit $m = 0$, producing a gap of $\Delta E = 2M$ in the quark spectrum. In analogy to BCS theory, Eq. (2.23) is therefore often referred to as "gap equation". M is often called "constituent quark mass". A closely related quantity is the quark condensate, which is generally given by

$$\langle\bar{q}q\rangle = -\mathrm{i} \int \frac{\mathrm{d}^4 p}{(2\pi)^4} \operatorname{Tr} S(p) \ , \tag{2.24}$$

Fig. 2.3. Dyson equation for the quark propagator in Hartree approximation. The bare (dressed) propagator is denoted by the thin (bold) line.

Fig. 2.4. Bethe–Salpeter equation for quark–antiquark T-matrix ("meson propagators", shaded boxes) in RPA. The solid lines correspond to the dressed quark propagators in Hartree approximation (Fig. 2.3).

and thus in the present case

$$\langle\bar{q}q\rangle = -\frac{M-m}{2G} \ . \tag{2.25}$$

Iterating the four-point vertex as shown in Fig. 2.4 yields the quark–antiquark T-matrix in random phase approximation (RPA),

$$T_M(q^2) = \frac{2G}{1-2G\Pi_M(q^2)} \ , \tag{2.26}$$

where

$$\Pi_M(q^2) = \mathrm{i}\int \frac{\mathrm{d}^4p}{(2\pi)^4}\,\mathrm{Tr}[\mathcal{O}_M S(p+q)\mathcal{O}_M S(p)] \tag{2.27}$$

is the quark–antiquark polarization in the channel with the quantum numbers $\{M\}$. For the Lagrangian Eq. (2.20) we have the sigma channel ($\mathcal{O}_\sigma = \mathbb{1}$) and three pion channels ($\mathcal{O}_{\pi_a} = \mathrm{i}\gamma_5\tau_a$, $a = 1, 2, 3$). Evaluating the traces and employing the gap equation for $M \neq 0$ one finds

$$\begin{aligned}\Pi_\sigma(q^2) &= \frac{1}{2G}\left(1-\frac{m}{M}\right) - \frac{1}{2}(q^2-4M^2)I(q^2) \ , \\ \Pi_{\pi_a}(q^2) &= \frac{1}{2G}\left(1-\frac{m}{M}\right) - \frac{1}{2}q^2 I(q^2) \ ,\end{aligned} \tag{2.28}$$

where

$$I(q^2) = 4N_f N_c \mathrm{i}\int \frac{\mathrm{d}^4p}{(2\pi)^4}\,\frac{1}{[(p+q)^2-M^2+\mathrm{i}\varepsilon][p^2-M^2+\mathrm{i}\varepsilon]} \ . \tag{2.29}$$

In order to determine meson properties one interpretes T_M as an effective meson exchange between the external quark legs in Fig. 2.4 and parametrizes the pole structure as

$$T_M(q^2) = \frac{-g_{Mqq}^2}{q^2-m_M^2} \ . \tag{2.30}$$

Fig. 2.5. One-pion-to-vacuum matrix element in RPA, giving rise to the weak pion decay: A pion with isospin index b is coupled via a quark loop to an axial current with isospin index a.

Thus

$$1 - 2G\Pi_M(q^2 = m_M^2) = 0 \quad \text{and} \quad g_{Mqq}^{-2} = \left.\frac{\mathrm{d}\Pi_M}{\mathrm{d}q^2}\right|_{q^2=m_M^2} . \tag{2.31}$$

Using Eq. (2.28), one immediately finds that $m_\pi = 0$ if $m = 0$, in accordance with the Goldstone theorem. For $m \neq 0$, m_π also becomes non-zero (see below).

The pion decay constant can be obtained from the one-pion-to-vacuum matrix element visualized in Fig. 2.5,

$$f_\pi q^\mu \delta_{ab} = g_{\pi qq} \int \frac{\mathrm{d}^4 p}{(2\pi)^4} \,\mathrm{Tr}\left[\gamma^\mu\gamma_5 \frac{\tau_a}{2} S(p+q)\mathrm{i}\gamma_5\tau_b S(p)\right] . \tag{2.32}$$

It is straightforward to show that in the chiral limit the generalized Goldberger–Treiman relation [97],

$$g_{\pi qq} f_\pi = M + \mathcal{O}(m) \tag{2.33}$$

holds. Moreover, in first non-vanishing order in m, the pion mass satisfies the Gell–Mann Oakes Renner relation [98],

$$f_\pi^2 m_\pi^2 = -m\langle\bar{q}q\rangle + \mathcal{O}(m^2) . \tag{2.34}$$

In the brief discussion presented above, we have ignored several problems:

- In general, the gap equation has more than one solution. For instance, in the chiral limit, $m = 0$, there is always a trivial solution $M = 0$, but there can be non-trivial solutions $M = \pm M_0 \neq 0$ as well. In this case, one has to find out which solution minimizes the vacuum energy.
  One way is to go back to the underlying mechanism of the gap equation, which is a Bogoliubov–Valatin rotation of the fields. Starting point is a variational ansatz for the non-trivial vacuum of the model [10,65,70],

$$|\mathrm{vac}\rangle = \prod_{\vec{p},s,f,c} [\cos\theta_s(\vec{p}) + \mathrm{e}^{\mathrm{i}\xi_s(\vec{p})}\sin\theta_s(\vec{p}) b^\dagger(\vec{p},s,f,c)\, d^\dagger(-\vec{p},-s,f,c)]|0\rangle , \tag{2.35}$$

  where $|0\rangle$ is the perturbative vacuum, and $b(\vec{p},s,f,c)$ and $d(\vec{p},s,f,c)$ are the corresponding annihilation operators for a quark or antiquark, respectively, with momentum $\vec{p}$, helicity s, flavor f, and color c. According to this ansatz, $|vac\rangle$ is a coherent state composed of quark–antiquark pairs with zero total momentum. This underlines once more the analogy to the BCS ground state. Minimizing the ground state energy,

$$\mathscr{E}_{\mathrm{vac}}[\theta_s(\vec{p}), \xi_s(\vec{p})] = \langle\mathrm{vac}|\hat{H}|\mathrm{vac}\rangle , \tag{2.36}$$

($\hat{H}$ = Hamiltonian of the model) with respect to variations of the functions $\theta_s(\vec{p})$ and $\xi_s(\vec{p})$ leads to a self-consistency equation, which is equivalent to the Hartree–Fock gap equation discussed above. (For the difference between Hartree and Hartree–Fock, see below.) It turns out that the vacuum energy is minimized by the solution with the largest M. In the chiral limit this means that the non-trivial solution is stable whenever it exists.

An alternative way to calculate the ground state energy will be presented in Section 2.3 in the context of the thermodynamics of the model. There we will discuss further details.

- The NJL model is not renormalizable. Since the above expressions contain divergent integrals, e.g., Eqs. (2.23), (2.29), and (2.32), we have to specify how to regularize these divergencies. This prescription is then part of the model. There are several regularization schemes which have been used in the literature, and each of them have certain advantages and disadvantages [70,72]. When the model is applied to thermodynamics, most authors prefer to regularize the integrals by a (sharp or smooth) 3-momentum cut-off. Besides being relatively simple, this has the advantage that it preserves the analytical structure, necessary, e.g., for the analytical continuation of functions given on imaginary Matsubara frequencies. Of course, 3-momentum cut-offs violate the Lorentz covariance of the model. It is often argued that this problem is less severe at finite temperature or density where manifest covariance is anyway broken by the medium. Although this argument is questionable, since it makes a difference whether the symmetry is broken by physical effects or by hand, it is perhaps true that a 3-momentum cut-off has the *least* impact on the medium parts of the regularized integrals, in particular at $T = 0$. This will become more clear in Section 2.3. In this report we will therefore regularize the model using a sharp 3-momentum cut-off Λ, unless stated otherwise.
- We already mentioned that the NJL model does not confine. Formally, this is reflected by the fact that the integral $I(q^2)$, and hence the polarization functions $\Pi_M(q^2)$, get an imaginary part above the $q\bar{q}$-threshold, i.e., for $q^2 > 4M^2$. As a consequence, mesons with a mass larger than $2M$ have a finite width, which indicates that they are unstable against decay into a quark–antiquark pair. The pion is of course not affected by this problem. However, as can be seen from Eqs. (2.28) and (2.31), $m_\sigma = 2M$ if $m = 0$ and it moves above the threshold if $m > 0$. If vector mesons are included, it depends on the parameters whether they have masses above or below the $q\bar{q}$ threshold, while axial vector mesons always decay into $q\bar{q}$ pairs in the model.
- The formulae given above correspond to the Hartree approximation and to RPA without Pauli exchange terms, respectively. However, because of the local four-point interaction, exchange diagrams can always be cast in the form of direct diagrams via a Fierz transformation (see Appendix A). This means, the Hartree–Fock approximation is equivalent to the Hartree approximation with appropriately redefined coupling constants. In this sense, Hartree is as good as Hartree–Fock, as long as the interaction terms in the Lagrangian are not fixed by some underlying theory.

  Extensions of the approximation scheme beyond Hartree–Fock+RPA are much more difficult. This topic will briefly be discussed in Section 2.3.5.

2.2.2. Parameter fit

As a basis for the subsequent discussions we perform a first parameter fit for the simple two-flavor model, Eq. (2.20), within the Hartree+RPA scheme. As mentioned above, we will regularize the integrals by a sharp 3-momentum cut-off. We thus have three parameters, the bare quark mass m, the coupling constant G, and the cut-off Λ. These parameters are usually fixed by fitting the pion mass, the pion

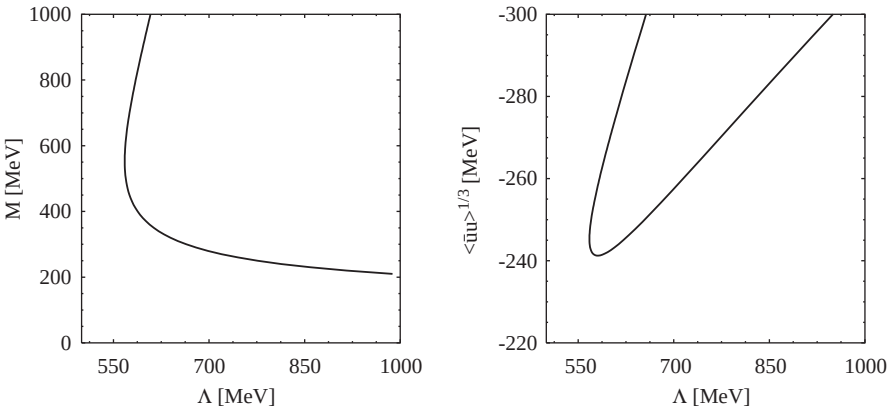

Fig. 2.6. Constituent quark mass (left) and quark condensate (right) as functions of the 3-momentum cut-off for fixed $f_\pi = 92.4\,\text{MeV}$ and $m_\pi = 135\,\text{MeV}$.

decay constant, and the quark condensate. Whereas the pion mass, $m_\pi = 135.0\,\text{MeV}$ [99][8] and the pion decay constant, $f_\pi = 92.4 \pm 0.2\,\text{MeV}$ [102], are known quite accurately, the uncertainties for the quark condensate are rather large. Limits extracted from sum rules are $190\,\text{MeV} \lesssim -\langle\bar{u}u\rangle^{1/3} \lesssim 260\,\text{MeV}$ at a renormalization scale of 1 GeV [103], while lattice calculations yield $\langle\bar{u}u\rangle^{1/3} = -(231 \pm 4 \pm 8 \pm 6)\,\text{MeV}$ [104].

In this situation we first fix G and m for arbitrary values of Λ by fitting f_π and m_π to their empirical values. The corresponding solutions of the gap equation are displayed in Fig. 2.6. In the left panel the constituent mass M is shown as a function of the cut-off. Obviously, Λ must be larger than some critical value (about $568\,\text{MeV} \hat{=} 6.1 f_\pi$) to find a solution. Above this value, there is a "low-mass" branch ($M \lesssim 550\,\text{MeV}$) and a "high-mass" branch of solutions. This kind of behavior is typical for the model and is also found within other regularization schemes [72].

On the r.h.s. of Fig. 2.6 we show the corresponding values of the quark condensate. We see that the model (together with the used regularization scheme) cannot accommodate values of $-\langle\bar{u}u\rangle^{1/3}$ smaller than 240 MeV. Taking the upper limit of Ref. [103], $-\langle\bar{u}u\rangle^{1/3} \lesssim 260\,\text{MeV}$, we find $\Lambda \lesssim 720\,\text{MeV}$ for the low-mass branch and $\Lambda \lesssim 585\,\text{MeV}$ for the high-mass branch. This restricts the constituent mass to lie between about 270 and 800 MeV. Taking the upper limit of $-\langle\bar{u}u\rangle^{1/3}$ to be 250 MeV, as suggested by the results of Ref. [104], would constrain M to an interval between about 300 and 640 MeV.

Four parameter sets, more or less representing this interval, are listed in Table 2.2. In the last column we also list the corresponding "bag constants", i.e., the energy gain per volume, due to the formation of the non-trivial vacuum state. Obviously, the uncertainty in M (caused by the uncertainty in the quark condensate and the peculiar behavior of having two solutions for the same value of $\langle\bar{u}u\rangle$) leads to a big uncertainty in the bag constant and thereby in the thermodynamic behavior of the model. This will be discussed in more detail in the next section.

[8] This corresponds to the mass of the π^0, which is not affected by $\mathcal{O}(\alpha)$ electromagnetic corrections [100]. For the NJL model, this was explicitly proven in Ref. [101]. Of course, having the other uncertainties in mind, fitting m_π to the charged pion mass would not cause any practical difference.

Table 2.2
Model parameters (3-momentum cut-off Λ, coupling constant G, and current quark mass m) and related quantities (constituent quark mass M, quark condensate $\langle\bar{u}u\rangle$, and bag constant B) for the two-flavor NJL model, Eq. (2.20), treated in Hartree+RPA approximation

set	Λ (MeV)	$G\Lambda^2$	m (MeV)	M (MeV)	$\langle\bar{u}u\rangle^{1/3}$ (MeV)	B (MeV/fm^3)
1	664.3	2.06	5.0	300	−250.8	76.3
2	587.9	2.44	5.6	400	−240.8	141.4
3	569.3	2.81	5.5	500	−242.4	234.1
4	568.6	3.17	5.1	600	−247.5	356.1

The parameters have been determined fitting the pion decay constant and the pion mass to their empirical values, f_π=92.4 MeV and $m_\pi = 135.0$ MeV. The definition of the bag constant is given in Section 2.3.1, Eq. (2.60).

2.3. Non-zero densities and temperatures

Soon after the reinterpretation of the NJL model as an effective quark model it has been employed to study quark and meson properties in hot or dense matter [105,106].

Applying standard techniques of thermal field theory [107] it is straightforward to evaluate the quark loop which enters the gap equation or the mesonic polarization diagrams at non-vanishing temperature or chemical potential. The results have basically the same structure as the vacuum expressions, but are modified by thermal occupation numbers. For instance, the gap equation Eq. (2.23) becomes

$$M = m + 4N_f N_c G \int \frac{\mathrm{d}^3 p}{(2\pi)^3} \frac{M}{E_p} (1 - n_p(T,\mu) - \bar{n}_p(T,\mu)) \ , \tag{2.37}$$

where $E_p = \sqrt{\vec{p}^2 + M^2}$ is the on-shell energy of the quark, self-consistently evaluated for the constituent mass M which solves the equation.[9] n_p and $\bar{n}_p$ are Fermi occupation numbers of quarks and antiquarks, respectively,

$$n_p(T,\mu) = \frac{1}{\mathrm{e}^{(E_p-\mu)/T}+1}, \quad \bar{n}_p(T,\mu) = \frac{1}{\mathrm{e}^{(E_p+\mu)/T}+1} \ . \tag{2.38}$$

They are related to the total quark number density in the standard way,

$$n(T,\mu) = 2N_f N_c \int \frac{\mathrm{d}^3 p}{(2\pi)^3} (n_p(T,\mu) - \bar{n}_p(T,\mu)) \ . \tag{2.39}$$

For $T = \mu = 0$, we have $n_p = \bar{n}_p = 0$ and Eq. (2.37) becomes identical to Eq. (2.23) if there the integration over p_0 is turned out.

In medium, the occupation numbers are non-zero and reduce the value of the constituent mass. For large temperatures or densities the factor $(1 - n_p - \bar{n}_p)$ goes to zero, and M approaches the value of the current mass m. This is illustrated in Fig. 2.7 for zero density and non-zero temperatures (left panel) and for zero temperature and non-zero densities (right panel). The solid lines indicate the (maximal)

[9] We will not use a special notation, like, e.g., M^*, to indicate in-medium quantities, since most quantities in this report correspond to non-zero temperature or density. Instead, we will sometimes indicate vacuum quantities by the suffix "vac", if necessary.

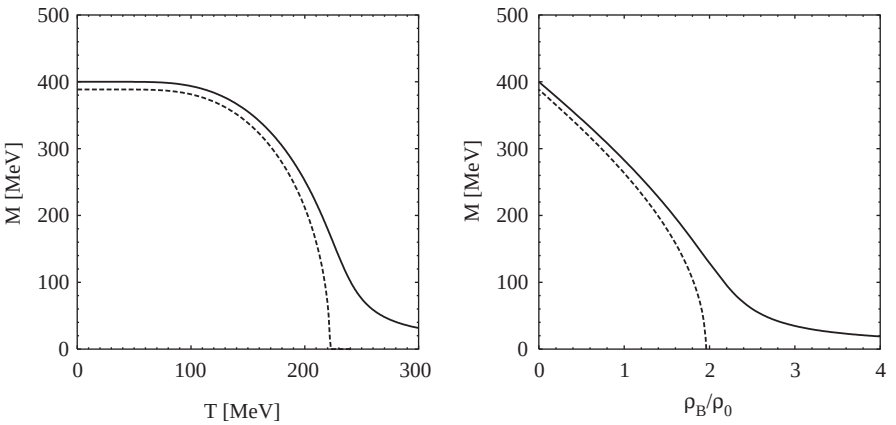

Fig. 2.7. Constituent quark mass at zero density as a function of temperature (left) and at zero temperature as a function of baryon number density in units of nuclear matter density $\rho_0 = 0.17\,\mathrm{fm}^{-3}$ (right). Solid lines: parameters of set 2 of Table 2.2, dashed lines: same parameters, but with $m = 0$ (chiral limit).

solutions of the gap equation for parameter set 2 of Table 2.2. Taking the chiral limit we arrive at the dashed lines. In this case Eq. (2.37) does no longer support non-trivial solutions for temperatures larger than $T_c = 222\,\mathrm{MeV}$ or densities larger than $\rho_c = 2.0\rho_0$. (For a detailed discussion of the critical line in the density–temperature plane, see, e.g., [108].) Note that the critical temperature at zero density is quite large compared with the lattice value of about 170 MeV, while the critical density at zero temperature seems to be rather low. As we will discuss in Section 2.3.4, this is a typical feature of an NJL mean-field calculation, which is mainly due to the fact that the phase transition is driven by the wrong degrees of freedom (unconfined quarks).

In the beginning, the smooth behavior of the constituent quark mass as a function of temperature or density lead several authors to believe that the phase transition is second order [105]. However, in order to decide on the order of the phase transition it is not sufficient to solve the gap equation. As we have seen in vacuum, the gap equation does not have a unique solution and one should look for the solution with the lowest energy. Similarly, at non-vanishing temperature or chemical potential, one should minimize the (grand canonical) thermodynamic potential. In this way it was revealed by Asakawa and Yazaki that the phase transition can indeed be first order, at least at low temperatures [59]. In the following we will basically adopt their method to calculate the thermodynamic potential.

2.3.1. Thermodynamic potential

We consider a two-flavor NJL-type Lagrangian of the form

$$\mathscr{L} = \bar{q}(\mathrm{i}\partial\!\!\!/ - m)q + G_S[(\bar{q}q)^2 + (\bar{q}\mathrm{i}\gamma_5\vec{\tau}q)^2] - G_V(\bar{q}\gamma^\mu q)^2 + \cdots\ . \tag{2.40}$$

To keep the discussion rather general we have not restricted ourselves to the standard NJL interaction term in the scalar and pseudoscalar-isovector channels, but we have added explicitly a term in the vector–isoscalar channel. It is known, e.g., from the Walecka model [109], that this channel is quite important at non-zero densities. In principle we allow for further channels (indicated by the ellipsis), which, however, do not contribute at mean-field level as long as we have only one common quark chemical potential.

The thermodynamic potential per volume V at temperature T and quark chemical potential μ is defined as

$$\Omega(T,\mu) = -\frac{T}{V}\,\ln\mathscr{Z} = -\frac{T}{V}\,\ln\mathbf{Tr}\exp\left(-\frac{1}{T}\int \mathrm{d}^3x(\mathscr{H}-\mu q^\dagger q)\right)\ , \tag{2.41}$$

where $\mathscr{H}$ is the Hamiltonian density and **Tr** a functional trace over all states of the system, i.e., spin, flavor, color and momentum. $\mathscr{Z}$ is the grand canonical partition function.

To calculate Ω in mean-field (Hartree) approximation we could in principle proceed in the way sketched in Section 2.2.1, i.e., we define a non-trivial ground state via a Bogoliubov rotation and then evaluate the free energy in this state. This method would have the advantage that it contains the full information about the structure of the ground state. On the other hand, the derivations become quite involved and extensions to include several condensates at the same time are very difficult. Therefore we follow Ref. [59] where an equivalent but much simpler method has been applied. To that end we consider two non-vanishing "condensates",

$$\phi = \langle\bar{q}q\rangle \quad \text{and} \quad n = \langle q^\dagger q\rangle \equiv \langle\bar{q}\gamma^0 q\rangle\ , \tag{2.42}$$

i.e., the quark condensate and the total quark number density. As long as we assume that—apart from chiral symmetry and Lorentz invariance (which is explicitly broken by the chemical potential)—all symmetries of the Lagrangian remain intact, these are the only allowed expectation values which are bilinear in the quark fields. (Later we will encounter many other condensates, due to both, explicit and spontaneous symmetry breaking.)

Next, we linearize the interaction terms of $\mathscr{L}$ in the presence of ϕ and n,[10]

$$(\bar{q}q)^2 \simeq 2\phi\bar{q}q - \phi^2, \quad (\bar{q}\gamma^\mu q)^2 \simeq 2nq^\dagger q - n^2\ , \tag{2.43}$$

where terms quadratic in the fluctuations, like $(\bar{q}q-\phi)^2$, have been neglected. In particular terms in channels without condensate, like $(\bar{q}\mathrm{i}\gamma_5\vec{\tau}q)^2$ or the space components in the vector vertex, drop out. In this approximation,

$$\begin{aligned}\mathscr{L}+\mu q^\dagger q &= \bar{q}(\mathrm{i}\partial\!\!\!/ - m + 2G_S\phi)q + (\mu - 2G_V n)q^\dagger q - G_S\phi^2 + G_V n^2 \\ &= \bar{q}(\mathrm{i}\partial\!\!\!/ - M)q + \tilde{\mu}q^\dagger q - \frac{(M-m)^2}{4G_S} - \frac{(\mu-\tilde{\mu})^2}{4G_V}\ ,\end{aligned} \tag{2.44}$$

where we have introduced the constituent mass M and the renormalized chemical potential $\tilde{\mu}$,

$$M = m - 2G_s\phi, \quad \tilde{\mu} = \mu - 2G_V n\ . \tag{2.45}$$

This means, apart from constant (i.e., field independent) terms, which give trivial contributions to the r.h.s. of Eq. (2.41), the problem is equivalent to a system of non-interacting particles with mass M at chemical potential $\tilde{\mu}$. Hence, the mean-field thermodynamic potential takes the form

$$\Omega(T,\mu;M,\tilde{\mu}) = \Omega_M(T,\tilde{\mu}) + \frac{(M-m)^2}{4G_S} - \frac{(\mu-\tilde{\mu})^2}{4G_V} + \text{const.}\ , \tag{2.46}$$

[10] A more formal, but essentially equivalent, method is to bosonize the model. In that context, ϕ and n emerge as auxiliary Bose fields which are introduced in the framework of a Hubbard–Stratonovich transformation.

with the free Fermi-gas contribution

$$\Omega_M(T,\tilde{\mu}) = -T\sum_n \int \frac{\mathrm{d}^3p}{(2\pi)^3}\,\mathrm{Tr}\,\ln\left(\frac{1}{T}\,S^{-1}(\mathrm{i}\omega_n,\vec{p})\right)\ . \tag{2.47}$$

Here $S^{-1}(p) = \not{p} - \tilde{\mu}\gamma^0 - M$ is the inverse fermion propagator at chemical potential $\tilde{\mu}$ which has to be evaluated at fermionic Matsubara frequencies, $p^0 = \mathrm{i}\omega_n = (2n+1)\pi T$.

The further evaluation of Ω_M can be found in textbooks [107], but for later comparison we summarize the main steps: The trace is to be taken in color, flavor, and Dirac space. Using

$$\mathrm{Tr}\,\ln(\not{Q} - M) = \ln\,\mathrm{Det}(\not{Q} - M) = 2N_fN_c\ln(Q^2 - M^2)\ , \tag{2.48}$$

this is readily done. Then, after some reordering, one can apply the relation [107]

$$T\sum_n \ln\left(\frac{1}{T^2}(\omega_n^2 + \lambda_k^2)\right) = \lambda_k + 2T\ln(1 + \mathrm{e}^{-\lambda_k/T}) \tag{2.49}$$

to turn out the Matsubara sum. One finally gets

$$\begin{aligned}\Omega_M(T,\tilde{\mu}) = &-2N_fN_c\int\frac{\mathrm{d}^3p}{(2\pi)^3}\left\{E_p + T\ln\left(1+\exp\left(-\frac{E_p-\tilde{\mu}}{T}\right)\right)\right.\\ &\left.+\,T\,\ln\left(1+\exp\left(-\frac{E_p+\tilde{\mu}}{T}\right)\right)\right\}\ .\end{aligned} \tag{2.50}$$

Note that Ω is physically meaningful only up to a constant, as indicated in Eq. (2.46).

Until this point, the result for Ω depends on M and $\tilde{\mu}$, i.e., on our choice of ϕ and n. On the other hand, in a thermodynamically consistent treatment, ϕ and n should follow from Ω as

$$\phi = \frac{\partial\Omega}{\partial m} \quad\text{and}\quad n = -\frac{\partial\Omega}{\partial\mu}\ . \tag{2.51}$$

Writing $M = M(m,T,\mu)$ and $\tilde{\mu} = \tilde{\mu}(m,T,\mu)$ and applying the chain rule we get from Eq. (2.46)

$$\frac{\partial\Omega}{\partial m} = \phi + \frac{\delta\Omega}{\delta M}\frac{\partial M}{\partial m} + \frac{\delta\Omega}{\delta\tilde{\mu}}\frac{\partial\tilde{\mu}}{\partial m},\quad \frac{\partial\Omega}{\partial\mu} = -n + \frac{\delta\Omega}{\delta M}\frac{\partial M}{\partial\mu} + \frac{\delta\Omega}{\delta\tilde{\mu}}\frac{\partial\tilde{\mu}}{\partial\mu}\ , \tag{2.52}$$

where we have used Eq. (2.45) to replace the *explicit* derivatives by ϕ and $-n$, respectively. Thus, to be consistent with Eq. (2.51) the *implicit* contributions have to vanish. This is obviously fulfilled if

$$\frac{\delta\Omega}{\delta M} = \frac{\delta\Omega}{\delta\tilde{\mu}} = 0\ , \tag{2.53}$$

i.e., the stationary points of Ω with respect to M and $\tilde{\mu}$ are automatically thermodynamically consistent. Explicitly, one gets

$$\frac{\delta\Omega}{\delta M} = \frac{M-m}{2G_S} - 2N_fN_c\int\frac{\mathrm{d}^3p}{(2\pi)^3}\frac{M}{E_p}\,(1 - n_p(T,\tilde{\mu}) - \bar{n}_p(T,\tilde{\mu})) = 0 \tag{2.54}$$

and

$$\frac{\delta\Omega}{\delta\tilde{\mu}} = \frac{\mu-\tilde{\mu}}{2G_V} - 2N_fN_c\int\frac{\mathrm{d}^3p}{(2\pi)^3}(n_p(T,\tilde{\mu}) - \bar{n}_p(T,\tilde{\mu})) = 0\ . \tag{2.55}$$

This is a coupled set of self-consistency equations for M and $\tilde{\mu}$, which generalizes the gap equation (2.37) to $G_V \neq 0$. In fact, for $G_V \to 0$, Eq. (2.55) yields $\tilde{\mu} = \mu$ and Eq. (2.54) goes over into Eq. (2.37). In general, $\tilde{\mu} \neq \mu$ and Eqs. (2.54) and (2.55) have to be solved simultaneously. If there is more than one solution, the stable one is the solution which corresponds to the lowest value of Ω.

In the following, we will restrict ourselves to repulsive vector interactions, $G_V \geqslant 0$. In this case $\tilde{\mu}$ is uniquely determined by Eq. (2.55) for given values of T, μ, and M. To see this we rewrite this equation in the form

$$\mu = \tilde{\mu} + 4N_f N_c G_V \int \frac{\mathrm{d}^3 p}{(2\pi)^3} (n_p(T,\tilde{\mu}) - \bar{n}_p(T,\tilde{\mu})) \ , \tag{2.56}$$

which formally defines μ as a function of $\tilde{\mu}$. It is easy to verify that this function is strictly rising. Therefore it can be inverted and $\tilde{\mu}$ is in turn a strictly rising function of μ. In particular we find that $\tilde{\mu}(\mu = 0) = 0$, which also implies $n = 0$ (see Eq. (2.45)).

Another important observation is that M, if written as a function of temperature and *density*, does not depend on the vector coupling G_V. This follows from the fact that, according to Eqs. (2.55) and (2.45), the density is given by

$$n(T,\tilde{\mu}) = 2N_f N_c \int \frac{\mathrm{d}^3 p}{(2\pi)^3} (n_p(T,\tilde{\mu}) - \bar{n}_p(T,\tilde{\mu})) \ , \tag{2.57}$$

i.e., just like in a free quark gas, Eq. (2.39), but with μ replaced by $\tilde{\mu}$. This equation can be inverted to calculate $\tilde{\mu}$ for given T and n, except for $T = 0$ and $n = 0$ which can be satisfied by any value of $\tilde{\mu}$ with $|\tilde{\mu}| \leqslant |M|$. However, in that case the occupation functions n_p and $\bar{n}_p$ are identically zero, which means that in any case n_p and $\bar{n}_p$, and thus all ingredients of the gap Eq. (2.54) are uniquely determined if the density is known.

Having found a pair of solutions M and $\tilde{\mu}$, other thermodynamic quantities can be obtained in the standard way. Since the system is uniform, pressure and energy density are given by

$$p(T,\mu) = -\Omega(T,\mu;M,\tilde{\mu}), \quad \epsilon(T,\mu) = -p(T,\mu) + Ts(T,\mu) + \mu n(T,\mu) \ . \tag{2.58}$$

The density n is given by Eq. (2.51) while the entropy density is $s = -\partial\Omega/\partial T$. As customary, we choose the irrelevant constant in Eq. (2.46) such that p and ϵ vanish in vacuum, i.e., we choose

$$\Omega(0,0;M_{\mathrm{vac}},0) = 0 \ . \tag{2.59}$$

Here M_{vac} corresponds to the *stable* solution for M at $T = \mu = 0$. We may also define the "bag constant",

$$B = \Omega(0,0;m,0) - \Omega(0,0;M_{\mathrm{vac}},0) = \Omega(0,0;m,0) \ , \tag{2.60}$$

where the second equality follows from our particular choice, Eq. (2.59), whereas the first equality is the more general expression. Like in the bag model, B describes the pressure difference between the trivial and the non-trivial vacuum, but it is not an input parameter of the model, but a dynamical consequence of the interaction, leading to vacuum masses $M_{\mathrm{vac}} \neq m$. Note that, except in the chiral limit, $M = m$ is not a solution of the gap equations, i.e., not even an unstable one, but corresponds to the perturbative vacuum.

In Table 2.2 we have listed the values of B for the various parameter sets. Obviously, B is extremely sensitive to the parameters, ranging from $76.3\,\mathrm{MeV/fm^3}$ for $M_{\mathrm{vac}} = 300\,\mathrm{MeV}$ to $356.1\,\mathrm{MeV/fm^3}$ for

$M_{\rm vac} = 600\,\text{MeV}$, i.e., more or less covering the same region as the bag-model fits listed in Table 2.1. It can be shown that for $\Lambda^2 \gg M_{\rm vac}^2$ the following relation holds in the chiral limit [110],

$$B = \frac{1}{2} M_{\rm vac}^2 f_\pi^2 + \frac{N_f N_c}{32\pi^2} M_{\rm vac}^4 + \mathcal{O}(M_{\rm vac}^2/\Lambda^2) \ . \tag{2.61}$$

In practice this formula works rather well, even for $M_{\rm vac}$ of the same order as the cut-off. Thus the strong parameter dependence of B can mainly be attributed to the $M_{\rm vac}^4$-term in Eq. (2.61).

2.3.2. Chiral phase transition and stable quark matter solutions at zero temperature

In the limit $T \to 0$, the thermal factors in Eq. (2.50) go over into step functions and the mean-field thermodynamic potential Eq. (2.46) becomes

$$\begin{aligned}\Omega(0,\mu;M,\tilde{\mu}) = & -2N_f N_c \int \frac{\mathrm{d}^3 p}{(2\pi)^3}\{E_p + (\tilde{\mu} - E_p)\theta(\tilde{\mu} - E_p)\} + \frac{(M-m)^2}{4G_S} \\ & - \frac{(\mu-\tilde{\mu})^2}{4G_V} + \text{const.} \ ,\end{aligned} \tag{2.62}$$

where we have assumed $\mu \geqslant 0$ and thus $\tilde{\mu} \geqslant 0$. When we also take $\mu \to 0$ and use the fact that in this case $\tilde{\mu}$ has to vanish as well, we obtain the vacuum thermodynamic potential

$$\Omega_{\rm vac}(M) := \Omega(0,0;M,0) = -2N_f N_c \int \frac{\mathrm{d}^3 p}{(2\pi)^3} E_p + \frac{(M-m)^2}{4G_S} + \text{const.} \tag{2.63}$$

Here we can nicely see, that the spontaneous symmetry breaking in vacuum comes about through the interplay between the negative contribution from the Dirac sea (first term on the r.h.s.), which favors large values of M^2, and the positive field energy of the condensate (second term) which favors values of M close to the current mass m. We should keep in mind that the integral, which would be strongly divergent otherwise, is regularized by a cut-off. One can easily check that it rises quadratically with M for small values of M and logarithmically if M is large. Thus for large M, the positive $(M-m)^2$ term always wins, whereas for small M the over-all behavior depends on the size of the coupling constant.

An example for the vacuum thermodynamic potential as a function of M is shown in the left panel of Fig. 2.8 (dotted line). We have used parameter set 2 of Table 2.2, but in the chiral limit ($m = 0$). In this case one obtains a vacuum mass $M_{\rm vac} = 388.5\,\text{MeV}$, which corresponds to a minimum $\Omega_{\rm vac}$, while the trivial solution $M = 0$ is a maximum.

For $\mu > 0$ (but still $T = 0$), Ω gets modified by the term

$$\delta\Omega_{\rm med}(0,\mu;M,\tilde{\mu}) = -2N_f N_c \int \frac{\mathrm{d}^3 p}{(2\pi)^3}(\tilde{\mu} - E_p)\theta(\tilde{\mu} - E_p) - \frac{(\mu-\tilde{\mu})^2}{4G_V} \ . \tag{2.64}$$

Unlike the vacuum part, this term is finite, even without regularization because the integral is cut off by the step function at the Fermi momentum $p_{\rm F} = \theta(\tilde{\mu} - M)\sqrt{\tilde{\mu}^2 - M^2}$. Thus, as long as $p_{\rm F} < \Lambda$, $\delta\Omega_{\rm med}$ is not affected by the cut-off. Taking a typical value, $\Lambda = 600\,\text{MeV}$, this corresponds to a baryon number density of about $11\rho_0$. This was what we had in mind, when we said that a sharp 3-momentum cut-off is probably the least severe regularization of medium integrals. (Note, however, that the cut-off does have an impact on the medium contributions at finite T or in color superconducting phases, when the Fermi surface is smeared out.)

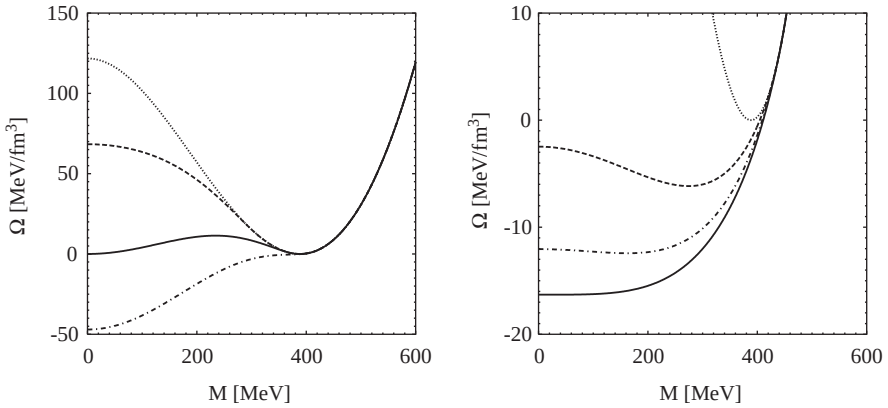

Fig. 2.8. Mean-field thermodynamic potential as a function of the auxiliary variable M ("constituent quark mass") for parameter set 2 of Table 2.2, but with $m = 0$ (chiral limit). For each value of M, the gap equation (2.55) has been solved to eliminate the auxiliary variable $\tilde{\mu}$. All functions are symmetric in M, but only the positive part is shown. Left: $G_V = 0$ and chemical potentials $\mu = 0$ (dotted), $\mu = 300\,\text{MeV}$ (dashed), $\mu = \mu_c = 368.6\,\text{MeV}$ (solid), and $\mu = 400\,\text{MeV}$ (dash–dotted). Right: $G_V = G_S$ and chemical potentials $\mu = 0$ (dotted), $\mu = 430\,\text{MeV}$ (dashed), $\mu = 440\,\text{MeV}$ (dash–dotted), and $\mu = \mu_c = 444.3\,\text{MeV}$ (solid). The vacuum result (dotted) is identical to that for $G_V = 0$.

For $\tilde{\mu} \leqslant M$, $p_F = 0$ and the integral vanishes. In this case the second term in Eq. (2.64) yields the stationary solution $\tilde{\mu} = \mu$, i.e., it vanishes, too.[11] Since $\tilde{\mu}$ is a strictly rising function of μ and vice versa, we conclude that $\tilde{\mu} = \mu$ for all $\mu \leqslant M$ and $\delta\Omega_{\text{med}}$ vanishes in this regime. From a physical point of view, this makes sense: At $T = 0$ the chemical potential corresponds to the Fermi energy of the system. As long as this is smaller than the constituent quark mass, no quark state can be populated, i.e., the density remains zero. Since $n = -\partial\Omega/\partial\mu$, this implies that Ω remains unchanged.[12] Moreover, according to Eq. (2.45), $\tilde{\mu} = \mu$ for $n = 0$.

For $\mu > M$, $\delta\Omega_{\text{med}}$ does not vanish and leads to a reduction of Ω, favoring small values of M. In the chiral limit this eventually leads to a restoration of chiral symmetry at some critical chemical potential μ_c. Above this value, the absolute minimum of the thermodynamic potential corresponds to $M = 0$. It turns out that there are three different ways how the restored phase can be reached in the model [111,112]. These scenarios are illustrated in Fig. 2.9 where the constituent quark masses (left panels) and the densities (right panel) are displayed as functions of μ. The plots are based on calculations with parameter set 2 of Table 2.2 and different values of the vector coupling constant G_V: $G_V = 0$ in the upper line ("case (a)"), $G_V = 0.5G_S$ in the second line ("case (b)"), and $G_V = G_S$ in the lower line ("case (c)"). The dashed lines correspond to the chiral limit, while for the solid lines we used the current mass $m = 5.6\,\text{MeV}$, as

[11] Note that for repulsive vector interactions, $G_V > 0$, the stationary solution corresponds to a *maximum* of Ω with respect to $\tilde{\mu}$. This phenomenon is well-known, e.g., from the Walecka model [109]. It means that the condition $\delta\Omega/\delta\tilde{\mu} = 0$ must not be viewed as a variational principle, but as a constraint: Values of $\tilde{\mu}$ which do not fulfill this condition are not thermodynamically consistent and should be discarded.

[12] Although one might think that this argument is only valid for thermodynamic consistent points, it applies to Ω at any fixed $M \geqslant \mu$ because $\delta\Omega_{\text{med}}$ does not "know" whether or not M corresponds to a stationary point of the total thermodynamic potential.

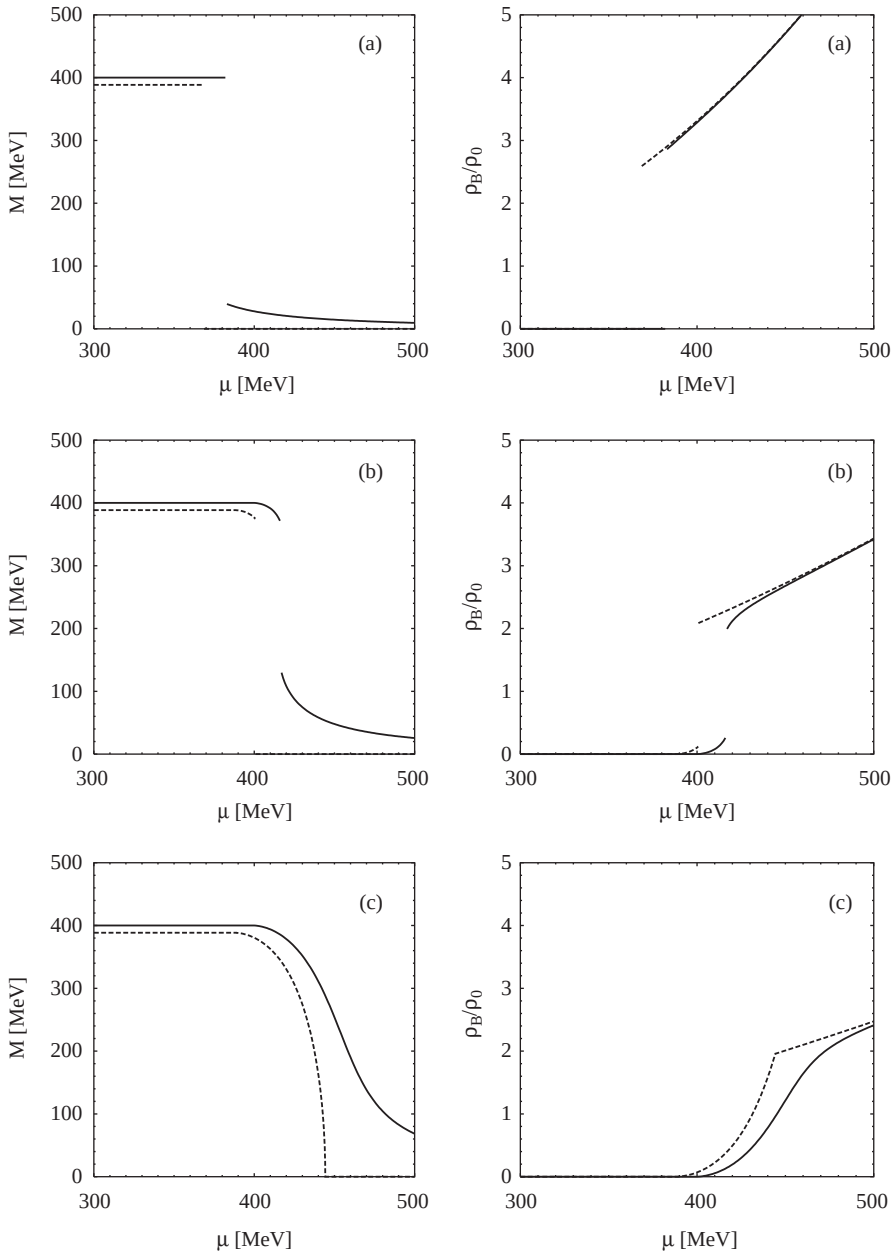

Fig. 2.9. Masses (left) and baryon number densities (right) as functions of the chemical potential μ, illustrating the three types of phase transitions in the NJL model at $T = 0$. The solid lines correspond to parameter set 2 of Table 2.2, the dashed lines to the chiral limit. The vector coupling is $G_V = 0$ (a), $G_V = 0.5G_S$ (b), and $G_V = G_S$ (c).

given in the table. In that case, chiral symmetry gets of course never restored exactly, but the main points discussed below remain the same.

(a) *First-order phase transition at* $\mu_c < M_{vac}$: If the reduction of the thermodynamic potential at low masses grows fast enough with μ, it may happen that the phase transition takes place at a critical potential μ_c which is smaller than the vacuum mass M_{vac} (see left panel of Fig. 2.8 for illustration). Since $\delta\Omega_{med} = 0$ for all $M \geqslant \mu$, this means that in the vicinity of the vacuum minimum, $M = M_{vac}$, the thermodynamic potential has still its vacuum form. In particular, the solution at $M = M_{vac}$ itself still exists and still corresponds to zero density. Thus, if this case is realized, there is a strong first-order phase transition from the vacuum solution $M = M_{vac}$ into the chirally restored phase with $M = 0$ (or $M =$ "small" if we are not in the chiral limit). At the same time the density jumps from zero to a relatively large value. Apart from the vacuum, there is no stable solution with broken chiral symmetry and no other stable solution with a smaller density than the critical one.

(b) *First-order phase transition at* $\mu_c > M_{vac}$: This case is similar to case (a), but with a slower reduction of the thermodynamic potential at low masses, such that the phase transition takes only place at a critical potential $\mu_c > M_{vac}$. This means, there is an interval $M_{vac} < \mu < \mu_c$, where the system is still in the chirally broken phase, but $\delta\Omega_{med}$ is already non-zero at $M = M_{vac}$ and shifts the minimum to lower values and its location to lower masses. Thus, in this interval, the constituent mass goes smoothly down and the density smoothly rises with μ. Eventually, at $\mu = \mu_c$ the phase transition takes place and constituent mass and density show a similar discontinuous behavior as in case (a).

(c) *Second-order phase transition* ($\mu_c > M_{vac}$): Unlike in (a) and (b) it is also possible that $\delta\Omega_{med}$ does not produce an extra minimum at $M = 0$ (in the chiral limit), and the "old" minimum moves all the way down to zero when μ is increased to sufficiently high values (see right panel of Fig. 2.8). As pointed out earlier, in the chiral limit Ω is symmetric in M. Thus below μ_c there are two degenerate minima with opposite sign. At $\mu = \mu_c$ they merge and turn the maximum at $M = 0$ into a minimum. Like in case (b) the constituent mass drops smoothly, beginning at $\mu = M_{vac}$, but this time there is no discontinuity at any higher value of μ. In the chiral limit, the second-order phase transition manifests itself in a discontinuous derivative of the mass and the density as a function of μ. For $m \neq 0$ there is only a cross-over, and all variables vary smoothly.

In principle, one could imagine further scenarios. For instance, there could be a discontinuous jump not directly into the restored phase but to a solution with a finite constituent quark mass, which eventually goes to zero at higher chemical potential. Such a behavior would imply that the thermodynamic potential develops another minimum at finite M which is different from the vacuum one. Inspecting the structure of Ω_{vac} and $\delta\Omega_{med}$, this seems to be difficult to realize although we have not proven it rigorously. In any case, we have not found such solutions. This can be different, however, if we go beyond mean-field approximation. In this context it is interesting that a behavior of the above type has recently been found within a renormalization group analysis of the quark-meson coupling model [113].

It should be reminded that, although the functions $M(\mu)$ and $\rho_B(\mu)$ depend on the vector coupling G_V and are therefore different for the three examples shown in Fig. 2.9, the function $M(\rho_B)$ is G_V-independent, as we have seen earlier. Thus if we plot the masses given in Fig. 2.9 for cases (a)–(c) against the respective densities they all fall on the same lines (one for the chiral limit and one for $m = 5.6\,\text{MeV}$) which agree with the functions plotted in the right panel of Fig. 2.7. However, G_V does influence the *stability* of the solutions. Whereas in case (c) all points shown in Fig. 2.7 are stable solutions, this is not the case for (a) and (b).

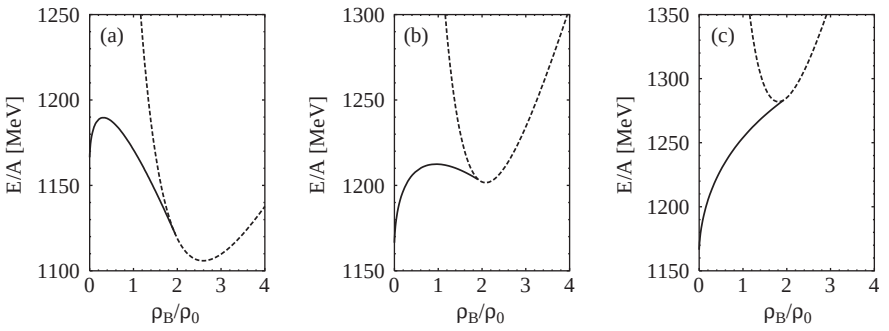

Fig. 2.10. Energy per baryon number for the three cases (a), (b), and (c) as functions of the baryon number density ρ_B. The parameters are the same as in Fig. 2.9 with $m = 0$. The solid lines correspond to the massive solutions of the gap equation, the dashed lines to the massless ones. Similar figures have been shown in Ref. [111] for slightly different parameters.

As demonstrated by the numerical examples, all three cases, (a)–(c), can be realized within the NJL model, depending on the choice of the parameters. However, from a physical point of view it is clear that cases (b) and (c) are unrealistic, because both of them predict the existence of a low-density phase of homogeneously distributed constituent quarks. This reflects the missing confinement of the model and obviously any prediction based on these solutions, like medium modifications of RPA mesons, should be taken with great care.

Case (a) is special, because it does *not* predict a stable quark phase at low density. The first-order phase transition directly from the vacuum phase to quark matter with baryon number density ρ^* implies that any homogeneous quark distribution of density $0 < \rho_B < \rho^*$ is unstable against separation into a mixed phase consisting of quark matter with density ρ^* and vacuum. Hence, instead of a homogeneous quark gas at low densities, in this case the model predicts the existence of quark "droplets" which are self-bound in vacuum [111].

To work this out more clearly, let us discuss the behavior of the energy per baryon,

$$\frac{E}{A} = \frac{\epsilon}{\rho_B} = -\frac{p}{\rho_B} + 3\mu \tag{2.65}$$

as a function of density. In Fig. 2.10 this is displayed for the three previous examples in the chiral limit. The dashed lines correspond to the massless solutions of the gap equation, the solid lines to the massive ones. As we have seen in Fig. 2.7, the latter only exist for densities $\rho_B < 2.0\rho_0$ for these parameters. Note that at fixed density the massive solutions, whenever they exist, are energetically favored.

The basic features of the curves can be understood by inspecting the points of zero pressure:

- The branch of the massive solutions starts with the non-trivial vacuum point which by definition has zero pressure. Approaching this point from above, $\rho_B \to 0^+$, we have $\mu \to M_{\text{vac}}$ while the pressure is proportional to $\rho_B^{5/3}$ [107]. Hence $E/A \to 3M_{\text{vac}}$ in this limit. On the other hand, applying Eq. (2.18), the derivative diverges at this point.
- For the massless solutions the pressure becomes zero at some chemical potential μ_0 corresponding to a non-vanishing density. Hence there is a minimum with $E/A = 3\mu_0$.

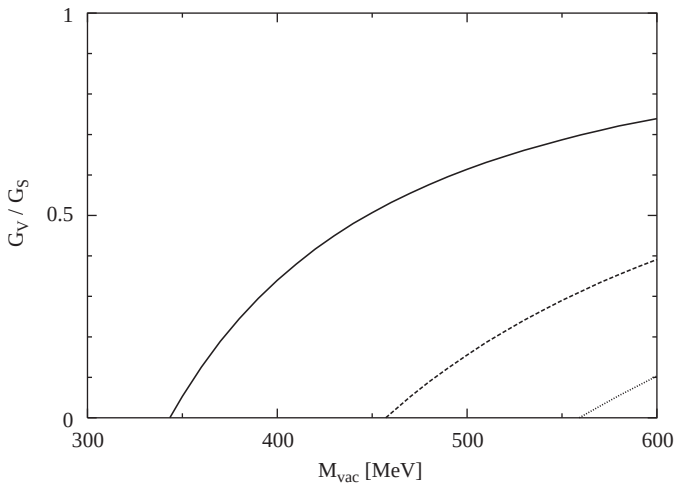

Fig. 2.11. Lines of constant binding energy per quark, E_b, for fixed $f_\pi = 92.4\,\mathrm{MeV}$, $m = 0$, and varying constituent quark masses M_vac and ratios of the vector and scalar coupling constants, G_V/G_S: $E_\mathrm{b} = 0$ (solid), $E_\mathrm{b} = 50\,\mathrm{MeV}$ (dashed), and $E_\mathrm{b} = 100\,\mathrm{MeV}$ (dotted). Adapted with permission from Ref. [112].

In case (a), μ_0 is identical to the critical chemical potential μ_c for the chiral phase transition and is smaller than M_vac. Therefore the minimum is an absolute minimum and corresponds to the state of self-bound quark matter mentioned above.
In cases (b) and (c), $\mu_0 > M_\mathrm{vac}$, and the point of lowest E/A is reached for $\rho_B \to 0$. This means, if not prohibited by external forces, the quark matter favors to become infinitely dilute. This is of course unrealistic.

- In cases (a) and (b), there is a maximum in the thermodynamic potential which separates the massive from the massless minimum (see Fig. 2.8). At some chemical potential μ_1 the pressure of this maximum becomes zero. This leads to a maximum in the massive branch of E/A. As a consequence the minimum of the massless branch corresponds to metastable quark matter in case (b).

It is obvious that the repulsive vector interaction disfavors the existence of bound quark matter and therefore case (a) is only realized for not too large values of G_V. Similarly, the attractive scalar interaction favors the existence of bound quark matter. In turn, if the attraction is too weak, case (a) is not even realized for vanishing G_V. This is illustrated in Fig. 2.11 where lines of constant binding energy per quark, $E_\mathrm{b} = M_\mathrm{vac} - (E/(3A))_\mathrm{min}$ are displayed in the $G_V/G_S - M_\mathrm{vac}$ space. The calculations have been performed in the chiral limit with G_S and Λ chosen to reproduce $f_\pi = 92.4\,\mathrm{MeV}$, see Fig. 2.6.[13] We find that there is no bound matter for $M_\mathrm{vac} \lesssim 343\,\mathrm{MeV}$.

[13] We have ignored that f_π should be somewhat smaller in the chiral limit. Also, from physical arguments it might be reasonable to consider vector–isovector and axial vector–isovector interactions with the same coupling strength G_V as in the vector–isoscalar channel. In this case, the pion decay constant gets modified by the order of 10%. These details, which have not been taken into account in the parameter fixing of Fig. 2.11, should, however, not change the overall picture.

This agrees well with the following simple estimate. For $M = m = 0$ the thermodynamic potential Eq. (2.62) is readily evaluated and one can derive E/A for the massless solutions analytically. One finds

$$\left(\frac{E}{A}\right)_{M=0} = \frac{B}{\rho_B} + \frac{9}{4}\left(\frac{3\pi^2}{2}\,\rho_B\right)^{1/3} + 9G_V\rho_B \ . \tag{2.66}$$

Minimizing this formula with respect to the density one finds for the minimum

$$\left(\frac{E}{A}\right)_{M=0,\min} \simeq 3(2\pi^2 B)^{1/4}\left[1 + 2G_V\left(\frac{2B}{\pi^2}\right)^{1/2}\right] , \tag{2.67}$$

where terms of order G_V^2 have been neglected. To be bound, this should be smaller than $3M_{\rm vac}$. If we use the approximate formula, Eq. (2.61), for the bag constant we find that for $G_V = 0$ this is the case if $M_{\rm vac} \gtrsim 4f_\pi$, in reasonable agreement with our numerical findings. Reinserting this into Eq. (2.61) we find that the minimal bag constant which allows for bound quark matter in the NJL model is given by $B \gtrsim 125\,{\rm MeV/fm}^3$, i.e., about twice the original MIT value [75].

Recently, it has been shown that the stability of NJL quark matter can increase if the matter is exposed to large magnetic fields [114]. In this case, even stable quark droplets consisting of massive quarks are possible. However, these effects require magnetic fields of the order 10^{19} G, which is unlikely to be realized even in magnetars.

We should recall, that we have not yet included diquark condensates, i.e., color superconductivity. In our later analysis, this will be an additional source of attraction which enhances the binding.

2.3.3. Comparison with the bag model

The bound quark matter solutions discussed in the end of the previous section show great similarities with the bag model equation of state. In fact, for $G_V = 0$ Eq. (2.66) is identical to the bag-model relation, Eq. (2.16). This is easily understood: Since Eq. (2.66) describes the energy per baryon number in the chirally restored phase, the quark condensate ϕ is equal to zero. Thus, if $G_V = 0$ the system is not coupled to any mean field, and energy and pressure are those of a free fermion gas, shifted by the bag constant, Eq. (2.60), because the zero-points have been calibrated to the non-trivial vacuum. In other words, the quark matter phase we have described in this way is completely trivial. What is non-trivial, is the vacuum.

For $G_V \neq 0$, the chirally restored phase becomes non-trivial as well. Nevertheless, at least qualitatively the effect of the vector coupling is similar to the perturbative corrections in the bag model, shifting the minimum of E/A to larger values and lower densities. (The quantitative behavior is, however, different: Whereas in Eq. (2.66) the correction term is of the order $G_V\rho_B$, in the bag model it is of the order $\alpha_s\rho_B^{1/3}$, as required by dimensions.)

In spite of the arguments above, the great similarity of the NJL-model and bag-model equations of state might be surprising, since the NJL model does not confine the quarks, whereas the bag model is confining by construction. The resolution is, of course, that Eq. (2.66) is only valid for the massless solutions (the dashed lines in Fig. 2.10). For these solutions, E/A diverges in the limit $\rho_B \to 0$. This could indeed be interpreted as "confinement" in the sense, that for a fixed number of massless quarks an infinite amount of energy would be needed to increase the bag radius to infinity. However, in the NJL model this is not the whole story. Here at low densities the quarks have the possibility to acquire a mass, and for these solutions only a finite amount of energy ($M_{\rm vac}$ times the number of quarks in the "bag") is required in the zero-density limit: Whereas the massless quarks, just like the bag-model quarks, are restricted to the chirally

restored phase, the massive NJL-model quarks are permitted to enter the non-trivial vacuum. Therefore, in the zero-density limit, instead of paying an infinite amount of energy to transform the vacuum, one only needs a finite amount to transform the quarks. Thus, unfortunately, the same mechanism which gives a microscopic explanation of the bag pressure—chiral symmetry breaking—prevents it from confining the quarks in the model.

Away from the chiral limit, the NJL model equation of state always differs from the bag model one. This is because for $m \neq 0$ chiral symmetry gets completely restored only asymptotically.[14] As we have seen in Fig. 2.7, M is a density dependent function which can stay relatively large up to rather high densities. Thus, whereas in a bag model the quarks have just those masses which have been given to them and which are usually identified with the current masses, the quarks in bound NJL matter can have considerably higher masses. For instance, for parameter set 2 and $G_V = 0$ we find bound quark matter with $M = 40\,\mathrm{MeV}$, much larger than the current quark mass $m = 5.6\,\mathrm{MeV}$.

For the discussion it is often useful to introduce an "effective bag constant". One possibility is to write the energy density of the NJL model in the form

$$\epsilon(\rho_B) = \epsilon_{\mathrm{free}}(\rho_B; M(\rho_B)) + B_{\mathrm{eff}}(\rho_B)\ , \tag{2.68}$$

where

$$\epsilon_{\mathrm{free}}(\rho_B; M(\rho_B)) = \frac{N_f N_c}{\pi^2} \int_0^{p_{\mathrm{F}}} \mathrm{d}p\, p^2 \sqrt{p^2 + M^2(\rho_B)} \tag{2.69}$$

is the pressure of a free gas of quarks with mass $M(\rho_B)$ (the density dependent constituent quark mass of the NJL model) at baryon number density $\rho_B = (N_f/3\pi^2)p_{\mathrm{F}}^3$.

B_{eff} as a function of ρ_B is plotted in Fig. 2.12 (solid lines). The calculations have been performed using parameter set 2 of Table 2.2 (right panel) and the corresponding chiral limit (left panel). In both cases the vector coupling has been set equal to zero. The general behavior of the results can be understood as follows: Since $\epsilon = \epsilon_{\mathrm{free}} = 0$ at $\rho_B = 0$, B_{eff} has to vanish at this point. On the other hand, when chiral symmetry is restored, ϵ behaves like ϵ_{free}, but shifted by the bag constant B. Thus, in the chiral limit, B_{eff} rises from zero to B and then stays constant. For $m \neq 0$, B_{eff} behaves similarly, but since there is no complete restoration of chiral symmetry, the curve is smoother and $B_{\mathrm{eff}} = B$ is reached only asymptotically.

In contrast to our results, it is sometimes argued that the bag constant should *decrease* with density, see, e.g., Refs. [117–119]. At first sight, this seems to be natural, because in Eq. (2.60) we defined the bag constant to be the pressure difference between the non-trivial vacuum and the trivial vacuum at $M = m$, which goes away upon chiral restoration. However, the physical meaning of B_{eff} as defined in Eq. (2.68) is different: Here the system is interpreted as a gas of quasi quarks with mass $M(\rho_B)$ in a vacuum with completely or partially restored symmetry. B_{eff} is the energy per volume which is needed for this (partial) restoration. Thus at low densities where only a small step towards symmetry restoration has been done, only a low "price" has to be paid, whereas the total amount of restoration energy, $B_{\mathrm{eff}} = B$, is only due

[14] In the NJL model with sharp 3-momentum cut-off, "asymptotically" means, when the Fermi momentum becomes equal to the cut-off. At this point one gets $\phi = 0$ and $M = m$. However, as we have seen, this only happens at very large densities, well above the phase transition. This is different in the so-called "scaled NJL model" [115]. In this model, the cut-off is taken to be proportional to a dilaton field in order to maintain scale invariance. As a consequence, the cut-off drops discontinuously at first-order phase boundaries. Since it drops easily below the Fermi momentum, this often limits the applicability of the model to the chirally broken phase [116].

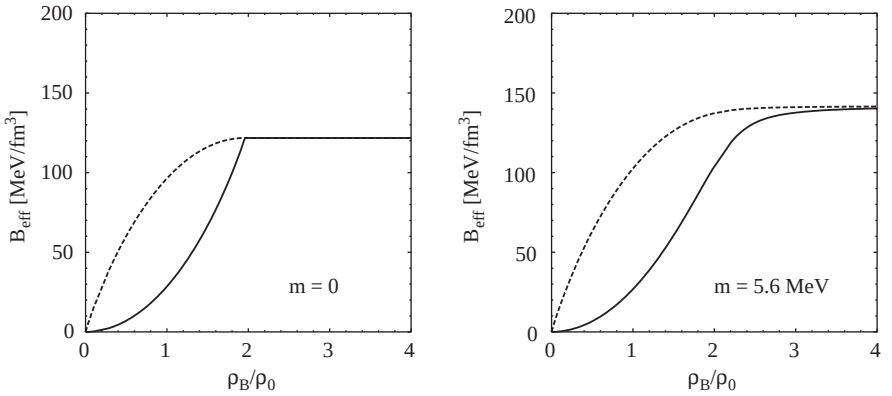

Fig. 2.12. Effective bag constants $B_{\rm eff}$ (Eq. (2.68), solid lines) and $B'_{\rm eff}$ (Eq. (2.70), dashed lines) as functions of the baryon number density ρ_B. Right: Parameters of set 2 of Table 2.2 and $G_V = 0$. Left: The same, but in the chiral limit.

at high densities. Of course, from a practical point of view, it still could make sense to use effective bag constants which decrease with density in order to parametrize missing physics, like short-range repulsion or excluded volume effects on the hadronic side. However, the naive argument that generalized bag models with decreasing bag constants are more physical because this accounts for chiral symmetry restoration is not correct.

In the above discussion we have identified two sources for the deviation of the NJL model equation of state from the bag model one: the density-dependent quark masses and the density-dependent effective bag constant. To see the net effect, we could alternatively start from a free gas of current quarks and attribute the entire interaction effects to the effective bag constant,

$$\epsilon(\rho_B) = \epsilon_{\rm free}(\rho_B; m) + B'_{\rm eff}(\rho_B) \ . \tag{2.70}$$

$B'_{\rm eff}$ is also displayed in Fig. 2.12 (dashed lines). Again, at zero density, ϵ and $\epsilon_{\rm free}$ vanish, and therefore $B'_{\rm eff}$ vanishes as well. On the other hand, at high densities, $M \to m$ and therefore $B_{\rm eff} \to B'_{\rm eff} \to B$. Between these two extremes, $B_{\rm eff}$ and $B'_{\rm eff}$ can differ considerably. As one can see in the figure, $B'_{\rm eff}$ stays longer close to the asymptotic value B than $B_{\rm eff}$ does. This means, the approximation of the NJL energy density by a bag model one with constant mass m and bag constant B works better than one would naively expect if one looks at M and $B_{\rm eff}$ as functions of the density.

In some models, density dependent bag constants are introduced *by hand* using some ad hoc parametrization, e.g., [117,118]. In these cases one has to be careful not to violate thermodynamic consistency. For instance, if we start from Eq. (2.70), there is an extra contribution to the chemical potential $\mu_B = \partial\epsilon/\partial\rho_B$ due to the density dependence of the bag constant and hence the pressure is *not* given by the bag model expression. This problem will not affect us, because we will never use effective bag constants to calculate other quantities, but only in order to interprete the results (which are consistently derived from the thermodynamic potential). Related to the above problem, there is of course some arbitrariness in the definition of $B_{\rm eff}$. For instance, we could have started from the bag model expression for the pressure, instead of the energy density. The results would be somewhat different, but the qualitative features of Fig. 2.12 would change only little.

Because of the great similarities between NJL model and bag model equations off state, it is tempting to identify the bound-matter solutions of the NJL model with baryons, at least in a very schematic sense [10,111]. In the previous section we pointed out that scenarios (b) and (c) for the chiral phase transition are unrealistic because they predict the existence of a homogeneous gas of constituent quarks at low densities. This contradicts confinement. This problem does not arise in case (a) where the dilute-gas solutions are unstable against phase separation, leading to droplets of dense quark matter in the chirally restored phase surrounded by vacuum. Clearly, at least for two flavors, this scenario would be unrealistic as well, unless we adopt the above interpretation of these droplets as baryons.

Therefore let us neglect for a while that we have solved a thermodynamic problem for infinite homogeneous mean fields and assume that the solutions can be extrapolated down to three quarks in a sphere of radius R. Taking the bound-matter solution of parameter set 2 with baryon number density $\rho^* = 2.8\rho_0$ we obtain a reasonable bag radius $R = (4\pi\rho_B/3)^{-1/3} = 0.8\,\text{fm}$. (For parameter set 4, we find $\rho^* = 5.8\rho_0$ corresponding to $R = 0.6\,\text{fm}$.) We may also calculate the $\bar{q}q$-content of the bag, which is defined as the difference of the quark condensate in the bag and in the vacuum, integrated over the bag volume,

$$\langle \text{bag}|\bar{q}q|\text{bag}\rangle = \frac{1}{\rho^*}\left(\phi|_{\rho_B=\rho^*} - \phi|_{\rho_B=0}\right) . \tag{2.71}$$

For parameter set 2 we find $\langle \text{bag}|\bar{q}q|\text{bag}\rangle \simeq 7$. This corresponds to a "sigma term" $\sigma_{\pi,\text{bag}} = m\langle \text{bag}|\bar{q}q|\text{bag}\rangle \simeq 39\,\text{MeV}$, not too far away from the most commonly quoted value $\sigma_{\pi N} \simeq 45\,\text{MeV}$, extracted from πN scattering data [120].[15] For parameter set 4 we find lower values, $\langle \text{bag}|\bar{q}q|\text{bag}\rangle \simeq 4$ and $\sigma_{\pi,\text{bag}} \simeq 20\,\text{MeV}$, mostly because of the smaller bag volume. On the other hand, if we include vector interactions, the density of the bound quark matter becomes smaller and, consequently, the bag radii, $\langle \text{bag}|\bar{q}q|\text{bag}\rangle$, and $\sigma_{\pi,\text{bag}}$ get larger.

Our method to determine a sigma term within the NJL model is rather different from that of Ref. [122]. In that reference a pion–quark sigma term, $\sigma_{\pi q}$ was extracted from the constituent quark masses in vacuum via the Feynman–Hellmann theorem. The authors could show that $\sigma_{\pi q}$ governs the low-density behavior of $\langle \bar{q}q\rangle$ in the NJL model in the same way as $\sigma_{\pi N}$ in chiral perturbation theory, Eq. (1.6). Identifying $\sigma_{\pi N} = 3\sigma_{\pi q}$ they obtained $\sigma_{\pi N} = 32\,\text{MeV}$. Although this is a reasonable number, the description of low-density nuclear matter by a low-density quark gas remains questionable. Comparison with our method might shed some light on this puzzle: Whereas in Ref. [122] the sigma term is proportional to the derivative of the quark condensate at $\rho_B = 0$, the value obtained from Eq. (2.71) is proportional to the slope of a straight line connecting $\langle \bar{q}q\rangle$ at $\rho_B = 0$ with $\langle \bar{q}q\rangle$ at $\rho_B = \rho^*$. Although this is not exactly the same, both numbers are quite similar, as one can see, e.g., from the density dependence of the constituent quark mass shown in Fig. 2.7 (Connect the points at $\rho_B = 0$ and $\rho^* = 2.8\rho_0$ on the solid line of the right panel by a straight line and compare the slope with the slope of the solid line at$\rho_B = 0$.). Thus, if we believe that our method gives the correct value of the sigma term, the method of Ref. [122] should also work rather well.

On the other hand, it is clear that our identification of the "droplets" of bound quark matter in the NJL model with baryons, i.e., our extrapolation from homogeneous infinite matter to three-quark system is too simplistic. Obviously, a realistic modeling of baryons requires to start from three valence quarks and to abandon the simplification of space-independent mean fields. In fact, much better jobs in this direction have already been done, describing baryons as chiral quark solitons [72,123,124] or solving a Fadeev equation for three constituent quarks [125,126]. Of course, even these approaches cannot explain why

[15] Note, however, that much larger values are found in some more recent analyses [121].

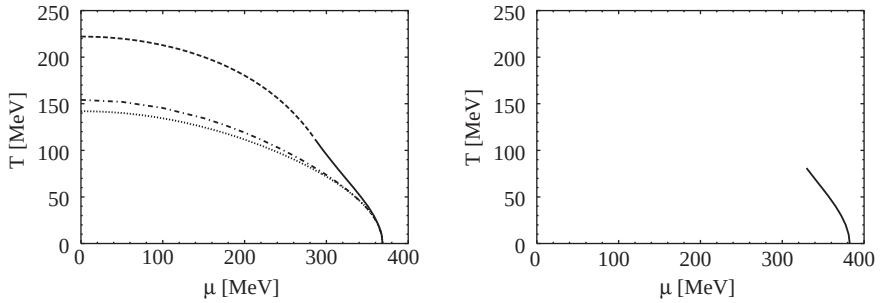

Fig. 2.13. NJL phase diagram for parameter set 2 and $G_V = 0$. Left: Phase diagram in the chiral limit. The first and second order phase boundaries are indicated by the solid or dashed line, respectively. The dash–dotted line indicates the location of massless solutions with vanishing pressure. The dotted line corresponds to the zero-pressure line in a bag model with the same bag constant and quark degrees of freedom only. Right: Phase diagram for $m = 5.6\,\mathrm{MeV}$.

three-quark systems are favored against larger multi-quark clusters, or, in other words, why nuclei consist of nucleons instead of being a single large bag. This would require a better understanding of confinement and the inclusion of repulsive short-range interactions which prevent the three-quark bags from merging.

Anyway, it is obvious that a realistic description of nuclei or nuclear matter with quark degrees of freedom is not possible within mean-field approximation. The bound quark-matter solutions of the NJL model describe at most some fictitious state of matter, which one would find if the bag pressure was the only relevant binding force. Once confining forces and residual interactions beyond a homogeneous mean field are taken into account, the quark-matter solutions become unstable and decay into baryonic matter. In this context it is remarkable that all bound quark-matter solutions we have found above have $E/A \gtrsim 3 \times 343\,\mathrm{MeV}$, i.e., at least 90 MeV above the nucleon mass.

As long as these mechanisms are not understood, the best way to describe hadronic matter is to start from phenomenological hadronic interactions. Eventually, at higher densities, homogeneous quark matter should become favored. Thus, a more pragmatic procedure would be to employ the NJL model only at high densities and to use a hadronic equation of state for the hadronic phase. This will be done in Chapter 7 where we investigate the structure of compact stars. On the other hand, for more schematic discussions of the phase diagram it is often more appealing to have a single model for all phases. An NJL mean-field description of the hadronic phase could then be acceptable, if one stays aware of the limitations of the model. Particular caution is in order at finite temperature, where effects of unconfined quarks in the "hadronic phase" are unavoidable. This will briefly be discussed in the next section.

2.3.4. Phase diagram

Applying the formalism developed in Section 2.3.1, it is straightforward to extend our numerical studies to non-vanishing temperatures and to investigate the chiral phase diagram in the T–μ plane. This has first been done by Asakawa and Yazaki [59], followed by many others.

A typical phase diagram obtained in this way is shown in Fig. 2.13. The calculations have been performed with parameter set 2 of Table 2.2 and $G_V = 0$. The phase diagram in the left panel corresponds to the chiral limit, $m = 0$. First and second-order phase boundaries are indicated by a solid or dashed line, respectively. We know already that for the present parameters the phase transition is first order at $T = 0$. On the other hand, along the T-axis, i.e., at $\mu = 0$, the phase transition is second order. Hence, as

argued in the Introduction, there must be a tricritical point at some intermediate temperature, where the first-order phase boundary turns into a second-order one. In the present example, this point is located at $\mu = 286\,\mathrm{MeV}$ and $T = 112\,\mathrm{MeV}$.

With finite quark masses, chiral symmetry is never restored exactly. Therefore, at high temperatures and low chemical potentials, instead of second-order phase transitions, we only have smooth cross-overs where the quark condensate gets rapidly (but continuously) reduced. In this case, the first-order phase boundary ends in a second-order endpoint. This is shown in the right panel of Fig. 2.13. For the position of the endpoint we find $\mu = 330\,\mathrm{MeV}$ and $T = 81\,\mathrm{MeV}$.

At first sight, Fig. 2.13 seems to be in qualitative agreement with common wisdom about the QCD phase diagram for two light or massless flavors. A closer inspection, however, reveals severe problems. Being a mean-field calculation, the phase transition is driven by quark and antiquark degrees of freedom. In particular the "hadronic phase", i.e., the phase with broken chiral symmetry is described as a gas of constituent quarks, instead of mesons and baryons. The only exception is the μ-axis at $T = 0$. There, as discussed in Section 2.3.2, we have a phase transition of "type (a)", i.e., the "hadronic phase" is identical to the vacuum. This scenario does no longer exist at finite temperature where the occupation numbers n_p and $\bar{n}_p$ are always non-zero. This underlines the difference between bound and confined quark matter: The finite binding energy for the self-bound solutions at $T = 0$ cannot prevent the evaporation of constituent quarks at arbitrary small (but non-zero) temperatures.

It is therefore not surprising that the NJL model results are at variance with several aspects of the QCD phase diagram which we have discussed in the Introduction:

- Without major modifications (like introducing temperature-dependent coupling constants) the NJL model gives a rather poor description of the lattice results at $\mu = 0$. In particular the critical temperature is typically too large.
- The curvature of the phase boundary at $\mu = 0$ is also larger than the lattice result [50], $T_c(\mathrm{d}^2 T_c/\mathrm{d}\mu^2)|_{\mu=0} = -0.14 \pm 0.06$. We find -0.40 in the chiral limit and about the same number for $m = 5.6\,\mathrm{MeV}$ if we define the cross-over line by the inflection points $\partial^2 M/\partial T^2 = 0$.
- The temperature of the critical endpoint is considerably smaller and the chemical potential is larger than for the lattice point of Fodor and Katz [54] who find $T = (162 \pm 2)\,\mathrm{MeV}$ and $\mu_B = (360 \pm 40)\,\mathrm{MeV}$, i.e., $\mu \simeq 120\,\mathrm{MeV}$.
- In a mean-field calculation, one finds of course mean-field critical exponents, rather than $O(4)$.
- At $\mu = 0$ and low temperature, the model is not in agreement with chiral perturbation theory, because the pionic degrees of freedom are not taken into account in mean-field approximation. This will be discussed in more details in Section 2.3.5.

Of course, the value of the critical temperature at $\mu = 0$ depends on the parameters. For parameter set 2 (in the chiral limit) we find $T_c = 222\,\mathrm{MeV}$, as we have already seen in Fig. 2.7. If we take parameter set 1 we get a more reasonable value, $T_c = 177\,\mathrm{MeV}$, but at the same time μ_c at $T = 0$ becomes unrealistically small: We find $\mu_c = 305\,\mathrm{MeV}$, i.e., the baryon chemical potential $\mu_B = 915\,\mathrm{MeV}$ is less than the nuclear matter value. Note that the large ratio between T_c at $\mu = 0$ and μ_c at $T = 0$ gives also a natural explanation for the too large curvature of the phase boundary, since on average the boundary must be steeper than for smaller ratios.

To shed some light on the possible sources of this behavior, we compare the NJL phase boundary with the line of zero pressure in a bag model with quark degrees of freedom only and the same bag constant

(left panel of Fig. 2.13, dotted line). Basically, this line corresponds to the dotted line in Fig. 2.1. At $T = 0$, as discussed in Section 2.3.3, both models agree. However, at small chemical potentials, i.e., at relatively high temperatures, the two lines become quite different. To some extent, this is due to the regularization which cuts off the high momenta in the NJL-model calculation. Therefore the pressure of the massless solutions is somewhat smaller than in the bag model and the line of zero pressure is shifted to higher temperatures (dash–dotted line). The remaining difference to the dashed or solid line must then be attributed to the presence of unconfined constituent quarks in the chirally broken phase which add to the pressure in that phase and thereby shift T_c to higher values. Also note that the bag-model T_c becomes further reduced if gluons are included (see Fig. 2.1).

This comparison suggests that the large critical temperatures in the NJL model at small chemical potentials are mainly due to unphysical effects, namely cut-off effects, missing gluonic degrees of freedom in the "QGP phase", and unconfined quarks in the "hadronic phase". Although the latter might partially account for the effect of the missing hadronic degrees of freedom, it is clear that quantitative predictions of the model, e.g., about the position of the critical endpoint, should not be trusted. We should also recall that the introduction of a repulsive vector interaction in the NJL model weakens—and finally removes—the first-order phase transition. We could thus move the endpoint to even lower temperatures until it vanishes completely. Therefore, any agreement of NJL and lattice results in this point would be accidental.

Before closing these critical reflections, we should note that the flaws listed above are rather general consequences of missing confinement, together with the mean-field treatment and are not restricted to NJL-type models. As pointed out before, it is quite obvious that, starting from quark degrees of freedom, one cannot get a realistic picture of the hadronic phase in mean-field approximation, no matter how sophisticated the interaction.

2.3.5. $1/N_c$ corrections

As an example for the shortcomings of the mean-field approximation and in order to illustrate how these problems are (partially) removed beyond mean field, we briefly discuss the temperature dependence of the quark condensate within a $1/N_c$ expansion scheme. More detailed discussions about the use of this scheme and other methods beyond mean field in the NJL model can be found in Refs. [127,128] and references therein.

According to chiral perturbation theory, the low-temperature and density behavior of the quark condensate in the chiral limit is given by Eq. (1.6). Hence, to leading order in T and at zero density, the change of the condensate should be proportional to $T^2/(8f_\pi^2)$. As mentioned in the Introduction, this can be attributed to the thermal excitation of massless pions. This is at variance with the NJL mean field, where the heat bath consists entirely of constituent quarks and antiquarks. However, since these are exponentially suppressed because of their mass, the quark condensate changes only very little at low temperatures [72,122]. This can be seen in Fig. 2.15 where $\langle\bar{q}q\rangle$, normalized to its value at $T=0$, is plotted as a function of temperature. The calculations have been performed in the chiral limit. The mean-field result is indicated by the dashed lines.[16]

[16] Fig. 2.15 is based on the results of Refs. [127,128] where the quark loops have been regularized using the Pauli-Villars scheme. However, this is an irrelevant detail for the present discussion. For a sharp $O(3)$ cut-off, the mean-field behavior is readily read off in Fig. 2.7 since in the chiral limit the mean-field quark condensate is directly proportional to the constituent quark mass, see Eq. (2.44).

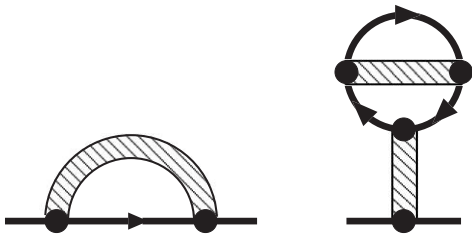

Fig. 2.14. Correction terms of order $1/N_c$ to the quark self-energy. The solid lines and shaded boxes symbolize quark propagators and RPA meson propagators, respectively.

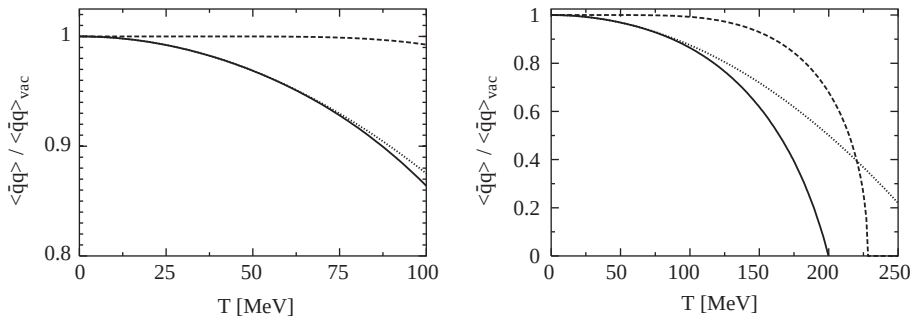

Fig. 2.15. Quark condensate in the chiral limit, normalized to its vacuum value, as a function of temperature: Hartree approximation (dashed line) and with $1/N_c$ corrections included (solid). The dotted line indicates a temperature expansion of the $1/N_c$ corrected result up to order T^2 (see Eq. (2.72)). The right figure has been adapted from Ref. [127]. The left figure is just an enlarged detail of the right one.

A method to include the effect of thermal pions in a systematic (and symmetry conserving) way, is an expansion in powers of the inverse number of colors, $1/N_c$. To that end, one assigns a factor $1/N_c$ to the NJL coupling constants. Since the closed quark loops yield a factor N_c, the quark propagator in Hartree approximation (Fig. 2.3) is of the order unity, while the exchange of an RPA meson (Fig. 2.4) is of the order $1/N_c$. Similarly, the quark condensate is of the order N_c and f_π is of the order $\sqrt{N_c}$.

Following these rules, one can construct two self-energy diagrams which contribute to the order $1/N_c$ to the quark propagator. They are shown in Fig. 2.14. Note that, unlike the Hartree term, these self-energy contributions must not be iterated, as this would be of higher order. The $1/N_c$ corrected quark condensate is then obtained as an integral over the trace of the $1/N_c$ corrected quark propagator, just as in Eq. (2.24).

The result is indicated by the solid lines in Fig. 2.15. Because of the meson loops, the $1/N_c$ correction terms are sensitive to thermally excited pions and therefore indeed cause a T^2-behavior at small temperatures. A careful examination of the corresponding diagrams yields [127,128]

$$\langle\bar{q}q\rangle(T) = \langle\bar{q}q\rangle_{\rm vac} - \langle\bar{q}q\rangle^{(0)}_{\rm vac}\frac{T^2}{8f_\pi^{(0)2}} + \cdots\ , \tag{2.72}$$

where the suffix (0) indicates quantities in leading order in $1/N_c$. Since $f_\pi^{(0)2}$ is of the order $1/N_c$, Eq. (2.72) corresponds to a consistent expansion of the χPT result, Eq. (1.6), at zero density to next-to-

leading order in $1/N_c$. To illustrate the quality of this expansion, the r.h.s. of Eq. (2.72) is also displayed in Fig. 2.15 (dotted lines). As one can see, the agreement with the solid line is excellent for $T \lesssim 80\,\mathrm{MeV}$.

In spite of its successes, the $1/N_c$-expansion scheme has also its limitations. First, it should be noted that the magnitude of the $1/N_c$-correction terms is not uniquely determined by the leading-order parameters. Instead, since the NJL model is non-renormalizable, new parameters appear at each order. In the model described above, the meson loops have been regularized by an independent cut-off parameter which has been fixed by fitting the width of the ρ meson [129].

For our purposes, the most severe problem is the fact that it is a perturbative scheme (as pointed out before, the diagrams shown in Fig. 2.14 must not be iterated) and therefore, it cannot be applied to the phase transition. A non-perturbative, but still symmetry conserving extension of the NJL model beyond mean field—the so-called meson-loop expansion (MLA)—has been developed in Refs. [130,131]. Within this scheme one also finds the correct low-temperature behavior of the quark condensate [127,128,132] and it is possible to construct a phase transition. Unfortunately, the latter turns out to be first order [127,128,132], which is likely to be an artifact of the approximation scheme.

We should also note that, while we have added the relevant degrees of freedom for low-temperature physics, we still need to include nucleons for a correct description of the low-density regime. Staying within the NJL model this means that one first has to solve a Fadeev equation. Work in this direction has been performed in Refs. [133,134].

Finally there remains the problem that the unphysical degrees of freedom—quarks and antiquarks—are not removed from the hadronic phase. Because of the relatively large constituent mass, they are suppressed at low temperatures, but since they have a large degeneracy factor, they become dominant at higher T. In Fig. 2.15 this is the case above $\simeq 100\,\mathrm{MeV}$.

2.4. Asymmetric matter

So far we have restricted our analysis to the case of a uniform chemical potential which is the same for up and down quarks. Together with the isospin symmetry in the Lagrangian, i.e., the assumption $m_u = m_d \equiv m$, this implies that all quantities related to up and down quarks, in particular constituent masses, quark condensates, and densities, are equal for both flavors. However, there are many situations in nature, where the numbers of up and down quarks are not equal. Neutron stars, for instance, must be electrically neutral to a very high degree. Therefore, if the core of a neutron star consists of deconfined up and down quarks, the number of down quarks must be about twice as large as the number of up quarks to ensure neutrality. (There are also electrons, but as we will see later on, in chemical equilibrium their fraction is very small.) Similarly, all heavy nuclei have an excess of neutrons over protons, which translates into an excess of down quarks over up quarks. Thus, if a quark–gluon plasma is formed in the collision of two neutron-rich nuclei, one would expect that it contains more down quarks than up quarks.

In order to describe these situations properly, we have to allow for different chemical potentials, μ_u and μ_d, for up and down quarks, respectively,

$$\mu_u = \mu + \delta\mu, \quad \mu_d = \mu - \delta\mu\ . \tag{2.73}$$

As before, $\mu = \mu_B/3$ is the chemical potential related to the total quark number density $n = n_u + n_d$. $\delta\mu$ is related to $n_u - n_d$ and in this way to the isospin density.[17]

[17] The isospin density is defined as $n_I = \frac{1}{2}(n_u - n_d)$. This implies $\mu_I = 2\delta\mu$.

The introduction of a new chemical potential adds a new axis to the phase diagram of strong interactions. Although most theoretical works describe the "standard" μ–T phase diagram with $\delta\mu = 0$, some authors have also studied other projections. For instance the case $\mu = 0$ but $\delta\mu \neq 0$ [135] is particularly interesting since it can be studied on the lattice [136]. On the other hand, for the application to neutron star interiors one can often neglect temperature effects, whereas $\mu \neq 0$ and $\delta\mu \neq 0$. This case (extended to three flavors) will be one of the main tasks of the present work.

In this section, however, we want to discuss the effect of a non-vanishing, but constant $\delta\mu$ on the structure of the μ–T phase diagram, which might be the most interesting case for the interpretation of heavy-ion collisions, although the isospin chemical potential is not strictly constant along the trajectory of the process. This case has been studied within a random matrix model [137] and within an NJL-type model [138]. The authors of these references reported the interesting result that, instead one, they found two first-order phase transitions at low temperature and high baryon chemical potential and thus two second-order endpoints. More recently, this result has been confirmed by further studies within the NJL model [139] and within a QCD-like model ("ladder QCD") [140]. Since second-order endpoints, as discussed in the Introduction, are potentially detectable in heavy-ion collisions [60,61], this could have important consequences.

In the references above an interaction was chosen, where the up and down quarks completely decouple, i.e., the presence of up quarks has no influence on the down quarks and vice versa. From this point of view, the fact that there are two phase transitions—one for up quarks and one for down quarks—is almost trivial. It is known, however, that instanton-induced interactions, like Eq. (2.21), mix different flavors. One can therefore ask, whether the existence of two phase boundaries persist, when instanton-type interactions are present, together with non-flavor mixing interactions. This has been investigated in Ref. [141], which we discuss in the following.

Starting point is the Lagrangian

$$\mathscr{L} = \mathscr{L}_0 + \mathscr{L}_1 + \mathscr{L}_2 \ , \tag{2.74}$$

which contains a free part

$$\mathscr{L}_0 = \bar{q}(\mathrm{i}\partial\!\!\!/ - m)q \ , \tag{2.75}$$

and two different interaction parts [70,59],

$$\mathscr{L}_1 = G_1\{(\bar{q}q)^2 + (\bar{q}\vec{\tau}q)^2 + (\bar{q}\,\mathrm{i}\gamma_5 q)^2 + (\bar{q}\,\mathrm{i}\gamma_5\vec{\tau}q)^2\} \tag{2.76}$$

and

$$\mathscr{L}_2 = G_2\{(\bar{q}q)^2 - (\bar{q}\vec{\tau}q)^2 - (\bar{q}\,\mathrm{i}\gamma_5 q)^2 + (\bar{q}\,\mathrm{i}\gamma_5\vec{\tau}q)^2\} \ . \tag{2.77}$$

$\mathscr{L}_2$ is identical to the instanton-induced ("'t Hooft") interaction $\mathscr{L}_{\text{inst}}$, Eq. (2.21), whereas the standard NJL Lagrangian, Eq. (2.20), is recovered when we choose $G_1 = G_2 = G/2$. Both terms are invariant under $SU(2)_L \times SU(2)_R \times U(1)$ transformations. $\mathscr{L}_1$ exhibits an additional $U_A(1)$ symmetry which is explicitly broken by $\mathscr{L}_2$.

To obtain the mean-field thermodynamic potential $\Omega(T, \mu, \delta\mu)$ we can basically apply the same techniques as before. Since isospin symmetry is broken by a non-vanishing $\delta\mu$, we assume the existence of two generally different quark condensates

$$\phi_u = \langle\bar{u}u\rangle \quad \text{and} \quad \phi_d = \langle\bar{d}d\rangle \ , \tag{2.78}$$

and linearize the Lagrangian in the presence of these condensates. In principle, we should also allow for non-vanishing expectation values with pionic quantum numbers, $\pi_a = \langle \bar{q} \mathrm{i}\gamma_5 \tau_a q \rangle$, to describe a possible pion condensation. Indeed, for $\mu = 0$, it can be shown that these condensates become non-zero if $\mu_I = 2|\delta\mu|$ exceeds the pion mass [142,135]. However, as we will see below, for our present purpose it is sufficient to restrict the model to lower values of $|\delta\mu|$ and we can safely assume $\pi_a = 0$. In this way we get

$$\Omega(T, \mu_u, \mu_d; \phi_u, \phi_d) = \sum_{f=u,d} \Omega_{M_f}(T, \mu_f) + 2G_1(\phi_u^2 + \phi_d^2) + 4G_2\phi_u\phi_d \ , \tag{2.79}$$

where $\Omega_{M_f}(T, \mu_f)$ corresponds to the contribution of a gas of quasiparticles of flavor f,

$$\begin{aligned}\Omega_{M_f}(T, \mu_f) = &-2N_c \int \frac{\mathrm{d}^3 p}{(2\pi)^3} \left\{ E_{p,f} + T \ln\left(1 + \exp\left(-\frac{1}{T}(E_{p,f} - \mu_f)\right)\right)\right. \\ &\left. + T \ln\left(1 + \exp\left(-\frac{1}{T}(E_{p,f} + \mu_f)\right)\right)\right\} \ . \end{aligned} \tag{2.80}$$

The constituent quark masses are now given by

$$M_i = m_i - 4G_1\phi_i - 4G_2\phi_j, \quad i \neq j \in \{u, d\} \ , \tag{2.81}$$

i.e., in general $M_u \neq M_d$. In order to determine the physical solutions, we have again to look for the stationary points of the thermodynamic potential, this time with respect to the two condensates ϕ_u and ϕ_d. This leads to the standard expression for the quark condensates

$$\phi_f = -2N_c \int \frac{\mathrm{d}^3 p}{(2\pi)^3} \frac{M_f}{E_{p,f}} \{1 - n_{p,f}(T, \mu_f) - \bar{n}_{p,f}(T, \mu_f)\} \ . \tag{2.82}$$

When these are inserted into Eq. (2.81), we obtain a set of two coupled gap equations for M_u and M_d which have to be solved self-consistently.

Note that the condensate ϕ_f only depends on the constituent mass M_f of the same flavor, whereas the constituent mass for one flavor depends in general on both condensates, and therefore the two flavors are coupled. If we switch off the "instanton part" $\mathscr{L}_2$, i.e., $G_2 = 0$, the two flavors decouple. In this case M_i depends only on the condensate of the same flavor ϕ_i and the mixed contribution to Ω (last term of Eq. (2.79)) vanishes. This limit corresponds basically to the case studied in Ref. [138]. In the opposite limit, i.e., $G_1 = 0$, we have "maximal" mixing: The constituent mass of flavor i only depends on the condensate ϕ_j with $i \neq j$. It is also interesting that for $G_1 = G_2$, i.e., for the original NJL Lagrangian Eq. (2.20) we always get $M_u = M_d$, even for large $\delta\mu$.

To study the effects of flavor mixing, let us now write

$$G_1 = (1 - \alpha)G_0, \quad G_2 = \alpha G_0 \tag{2.83}$$

and calculate the phase diagram for fixed G_0 but different values of α. The degree of flavor mixing is thereby controlled by the particular value of α while the values of the vacuum constituent quark masses M_{vac} are kept constant.

For our numerical studies we use the parameters $m_u = m_d = 6\,\mathrm{MeV}$, $\Lambda = 590\,\mathrm{MeV}$, and $G_0\Lambda^2 = 2.435$ [141]. They are close to set 2 of Table 2.2 and yield $M_{\mathrm{vac}} = 400\,\mathrm{MeV}$, $m_\pi = 140.2\,\mathrm{MeV}$, $f_\pi = 92.6\,\mathrm{MeV}$ and $\langle \bar{u}u \rangle = (-241.5\,\mathrm{MeV})^3$.

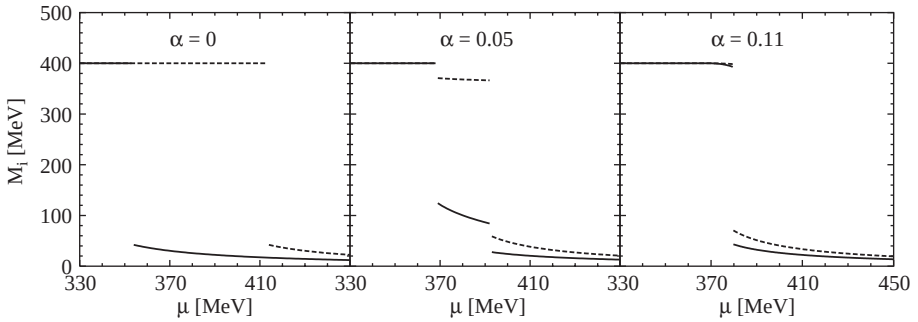

Fig. 2.16. Constituent quark masses M_u (solid) and M_d (dashed) at $T = 0$ as functions of quark number chemical potential μ for $\delta\mu = 30\,\text{MeV}$ and $\alpha = 0$ (left), $\alpha = 0.05$ (center), and $\alpha = 0.11$ (right). Reprinted with permission from Ref. [141].

We begin our discussion with the results at $T = 0$. In Fig. 2.16 we display the values of M_u and M_d as functions of the quark number chemical potential μ for fixed $\delta\mu = 30\,\text{MeV}$.[18] The left panel corresponds to $\alpha = 0$. We observe two distinct phase transitions at $\mu = 353\,\text{MeV}$ for the up quarks and at $\mu = 413\,\text{MeV}$ for the down quarks. This behavior is easily understood when we recall that at $\alpha = 0$ the up and down quark contributions to the thermodynamic potential decouple. Hence, if we had plotted M_u and M_d, in terms of the corresponding *flavor* chemical potential μ_u and μ_d, respectively, we would have found two identical functions with a phase transition at $\mu_f = 383\,\text{MeV}$. This is basically the result reported in Refs. [137,138].

Now we study the influence of a non-vanishing flavor mixing. In the central panel of Fig. 2.16 we show the behavior of the constituent quark masses for $\alpha = 0.05$. The situation remains qualitatively unchanged, i.e., we still find two distinct phase transitions. However, because M_d now also depends on ϕ_u (and thus on M_u), and vice versa, both constituent masses drop at both critical chemical potentials. Moreover, this small amount of flavor mixing already diminishes the difference between the two critical quark number chemical potentials considerably. Finally, for α larger than a critical value of 0.104 we find only one *single* first-order phase transition. This is illustrated in the right panel of Fig. 2.16, which corresponds to $\alpha = 0.11$.

Next, we extend our analysis to non-vanishing temperature. The phase diagrams in the μ–T plane for fixed $\delta\mu = 30\,\text{MeV}$ and three different values of α are shown in Fig. 2.17. At $\alpha = 0$ (left panel) we qualitatively reproduce the results reported in Refs. [137,138], i.e., two separate first-order phase boundaries which end in two second-order endpoints. Again, since for $\alpha = 0$ the up and down quarks decouple, we would obtain two identical phase diagrams if we plotted the phase structure of flavor f in the μ_f–T plane. In the central panel of Fig. 2.17 we consider $\alpha = 0.11$, i.e., slightly larger than the critical value $\alpha^c(T = 0) = 0.104$ for a single phase transition at $T = 0$. Accordingly, there is only one phase boundary at low temperatures. However, at $T = 25\,\text{MeV}$ it splits into two lines which end at two different second-order endpoints. The two branches are very close to each other though, and already at $\alpha = 0.12$ we find only one phase boundary with a single endpoint. This is illustrated by the diagram on the right, which corresponds to $\alpha = 0.15$.

[18] Following common practice (e.g., Refs. [138,143,144]) we take a positive value of $\delta\mu$, although for the description of heavy-ion collisions $\delta\mu < 0$ would be more appropriate. However, since changing the sign of $\delta\mu$ does only interchange the roles of up and down quarks, this does not alter our conclusions.

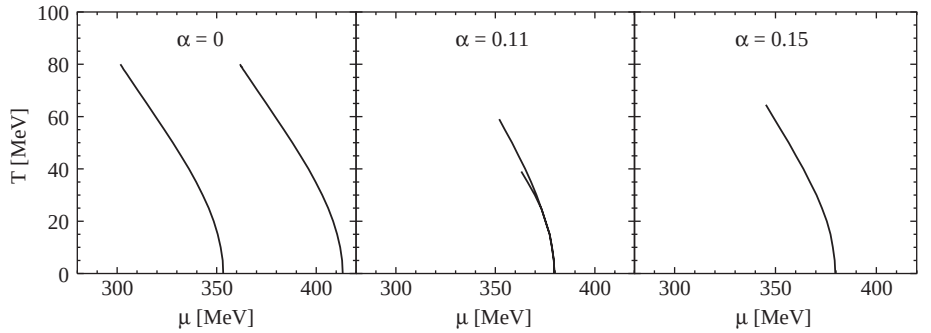

Fig. 2.17. Phase diagrams in the μ–T plane for $\delta\mu = 30\,\mathrm{MeV}$ and $\alpha = 0$ (left), $\alpha = 0.11$ (center), and $\alpha = 0.15$ (right). The lines correspond to first-order phase boundaries which end in second-order endpoints. Reprinted with permission from Ref. [141].

In our example a rather small amount of flavor mixing is sufficient to remove the existence of the second phase transition: Of course, there *must* be a single phase transition at $\alpha = 0.5$, where M_u and M_d are equal (see Eq. (2.81)). (This was the case studied in Ref. [144].) However, the critical value $\alpha^{\mathrm{c}} \simeq 0.12$ we found in our example is much smaller. At $T = 0$, a rough, but perhaps more general estimate for the critical α can be obtained from the observation that the phase transition takes place when the chemical potential of quark f comes close to its constituent mass, i.e., $\mu_f \approx M_i$. Applying this condition to the up quark we expect the first phase transition to take place at $\mu_u \approx M_{\mathrm{vac}}$, i.e, at $\mu \approx M_{\mathrm{vac}} - \delta\mu$. At this point M_u drops and, according to Eq. (2.81), M_d drops as well. Neglecting the current quark mass, we find

$$M_d \approx -(1-\alpha)4G_0\phi_d \lesssim (1-\alpha)\, M_{\mathrm{vac}} \ . \tag{2.84}$$

If this value becomes smaller than the value of μ_d, we expect the down quarks to exhibit a phase transition as well. Hence, we estimate

$$\alpha^{\mathrm{c}}(T=0) \lesssim \frac{2\delta\mu}{M_{\mathrm{vac}}} \ . \tag{2.85}$$

Note that this estimate would not be affected by a possible restoration of the $U_A(1)$ symmetry at the phase boundary. Obviously, if G_2 goes to zero, M_d would drop as well.

For our example, Eq. (2.85) gives $\alpha^{\mathrm{c}}(T=0) \lesssim 0.15$. Comparing this value with the numerical result $\alpha^{\mathrm{c}}(T=0) = 0.104$, we see that Eq. (2.85) is a quite conservative estimate. This is easily understood, since in the second step of Eq. (2.84) we have neglected the fact, that ϕ_d also becomes smaller. Our estimate does also not include the observation, that the critical chemical potential for the first phase transition *rises* with α. In any case, we have to admit that our arguments cannot explain quantitatively why Eq. (2.85) seems to hold even for temperatures approaching the critical endpoint where the quark masses do no longer drop discontinuously.

At this point one can ask, which value of α is "realistic". All observables we have used so far to fix the parameters (f_π, m_π, and $\langle\bar{q}q\rangle$) do not depend on α. However, as already mentioned, for $\alpha = 0$ the interaction would be symmetric under $U_A(1)$ transformations and consequently there would be another pseudo-Goldstone boson, namely an isoscalar pseudoscalar particle, degenerate with the pions. This is of course unrealistic. Turning on α, the $U_A(1)$ symmetry becomes explicitly broken (in addition to the mass term in the Lagrangian) and the mass of the isoscalar meson is shifted upwards. Since in a pure

two-flavor world this particle should be identified with the η meson, one way to fix α is to fit the physical η mass. In this way one finds $\alpha = 0.11$.

However, the description of the η meson without strange quarks is not very realistic. For a better way to determine α we should therefore refer to the three-flavor NJL model. For three flavors the instanton-induced interaction which plays the role of $\mathscr{L}_2$ is a six-point interaction (in general, for N_f flavors it is a $2N_f$-point interaction), and gives rise to the $\eta - \eta'$ splitting. More details of the three-flavor NJL model will be discussed in the next chapter. Here we just refer to Eq. (3.5) for the constituent quark masses. When we compare this equation with Eq. (2.81) we can identify $G_1 = G$ and $G_2 = -\frac{1}{2} K\phi_s$ and thus

$$\alpha = \frac{-K\phi_s}{2G - K\phi_s} \ . \tag{2.86}$$

The parameters G and K and the quark condensate ϕ_s have been determined by several authors by fitting the masses of the pseudoscalar octet and are listed in Table 3.1. If we take, for instance, the values of set RKH [145], we find $\alpha \simeq 0.21$. For the parameters of set HK [71] we get a somewhat smaller value, $\alpha \simeq 0.16$. On the other hand, the success of the instanton liquid model to describe vacuum correlators [37] would suggest that $\mathscr{L}_2$ is the dominant part of our Lagrangian, i.e., $\alpha \simeq 1$. In all these cases we would find only one phase transition for $\delta\mu = 30$ MeV. (For the pure $SU(2)$ fit of the η meson we would just be at the intermediate case depicted in the central panel of Fig. 2.17.)

Typical values of $|\delta\mu|$ in heavy-ion collisions are likely to be smaller than that. A simple estimate, assuming the density ratio $n_u : n_d = 290 : 334$ as in ^{208}Pb, and the approximate relation $n_u : n_d \approx (\mu_u : \mu_d)^3$ yields $\delta\mu \approx -10$ MeV for $\mu = 400$ MeV. Empirically, one finds $\delta\mu = -2.5$ MeV, at chemical freeze-out for Pb–Pb collisions at SPS [44] and $\delta\mu = -6$ MeV for Si+Au collisions at AGS [146]. This would mean, that it is very unlikely to "see" two phase boundaries in heavy-ion collisions.

Of course, before drawing quantitative conclusions, we should recall the shortcomings of the model. As pointed out earlier, the description of the "hadronic phase" as a gas of quarks, rather than hadrons, is unrealistic and any prediction of the critical endpoint(s) in non-confining mean-field models should not be trusted. However, keeping this in mind, our results show that flavor-mixing effects cannot be neglected in the discussion of the phase diagram. The very existence of these effects is related to instantons and the $U_A(1)$-anomaly of QCD. Of course their magnitude is a matter of debate, but they are likely to cancel the interesting phenomena discussed in Refs. [137,138].

3. Three-flavor systems

In this chapter we extend our analysis to three quark flavors. While most features of the two-flavor NJL model which we have discussed in the previous chapter remain qualitatively unaffected, the main difference comes about from the fact that the mass of the strange quark cannot be chosen equal to the non-strange quark mass in realistic calculations. This means we have to deal with an explicitly broken $SU(3)$ symmetry, and thus $\langle\bar{s}s\rangle \neq \langle\bar{u}u\rangle$, even for equal chemical potentials. In particular the chiral limit is in general not a good approximation to the model with realistic masses. Therefore the finite-mass effects we have already encountered in the two-flavor case become much more pronounced in the three-flavor model.

3.1. Vacuum properties

3.1.1. Lagrangian

The three-flavor version of the NJL model has been developed in the mid-1980s [147–149] and has been investigated by many authors since then. The most commonly used Lagrangian reads [145,150]

$$\mathscr{L} = \bar{q}(\mathrm{i}\partial\!\!\!/ - \hat{m})q + \mathscr{L}_{\mathrm{sym}} + \mathscr{L}_{\mathrm{det}} \ , \tag{3.1}$$

where $q = (u, d, s)^{\mathrm{T}}$ denotes a quark field with three flavors, and $\hat{m} = \mathrm{diag}_f(m_u, m_d, m_s)$ is the corresponding mass matrix. Throughout this report we will assume isospin symmetry on the Lagrangian level, $m_u = m_d$, whereas m_s will in general be different, thus explicitly breaking $SU(3)$-flavor symmetry. The Lagrangian contains two independent interaction terms which are given by

$$\mathscr{L}_{\mathrm{sym}} = G \sum_{a=0}^{8} [(\bar{q}\tau_a q)^2 + (\bar{q}\mathrm{i}\gamma_5\tau_a q)^2] \tag{3.2}$$

and

$$\mathscr{L}_{\mathrm{det}} = -K[\det{}_f(\bar{q}(1+\gamma_5)q) + \det{}_f(\bar{q}(1-\gamma_5)q)] \ . \tag{3.3}$$

These terms may be seen as the three-flavor version of Eqs. (2.76) and (2.77) and can straightforwardly be generalized to any number of flavors, N_f. $\mathscr{L}_{\mathrm{sym}}$ is then a $U(N_f)_L \times U(N_f)_R$ symmetric four-point interaction, where τ_a, $a = 1, \ldots, (N_f^2 - 1)$ denote the generators of $SU(N_f)$, while τ_0 is proportional to the unit matrix. All τ_a are normalized such that $\mathrm{tr}\,\tau_a\tau_b = 2\delta_{ab}$. For two flavors, this is fulfilled by $\tau_0 = \mathbb{1}_f$ and the Pauli matrices τ_a, $a = 1, 2, 3$. Then $\mathscr{L}_{\mathrm{sym}}$ becomes identical to $\mathscr{L}_1$ in Eq. (2.76) with $G_1 = G$. Now, for three flavors, $\tau_0 = \sqrt{\frac{2}{3}}\mathbb{1}_f$ and τ_a, $a = 1, \ldots, 8$ are the eight Gell–Mann matrices.[19]

The second term, $\mathscr{L}_{\mathrm{det}}$, corresponds to the 't Hooft interaction and is a determinant in flavor space. This means, it is a maximally flavor-mixing $2N_f$-point interaction, involving an incoming and an outgoing quark of each flavor. Thus, for two flavors, $\mathscr{L}_{\mathrm{det}}$ is a four-point interaction and one can easily check that it is equal to $\mathscr{L}_2$ in Eq. (2.77) with $G_2 = -K$. For three flavors we have a six-point interaction of the form

$$\det{}_f(\bar{q}\mathcal{O}q) := \sum_{i,j,k} \varepsilon_{ijk}(\bar{u}\mathcal{O}q_i)(\bar{d}\mathcal{O}q_j)(\bar{s}\mathcal{O}q_k) \ , \tag{3.4}$$

where i, j, k are flavor indices (see Fig. 3.1).

$\mathscr{L}_{\mathrm{det}}$ is $SU(N_f)_L \times SU(N_f)_R$ symmetric, but it breaks the $U_A(1)$ symmetry which was left unbroken by $\mathscr{L}_{\mathrm{sym}}$. It thus translates the $U_A(1)$ anomaly, which in QCD arises at quantum level from the gluon sector, to a tree-level interaction in a pure quark model. As discussed earlier, this term is phenomenologically important to get the correct mass splitting of the η and η' mesons. In the chiral limit ($m_u = m_d = m_s = 0$), the η' mass is lifted to a finite value by $\mathscr{L}_{\mathrm{det}}$, while the other pseudoscalar mesons, including the η, remain massless.

Like in the two-flavor case, there are many other terms which are consistent with the symmetries and which could be added to the Lagrangian. For instance, in Ref. [122] vector and axial-vector four-point

[19] Traditionally, the Gell–Mann matrices are denoted by λ_a. However, for later convenience we reserve this symbol for $SU(3)$-color generators and keep the notation τ_a for $SU(3)$-flavor generators.

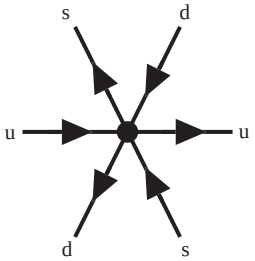

Fig. 3.1. Flavor structure of the six-point vertex ('t Hooft interaction).

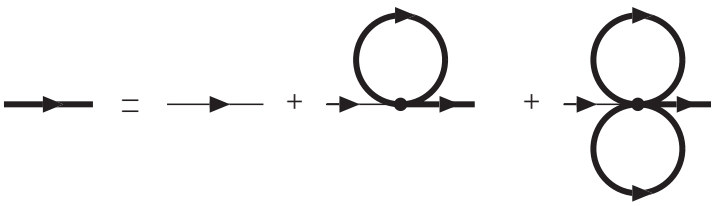

Fig. 3.2. Dyson equation for the quark propagator in the three-flavor NJL model (Hartree approximation).

interactions have been taken into account in addition to the terms given above. A complete list of possible four-point and six-point terms is discussed in Ref. [151]. For simplicity, however, we will restrict ourselves to the Lagrangian defined above.

3.1.2. Gap equation and meson spectrum

Apart from the explicit $SU(3)$-flavor breaking by the strange quark mass, the main complication of the three-flavor version of the NJL model as compared with the two-flavor case is caused by the six-point vertices which arise from the 't Hooft interaction. For the gap equation this means that there is an additional term involving two quark loops. This gives rise to the equation

$$M_i = m_i - 4G\phi_i + 2K\phi_j\phi_k, \quad (i,j,k) = \text{any permutation of } (u,d,s)\ , \tag{3.5}$$

which is diagrammatically shown in Fig. 3.2. It contains a non-flavor mixing term proportional to the coupling constant G and a flavor mixing term proportional to the coupling constant K.

For describing mesons one first constructs effective four-point vertices as a sum of the genuine four-point vertices and the six-point vertices with one closed loop, see Fig. 3.3. These effective four-point vertices are then used as scattering kernels in the Bethe–Salpeter equation (Fig. 2.4). Although technically more involved, mostly because of the unequal strange and non-strange quark masses (leading, among other things, to octet–singlet mixing in the η-η' subspace), the basic mechanism is the same and will not be presented here. For further details see, e.g., Refs. [145,151].

The model specified in Section 3.1.1 contains five parameters: the bare masses m_s and m_u, the coupling constants G and K, and the cut-off Λ. Thus, compared with the simplest version of the two-flavor model, Eq. (2.20), we have two more parameters: m_s and the six-point coupling. (As we have seen in Section 2.4, Eq. (2.20) corresponds to a particular choice of the more general Lagrangian Eq. (2.74). From this point of view, there is even only one additional parameter.) On the other hand there are at least three

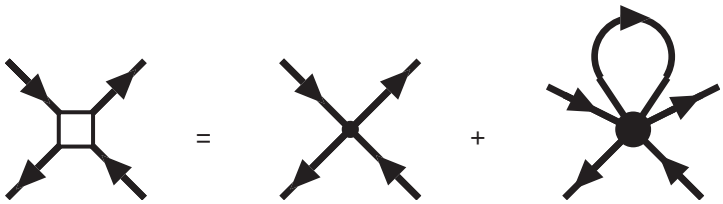

Fig. 3.3. Effective four-point vertex.

Table 3.1
Three sets of parameters and related quark and meson properties in the three-flavor NJL model

	RKH [145]	HK [71]	LKW [122]	Empirical [99]
Λ (MeV)	602.3	631.4	750	
$G\Lambda^2$	1.835	1.835	1.82	
$K\Lambda^5$	12.36	9.29	8.9	
$m_{u,d}$ (MeV)	5.5	5.5	3.6	3.5–7.5
m_s (MeV)	140.7	135.7	87	110– 210
G_V/G	—	—	1.1	
$M_{u,d}$ (MeV)	367.7	335	361	
M_s (MeV)	549.5	527	501	
$(\langle\bar{u}u\rangle)^{1/3}$ (MeV)	−241.9	−246.9	−287	
$(\langle\bar{s}s\rangle)^{1/3}$ (MeV)	−257.7	−267.0	−306	
B (MeV/fm^3)	291.7	295.5	350.0	
f_π (MeV)	92.4	93.0	93	92.4 [102]
m_π (MeV)	135.0	138	139	135.0, 139.6
m_K (MeV)	497.7	496	498	493.7, 497.7
m_η (MeV)	514.8	487	519	547.3
$m_{\eta'}$(MeV)	957.8	958	963	957.8
$m_{\rho,\omega}$ (MeV)	—	—	765	771.1, 782.6
m_{K^*} (MeV)	—	—	864	891.7, 896.1
m_ϕ (MeV)	—	—	997	1019.5

The empirical quark masses listed in Ref. [99] have been rescaled to a renormalization scale of 1 GeV by multiplying them by 1.35 [99]. The values given for the light quarks correspond to the average $(m_u + m_d)/2$.

additional observables, namely the masses of the pseudoscalar mesons K, η, and η'. Therefore, in the three-flavor model, the parameters are in principle much better constrained than in the two-flavor model. In fact, whereas for two flavors we had to invoke the poorly known quark condensate, we now have five well-known observables, f_π, m_π, m_K, m_η, and $m_{\eta'}$, and one would naively expect that one can uniquely fix the five parameters.

It turns out that this is not quite the case. In Table 3.1 we have listed three different parameter sets taken from the literature, together with related quantities in the quark and meson sectors. The first two sets correspond to the fits of Rehberg, Klevansky, and Hüfner (RKH) [145] and of Hatsuda and Kunihiro

(HK) [71],[20] respectively. Instead of fitting five mesonic quantities, both groups have set m_u to a value of 5.5 MeV, taken from Refs. [30,152], and fixed the remaining four parameters by fitting f_π, m_π, m_K, and $m_{\eta'}$ to their empirical values. In this way the mass of the η-meson is underestimated by 6% in RKH and 11% in HK.

However, although both groups apparently used the same prescription, the resulting parameter sets are not identical. The most striking difference is found in the six-point coupling. Comparing the dimensionless combinations $K\Lambda^5$, the RKH value is more than 30% larger than the HK value. (If we compare the values of K the difference is even 70%.) The reason for this discrepancy lies in the different treatment of the η'-meson [153]. Because of its large mass ($m_{\eta'} = 958$ MeV), in both cases the η' is above the threshold for $q\bar{q}$-decay, and the $q\bar{q}$-polarization diagram receives an unphysical imaginary part. In RKH this was accepted as an unavoidable feature of the NJL model and the authors defined the η'-mass as the real part of the corresponding pole in the complex plane. In HK, on the contrary, the imaginary part of the polarization function has been discarded by hand and only the real part was retained in order to determine $m_{\eta'}$. Of course, since the real part is linked to the imaginary part via dispersion relations, this prescription does not completely remove the unphysical effects. This leaves a general uncertainty which is reflected in the difference between the parameter sets RKH and HK.

As a third example, the parameters of Lutz, Klimt, and Weise (LKW) [122] are also shown in Table 3.1. In addition to Eqs. (3.2) and (3.3), the authors considered a vector and axial-vector interaction term, which enabled them to fit the vector-meson nonet (ρ, ω, K^*, and ϕ) as well. In the pseudoscalar meson sector they obtained similar results as RKH and HK. However, because the longitudinal part of the axial-vector interaction mixes with the pseudoscalar interaction ("πa_1-mixing"), this sector is not independent of the vector coupling constant G_V. As a consequence, LKW find a relatively large cut-off and relatively small bare quark masses. Moreover, the six-point coupling is even weaker than in HK.

In spite of these differences, it remains generally true that the parameters of the three-flavor model are much better constrained than in the two-flavor case. In fact, the resulting constituent quark masses in vacuum are quite similar for the three parameter sets, ranging from about 335 to 370 MeV for up and down quarks and from 500 to 550 MeV for strange quarks. The same is true for the bag constants, which are defined in an analogous way to the two-flavor case (see below). They are almost equal for RKH and HK, while the value for LKW is about 20% larger. In the numerical calculations presented in this work, we will mostly employ the parameters of RKH.

3.2. Thermodynamics

3.2.1. Formalism

The formalism of Sections 2.3.1 and 2.4 is straightforwardly generalized to the three-flavor model. Allowing for three independent chemical potentials μ_f for the three flavors $f = u, d, s$, the mean-field thermodynamic potential in the presence of the quark condensates $\phi_f = \langle \bar{q}_f q_f \rangle$ reads

$$\Omega(T, \{\mu_f\}; \{\phi_f\}) = \sum_{f=u,d,s} \Omega_{M_f}(T, \mu_f) + 2G(\phi_u^2 + \phi_d^2 + \phi_s^2) - 4K\phi_u\phi_d\phi_s + \text{const.}\,, \qquad (3.6)$$

where $\Omega_{M_f}(T, \mu_f)$ is given in Eq. (2.80) and corresponds to the contribution of a gas of quasi-particles with mass M_f. The latter is related to the various ϕ_i via Eq. (3.5). Again, the thermodynamically consistent

[20] The parameters of Ref. [71] are almost, but not exactly the same as the parameters of the earlier fit by Kunihiro [150].

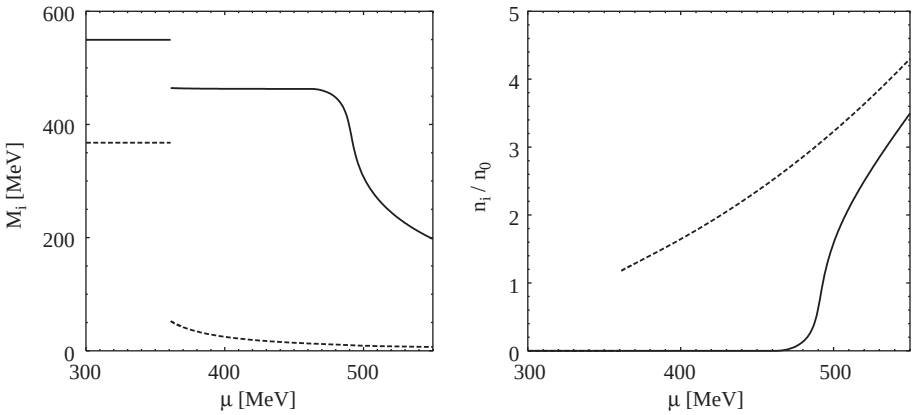

Fig. 3.4. Quark matter properties as functions of a common quark number chemical potential μ (parameter set RKH [145]). Left: Constituent quark masses $M_u = M_d$ (dashed) and M_s (solid). Right: Number densities $n_u = n_d$ (dashed) and n_s (solid) in units of $n_0 = 3\rho_0 = 0.51\,\mathrm{fm}^{-3}$.

solutions correspond to the stationary points of Ω, where $\delta\Omega/\delta\phi_f = 0$. One finds that ϕ_f is given by Eq. (2.82), which now has to be evaluated self-consistently with Eq. (3.5), forming a set of three coupled gap equations for the constituent masses. The irrelevant constant in Eq. (3.6) is conveniently chosen such that the minimal solution of Ω in vacuum is zero.

Once the self-consistent solutions are found, other thermodynamic quantities can be derived in the standard way. In particular we can calculate the pressure and the energy density,

$$p = -\Omega, \quad \epsilon = \Omega + Ts + \sum_f \mu_f n_f \ , \tag{3.7}$$

where $s = \partial\Omega/\partial T$ is the entropy density and $n_f = -\partial\Omega/\partial\mu_f$ are the number densities of the quarks of flavor f. The total quark number density and the baryon number density are given by $n = \sum_f n_f$ and $\rho_B = n/3$, respectively.

Finally, in analogy to Eq. (2.60), we define the bag constant as

$$B = \Omega(T = 0, \{\mu_f = 0\}; \{\phi_f = 0\}) \ . \tag{3.8}$$

3.2.2. Quark masses and effective bag constants at non-zero density

In the following we restrict ourselves to $T = 0$. In Fig. 3.4 the constituent quark masses M_i (left panel) and the flavor densities n_i (right panel) are plotted as functions of a common quark number chemical potential μ. Quantities related to the up and down quarks are indicated by dashed lines, those related to the strange quarks by solid lines. The results were obtained using the model parameters RKH [145].

At $\mu = \mu_c = 361\,\mathrm{MeV}$ we find a first-order phase transition, where $M_u = M_d$ (dashed line) drops from 367.6 to 52.5 MeV. At this point the total baryon number density jumps from zero to about $2.4\rho_0$, equally carried by up and down quarks, while the density of strange quarks remains zero. Nevertheless, because of flavor-mixing, M_s does not stay constant but drops at μ_c from 549.5 to 464.4 MeV. Above μ_c, the contributions of ϕ_u and ϕ_d to M_s are negligible and M_s stays almost constant until μ exceeds M_s and n_s becomes non-zero as well. The behavior of the constituent masses shows some similarities

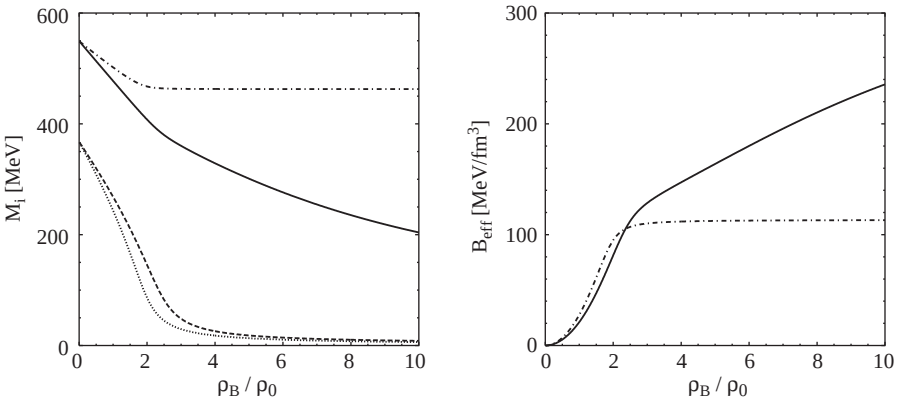

Fig. 3.5. Various quantities for isospin symmetric matter, $n_u = n_d$, as functions of the total baryon number density ρ_B (parameter set RKH [145]). Left: Constituent quark masses for symmetric matter, $n_u = n_d = n_s$: $M_u = M_d$ (dashed) and M_s (solid), and without strangeness, $n_s = 0$: $M_u = M_d$ (dotted) and M_s (dash–dotted). Right: Effective bag constant B_{eff} for symmetric matter (solid) and for $n_s = 0$ (dash–dotted).

with the two-flavor model at finite isospin chemical potential with small flavor mixing (central panel of Fig. 2.16), although instead of a second phase transition we now find a smooth cross-over above the strange quark threshold. The main difference is that in the present example the flavor symmetry is not broken by unequal chemical potentials, but be unequal masses.

It is again instructive to compare the NJL-model equation of state with the bag model one. As discussed in Section 2.3.3, both models behave almost identically in the chiral limit, but already for bare quark masses of a few MeV we found some differences, which could be expressed in terms of density dependent effective quark masses and bag constants. In the three-flavor case, where chiral symmetry is broken much stronger by the strange quark, we should expect much bigger effects.

Already in the two-flavor model, both, the constituent quark masses and the effective bag constants, are in general not only functions of the total density, but also on the flavor composition, i.e., they depend on each flavor density n_i separately. This point has not been discussed in Section 2.3.3 where we only considered isospin symmetric quark matter. However, in three-flavor systems, a restriction to equal flavor densities is no longer a natural choice, as obvious from Fig. 3.4. Therefore we generalize our previous definition of B_{eff}, Eq. (2.68), to include arbitrary flavor compositions,

$$\epsilon(n_u, n_d, n_s) = \frac{N_c}{\pi^2} \sum_f \int_0^{p_{\text{F}}^f} \mathrm{d}p\, p^2 \sqrt{p^2 + M_f^2(n_u, n_d, n_s)} + B_{\text{eff}}(n_u, n_d, n_s) \ , \tag{3.9}$$

where p_{F}^f is the Fermi momentum of flavor f.

To illustrate both, density dependence and dependence on flavor composition, the constituent quark masses and the effective bag constant are displayed in Fig. 3.5 for two different cases. The first case corresponds to equal densities $n_u = n_d = n_s$. The corresponding constituent quark masses as functions of ρ_B are indicated by the dashed line ($M_u = M_d$) and by the solid line (M_s) in the left panel of the figure. As we have seen earlier, the constituent masses become equal to the current masses only at "asymptotic" densities, i.e., when the Fermi momentum reaches the cut-off. (In the present example this is $\rho_B = 17\rho_0$.)

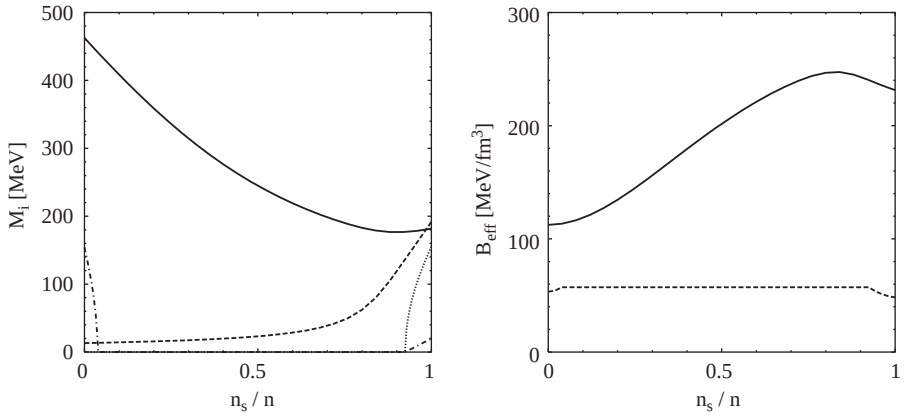

Fig. 3.6. Various quantities as functions of the fraction of strange quarks, n_s/n, for isospin symmetric matter ($n_u = n_d$) at fixed total baryon number density $\rho_B = 5\rho_0$. The results were obtained using the model parameters RKH (see Table 3.1) and the corresponding chiral limit ($m_u = m_d = m_s = 0$). Left: constituent quark masses $M_u = M_d$ (RKH: dashed, chiral limit: dotted), M_s (RKH: solid, chiral limit: dash–dotted). Right: effective bag constant B_{eff} (RKH: solid, chiral limit: dashed).

At this point all condensates vanish and the effective bag constant B_{eff} (solid line in the right panel) reaches the value of the bag constant $B = 291.7\,\text{MeV/fm}^3$. However, whereas in the non-strange sector chiral symmetry gets quickly restored, at least on an absolute scale, this is not the case for the strange sector, and neither M_s nor B_{eff} can be approximated by a constant above a certain density.

In the second case we consider equal non-strange densities $n_u = n_d$, but vanishing strangeness, $n_s = 0$. In this case the strange quark mass (dash–dotted line in the left panel) only drops through its mixing with the up and down masses (dashed line) and stays practically constant above $\rho_B \simeq 2\rho_0$, where the latter are small. Obviously, the asymptotic value M_s^∞ is just the vacuum mass one would obtain for a vanishing six-point coupling. For the present example one finds $M_s^\infty = 462.8\,\text{MeV}$, corresponding to a strange quark condensate $\phi_s^\infty = (-251.6\,\text{MeV})^3$. This means, chiral symmetry never gets restored in the strange sector, and, as a consequence, B_{eff} (dash–dotted line in the right panel) does not approach the bag constant B, but the asymptotic value

$$B_\infty = \Omega(T = 0, \{\mu_f = 0\}; \phi_u = 0, \phi_d = 0, \phi_s = \phi_s^\infty)\ . \tag{3.10}$$

This can be considerably smaller than B: In the present example $B_\infty = 113.2\,\text{MeV/fm}^3$, compared with $B = 291.7\,\text{MeV/fm}^3$. Hence, at high enough densities, the system behaves like a two-flavor bag model with a bag constant B_∞.

The two examples demonstrate, that the dependence of the effective quark masses and bag constants on the flavor composition can be large. A complementary view on this point is given in Fig. 3.6 where the constituent masses and the effective bag constant are displayed as functions of the strangeness fraction n_s/n for $n_u = n_d$ at fixed baryon number density $\rho_B = 5\rho_0$. At not too large values of n_s/n we find a strong decrease of M_s (left panel, solid line) and a weak increase of the non-strange masses (dashed line) with increasing n_s/n. This is easily understood from the fact that the density of strange quarks increases while the density of non-strange quarks is large, but decreases. The small increase of M_s at very large n_s/n is a flavor-mixing effect and related to the steeper increase of $M_u = M_d$ in this regime. From the behavior

of the constituent masses (and thus the condensates) we can also qualitatively understand the behavior of the effective bag constant (right panel, solid line), which is mostly rising and only turns around at large n_s/n.

For comparison we have also plotted the results for the corresponding chiral limit, ($m_u = m_d = m_s = 0$). In this case one finds a large regime ($0.04 < n_s/n < 0.92$) where chiral symmetry is exactly restored, i.e., all constituent masses vanish. In this regime B_{eff} is equal to B ($=57.3\,\text{MeV/fm}^3$ in the chiral limit) and therefore constant. While this is in agreement with a bag model description, it is in sharp contrast to the NJL-model with realistic quark masses where B_{eff} approximately doubles its value in the same regime.

3.3. Stability of strange quark matter

3.3.1. The strange quark matter hypothesis

The results of the previous sections may have interesting consequences for the existence of absolutely stable strange quark matter.

In 1984 Witten suggested that there could be a so-far unobserved form of matter, "strange quark matter" (SQM), which is bound more strongly than ordinary nuclei and thus forms the true ground state of strongly interacting matter [40]. In contrast to nuclei, where quarks are confined to individual colorless nucleons, SQM is supposed to be an extended or even macroscopic piece of matter which is composed of *deconfined* up, down, and strange quarks. Witten's paper immediately attracted great attention and stimulated a large number of further investigations, although similar ideas had come up much earlier [39].

Witten's original motivation for his conjecture was to give a possible solution to the dark matter problem in terms of QCD effects. Later it was shown that most of the SQM possibly produced in the early universe would quickly have converted into normal hadronic matter by evaporating nucleons [154]. Therefore SQM cannot be of cosmological importance, even if it is the absolute ground state of matter.

Nevertheless, the existence of absolutely stable SQM—besides being interesting by itself—could have other interesting consequences. For instance, there could be so-called "strange stars", i.e., compact stars entirely made of SQM. Being self-bound objects they could be arbitrarily small, in sharp contrast to conventional neutron stars, which are bound by gravitation and therefore have a minimal radius of about 10 km (see, e.g., Ref. [155]) or even 12 km [156]. Consequently, the reported discovery of a compact star with a radius of 3.8–8.2 km [157] received tremendous attention. However, the determination of compact star radii is of course very difficult and a radius of 10–14 km was obtained in Ref. [158] for the same object. In fact, so far all strange star candidates are highly controversial.

Another interesting scenario is the production of small lumps of SQM, so-called "strangelets", in heavy-ion collisions. For this it would be sufficient if SQM was stable with respect to strong interactions, but not necessarily against weak decays. On the other hand, the production of positively charged absolutely stable strangelets could in principle trigger a conversion of the Earth into SQM. This was one of the "disaster scenarios" discussed when RHIC was commissioned [159]. Clearly, the most convincing argument against this possibility is the existence of the Moon in spite of its long-term exposure to high energetic cosmic rays [159].

At first sight, the hypothesis of absolutely stable SQM seems to contradict the empirical stability of nuclei. In fact, we can immediately exclude the stability of non-strange quark matter (NSQM) consisting of deconfined up and down quarks. The essential point is that SQM may only be stable if it contains a large fraction of strange quarks, $n_s \approx n_u \approx n_d$. Since hypernuclei, i.e., nuclei which contain hyperons, have higher masses than ordinary nuclei of the same mass number, this state cannot be reached via a series

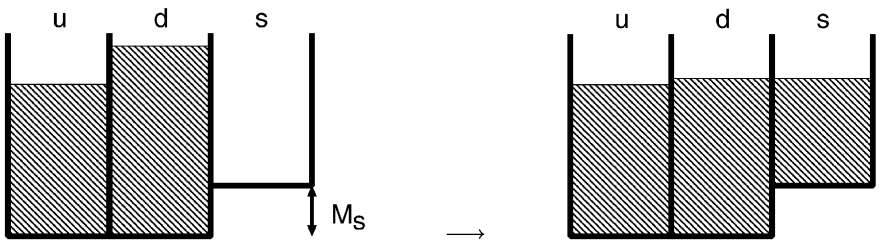

Fig. 3.7. Basic principle of the SQM hypothesis (schematic): For $\mu_d > M_s$, NSQM (left) can lower its energy by converting into SQM (right) via weak decay of d quarks into s quarks.

of subsequent weak decay processes, but only via the simultaneous decay of many quarks, associated with a very long lifetime.[21]

A somewhat oversimplified picture of the basic idea is sketched in Fig. 3.7. Suppose we have a system of massless up and down quarks in a given volume. To be electrically neutral, the number of down quarks should be twice as large as the number of up quarks and hence $\mu_d = 2^{1/3}\mu_u$ (left). Obviously, if this value is larger than the mass of the strange quark, the system could lower its energy by transforming some of the down quarks into strange quarks until they have equal Fermi energies (right). Thus, if the actual numbers are such that

$$\left(\frac{E}{A}\right)_{\text{SQM}} < \left(\frac{E}{A}\right)_{\text{nuclei}} < \left(\frac{E}{A}\right)_{\text{NSQM}} \tag{3.11}$$

absolute stable SQM could exist without contradicting the empirical facts. Of course, to be more realistic one should add electrons to the system and consider neutral matter in weak equilibrium. Moreover, unlike Fig. 3.7 there is no fixed volume, but the system should be bound by itself and the respective densities of SQM and NSQM could be different.

Right after Witten's paper, Farhi and Jaffe have performed an investigation within the MIT bag model [92]. To that end, they treated the bag constant, the strange quark mass and α_s as free parameters and searched for a window in parameter space, where Eq. (3.11) is fulfilled. It turned out that there are indeed "reasonable" parameters for which this could be achieved. For instance, for $\alpha_s = 0$ and $m_s = 150\,\text{MeV}$, Eq. (3.11) would be fulfilled for $60\,\text{MeV/fm}^3 \lesssim B \lesssim 80\,\text{MeV/fm}^3$. For larger values of m_s the upper limit of B becomes reduced, while with increasing α_s both, upper and lower limit, are shifted to lower values.

Although none of the parameter fits listed in Table 2.1 falls into Farhi and Jaffe's window, the authors pointed out that these parameters might not be applicable to describe dense quark matter. First, as we have seen earlier, the hadron spectra strongly depend on parameters which become irrelevant in infinite systems, like the zero-point energy or the treatment of the center of momentum motion. But even those parameters which survive, could be effectively density dependent. This is quite obvious for α_s which should become smaller with increasing density. The relatively large values for m_s (as compared with the particle data book), point into the same direction. In this context it is certainly interesting to redo Farhi and Jaffe's analysis within the NJL model, where density-dependent masses emerge naturally. This has been done in Ref. [160]. In the following we discuss the results.

[21] In addition it is possible that, because of surface effects, SQM is only absolutely stable for a very large number of particles, e.g., $N > 10^7$. Then the decay of nuclei would not even be favored energetically.

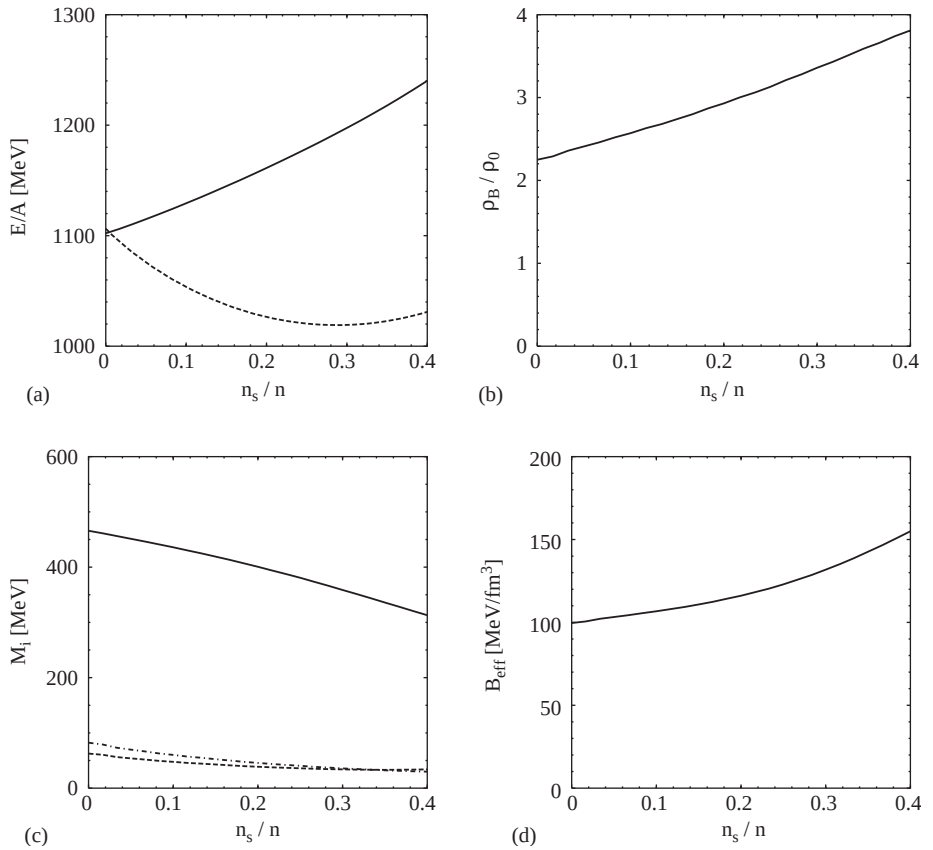

Fig. 3.8. Properties of neutral NJL quark matter at zero pressure as functions of the fraction of strange quarks, n_s/n. (parameter set RKH [145]). (a) Energy per baryon number. Solid line: NJL model. Dashed line: bag model with $m_u = m_d = 5.5\,\text{MeV}$, $m_s = 140.7\,\text{MeV}$, and $B = 113.2\,\text{MeV/fm}^3$. (b) Total baryon number density. (c) Constituent quark masses M_u (dash–dotted), M_d (dashed), and M_s (solid). (d) Effective bag constant.

3.3.2. NJL-model analysis

When we compare the constituent masses and effective bag constants which we typically got in Section 3.2.2 with Farhi and Jaffe's window, we can already anticipate that it will be hard to fulfill Eq. (3.11). This is confirmed by another pre-study which is displayed in Fig. 3.8. In that figure various quantities are plotted as functions of the fraction of strange quarks n_s/n. However, unlike in Fig. 3.6, matter is kept neutral by choosing $n_u/n = \frac{1}{3}$ and $n_d/n = \frac{2}{3} - n_s/n$. Moreover, the results do not correspond to a fixed total density, but to vanishing pressure. The corresponding total baryon number density is shown in panel (b), the constituent masses and the effective bag constant are given in panels (c) and (d), respectively.

The resulting values of E/A are shown in panel (a). The NJL-model result is indicated by the solid line. Since the pressure vanishes, each point corresponds to a minimum of E/A as a function of the total baryon density for fixed n_s. However, the lowest value is reached at $n_s = 0$, i.e., it is not favorable for the non-strange matter to convert down quarks into strange quarks. The reason for this behavior is

of course the large strange quark mass $M_s = 466\,\mathrm{MeV}$. Therefore, since $\mu_d = 392\,\mathrm{MeV}$ at this point,[22] the conversion of a down quark into a strange quark costs 74 MeV.

For comparison we also show the result of a bag model calculation with quark masses equal to the NJL current quark masses, i.e., $m_u = m_d = 5.5\,\mathrm{MeV}$ and $m_s = 140.7\,\mathrm{MeV}$. The bag constant was taken to be equal to $B_\infty = 113.2\,\mathrm{MeV/fm^3}$, i.e., the asymptotic value of the dash–dotted line in the right panel of Fig. 3.5. The resulting E/A is indicated by the dashed line in panel (a) of Fig. 3.8. As one can see, for $n_s = 0$ the bag-model result agrees quite well with the NJL result. However, because of the much smaller strange quark mass, in the bag model the conversion of down quarks to strange quarks is energetically favored, and there is a minimum $E/A = 1019\,\mathrm{MeV/fm^3}$ at $n_s = 0.29$. Note, however, that even this value is about $100\,\mathrm{MeV/fm^3}$ larger than E/A in atomic nuclei. This reflects the fact that the bag constant is above Farhi and Jaffe's limit for $m_s \simeq 140\,\mathrm{MeV}$.

So far, we have only considered quarks. Of course, for a more realistic treatment of the problem, we have to take into account weak decays, like

$$d \leftrightarrow u + e + \bar{\nu}_e \leftrightarrow s \ , \tag{3.12}$$

and related processes. This implies that we have to include electrons and (in principle) neutrinos. To large extent we can adopt the model of Farhi and Jaffe [92], but replacing the MIT bag by the NJL mean field: Since we are interested in static properties of potentially stable matter, we can safely assume that the neutrinos have enough time to leave the system. The electrons are described by a non-interacting gas of massless fermions,

$$\Omega_e(T = 0, \mu_e) = -\frac{\mu_e^4}{12\pi^2} \ , \tag{3.13}$$

where μ_e is the electron chemical potential. The total thermodynamic potential is then simply the sum of the quark part, Eq. (3.6), and Ω_e, and consequently,

$$\epsilon_{\mathrm{tot}} = \epsilon + \frac{\mu_e^4}{4\pi^2} \ , \quad p_{\mathrm{tot}} = p + \frac{\mu_e^4}{12\pi^2} \ , \tag{3.14}$$

where ϵ and p refer to the quark contributions. The electron density is given by $n_e = \mu_e^3/(3\pi^2)$.

Since the neutrinos can leave the system, lepton number is not conserved and we effectively have two conserved charges, namely baryon number and electric charge. Hence, in chemical equilibrium, only two of the four chemical potentials which enter into the thermodynamic potential (μ_e and the three quark chemical potentials μ_u, μ_d, and μ_s) are independent and could be expressed, e.g., in terms of a quark number chemical potential μ and an electric charge chemical potential μ_Q,

$$\mu_u = \mu + \tfrac{2}{3}\,\mu_Q, \quad \mu_d = \mu_s = \mu - \tfrac{1}{3}\,\mu_Q, \quad \mu_e = -\mu_Q \ . \tag{3.15}$$

[22] Note that $\mu_d > M_d^{\mathrm{vac}}$. This means that the neutral non-strange quark matter is unstable as well and could in principle reduce its energy by evaporating massive down quarks into the vacuum. However, this is irrelevant for the present discussion.

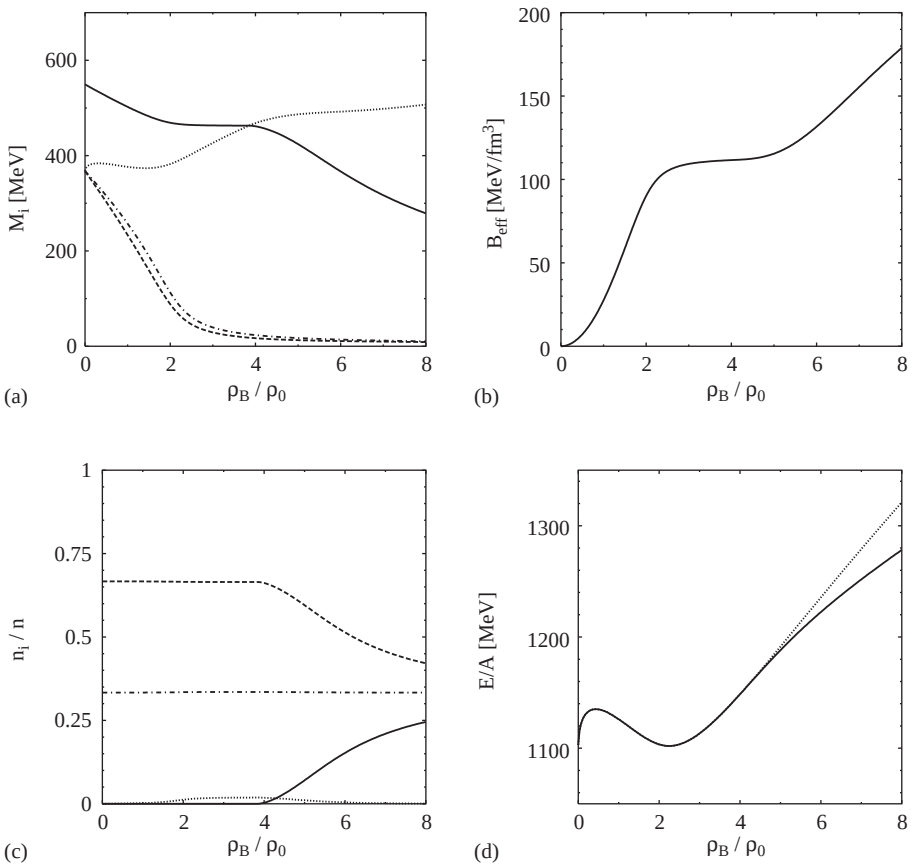

Fig. 3.9. Properties of neutral matter of NJL model quarks in beta equilibrium with electrons as functions of the total baryon number density ρ_B (parameter set RKH [145]). (a) Constituent quark masses M_u (dash–dotted), M_d (dashed), and M_s (solid). The dotted line indicates the chemical potential $\mu_d = \mu_s$. (b) Effective bag constant. (c) Number densities n_i divided by the total quark number density n: up quarks (dash–dotted), down quarks (dashed), strange quarks (solid), and electrons multiplied by 10 (dotted). (d) Energy per baryon number with (solid) and without (dotted) strangeness degrees of freedom. (a),(c), and (d) have been adapted with permission from Ref. [160].

Furthermore we demand charge neutrality,

$$\tfrac{2}{3}\, n_u - \tfrac{1}{3}\,(n_d + n_s) - n_e = 0\ . \tag{3.16}$$

Thus, the system can be characterized by one independent variable, e.g., the baryon number density ρ_B.

The results of our analysis are shown in Fig. 3.9. The energy per baryon number, $E/A = \epsilon_{\rm tot}/\rho_B$, is displayed in panel (d). The solid line corresponds to the model described above, the dotted line to non-strange quark matter, where the strange quarks have artificially been suppressed. Obviously the two curves only differ above $\sim 4\rho_0$. The reason for this is that below $\rho_B = 3.85\rho_0$ the density of strange quarks vanishes. This can be seen in panel (c) where the fractions n_i/n of the various particles are plotted. Since electrons (dotted line) play practically no role (note that their fraction has been multiplied by a factor of 10 to be visible in the plot) the fraction of up quarks (dash–dotted) is fixed by charge neutrality

(Eq. (3.16)) to about $\frac{1}{3}$. Thus, as long as $n_s = 0$, the remaining $\frac{2}{3}$ are mostly down quarks (dashed). For $\rho_B > 3.85\rho_0$, n_s/n becomes non-zero (solid) and n_d/n drops accordingly.[23]

The fact that there is no strangeness at lower densities is again due to the relatively large mass of the strange quark. The dynamical quark masses are displayed in panel (a) of Fig. 3.9. The strange quark mass is indicated by the solid line. For comparison we also show the chemical potential μ_s (dotted line). For $\rho_B < 3.85\rho_0$, μ_s is smaller than M_s, which is the reason why n_s vanishes in this regime. The decrease of M_s at small densities ($\rho_B \lesssim 2\rho_0$) is again a flavor-mixing effect and related to the drop of M_u and M_d. Above $2\rho_0$, this contribution can be neglected and M_s stays almost constant until it starts decreasing again when n_s becomes non-zero.[24]

A similar plateau structure is also seen in the effective bag constant which is shown in panel (b). At low densities, $\rho_B \lesssim 2\rho_0$, and at high densities $\rho_B \gtrsim 4\rho_0$, B_{eff} rises due to the symmetry restoration in the non-strange and in the strange sector, respectively, while in the intermediate region B_{eff} is almost constant. Note that the plateau values of M_s and B_{eff} are roughly the same as the asymptotic values $M_s^\infty = 462.8\,\text{MeV}$ and $B_\infty = 113.2\,\text{MeV/fm}^3$ of the dash–dotted lines in Fig. 3.5.

Let us come back to the energy per baryon (panel (d)) which is the main result of this analysis. At those densities where strange quarks exist, they indeed lead to a reduction of the energy, as can be seen by comparing the solid curve with the dotted one. However, the minimum of E/A does not belong to this regime, but is located at a much lower density, $\rho_B = 2.25\rho_0$. Here we find $E/A = 1102\,\text{MeV}$. Compared with the energy per baryon in an iron nucleus, $E/A \simeq 930\,\text{MeV}$, this is still very large. In this sense our results are consistent with the empirical fact that stable NSQM does not exist. However, since the energy of strange quark matter is even higher, our calculation predicts that also SQM is not the absolute ground state of strongly interacting matter.

This result is very robust with respect to changes of the model parameters. Obviously, stable quark matter with finite strangeness is only possible if the in-medium strange quark mass is much lower than the values we obtained above. The easiest way to reduce M_s is to choose a lower value of the current mass m_s. If we leave all other parameters unchanged, m_s must not be larger than 85 MeV if we require $n_s \neq 0$ at the minimum of E/A. With this value, we obtain much too low masses for K and η ($m_K \simeq 390\,\text{MeV}$, $m_\eta \simeq 420\,\text{MeV}$), while E/A is still relatively large (1075 MeV). If we want to come down to $E/A \simeq 930\,\text{MeV}$ we have to choose $m_s = 10\,\text{MeV}$ or, alternatively, $m_s = 25\,\text{MeV}$ and $m_u = m_d = 0$. This is of course completely out of range.

We could also try to lower M_s by choosing a smaller coupling constant G. (Since $\phi_u\phi_d$ is already very small at the densities of interest, M_s is almost insensitive to the coupling constant K.) However, with a lower G the vacuum masses of all quarks drop and correspondingly the bag constant B. This shifts the

[23] The small fraction of electrons can easily be understood in the following way: Suppose there were no electrons at all and no strange quarks. Then, for charge neutrality, we must have $n_d = 2n_u$ and thus $\mu_d \simeq 2^{1/3}\mu_u$, where we have neglected the masses of the up and down quarks. Employing beta equilibrium, Eq. (3.15), yields $\mu_e \simeq (2^{1/3} - 1)\mu_u$ and therefore $n_e/n \simeq N_c^{-1}(2^{1/3} - 1)^3 n_u/n \simeq 0.002$. This result justifies the neglect of n_e in the first step, and one can easily convince oneself that all neglected effects lead to a further reduction of n_e. In fact, this estimate agrees well with the maximum value of n_e/n.

[24] This behavior is rather different from typical *parametrizations* which have been invented to obtain density dependent quark masses. Usually, these parametrizations depend on the total baryon number density ρ_B only and show no plateau (see, e.g., [161–163]).

minimum of E/A to lower densities and reduces the values of the chemical potentials at the minimum. In fact, μ_s at the minimum drops faster than M_s at the minimum and hence the density of strange quarks remains zero. To avoid this effect we could increase the coupling constant K while decreasing G, e.g., in such a way that the vacuum masses of up and down quarks are kept constant. In order to get $n_s \neq 0$ at the minimum of E/A we have to lower $G\Lambda^2$ to 1.5 and to increase $K\Lambda^5$ to 21.27, almost twice the value of parameter set RKH [145] and more than twice the values of HK [71] or LKW [122]. For these parameters the energy per baryon number is still 1077 MeV. On the other hand, if we decrease the ratio G/K further, this would flip the sign of the effective $q\bar{q}$ coupling in the pseudoscalar-flavor singlet channel, which is dominated by the combination $2G + \frac{2}{3}K(\langle\bar{u}u\rangle + \langle\bar{d}d\rangle + \langle\bar{s}s\rangle)$. In that case there would be no solution for the η'-meson in vacuum.

We could ask whether additional terms in the Lagrangian could help. In particular vector interactions can be quite important at finite density, as we have seen earlier. However, since vector mean fields are repulsive[25] the energy per baryon number will be even larger than before and SQM remains strongly disfavored compared with ordinary nuclei.

We thus conclude that the NJL model does not support the idea of absolutely stable SQM if we want to keep the vacuum properties of the model at least qualitatively unchanged. The main reason is that the strange quark mass stays rather large at densities where chiral symmetry is already approximately restored in the non-strange sector. As a consequence SQM tends to be disfavored against NSQM. But also the effective bag constant in that region is larger than the upper limit of Farhi and Jaffe's window for any value of m_s. This combination is hard to beat. Of course, we cannot exclude that the parameters which have been fixed in vacuum are not appropriate to describe high densities. However, in order to change our conclusions, rather drastic variations would be required.

The situation is not as clear for the possibility of strangelets to be stable against strong but not against weak decays. With the parameters used above (set RKH [145]) we find $E/A = 1210.8\,\text{MeV}$ for quark matter consisting of equal numbers of up, down, and strange quarks. Although this would still be unstable against decay into Λ or Σ baryons ($M_\Lambda = 1116\,\text{MeV}$, $M_\Sigma = 1190\,\text{MeV}$), the difference is smaller than before and could be more sensitive to the parameters (also see Refs. [166,167]).

A quite important effect which has not been taken into account in our analysis is the condensation of diquark pairs ("color superconductivity"). As we will see, color superconductivity indeed provides an additional binding mechanism which is more effective for strange matter ("color–flavor locking") than for non-strange matter. To include these effects, major extensions of the model are necessary. This will be the central issue of the remaining part of this work. In Section 6.2.3 we will come back to the SQM hypothesis and investigate to what extent our conclusions change when diquark condensates are taken into account.

---

[25] This depends of course on the sign of the coupling constant G_V. In a different context, the authors of Refs. [164,165] have employed a vector interaction with an unconventional sign, leading to attractive mean fields. Although this cannot be excluded in general, there are several arguments in favor of the "conventional" choice of sign: (i) This sign emerges naturally, if the interaction is mediated via a heavy boson in the s-channel. For instance, in the Walecka model [109], the ω mean field is repulsive. (ii) This sign can also be derived from a single gluon exchange via Fierz transformation. (iii) In order to describe vector mesons within the NJL model, the vector interaction must be attractive in the space-like components. It is then repulsive in the time-like components, which are relevant in the mean field. In particular, the fitted vector coupling of parameter set LKW [122], has the "conventional" sign and leads to a repulsive vector mean field.

4. Two-flavor color superconductors

So far our discussion was restricted to quark–antiquark condensates, $\langle\bar{q}\Gamma q\rangle$, most importantly the "quark condensate" $\phi = \langle\bar{q}q\rangle$, related to spontaneous chiral symmetry breaking. At low temperatures and densities this led us to a non-trivial phase with $\phi \neq 0$, while the structure of the high-temperature or density regime was rather simple. In fact, if we neglect the current quark masses (chiral limit) and possible vector interactions, the chirally restored phase is completely trivial in the NJL mean-field, and the high-density effects discussed in the previous chapters were mainly based on the imperfect chiral restoration in the presence of quark masses.

It is known, however, that any Fermi system at sufficiently low temperatures is subject to a Cooper instability, as soon as an arbitrarily weak attraction is present ("Cooper theorem" [168]). The heuristic argument is very simple: Consider an infinite system of non-interacting fermions. At $T = 0$ they will form a Fermi sphere, with all states occupied up to the Fermi momentum p_F, and all other states empty. Since the free energy $|E_{\vec{p}} - \mu|$ to create a particle or a hole with momentum $\vec{p}$ vanishes at the Fermi surface, one could create a pair of particles (or holes) directly at the Fermi surface without any free energy cost. If we now turn on a small attraction between the particles, this will further lower the free energy, and thus the original Fermi sphere becomes unstable.

In BCS theory this problem is cured by the formation of a Cooper pair condensate [67]. This leads to a gap in the excitation spectrum, i.e., excitations with vanishing free energy do no longer exist. In ordinary (metallic) superconductors, Cooper pairs are pairs of electrons with opposite momentum and opposite spin. In analogy we should expect that cold deconfined quark matter becomes a "color superconductor" where pairs of quarks condense ("diquark condensate"). In fact, whereas the elementary interaction between electrons, i.e., photon exchange, is repulsive and the Cooper instability in metals only comes about as a subtle effect of phonon exchange in the presence of a screened photon field [169] (see also Ref. [170]), the situation appears much more straightforward in QCD, where already the elementary interaction, i.e., gluon exchange is attractive in certain channels. Therefore the possibility of color superconductivity in high-density QCD matter has already been suggested in 1975 [1], only 2 years after the discovery of asymptotic freedom. However, in spite of further investigations in the 1970s [7,8][26] and 1980s [9], until quite recently not much attention has been payed to this possibility by a wider audience.

This changed at the end of the 1990s, after it had been discovered that in the region of interest, i.e., $\mu \sim 500\,\text{MeV}$, the color superconducting gaps could be of the order of $\Delta \sim 100\,\text{MeV}$ [10,11], much larger than originally expected. Since in standard weak-coupling BCS theory the critical temperature for $J^P = 0^+$-pairing is given by $T_c \simeq 0.57\Delta(T = 0)$ [171], this would also imply a sizeable extension of the color superconducting phases into the temperature direction [172]. Hence, color superconducting phases could be relevant for neutron stars [173,174] and—if we are very lucky—even for heavy-ion collisions [175].

The calculations of Refs. [10,11] have been performed within NJL-type models with instanton-inspired interactions. Later, similar results (sometimes even larger gaps) have been obtained within the instanton model [176,177]. The large gaps have therefore first been attributed to non-perturbative effects which are effectively contained in these interactions, whereas the old analyses were based on a single-gluon exchange. On the other hand, improved treatments of the gluon exchange, which took into account that

[26] Interestingly, the main intention of Barrois' paper, Ref. [7], was to argue in favor of a six-quark condensate as an alternative to a BCS-like diquark pairing.

static magnetic gluons remain unscreened [178], revealed gaps of similar size when the leading-order results are extrapolated from asymptotic densities down to chemical potentials below 1 GeV [179]. Further improvements, however, seem to reduce the gap again by almost one order of magnitude [180].

Soon after the rediscovery of color superconductivity it was realized that the consideration of diquark condensates opens the possibility for a wealth of new phases in the QCD phase diagram (see Fig. 1.1 in the Introduction). For the exploration of these phases, often NJL-type models play a pioneering role. Since the models are relatively simple, they allow for the simultaneous consideration of several different condensates in order to investigate their competition and mutual influence. As we will discuss in the next chapter, this will again be most important when strange quarks are involved. We begin, however, with the two-flavor case. Besides being a somewhat simpler warm-up exercise, it turns out that interesting results can already be obtained for this case.

4.1. Diquark condensates

A diquark condensate is defined as an expectation value

$$\langle q^{\mathrm{T}} \mathcal{O} q \rangle \ , \tag{4.1}$$

where q is a quark field with spin, flavor and color degrees of freedom, and is q^{T} the transposed (not adjoined!) field operator. $\mathcal{O}$ denotes an operator acting in Dirac, flavor and color space,

$$\mathcal{O} = \mathcal{O}_{\mathrm{Dirac}} \otimes \mathcal{O}_{\mathrm{flavor}} \otimes \mathcal{O}_{\mathrm{color}} \ . \tag{4.2}$$

It can also contain derivatives, but we will not consider this possibility here.

4.1.1. Pauli principle

A priori, the only restriction to $\mathcal{O}$ is provided by the Pauli principle. Since

$$q^{\mathrm{T}} \mathcal{O} q = \mathcal{O}_{ij} q_i q_j = -\mathcal{O}_{ij} q_j q_i = -q^{\mathrm{T}} \mathcal{O}^{\mathrm{T}} q \ , \tag{4.3}$$

only totally antisymmetric operators $\mathcal{O}^{\mathrm{T}} = -\mathcal{O}$ survive.

The symmetry properties of various operators under transposition are given in Table 4.1 . In the first line operators in Dirac space are listed. Here $C = \mathrm{i}\gamma^2\gamma^0$ is the matrix of charge conjugation. The five combinations correspond to definite properties of the bilinears $q^{\mathrm{T}} \mathcal{O} q$ under Lorentz transformations, as indicated below, i.e., scalar, pseudoscalar, vector, axial vector, and tensor. In the second and the third line of Table 4.1 we have listed the generators of $U(2)$ and $U(3)$, respectively. The generators of $U(2)$ form a basis for the operator $\mathcal{O}_{\mathrm{flavor}}$ in the two-flavor case. The corresponding diquark bilinears transform as a singlet and a triplet under isospin rotations, i.e., isospin 0 and isospin 1, respectively. Finally, the generators of $U(3)$ form a basis for the operator $\mathcal{O}_{\mathrm{color}}$ or for the operator $\mathcal{O}_{\mathrm{flavor}}$ in the three-flavor case. Here the diquark bilinears can be decomposed into an antisymmetric antitriplet and a symmetric sextet.

Since a totally antisymmetric operator $\mathcal{O}$ can be built as a product of three antisymmetric operators $\mathcal{O}_{\mathrm{Dirac}}$, $\mathcal{O}_{\mathrm{flavor}}$, and $\mathcal{O}_{\mathrm{color}}$, or of one antisymmetric and two symmetric operators, there are obviously many combinations which are in principle permitted. This highlights an important difference to ordinary superconductors where color and flavor degrees of freedom do not exist. In which of these channels condensation takes place cannot be decided on the basis of the Pauli principle alone, but depends on the details of the interaction. (For a general overview about the classification of color superconducting phases, see also Ref. [15].)

Table 4.1
Dirac operators and generators of $U(2)$ and $U(3)$, and their symmetries under transposition. In this table τ_i denote Pauli matrices, and λ_i denote Gell–Mann matrices. $C = i\gamma^2\gamma^0$ is the matrix of charge conjugation

	Antisymmetric	Symmetric
Dirac	$C\gamma_5,\ C,\ C\gamma^\mu\gamma_5$ (S) (P) (V)	$C\gamma^\mu,\ C\sigma^{\mu\nu}$ (A) (T)
$U(2)$	τ_2 singlet	$\underbrace{\mathbb{1},\ \tau_1,\ \tau_3}$ triplet
$U(3)$	$\underbrace{\lambda_2,\ \lambda_5,\ \lambda_7}$ antitriplet	$\underbrace{\mathbb{1},\ \lambda_1,\ \lambda_3,\ \lambda_4,\ \lambda_6,\ \lambda_8}$ sextet

4.1.2. Scalar color-antitriplet diquark condensate

The most important example is the diquark condensate

$$s_{AA'} = \langle q^{\mathrm{T}} C\gamma_5\tau_A\lambda_{A'} q\rangle \ , \tag{4.4}$$

where τ_A and $\lambda_{A'}$ are the antisymmetric generators of $U(N_f)$ and $U(N_c)$, acting in flavor space and in color space, respectively. In this work, we only consider the physical number of colors, $N_c = 3$. Then the $\lambda_{A'}$ denote the three antisymmetric Gell–Mann matrices, λ_2, λ_5, and λ_7. Hence $s_{AA'}$ describes a diquark condensate in the scalar ($J^P = 0^+$) color-antitriplet channel. This corresponds to the most attractive diquark channel for both, one-gluon exchange and instanton-mediated interactions (see Appendix A.3).

In this chapter we discuss the case of two flavors ($N_f = 2$). Then the flavor index in Eq. (4.4) is restricted to $A = 2$, i.e., $s_{AA'}$ is a flavor singlet, describing the pairing of an up quark with a down quark. The three condensates $s_{2A'}$, $A' = 2, 5, 7$, form a vector in color space. Since this vector can always be rotated into the $A' = 2$-direction by a global $SU(3)$-color transformation, we may assume $s_{2A'} = s_{22}\delta_{A'2}$, without loss of generality. In the following, for convenience, we will denote s_{22} by δ,

$$\delta \equiv s_{22} = \langle q^{\mathrm{T}} C\gamma_5\tau_2\lambda_2 q\rangle \ . \tag{4.5}$$

Let us briefly summarize the main properties of a phase with non-vanishing δ. (For further details, see Ref. [12] and references therein.)

As already mentioned, the vector $s_{2A'}$ transforms as an antitriplet under $SU(3)$-color. Denoting the three colors by "red", "green", and "blue", the explicit color–flavor structure of δ reads

$$\delta = -\langle u_r^{\mathrm{T}} C\gamma_5 d_g\rangle + \langle u_g^{\mathrm{T}} C\gamma_5 d_r\rangle + \langle d_r^{\mathrm{T}} C\gamma_5 u_g\rangle - \langle d_g^{\mathrm{T}} C\gamma_5 u_r\rangle \ , \tag{4.6}$$

where u_r corresponds to a red up quark, and so on. This means, with this particular choice, only the red and green quarks participate in the condensate, while the blue ones do not: $SU(3)$-color is broken

down to $SU(2)$.[27] Accordingly, five of the eight gluons receive a mass through the Anderson–Higgs mechanism ("Meissner effect"). The corresponding Meissner masses have been calculated in Ref. [183] (together with the Debye masses) for asymptotically high densities and in Ref. [184] in the instanton liquid model.

Similarly, since the condensate carries a net electric charge, one might expect that also the photon acquires a mass, giving rise to an ordinary (electromagnetic) Meissner effect. In fact, δ is not invariant under a diagonal transformation generated by the electric charge operator. One finds

$$q \to \mathrm{e}^{\mathrm{i}\alpha Q} q \quad \Rightarrow \quad \delta \to \mathrm{e}^{\mathrm{i}\alpha/3}\delta, \quad \text{where } Q = \mathrm{diag}_f(\tfrac{2}{3}, -\tfrac{1}{3}) \ . \tag{4.7}$$

However, since δ transforms in a similar way under the color rotation

$$q \to \mathrm{e}^{\mathrm{i}\alpha' \lambda_8} q \quad \Rightarrow \quad \delta \to \mathrm{e}^{2\mathrm{i}\alpha'/\sqrt{3}}\delta \ , \tag{4.8}$$

one can find a linear combination

$$\tilde{Q} = Q - \tfrac{1}{2\sqrt{3}}\lambda_8 \equiv Q - \mathrm{diag}_c(\tfrac{1}{6}, \tfrac{1}{6}, -\tfrac{1}{3}) \ , \tag{4.9}$$

under which δ remains invariant. Indeed, the pairs in Eq. (4.6) have vanishing $\tilde{Q}$ charge, i.e., δ is $\tilde{Q}$ neutral. The physical relevance of $\tilde{Q}$ is related to the fact that the photon and the eighth gluon mix in the presence of δ, resulting in a state which becomes massive, while the orthogonal state remains massless. This is quite analogous to the mixing which gives rise to the massive Z-boson and the massless photon in electroweak theory. In the present case $\tilde{Q}$ is the charge the massless combination (the "rotated photon") is coupled to.

Like all diquark condensates, δ breaks the $U(1)$ symmetry, related to baryon number conservation, down to Z_2.[28] However, analogously to the case of electromagnetism, one can construct a new unbroken global symmetry as a combination of $U(1)$ with the color rotation Eq. (4.8). Thus, there is a conserved "rotated" baryon number.

As a flavor singlet, δ is invariant under isospin transformations $SU(2)_V$. One can easily show that δ is also invariant under the corresponding axial transformations $SU(2)_A$, i.e., δ leaves chiral symmetry unbroken. Hence, there is no global symmetry broken by δ and, consequently, there are no Goldstone bosons.

---

[27] Strictly speaking, gauge symmetries cannot be broken spontaneously [181] (see, however, Ref. [182] for possible caveats). This also applies to the "spontaneous breaking" of the electromagnetic $U(1)$ in ordinary superconductors or the breaking of the $SU(2)_L \times U(1)_Y$ in electroweak theory. In all these cases the spontaneous symmetry breaking can only be discussed after gauge fixing. Adopting Rajagopal and Wilczek's point of view, we therefore interpret the spontaneous breaking of a gauge symmetry as a "convenient fiction" [12] in a fixed gauge. The important point is that this "fiction" leads to correct predictions for "real", i.e., gauge invariant, observables. Whereas the vector $(s_{2A'})$, and thus δ, is not a gauge invariant quantity, the gap in the quasiparticle spectrum only depends on its "length", $|\delta| = \sqrt{|s_{22}|^2 + |s_{25}|^2 + |s_{27}|^2}$, which is gauge invariant. This may also be taken as some justification for studying color superconductivity within NJL-type models, although these models are only symmetric under global $SU(3)$-color.

[28] In finite systems, the total baryon number is of course conserved. The correct interpretation is that there are long-range correlations $C(y,x) \sim \langle q^\dagger(y) q^\dagger(y) q(x) q(x) \rangle$, describing the superfluid transport of a fermion pair from a point x to a distant point y. In the grand canonical treatment of infinite systems this is a result of the factorization $C(y,x) \sim \langle q^\dagger(y) q^\dagger(y) \rangle \langle q(x) q(x) \rangle = |\langle qq \rangle|^2$.

We have already pointed out in the introduction to this chapter that a non-vanishing diquark condensate leads to a gap in the quark excitation spectrum. Typically, the quasiparticle dispersion laws take the form

$$\omega_{\mp}(\vec{p}) = \sqrt{(E_p \mp \mu)^2 + |\Delta|^2}\ , \tag{4.10}$$

where ω_- corresponds to the free energy needed to create a particle above or a hole below the Fermi surface and ω_+ is the corresponding antiparticle term. $E_p = \sqrt{\vec{p}^2 + m^2}$ is again the on-shell energy of a non-interacting quark with mass m. Thus, there is a minimal free energy, $\delta F = 2|\Delta|$, which is needed to excite a particle–hole pair from the ground state. In general, Δ is an energy and momentum dependent quantity and can be different for quarks and antiquarks, but we may ignore this in this more qualitative discussion.

Like in the case of chiral symmetry breaking, the most transparent, but also most elaborate way to derive Δ is via an explicit pairing ansatz for the ground state $|\text{g.s.}\rangle$ as a coherent state of red and green up and down quarks with zero total momentum [10,12],

$$\begin{aligned}|\text{g.s.}\rangle = \prod_{\vec{p},s,c,c'} & [\cos\theta_s^b(\vec{p}) + \varepsilon_{3cc'}\, \mathrm{e}^{\mathrm{i}\xi_s^b(\vec{p})}\, \sin\theta_s^b(\vec{p}) b^\dagger(\vec{p},s,u,c) b^\dagger(-\vec{p},s,d,c')] \\ & \times [\cos\theta_s^d(\vec{p}) + \varepsilon_{3cc'}\mathrm{e}^{\mathrm{i}\xi_s^d(\vec{p})} \sin\theta_s^d(\vec{p}) d^\dagger(\vec{p},s,u,c) d^\dagger(-\vec{p},s,d,c')]|0\rangle\ .\end{aligned} \tag{4.11}$$

Here we have used the same notation as in Eq. (2.35). We have left out the part of the unpaired blue quarks, which decouples from the paired sector. The upper line describes particle–particle and, if measured relative to a filled Fermi sea, hole–hole pairing and basically corresponds to a standard BCS ansatz. The lower line corresponds to antiparticle–antiparticle pairing. This term is of course missing in non-relativistic descriptions.

For given chemical potential μ, the variational functions $\theta_s^{b,d}(\vec{p})$ and $\xi_s^{b,d}(\vec{p})$ are fixed by minimizing the free energy $\langle\text{g.s.}|\hat{H} - \mu\hat{N}|\text{g.s.}\rangle$, where $\hat{H}$ is the Hamiltonian and $\hat{N}$ is the quark number operator. This minimization problem can be transformed into a self-consistency problem for the gap parameter Δ. Details of this gap equation depend of course on the interaction. For NJL-type models where the interaction is short ranged it is typically of the form

$$\Delta = 8H\Delta \int \frac{\mathrm{d}^3p}{(2\pi)^3} \left\{ \frac{1}{\omega_-(\vec{p})} + \frac{1}{\omega_+(\vec{p})} \right\}\ , \tag{4.12}$$

where H is the coupling constant in the scalar color-antitriplet channel. (This particular equation will be derived in Section 4.3.2 within a more generalized framework.)

Obviously, Eq. (4.12) always has a trivial solution, $\Delta = 0$. On the other hand, for $\mu > m$ and $\Delta \to 0$, the integral on the r.h.s. becomes logarithmically divergent, due to a pole of $1/\omega_-$ at the Fermi surface. Thus, even for arbitrarily small positive (attractive) values of H, there is always a non-trivial solution which approximately behaves like

$$\Delta \propto \exp\left(-\frac{\text{const.}}{H}\right)\ . \tag{4.13}$$

The logarithmic divergence which guarantees the existence of the non-trivial solution is the formal manifestation of the Cooper instability. This feature is qualitatively different from the chiral gap

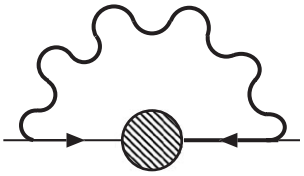

Fig. 4.1. Anomalous quark self-energy diagram determining the diquark gap at asymptotically large density. The wavy line symbolizes a gluon. The shaded blob corresponds to the insertion of a diquark condensate.

equation, Eq. (2.23), where non-trivial solutions require a certain minimal value of the coupling constant.[29]

4.2. Interaction

For the explicit computation of the color superconducting gaps and related quantities, we have, of course, to specify the quark–quark interaction. Unfortunately, this interaction in poorly known in the most interesting regime of a few times nuclear matter density. Before we introduce the NJL-type interactions which will be the main basis of our further investigations, we briefly discuss the microscopic (QCD based) approach at asymptotically large densities.

4.2.1. Asymptotic densities

Because of asymptotic freedom, the QCD coupling constant becomes small at large momentum scales and QCD can be treated perturbatively (see Eq. (1.4)). Since at finite density the scale is set by the Fermi momentum, it was realized rather early that QCD becomes relatively simple in the high-density phase [1] and a description starting from first principles should be possible. This was also the basis of the early studies of color superconductivity [7–9]. More recently, the large gaps which have been found within the more phenomenological approaches of Refs. [10,11] have also evoked renewed interest in asymptotic studies (see Refs. [14,15] for recent reviews).

The gap equation for the color superconducting phase can be derived within Dyson–Schwinger formalism [175,179,188]. In the weak-coupling limit, the interaction between quarks is dominated by single gluon exchange. This amounts to evaluating the quark self-energy

$$\Sigma(p) = -\mathrm{i}g^2 \int \frac{\mathrm{d}^4k}{(2\pi)^4}\, \Gamma^\mu_a S(k) \Gamma^\nu_b D^{ab}_{\mu\nu}(k-p)\ , \tag{4.14}$$

where $S(k)$ and $D^{ab}_{\mu\nu}(k-p)$ denote quark and gluon propagators, respectively, g is the QCD coupling constant, and Γ^μ_a is the quark–gluon vertex. To leading order it is basically the free vertex $\gamma^\mu\lambda_a$. The essential part of this diagram is depicted in Fig. 4.1. Because of the non-conservation of (ordinary) baryon number, two quarks can be absorbed or created by the condensate (shaded blob). This gives rise to a so-called anomalous contribution to the self-energy which is proportional to the gap. This will be discussed in more details in Section 4.3.1.

[29] Formally, in Eq. (4.12) the same is true for $\mu < m$. Then the trivial solution corresponds to zero density, i.e., there is no Fermi sphere which could become unstable. Nevertheless, there could be a non-trivial solution of the gap equation, if H is sufficiently strong [176,185–187].

If the gluon in Eq. (4.14) is replaced by a point interaction we arrive at a standard BCS-type gap equation, like in Eq. (4.12). Originally, it was concluded from this analogy that the gap should behave like $\exp(-\text{const.}/g^2)$ at weak coupling, leading to rather small gaps [9]. However, it has long been known for ordinary superconductors that the behavior can be rather different for long-range forces due to retardation effects [189].

In Ref. [179], the gluon propagator was taken to be of the general form [107],

$$D^{ab}_{\mu\nu}(q) = \left(\frac{P^{\mathrm{L}}_{\mu\nu}}{q^2 - F(q_0, |\vec{q}|)} + \frac{P^{\mathrm{T}}_{\mu\nu}}{q^2 - G(q_0, |\vec{q}|)} - \xi \frac{q_\mu q_\nu}{q^4} \right) \delta_{ab} \ , \tag{4.15}$$

where $P^{\mathrm{L,T}}_{\mu\nu}$ are longitudinal and transverse projectors, respectively, and ξ is a gauge parameter. The function F describes the Debye screening of the longitudinal (electric) gluons. The transverse (magnetic) gluons are dynamically screened due to Landau damping, but there is no screening of the static ($q_0 = 0$) modes. To first approximation [179]

$$F = 2N_f \frac{g^2\mu^2}{4\pi^2} \quad \text{and} \quad G = \frac{\pi}{4} \frac{q^0}{|\vec{q}|} F \ . \tag{4.16}$$

Since typical frequencies are of the order of the gap, $q^0 \sim \Delta$, the magnetic gluons cause a second logarithmic divergence, such that the integral in Eq. (4.14) diverges like $(\ln \Delta)^2$, rather than $\ln \Delta$. In this way the behavior of the gap is changed to

$$\frac{\Delta}{\mu} \propto \exp\left(-\frac{3\pi^2}{\sqrt{2}g} \right) \ , \tag{4.17}$$

which has first been found by Son [178] based on a renormalization group study. Afterwards this has been confirmed by several authors within the Dyson–Schwinger approach [172,175,179,188]. In particular, Eq. (4.17) remains valid if, instead of Eq. (4.16), F and G are calculated within hard dense loop approximation [179].

Eq. (4.17) has the striking consequence that asymptotically Δ grows to arbitrarily large values although the coupling becomes weaker. Note that $g = \sqrt{4\pi\alpha_s}$ behaves like $1/\sqrt{\ln \mu}$, where we have assumed that the momentum scale Q is proportional to μ. But also when the leading-order results are extrapolated downwards into the (astro-) physically more interesting regime below 1 GeV, gaps of the order ~ 100 MeV are found [179].

However, although appreciated as nice support for the results based on phenomenological interactions it is clear that the perturbative approach (i.e., one-gluon exchange) cannot be trusted at densities of relevance. To estimate the range of validity of these calculations let us assume (quite optimistically) that the perturbative regime begins at $Q \approx 1.5\,\mathrm{GeV}$ and identify this momentum scale with the chemical potential. For two massless flavors this corresponds to a baryon number density $\rho_B = 2/(3\pi^2)\mu^3 \approx 30\,\mathrm{fm}^{-3}$, which is about 175 times nuclear saturation density, well beyond the maximum densities of about $10\rho_0$ expected in the centers of compact stars. On the other hand, at $Q \approx 1.5\,\mathrm{GeV}$ the coupling is still rather large, $\alpha_s \simeq 0.35$ [27], i.e., $g \simeq 2$.

In Ref. [64] Rajagopal and Shuster employed the gauge parameter ξ in Eq. (4.15) to study the relevance of higher-order terms. Since (in principle) the gap in the excitation spectrum is an observable and thus a gauge invariant quantity, it must not depend on ξ. In Ref. [179] Schäfer and Wilczek showed, that the gap equation indeed becomes independent of ξ at infinitely large chemical potential and therefore

they dropped the ξ-dependent terms in their calculations. In contrast, the authors of Ref. [64] kept these terms and investigated the ξ-dependence of the result at given chemical potential. While they confirmed that these terms become negligible for $\mu \to \infty$, they found that they only begin to become small for couplings $g \lesssim 0.8$. Again identifying the momentum scale Q with the chemical potential, this corresponds to $\mu \gg 10^8$ MeV ($\rho_B \gg 5 \times 10^{16} \rho_0$)! Moreover, since the gap is dominated by almost collinear scattering, $|\vec{k} - \vec{p}| \ll \mu$, it is likely that the relevant momentum scale is much lower than μ, as also indicated by renormalization group studies [190]. This would push up the "asymptotic regime" even further.

Of course, the range of validity of the calculations can be extended by taking into account higher-order corrections. In the mean time a complete analysis to subleading order in g has been performed [180,191]. Nevertheless, in view of our "optimistic estimate" above, it is very unlikely that any calculation that is based on the use of perturbation theory can be reliably extrapolated down to the physically interesting regime.

4.2.2. NJL-type interactions

Alternatively, color superconductivity can be studied within models which are based on vacuum phenomenology, like instanton models [176,177] or NJL-type models, e.g., Refs. [10,11,68,108]. It is obvious that the use of models cannot overcome the problems discussed at the end of the previous section: While the gluon-exchange based studies become exact at asymptotic densities, but cannot reliably be extrapolated down to densities at physical relevance, NJL-type interactions are mostly constrained by fitting vacuum properties, and it is not clear whether the parameters obtained in this way can still be trusted in the deconfined phase.

In principle, instanton models are in a somewhat better situation, since they are based on a semiclassical description of the QCD vacuum and therefore less phenomenological. In fact, the single instanton solutions and the corresponding zero modes at finite chemical potential are known [192,193]. However, in the instanton liquid model there are additional parameters, namely the average instanton size $\bar{\rho}$ and the instanton density $1/\bar{R}^4$, which are well constrained in vacuum but not yet fully under control at finite density. In Ref. [176] these parameters have been kept constant. On the other hand, at finite density, instantons and anti-instantons could cluster to molecules, rather than being randomly distributed [177]. In this way the characteristics of the effective quark–antiquark and quark–quark interactions can change considerably since the strength of the vertices related to isolated instantons (the 't Hooft interaction) decreases, while new vertices with different quantum numbers emerge [194]. In particular, in contrast to isolated instantons, molecules do not break the $U_A(1)$ symmetry. As suggested in Ref. [195], instantons could also be lined up in long diquark chains. The competition between these possibilities has been investigated in Ref. [194] within a simple statistical mechanics approach, but the issue is not yet completely settled.

It is clear that these uncertainties remain, if instanton effects are approximated by NJL-type interactions (e.g., neglecting the momentum dependence of the vertices), and the situation is even worse for general NJL models, which are based on symmetries and vacuum phenomenology only. Another problem which arises in this case is the fact that the coupling constants in the quark–quark channel cannot unambiguously be related to the coupling constants in the quark–antiquark channel. To see this, consider an NJL-type interaction of the form

$$\mathscr{L}_{\text{int}} = g_I (\bar{q} \hat{\Gamma}^{(I)} q)^2 \ , \tag{4.18}$$

where $\hat{\Gamma}^{(I)}$ is an operator corresponding to the quark–antiquark channel I. As detailed in Appendix A, we can perform a Fierz transformation to describe the effect of the total (direct plus exchange) interaction by a Lagrangian

$$\mathscr{L}_{q\bar{q}} = \sum_M G_M (\bar{q}\hat{\Gamma}^{(M)} q)^2 \ , \tag{4.19}$$

where the sum runs over all quark–antiquark channels M and the effective coupling constants G_M can be calculated from the g_I. Of course, in order to avoid double counting, exchange diagrams should not be evaluated explicitly when using this Lagrangian instead of $\mathscr{L}_{\rm int}$.

Analogously, we can perform a Fierz transformation into the particle–particle channel to derive an effective quark–quark interaction

$$\mathscr{L}_{qq} = \sum_D H_D (\bar{q}\hat{\Gamma}^{(D)} C\bar{q}^{\rm T})(q^{\rm T} C\hat{\Gamma}^{(D)} q) \ , \tag{4.20}$$

where D corresponds to the various diquark channels. Thus, if we know the underlying Lagrangian $\mathscr{L}_{\rm int}$, the quark–antiquark coupling constants G_M and the quark–quark coupling constants H_D are uniquely fixed.

However, often we do not have an underlying theory. In this case we may directly start from $\mathscr{L}_{q\bar{q}}$, e.g., in order to describe the meson sector in vacuum, and only impose constraints according to the symmetries. This is, what we have usually done in this work. In this case, if we know *all* G_M (including those in the color octet channels), we still can calculate the H_D. However, usually only an incomplete subset of the coupling constants G_M can be determined by fitting data. In this case, and without underlying theory, there is no unique solution for the quark–quark coupling constants H_D.

A popular example for $\mathscr{L}_{\rm int}$ is the color current interaction

$$\mathscr{L}_{\rm int} = -g(\bar{q}\gamma^\mu \lambda_a q)^2 \ , \tag{4.21}$$

which can be thought of as abstracted from the QCD Lagrangian by converting the original $SU(N_c)$ gauge symmetry into a global symmetry of the quark color currents. For two flavors and three colors, the corresponding effective quark–antiquark Lagrangian reads (see Appendix A.3)

$$\mathscr{L}_{q\bar{q}} = G_S[(\bar{q}q)^2 + (\bar{q}\,\vec{\tau} q)^2 + (\bar{q}\mathrm{i}\gamma_5 q)^2 + (\bar{q}\mathrm{i}\gamma_5\vec{\tau} q)^2] + \cdots \ , \tag{4.22}$$

with $G_S = \frac{8}{9}\, g$. The ellipsis stands for vector and axial-vector terms and for color-octet terms. (Note that the terms we have written explicitly are just the Lagrangian $\mathscr{L}_1$ defined in Eq. (2.76).)

For the effective quark–quark Lagrangian one obtains

$$\mathscr{L}_{qq} = H_S \sum_{A=2,5,7} [(\bar{q}\mathrm{i}\gamma_5\tau_2\lambda_A C\bar{q}^{\rm T})(q^{\rm T} C\mathrm{i}\gamma_5\tau_2\lambda_A q) + (\bar{q}\tau_2\lambda_A C\bar{q}^{\rm T})(q^{\rm T} C\tau_2\lambda_A q)] + \cdots , \tag{4.23}$$

with $H_S = \frac{2}{3}\, g$. Here the ellipsis comprises vector and axial-vector terms, as well as color-sextet terms.

Comparing these results, we find that the coupling constant H_S in the scalar diquark channel is related to the coupling constant G_S in the scalar quark–antiquark channel as $H_S : G_S = 3 : 4$. Accidentally, the same relation follows if we start from a two-flavor instanton-induced interaction (see Appendix A.3). Nevertheless, this relation is not universal. For instance, if we choose $\mathscr{L}_{\rm int} = \mathscr{L}_1$ as defined in Eq. (2.76),

we still obtain effective interactions of the form of Eqs. (4.22) and (4.23), but with $G_S = G_1$ and $H_S = 0$. Thus, if we only know the value of G_S, e.g., from a fit to the pseudoscalar spectrum, we cannot infer the value of H_S without making assumptions about the underlying interaction.

If the quark–antiquark interaction has been constrained empirically, the most natural solution to this problem would be to determine the quark–quark coupling constants empirically, too. Unfortunately, the analog to the meson spectrum would be a diquark spectrum, which of course does not exist in nature. This means, one would have to fit the baryon spectrum by solving Fadeev equations, which is much more difficult. Fits which have been performed so far seem to be consistent with the one-gluon relation $H_S : G_S = 3 : 4$, but there are large uncertainties. In this context it would also be interesting to look at the recently discovered $\Theta^+(1540)$ baryon [196–200] which is a candidate to be a $uudd\bar{s}$ pentaquark, being a member of a flavor antidecuplet. This state and in particular its small width have been predicted some time ago by Praszalowicz [201] and by Diakonov et al. [202] within the chiral soliton model (but see Refs. [203,204] for controversial opinions). However, as recently suggested by Jaffe and Wilczek [205], it could also be understood as two highly correlated *ud* pairs, forming a scalar color and flavor antitriplet, bound to an $\bar{s}$ quark. If true, this could provide interesting information about the interaction in the scalar diquark channel. Unfortunately, there are many competing scenarios, like the model of Shuryak and Zahed, where one of the scalar diquarks is replaced by a tensor one [206].

It is clear that NJL-type models cannot yield quantitative predictions, e.g., about the size of the color superconducting gap, until more information about the parameters is available. Ultimately, this information must come from "outside", e.g., from Dyson–Schwinger calculations, improved instanton models or, if possible, from lattice calculations. The NJL coupling constants may then play the role of Fermi liquid parameters, possibly derived using renormalization group techniques [207,208], allowing for a simplified description of the quark matter in a given density regime.[30]

At present, NJL models are basically used in this way although, of course, on a much more speculative basis. We have already pointed out that the simplicity of the NJL interactions allows for the simultaneous investigation of several different condensates, uncovering important interdependencies which are much harder to explore in other approaches. This will be discussed in more technical details in the next section and stays the most important theme of this work. Lacking better prescriptions, we will usually employ vacuum parameters and simple relations, like $H_S : G_S = 3 : 4$, to fix the diquark coupling. With these parameters, we typically find a scalar diquark gap of the order $\sim 100\,\mathrm{MeV}$, in agreement with other calculations, e.g. [10,11]. Of course, since the latter were based on similar assumptions, this cannot be taken as a proof for the correctness of these numbers. However, we can study what happens to them if additional effects are taken into account. Our following investigations should mainly be interpreted in this way.

When dealing with NJL-type models we should also keep in mind that the Lagrangian is only *globally* symmetric under $SU(3)$-color. Hence, strictly speaking, there is no color superconductivity, but only "color superfluidity". The spontaneous breaking of the global $SU(3)$-color symmetry leads to false Goldstone modes which are absent in QCD due to the Meissner effect. (The "would-be" Goldstone bosons are "eaten" by the gluons.) Therefore the spectrum of bosonic excitations has to be interpreted with great care. For the fermionic degrees of freedom the replacement of a gauge symmetry by a global one should be less problematic.

[30] Non-Fermi liquid corrections to normal conducting quark matter have been investigated in Refs. [209–211].

4.3. Interplay with other condensates

In Chapter 2 we have discussed the properties of two-flavor quark matter, mostly concentrating on the role of the quark (–antiquark) condensate

$$\phi = \langle \bar{q} q \rangle \ , \tag{4.24}$$

which is related to chiral symmetry breaking and the non-trivial vacuum structure. We have now seen that there are good arguments to believe that two-flavor quark matter at high density is dominated by the scalar diquark condensate δ (Eq. (4.5)), which has been discussed in some details in Section 4.1.2. In the chiral limit, and assuming that the chiral phase transition coincides with the deconfinement one, it is clear that δ and ϕ characterize two disjoint regimes: In the hadronic phase we have $\phi \neq 0$ but there are no free quarks which could condense, while in the deconfined phase $\phi = 0$ if chiral symmetry is restored. The situation is of course different when chiral symmetry is explicitly broken by a non-vanishing current quark mass. In this case, as we have seen before, ϕ cannot vanish completely and coexists with the diquark condensate above μ_c. The question is then, whether this has sizeable effects or whether we can safely neglect the influence of ϕ in the deconfined phase.

Obviously, NJL-type models which have been employed for studying both, spontaneous chiral symmetry breaking and diquark condensation, offer the nice possibility to study both condensates and their interplay on the same footing. This has been done first by Berges and Rajagopal [68]. Their results are in qualitative agreement with our general considerations above: In the chiral limit, they find a first-order phase transition from the vacuum where $\phi \neq 0$ and $\delta = 0$ to a high-density phase with $\delta \neq 0$ and $\phi = 0$. After including a non-vanishing current quark mass, δ remains zero below the phase transition, but ϕ does no longer drop to zero at the transition point. In fact, just above μ_c, the gaps related to δ and ϕ are of similar magnitude.

We can go further [212]: In a fully self-consistent treatment, one has to include all possible condensates which are not protected by unbroken symmetries.[31] First of all, at finite density, Lorentz invariance is broken and therefore the existence of Lorentz non-invariant expectation values becomes possible. The most obvious example is of course the density itself,

$$n = \langle \bar{q} \gamma^0 q \rangle \ , \tag{4.25}$$

which transforms like the time component of a 4-vector. We have already seen in Section 2.3.2 that the influence of n on the phase structure can be quite large if vector interactions are present.

In a similar way, there could be a Lorentz non-invariant diquark condensate [9,165,213],

$$\delta_0 = \langle q^{\mathrm{T}} C \gamma^0 \gamma_5 \tau_2 \lambda_2 q \rangle \ , \tag{4.26}$$

which also transforms like the time component of a 4-vector.

Moreover, since in the presence of δ or δ_0 color $SU(3)$ is broken, there is no reason to assume that all other condensates are color-$SU(3)$ invariant in this state. For instance, we should expect that the contributions of red and blue quarks, ϕ_r and ϕ_b, to the quark condensate ϕ could be different, thus giving

[31] This does not include equivalent condensates, i.e., condensates which can be obtained from the considered ones by one of the spontaneously broken symmetry transformations.

Table 4.2
Symmetries conserved (✓) or not conserved (**x**) by the condensates considered in this section

	n	n_8	ϕ	ϕ_8	δ	δ_0
Lorentz	x	x	✓	✓	✓	x
$U(1)$	✓	✓	✓	✓	x	x
$U_A(1)$	✓	✓	x	x	x	✓
$SU(2)_V$	✓	✓	✓	✓	✓	✓
$SU(2)_A$	✓	✓	x	x	✓	x
$SU(3)_c$	✓	x	✓	x	x	x

rise to a non-vanishing expectation value

$$\phi_8 = \langle \bar{q}\lambda_8 q\rangle = \frac{2}{\sqrt{3}}\,(\phi_r - \phi_b)\ . \tag{4.27}$$

Here we have assumed that the condensate of green quarks and antiquarks, ϕ_g, is equal to ϕ_r, because we do not want to break the color-$SU(2)$ subgroup which was left unbroken by δ and δ_0.

Similarly, the densities of red and blue quarks will in general not be the same, i.e., in addition to the total number density $n = 2n_r + n_b$ there could be a non-vanishing expectation value

$$n_8 = \langle \bar{q}\gamma^0\lambda_8 q\rangle = \frac{2}{\sqrt{3}}(n_r - n_b)\ . \tag{4.28}$$

Since these color-symmetry breaking expectation values, induced by the presence of color-symmetry breaking diquark condensates, could in turn influence the properties of the diquark condensates, in principle, all condensates should be studied in a self-consistent way.

The various condensates and their symmetry properties are listed in Table 4.2. Given that Lorentz invariance, color $SU(3)$, and chiral symmetry are broken, this is the minimal set of condensates one has to take into account in a fully self-consistent calculation. Of course, if favored by the interaction, other condensates which break additional symmetries are possible. One example, a spin-1 condensate which breaks the rotational invariance, will be discussed in Section 4.4.

4.3.1. Hartree–Fock approach

To illustrate the necessity of including the additional condensates, Eqs. (4.25)–(4.28), in a "fully self-consistent calculation" and what we mean by this term we consider the generic NJL-type Lagrangian

$$\hat{\mathscr{L}} = \mathscr{L} + \mu q^\dagger q = \bar{q}(\mathrm{i}\partial\!\!\!/ - m + \mu\gamma^0)q + g_i(\bar{q}\Gamma_i q)^2\ , \tag{4.29}$$

where Γ_i are arbitrary local operators in Dirac, flavor and color space, and g_i are the corresponding coupling constants. (We implicitly assume a sum over i.) We have already added a chemical potential term $\mu q^\dagger q$, which is formally equivalent to a Lorentz non-invariant energy term in the Lagrangian.

It is quite obvious that the fundamental Bogoliubov–Valatin approach to derive the gap equation becomes extremely involved when more than one condensate is present.[32] In this case it is most convenient

[32] A variational analysis, which includes several color and flavor-dependent diquark and quark–antiquark condensates has recently been presented in Ref. [214].

to apply Nambu–Gorkov formalism [215] (see also [171,216]). To that end, one introduces charge conjugated fields and operators,

$$q^{\mathrm{C}}(x) = C\bar{q}^{\mathrm{T}}(x), \quad \bar{q}^{\mathrm{C}}(x) = q^{\mathrm{T}}(x)C, \quad \Gamma_i^{\mathrm{C}} = -C\Gamma^{\mathrm{T}}C \ , \tag{4.30}$$

and rewrites Eq. (4.29) as

$$\hat{\mathscr{L}} = \tfrac{1}{2}\,[\bar{q}\,(\mathrm{i}\partial\!\!\!/ - m + \mu\gamma^0)q + \bar{q}^{\mathrm{C}}(-\mathrm{i}\overleftarrow{\partial\!\!\!/} - m - \mu\gamma^0)q^{\mathrm{C}}] + \tfrac{1}{4}\,g_i[(\bar{q}\Gamma_i q) + (\bar{q}^{\mathrm{C}}\Gamma_i^{\mathrm{C}}q^{\mathrm{C}})]^2 \ . \tag{4.31}$$

Next, one formally doubles the number of degrees of freedom by treating q and q^{C} as independent variables. To this end one defines a bispinor field Ψ and operators $\hat{\Gamma}_i$ in the corresponding bispinor space,

$$\Psi(x) = \frac{1}{\sqrt{2}}\begin{pmatrix} q(x) \\ q^{\mathrm{C}}(x) \end{pmatrix}, \quad \hat{\Gamma}_i = \begin{pmatrix} \Gamma_i & 0 \\ 0 & \Gamma_i^{\mathrm{C}} \end{pmatrix} \ . \tag{4.32}$$

In this way the Lagrangian can be written in a rather compact form

$$\hat{\mathscr{L}} = \bar{\Psi}\tilde{S}_0^{-1}(x)\Psi + g_i(\bar{\Psi}\hat{\Gamma}_i\Psi)^2 \ , \tag{4.33}$$

quite similar to the original Lagrangian, Eq. (4.29). Here $\tilde{S}_0^{-1}(x)$ plays the role of the inverse bare propagator of the bispinor fields in coordinate space. Its Fourier transform in momentum space is given by

$$S_0^{-1}(p) = \begin{pmatrix} p\!\!\!/ + \mu\gamma^0 - m & 0 \\ 0 & p\!\!\!/ - \mu\gamma^0 - m \end{pmatrix} \ . \tag{4.34}$$

Now we want to take into account self-energy contributions to the propagator due to the interaction. According to the quantum numbers of the six different condensates discussed in the previous section we make the following ansatz:

$$S^{-1}(p) = S_0^{-1}(p) - \hat{\Sigma}(p) = \begin{pmatrix} p\!\!\!/ + \hat{\mu}\gamma^0 - \hat{M} & (\Delta + \Delta_0\gamma^0)\gamma_5\tau_2\lambda_2 \\ (-\Delta^* + \Delta_0^*\gamma^0)\gamma_5\tau_2\lambda_2 & p\!\!\!/ - \hat{\mu}\gamma^0 - \hat{M} \end{pmatrix} \ , \tag{4.35}$$

where

$$\hat{M} = M_0 + M_8\lambda_8 \quad \text{and} \quad \hat{\mu} = \tilde{\mu} + \tilde{\mu}_8\lambda_8 \tag{4.36}$$

are matrices in color space, describing color dependent constituent quark masses and color-dependent effective chemical potentials. Unlike the bare inverse propagator, Eq. (4.35) also contains non-diagonal elements in Nambu–Gorkov space. These connect quark fields with charge conjugated quark fields and thus describe self-energy contributions due to diquark condensates. Here the advantage of the bispinor notation becomes obvious.

We can now proceed analogously to Section 2.2.1: We first invert Eq. (4.35) to calculate the propagator $S(p)$. The result is a rather lengthy expression which is given in Appendix B. Here we just mention that, due to the non-diagonal Nambu–Gorkov components in Eq. (4.35), the propagator also gets non-diagonal components which are the origin of the anomalous propagation mentioned earlier. Using this propagator we then calculate the quark self-energy in some given approximation scheme. Identifying this with $\hat{\Sigma}$ in Eq. (4.35) we finally obtain a set of self-consistent gap equations for the parameters M_0, M_8, $\tilde{\mu}$, $\tilde{\mu}_8$, Δ, and Δ_0 of our ansatz.

Fig. 4.2. Hartree (left) and Fock (right) contribution to the quark self-energy. The bold solid lines indicate dressed Nambu–Gorkov propagators. The dotted lines symbolize the interaction.

In the following, we consider the quark self-energy in Hartree–Fock approximation,

$$\hat{\Sigma} = \hat{\Sigma}_{\mathrm{H}} + \hat{\Sigma}_{\mathrm{F}} \tag{4.37}$$

which is illustrated in Fig. 4.2. The Hartree term (left) is given by

$$\hat{\Sigma}_{\mathrm{H}} = 2\mathrm{i}g_i \int \frac{\mathrm{d}^4 p}{(2\pi)^4} \frac{1}{2} \mathrm{Tr}[\hat{\Gamma}_i S(p)] \hat{\Gamma}_i \ . \tag{4.38}$$

Here the trace is to be taken over Dirac, flavor, color, and the two bispinor degrees of freedom. Note that in order to correct for the artificial doubling of the number of degrees of freedom we have to introduce a factor $\frac{1}{2}$ in front of the trace.[33] It is immediately clear from Eq. (4.38) that in Hartree approximation only self-energy contributions proportional to the operators $\hat{\Gamma}_i$ can arise. In particular, since in our case all operators are diagonal in Nambu–Gorkov space, Σ_{H} is also diagonal, and hence $\Delta = \Delta_0 = 0$. In order to obtain non-vanishing diquark gaps we must therefore consider the Fock contribution to the self-energy, which is given by

$$\hat{\Sigma}_{\mathrm{F}} = -2\mathrm{i}g_i \int \frac{\mathrm{d}^4 p}{(2\pi)^4} \hat{\Gamma}_i S(p) \hat{\Gamma}_i \ . \tag{4.39}$$

Unlike the Hartree term its operator structure is not restricted to terms proportional to the $\hat{\Gamma}_i$. In fact, because of the rather complicated form of the propagator, it is quite difficult to "see" without explicit calculation how the matrix $\hat{\Gamma}_i S(p) \hat{\Gamma}_i$ looks like. Thus, if we started with some arbitrary inverse propagator $S^{-1}(p)$, it could happen that the Hartree–Fock self-energy calculated from the corresponding propagator contains operators which are not present in the original ansatz. For instance, if we started from Eq. (4.35), but without allowing for color dependent constituent quark masses (i.e., terms proportional to λ_8 in the diagonal Nambu–Gorkov components) it could turn out that the resulting Hartree–Fock self-energy contains such terms, and the equations cannot be closed. If in such a case we simply ignored the extra terms, this would be an example of a "not fully self-consistent" calculation.

As pointed out in the previous section, the only way to prevent this problem is to allow for all possible terms which are consistent with the unbroken symmetries of the system. Here "unbroken" means unbroken, including all other condensates. Hence, if we add a new condensate which breaks additional symmetries, this can induce further condensates which then have to be taken into account. Since

[33] This can be seen most easily if we consider a scalar interaction $\Gamma_i = \Gamma_i^{\mathrm{C}} = \mathbb{1}$ and the simplified case $M_0 \neq 0$, but $M_8 = \tilde{\mu} = \tilde{\mu}_8 = \Delta = \Delta_0 = 0$. In this case $S^{-1}(p)$ is easily inverted and $S(p)$ is diagonal in Nambu–Gorkov space with $S_{11} = S_{22}$ being ordinary fermion propagators with mass M_0. Taking the trace gives thus twice the result without fermion doubling, which has to be corrected by the factor $\frac{1}{2}$. A more general derivation of the factor $\frac{1}{2}$ can be found, e.g., in Ref. [183].

Eq. (4.35) has been constructed in this way, we can be sure that this ansatz will lead to a closed set of gap equations.

4.3.2. Thermodynamic potential

As we have seen earlier, it is often advantageous to derive the gap equations from a thermodynamic potential, rather than directly from a Dyson series. In the present case this even turns out to be simpler. Therefore we do not pursue the programme outlined in Section 4.3.1 in detail, but start over again and first calculate the thermodynamic potential of the system.

As before, the first step will be that we linearize the interaction terms of the Lagrangian in the presence of the condensates we want to take into account. In this way, however, obviously only those condensates can contribute which correspond to an interaction channel of the Lagrangian. In particular, when the Lagrangian contains only quark–antiquark interactions, like Eq. (4.29), there will be no contribution from diquark condensates to the linearized Lagrangian. This is because the linearization procedure corresponds to a Hartree approximation. However, as briefly discussed in Section 4.2.2, particle–particle terms can be included via Fierz transformation. Starting from a given Lagrangian, one transforms the interaction terms into the particle–particle channel (as well as into the particle–antiparticle exchange channel) and adds the resulting terms to the original Lagrangian. In this way one gets a new Lagrangian $\mathscr{L}_{\text{eff}}$ which contains both, particle–antiparticle and particle–particle interactions. By construction, this new Lagrangian is meant to be used in Hartree approximation only. A few examples for $\mathscr{L}_{\text{eff}}$ are given in Appendix A.3.

At this point we stay rather general and consider the Lagrangian

$$\mathscr{L}_{\text{eff}} = \bar{q}(\mathrm{i}\partial\!\!\!/ - m)q + \mathscr{L}_{q\bar{q}} + \mathscr{L}_{qq} \tag{4.40}$$

with a quark–antiquark interaction of the form

$$\mathscr{L}_{q\bar{q}} = G_s^{(0)}(\bar{q}q)^2 + G_s^{(8)}\,(\bar{q}\lambda_a q)^2 + G_v^{(0)}\,(\bar{q}\gamma^0 q)^2 + G_v^{(8)}\,(\bar{q}\gamma^0\lambda_a q)^2 + \cdots\ , \tag{4.41}$$

and a quark–quark interaction

$$\mathscr{L}_{qq} = H(\bar{q}\mathrm{i}\gamma_5 C\tau_2\lambda_A\bar{q}^{\mathrm{T}})(q^{\mathrm{T}}C\mathrm{i}\gamma_5\tau_2\lambda_A q) + H_0(\bar{q}\gamma^0\gamma_5 C\tau_2\lambda_A\bar{q}^{\mathrm{T}})(q^{\mathrm{T}}C\gamma^0\gamma_5\tau_2\lambda_A q) + \cdots\ . \tag{4.42}$$

Here the dots indicate possible other channels, not related to the condensates ϕ, ϕ_8, ρ, ρ_8, δ, or δ_0. In Eq. (4.41) λ_a, $a = 1,\ldots,8$, denotes the eight Gell–Mann matrices, while in Eq. (4.42) λ_A, $A = 2, 5, 7$, denotes the antisymmetric Gell–Mann matrices. All color indices are understood to be summed over, i.e., the Lagrangian is invariant under a global $SU(3)_c$.

Now we linearize this Lagrangian in the presence of the six condensates and then express the result in terms of bispinor fields, Eq. (4.32). In this way one finds

$$\mathscr{L}_{\text{eff}}^{\text{mean field}} + \mu q^\dagger q = \bar{\Psi}\tilde{S}^{-1}\Psi - V\ , \tag{4.43}$$

where $\tilde{S}^{-1}$ is the Fourier transform of the *dressed* inverse Nambu–Gorkov propagator given in Eq. (4.35), and

$$V = \frac{(M_0 - m)^2}{4G_s^{(0)}} + \frac{M_8^2}{4G_s^{(8)}} + \frac{(\tilde{\mu} - \mu)^2}{4G_v^{(0)}} + \frac{\tilde{\mu}_8^2}{4G_v^{(8)}} + \frac{|\Delta|^2}{4H} + \frac{|\Delta_0|^2}{4H_0}\ . \tag{4.44}$$

Here we have identified the constituent quark masses

$$M_0 = m - 2G_s^{(0)}\phi, \quad M_8 = -2G_s^{(8)}\phi_8\ , \tag{4.45}$$

the effective chemical potentials

$$\tilde{\mu} = \mu + 2G_v^{(0)} n, \quad \tilde{\mu}_8 = 2G_v^{(8)} n_8 \ , \tag{4.46}$$

and the diquark gaps

$$\Delta = -2H\delta, \quad \Delta_0 = 2H_0\delta_0 \ . \tag{4.47}$$

For later convenience, but also for the interpretation of the results, it is useful to perform linear combinations to get red and blue quantities, e.g., red and blue constituent quark masses $M_r = M_0 + \frac{1}{\sqrt{3}} M_8$ and $M_b = M_0 - \frac{2}{\sqrt{3}} M_8$. We then find

$$\begin{aligned}
M_r &= m - \tfrac{2}{3}(6G_s^{(0)} + 2G_s^{(8)})\phi_r - \tfrac{2}{3}(3G_s^{(0)} - 2G_s^{(8)})\phi_b \ , \\
M_b &= m - \tfrac{2}{3}(6G_s^{(0)} - 4G_s^{(8)})\phi_r - \tfrac{2}{3}(3G_s^{(0)} + 4G_s^{(8)})\phi_b \ , \\
\tilde{\mu}_r &= \mu + \tfrac{2}{3}(6G_v^{(0)} + 2G_v^{(8)})n_r + \tfrac{2}{3}(3G_v^{(0)} - 2G_v^{(8)})n_b \ , \\
\tilde{\mu}_b &= \mu + \tfrac{2}{3}(6G_v^{(0)} - 4G_v^{(8)})n_r + \tfrac{2}{3}(3G_v^{(0)} + 4G_v^{(8)})n_b \ .
\end{aligned} \tag{4.48}$$

Since Eq. (4.43) is bilinear in the bispinor fields Ψ (+ the constant V), the thermodynamic potential at temperature T and chemical potential μ is evaluated straightforwardly,

$$\Omega(T,\mu) = -T \sum_n \int \frac{\mathrm{d}^3 p}{(2\pi)^3} \frac{1}{2} \,\mathrm{Tr}\, \ln\left(\frac{1}{T} S^{-1}(\mathrm{i}\omega_n, \vec{p})\right) + V \ . \tag{4.49}$$

Formally, the main difference to the earlier expression, Eqs. (2.46) and (2.47), is that the trace has now been extended to the bispinor space, which must again be corrected by a factor $\frac{1}{2}$ in front. In practice, Eq. (4.49) is more complicated because the inverse propagator S^{-1}, Eq. (4.35), has not the form of a free fermion inverse propagator, i.e., we cannot simply copy a textbook result.

Evaluating the trace and performing the Matsubara sum one obtains

$$\begin{aligned}
\Omega(T,\mu) = & -4 \int \frac{\mathrm{d}^3 p}{(2\pi)^3} \left\{ 2 \left(\frac{\omega_- + \omega_+}{2} + T \,\ln(1 + \mathrm{e}^{-\omega_-/T}) + T \,\ln(1 + \mathrm{e}^{-\omega_+/T}) \right) \right. \\
& \left. + (E_{p,b} + T \,\ln(1 + \mathrm{e}^{-E_-/T}) + T \,\ln(1 + \mathrm{e}^{-E_+/T})) \right\} + V + \text{const.}
\end{aligned} \tag{4.50}$$

The factor 4 in front of the integral corresponds to the spin and flavor degeneracy, while the factor 2 in the first line of the integrand reflects the two paired colors. The second line corresponds to the blue quarks which do not participate in a diquark condensate. Their dispersion laws are therefore the standard ones,

$$E_\mp = E_{p,b} \mp \tilde{\mu}_b = \sqrt{\vec{p}^2 + M_b^2} \mp \tilde{\mu}_b \ . \tag{4.51}$$

On the other hand, the dispersion laws of the red and green quarks which enter the first line of Eq. (4.50) are much more complicated,

$$\omega_\mp = \sqrt{\vec{p}^2 + M_r^2 + \tilde{\mu}_r^2 + |\Delta|^2 + |\Delta_0|^2 \mp 2s} \tag{4.52}$$

with

$$s = \sqrt{(\tilde{\mu}_r^2 + |\Delta_0|^2)\,\vec{p}^2 + t^2}, \quad t = M_r\tilde{\mu}_r - \mathrm{Re}(\Delta\Delta_0^*) \ . \tag{4.53}$$

These dispersion laws will be discussed in more detail in Section 4.3.3.

The self-consistent solutions of the condensates correspond again to the stationary points of the thermodynamic potential,

$$\frac{\delta\Omega}{\delta M_0} = \frac{\delta\Omega}{\delta M_8} = \frac{\delta\Omega}{\delta\tilde{\mu}} = \frac{\delta\Omega}{\delta\tilde{\mu}_8} = \frac{\delta\Omega}{\delta\Delta^*} = \frac{\delta\Omega}{\delta\Delta_0^*} = 0 \ . \tag{4.54}$$

This leads to the following expressions for the various expectation values:

$$\begin{aligned}
\phi_r &= -4\int\frac{\mathrm{d}^3p}{(2\pi)^3}\left\{\frac{M_r s-\tilde{\mu}_r t}{2s\omega_-}\tanh\left(\frac{\omega_-}{2T}\right)+\frac{M_r s+\tilde{\mu}_r t}{2s\omega_+}\tanh\left(\frac{\omega_+}{2T}\right)\right\} \ ,\\
\phi_b &= -4\int\frac{\mathrm{d}^3p}{(2\pi)^3}\frac{M_b}{E_{p,b}}\left(1-n_{p,b}(T,\tilde{\mu}_b)-\bar{n}_{p,b}(T,\tilde{\mu}_b)\right) \ ,\\
n_r &= 4\int\frac{\mathrm{d}^3p}{(2\pi)^3}\left\{\frac{\tilde{\mu}_r(s-\vec{p}^2)-M_r t}{2s\omega_-}\tanh\left(\frac{\omega_-}{2T}\right)+\frac{\tilde{\mu}_r(s+\vec{p}^2)+M_r t}{2s\omega_+}\tanh\left(\frac{\omega_+}{2T}\right)\right\} \ ,\\
n_b &= 4\int\frac{\mathrm{d}^3p}{(2\pi)^3}\left(n_{p,b}(T,\tilde{\mu}_b)-\bar{n}_{p,b}(T,\tilde{\mu}_b)\right) \ ,\\
\delta &= -8\int\frac{\mathrm{d}^3p}{(2\pi)^3}\left\{\frac{\Delta s+\Delta_0 t}{2s\omega_-}\tanh\left(\frac{\omega_-}{2T}\right)+\frac{\Delta s-\Delta_0 t}{2s\omega_+}\tanh\left(\frac{\omega_+}{2T}\right)\right\} \ ,\\
\delta_0 &= 8\int\frac{\mathrm{d}^3p}{(2\pi)^3}\left\{\frac{\Delta_0(s-\vec{p}^2)+\Delta t}{2s\omega_-}\tanh\left(\frac{\omega_-}{2T}\right)+\frac{\Delta_0(s+\vec{p}^2)-\Delta t}{2s\omega_+}\tanh\left(\frac{\omega_+}{2T}\right)\right\} \ ,
\end{aligned} \tag{4.55}$$

where $n_{p,b}$ and $\bar{n}_{p,b}$ are the usual Fermi occupation functions for the blue quarks and antiquarks. Note that the thermal factors $\tanh(\omega_\pm/2T)$ which arise in the expressions related to the paired quarks go to 1 for $T \to 0$.

Together with Eqs. (4.47) and (4.48) the above equations form a set of six coupled gap equations for M_r, M_b, $\tilde{\mu}_r$, $\tilde{\mu}_b$, Δ, and Δ_0. Although the expressions for the blue expectation values ϕ_b and n_b formally look like the corresponding formulae for free particles (cf. Eq. (2.82)), they depend on the effective quantities M_b and $\tilde{\mu}_b$, which are influenced by the red quarks via Eq. (4.48).

The above equations illustrate nicely the emergence of induced condensates which are not protected by symmetries. One immediately sees that the red and blue quark condensates and densities are in general different from each other, i.e., ϕ_8 and n_8 do not vanish. Also, in general δ and δ_0 cannot vanish separately. This means, the standard scalar diquark condensate δ is in general accompanied by an induced non-vanishing expectation value δ_0, even when the coupling in the δ_0-channel is repulsive [213]. This is not the case, however, for $m = 0$. In this case there are solutions with $\phi_r = \phi_b = \delta_0 = 0$, even for $\delta \neq 0$, corresponding to unbroken chiral symmetry, but also solutions with $\phi_r = \phi_b = \delta = 0$ and $\delta_0 \neq 0$ which correspond to an unbroken $U_A(1)$ symmetry (see Table 4.2). Also, there is always a solution $\delta = \delta_0 = 0$, corresponding to unbroken $U(1)$ symmetry. In this case the expressions for ϕ_r and n_r get the same structure as the analogous expressions for the blue quarks and become equal to them, unless the interaction favors the breaking of $SU(3)_c$, even without diquark condensates.

Note that this discussion could only be performed a posteriori: After we have included, e.g., δ_0 we see that the resulting gap equations do in general not allow for $\delta_0 = 0$. However, if we had not taken into account δ_0 we would not immediately have noticed an inconsistency. This is different from the Hartree–Fock scheme discussed in the previous section.

On the other hand, usually not all condensates which are there are relevant. For instance for $H_0 = 0$, which is the case, e.g., for instanton mediated interactions (see Appendix A.3), we have $\Delta_0 = 0$. Thus, although δ_0 does in general not vanish and could be calculated from Eq. (4.55), it does not influence the other quantities. For instance the dispersion law for the red and green quarks and the gap equation for Δ reduce to the "standard forms" (cf. Eqs. (4.10) and (4.12)),

$$\omega_{\mp}(\vec{p}) = \sqrt{(\sqrt{\vec{p}^2 + M_r^2} \mp \tilde{\mu}_r)^2 + |\Delta|^2} \tag{4.56}$$

and

$$\Delta = 8H\Delta \int \frac{\mathrm{d}^3 p}{(2\pi)^3} \left\{ \frac{1}{\omega_-} \tanh\left(\frac{\omega_-}{2T}\right) + \frac{1}{\omega_+} \tanh\left(\frac{\omega_+}{2T}\right) \right\} , \tag{4.57}$$

which are obviously much simpler than the general expression given above. (They are, however, less "standard" than they appear, because in general $\tilde{\mu}_r \neq \mu$ and $M_r \neq m$.)

But even when $H_0 \neq 0$, Δ_0 (or other induced gap parameters) might be small and have only a small impact on other quantities. In this case it makes certainly more sense to neglect these condensates and include others, imposed by physics arguments, than dealing with a fully self-consistent set, which misses important channels. For the remainder of Section 4.3, however, we will keep all condensates discussed above to get some flavor of their possible importance.

4.3.3. Dispersion laws and gapless solutions

We have just seen that the dispersion laws Eq. (4.52) reduce to the standard form, Eq. (4.56), when $\Delta_0 = 0$. In this case, there is a gap of 2Δ in the particle–hole excitation spectrum of the red and green components. Among others, this has the consequence that their specific heat at $T \ll \Delta$ is exponentially suppressed, like in ordinary superconductors. (The specific heat of color superconducting quark matter will be discussed in more details in Section 4.4.3.)

In this section we want to discuss the modification of the dispersion law, assuming that the interaction gives rise to a non-negligible gap parameter Δ_0. To that end we first notice that the general expression for ω_-, Eq. (4.52), can be written in a way, analogous to Eq. (4.56),

$$\omega_-(\vec{p}) = \sqrt{(\sqrt{\vec{p}^2 + M_{\mathrm{eff}}^2} - \mu_{\mathrm{eff}})^2 + |\Delta_{\mathrm{eff}}|^2} , \tag{4.58}$$

where

$$\mu_{\mathrm{eff}} = \sqrt{\tilde{\mu}_r^2 + |\Delta_0|^2}, \quad M_{\mathrm{eff}}^2 = \frac{(M_r \tilde{\mu}_r - \mathrm{Re}\,(\Delta\Delta_0^*))^2}{\mu_{\mathrm{eff}}^2} \tag{4.59}$$

and

$$|\Delta_{\mathrm{eff}}|^2 = |\Delta|^2 + M_r^2 - M_{\mathrm{eff}}^2 . \tag{4.60}$$

Thus, the gap in the spectrum is now given by $\Delta_{\rm eff}$ not by Δ or Δ_0. Formally, this implies the interesting possibility that, even for non-vanishing Δ or Δ_0, the gap vanishes if

$$M_r\Delta_0 = -\tilde{\mu}_r\Delta \ . \tag{4.61}$$

In this case ω_- would have a node at

$$\vec{p}^{\,2}_{\rm node} = \mu^2_{\rm eff} - M^2_{\rm eff} \ , \tag{4.62}$$

provided the r.h.s. is positive. For $\tilde{\mu}_r \neq 0$ Eq. (4.61) can be used to eliminate Δ in Eq. (4.59),

$$\mu^2_{\rm eff} = \tilde{\mu}_r^2\left(1+\frac{|\Delta_0|^2}{\tilde{\mu}_r^2}\right), \quad M^2_{\rm eff} = M_r^2\left(1+\frac{|\Delta_0|^2}{\tilde{\mu}_r^2}\right) \ , \tag{4.63}$$

and hence

$$\vec{p}^{\,2}_{\rm node} = (\tilde{\mu}_r^2 - M_r^2)\left(1+\frac{|\Delta_0|^2}{\tilde{\mu}_r^2}\right) \ . \tag{4.64}$$

This means, $\tilde{\mu}_r^2$ must be greater or equal to M_r^2 and it immediately follows from Eq. (4.61) that a node in the quasiparticle spectrum is only possible if $|\Delta_0| \geqslant |\Delta|$.

In the vicinity of the node the quasiparticle takes the form of a non-relativistic fermion,

$$\omega_-(\vec{p}) \approx \frac{\vec{p}^{\,2}}{2\mu_{\rm eff}} - \frac{\mu^2_{\rm eff} - M^2_{\rm eff}}{2\mu_{\rm eff}} \equiv \frac{\vec{p}^{\,2}}{2m^*} - \mu^* \ . \tag{4.65}$$

Therefore, in spite of non-vanishing diquark condensates, the specific heat of such a system would be linear in T.

In the above discussion it is tacitly assumed that there is an interaction which yields solutions of the coupled gap equations for which Eq. (4.61) holds. How realistic is this assumption? Since all quantities which enter Eq. (4.61) are in general μ dependent, it is obvious, that the gapless solutions can exist at most at certain values of μ. The only exception would be that both sides of Eq. (4.61) vanish. Apart from the trivial case $\Delta = \Delta_0 = 0$ this could be realized in the form $M_r = \Delta = 0$. It is instructive to study this possibility in a simple toy model with $m = G_i^{(k)} = H = 0$ and only $H_0 \neq 0$. If we regularize the divergent integrals by a sharp 3-momentum cut-off Λ and restrict ourselves to $T = 0$, the thermodynamic potential of this schematic model is readily calculated:

$$\Omega_{\rm schem}(T=0,\mu;\Delta_0) = -\frac{1}{6\pi^2}(2(\mu^2+|\Delta_0|^2)^2+\mu^4) + \frac{|\Delta_0|^2}{4H_0} + \text{const.} \tag{4.66}$$

As a function of Δ_0, $\Omega_{\rm schem}$ is not bounded from below. However, as discussed earlier, only the self-consistent solutions are physically meaningful, i.e., Δ_0 is constrained to the stationary points, $\delta\Omega_{\rm schem}/\delta\Delta_0 = 0$. There is always a trivial solution with $\Delta_0 = 0$. For $0 < H_0 < 3\pi^2/8\mu^2$ there are also non-trivial solutions with $|\Delta_0|^2 = 3\pi^2/8H_0 - \mu^2$. However, whenever these non-trivial solutions exist, they correspond to maxima of $\Omega_{\rm schem}$, while at same time the trivial solution is a local minimum with a lower value of $\Omega_{\rm schem}$. This means, the non-trivial gapless solution is unstable. We will come back to this point in the end of the next section.

4.3.4. Numerical results

In the schematic example discussed in the end of the previous section the problem was reduced to a single condensate. In this section we want to present the results of a numerical study of the full coupled set of gap equations derived in Section 4.3.2 [212]. As an example we consider color current interaction

$$\mathscr{L}_{\rm col} = \bar{q}(\mathrm{i}\partial\!\!\!/ - m)q - g_{\rm E}(\bar{q}\gamma^0\lambda_a q)^2 + g_{\rm M}(\bar{q}\vec{\gamma}\lambda_a q)^2 \ , \tag{4.67}$$

because it allows to study the interplay of all condensates discussed above. (As mentioned earlier, for instanton-type interactions Δ_0 would vanish.) The effective Lagrangian at finite densities does not need to be Lorentz invariant. We underline this by explicitly allowing for different "electric" and "magnetic" coupling constants, $g_{\rm E}$ and $g_{\rm M}$. In the following we will study two cases, namely a Lorentz-invariant interaction, $g_{\rm E} = g_{\rm M}$, and a purely magnetic interaction, $g_{\rm E} = 0$. The latter might be motivated by the fact that at high densities electric gluons are Debye screened, whereas, as mentioned earlier, magnetic gluons are only dynamically screened and therefore dominate the interaction.

The effective quark–antiquark interaction $\mathscr{L}_{q\bar{q}}$ and the effective quark–quark interaction $\mathscr{L}_{qq}$ as given in Eqs. (4.41) and (4.42) can be derived from $\mathscr{L}_{\rm col}$ by performing the appropriate Fierz transformations, see Appendix A.3. The resulting coupling constants are

$$\begin{aligned} G_s^{(0)} &= \tfrac{2}{9}\,(g_{\rm E} + 3g_{\rm M}), \quad G_s^{(8)} = -\tfrac{1}{24}\,(g_{\rm E} + 3g_{\rm M}), \quad H = \tfrac{1}{6}\,(g_{\rm E} + 3g_{\rm M})\ , \\ G_v^{(0)} &= \tfrac{2}{9}\,(g_{\rm E} - 3g_{\rm M}), \quad G_v^{(8)} = -g_{\rm E} - \tfrac{1}{24}\,(g_{\rm E} - 3g_{\rm M}), \quad H_0 = \tfrac{1}{6}\,(g_{\rm E} - 3g_{\rm M})\ . \end{aligned} \tag{4.68}$$

We begin our discussion with the case of a Lorentz-invariant interaction,

$$g := g_{\rm E} = g_{\rm M}\ . \tag{4.69}$$

Of course, this does not mean that there are only Lorentz-invariant condensates, since Lorentz-invariance is still broken by the chemical potential.

If we insert Eq. (4.69) into Eq. (4.68) we find that for $g > 0$ the interaction is attractive in the scalar quark–antiquark channel and in the scalar diquark channel and repulsive in all other channels of interest. Of course, non-vanishing expectation values in the repulsive channels do not develop spontaneously, but only as a result of an external source, like the chemical potential, or induced by non-vanishing expectation values in attractive channels. In fact, as we have already seen in Section 2.3 in the context of the repulsive vector interaction, the solutions of the gap equations correspond to maxima of the thermodynamic potential with respect to variations in the repulsive channels, whereas they can be maxima or minima with respect to variations in the attractive channels.

In our numerical calculations we restrict ourselves again to $T = 0$ and take a sharp 3-momentum cut-off Λ to regularize the integrals. In the following we take $\Lambda = 600\,\mathrm{MeV}$, $g\Lambda^2 = 2.75$, and a bare quark mass $m = 5\,\mathrm{MeV}$ [212]. With these parameter values we obtain a vacuum constituent quark mass $M_r = M_b = 407.7\,\mathrm{MeV}$. This corresponds to a quark condensate $\phi = -2(245.7\,\mathrm{MeV})^3$, while ϕ_8, n, n_8, δ and δ_0 vanish in vacuum.

When we increase the quark chemical potential nothing happens up to a critical value $\mu_{\rm crit} = 403.3\,\mathrm{MeV}$. At this point a first-order phase transition takes place (type (a) in the classification of Section 2.3.2) and all expectation values under consideration receive non-vanishing values. This can be inferred from Fig. 4.3 where various quantities are displayed as functions of μ. In the left panel we show the constituent quark mass M_r, the diquark gap Δ, and the effective chemical potentials $\tilde{\mu}_r$ and $\tilde{\mu}_b$. In the right panel the mass

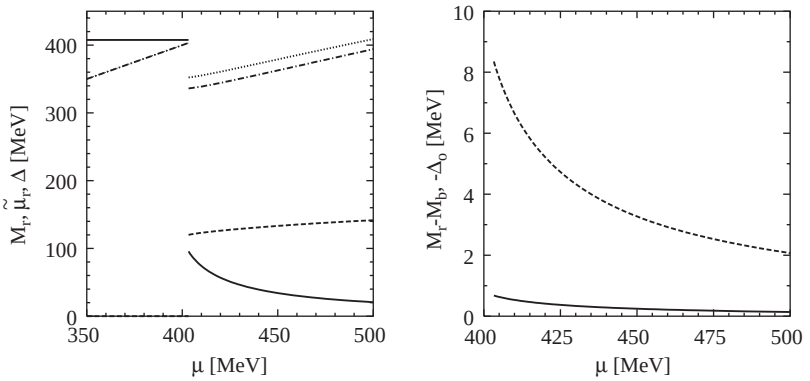

Fig. 4.3. Various quantities obtained with the Lorentz invariant interaction $g_E = g_M = 2.75/\Lambda^2$ as functions of the quark chemical potential μ. Left panel: M_r (solid), Δ (dashed), $\tilde{\mu}_r$ (dash–dotted), $\tilde{\mu}_b$ (dotted). Right panel: $M_r - M_b$ (solid), $-\Delta_0$ (dashed). Reprinted with permission from Ref. [212]. Copyright (2002) by the American Physical Society.

difference $M_r - M_b$ and the diquark gap $-\Delta_0$ are plotted.[34] At $\mu = \mu_{\text{crit}}$ the constituent quark masses drop by more than 300 MeV and are no longer identical. The difference, however, is small, $M_r = 95.7$ MeV and $M_b = 95.0$ MeV. With increasing chemical potential, both, the masses and their difference, decrease further. In the diquark channel we find $\Delta = 120.0$ MeV at $\mu = \mu_{\text{crit}}$, whereas—similar to what has been found in Ref. [213]—the second diquark gap parameter is more than one order of magnitude smaller, $\Delta_0 = -8.4$ MeV. Like the constituent masses, it decreases with increasingμ, while Δ is slightly growing in the regime shown in Fig. 4.3.

Below the phase transition the densities are zero and, thus, the effective chemical potentials $\tilde{\mu}_r$ and $\tilde{\mu}_b$ are equal to the external chemical potential μ. At the phase transition point, $\tilde{\mu}_r$ and $\tilde{\mu}_b$ drop by 67 and 51 MeV, respectively, and then grow again as functions of μ. The corresponding number densities of red and blue quarks are shown in Fig. 4.4. At $\mu = \mu_{\text{crit}}$, n_r (solid line) jumps from zero to 0.42 fm^{-3}, whereas the density of blue quarks (dashed line) reaches only $n_b = 0.34$ fm^{-3} at this point. Both densities grow of course with increasing chemical potential, but their difference remains nearly constant.

The unequal densities of red and blue quarks in this state can be understood as follows [217]: For the (unpaired) blue quarks the occupation number is of course a step function, whereas for the red and green quarks it is smoothened by the gap, leading to a depletion below and to an enhancement above the nominal Fermi surface. However, because of phase space, i.e., the integral measure $p^2\,\mathrm{d}p$, this leads to an overall enhancement of the number of red and green quarks at fixed Fermi momentum.

On the other hand, it was argued in a recent paper that in QCD the two-flavor color superconducting phase is automatically color neutral [218]. The arguments are based on gauge invariance and therefore they do not apply directly to NJL-type models. However, a key role in neutralizing color was attributed to the so-called “gluon tadpole” which is basically the Hartree diagram shown in Fig. 4.2 with the dotted line identified with a gluon. It is therefore interesting to analyze the effect of this diagram for our color current interaction.

[34] The gap equations fix Δ and Δ_0 only up to a common phase. Here we choose Δ to be real and positive. It then follows that Δ_0 is real and negative.

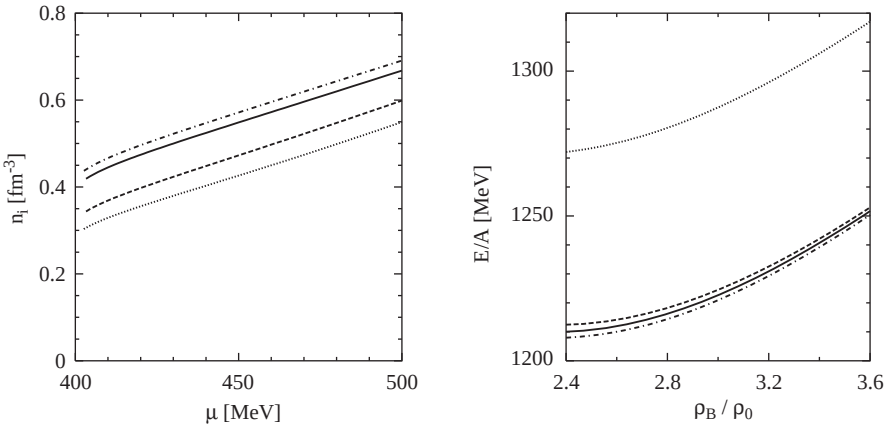

Fig. 4.4. Left: Quark number densities as functions of the quark chemical potential μ, obtained with the Lorentz-invariant interaction $g_{\rm E} = g_{\rm M} = 2.75/\Lambda^2$: $n_r = n_g$ (solid), n_b (dashed). The two other lines indicate the results without the contribution of the Hartree term ("gluon tadpoles"): $n_r = n_g$ (dash–dotted), n_b (dotted). Right: Energy per baryon number as function of the total baryon number density for a color superconducting system with equal densities of gapped and ungapped colors (dashed) and equal chemical potentials, $\mu_8 = 0$ (solid). The dash–dotted line corresponds to the calculation without "gluon tadpoles", the dotted line to a calculation without diquark pairing.

In our calculations the contribution of the Hartree term is hidden in the "$-g_{\rm E}$" in the expression for the effective coupling constant $G_v^{(8)}$ in Eq. (4.68), whereas all other couplings correspond to the Fock diagram (see Appendix A.3). First of all, this means that the "gluon tadpole" is already contained in our calculations but, obviously, this is not sufficient to get a color neutral result. Nevertheless, it does lead to a reduction of the color charge. To demonstrate this, we have switched off the Hartree contribution to $G_v^{(8)}$ and kept only the Fock terms. The resulting red and blue quark number densities are also displayed in Fig. 4.4 (dash–dotted and dotted lines in the left panel). As one can see, the effect of the "gluon tadpole" is to reduce the difference by about 50%. Qualitatively, this is due to the fact that the Hartree contribution to $G_v^{(8)}$ is repulsive, i.e., n_8 is reduced by this term. (Note that, due to this term, $\tilde{\mu}_r < \tilde{\mu}_b$.) We should stress again that our results do not contradict the claim Ref. [218] which is based on gauge invariance. It would be nice to see, however, how this comes about in QCD in terms of explicit diagrams. In fact, more recently it has been shown that the color neutralization is provided by constant gluon field [217] which is of course missed in an NJL-model description. Similar results have also been obtained for three-flavor QCD [219].

But even though color neutrality is not guaranteed to be automatically fulfilled in our model, the total number of quarks of each color is a conserved quantity because the Lagrangian $\mathscr{L}_{\rm col}$ is symmetric under global color $SU(3)$ transformations. One could therefore ask what happens if we start with a large but finite system with equal numbers of red, green and blue quarks at low densities and then compress it. Obviously, we cannot get one single color superconducting phase with the properties discussed above, i.e., with unequal numbers of red and blue quarks. A possible scenario could be that several domains emerge in which the symmetry is broken into different color directions, such that the total number of red, green and blue quarks remains unchanged. Clearly, in a realistic system, large colored domains would be disfavored because of the color-electric energy, related to long-range color forces, which are not included

in our NJL mean-field description. For small domains, on the other hand, surface effects should be taken into account.

Alternatively, we can construct a homogeneous superconducting state with equal densities for the gapped and ungapped quarks. To that end we have to introduce different *external* chemical potentials for red and blue quarks, or, equivalently, an additional external chemical potential $\mu_8 = (\frac{2}{\sqrt{3}})(\mu_r - \mu_b)$. Then the second equation in Eq. (4.46) becomes

$$\tilde{\mu}_8 = \mu_8 + 2G_v^{(8)} n_8 \ , \tag{4.70}$$

and in Eq. (4.44) we should replace $\tilde{\mu}_8^2$ by $(\tilde{\mu}_8 - \mu_8)^2$. With this additional external parameter we can enforce the densities of all colors to be equal, even in the superconducting state. Obviously this is the case if $\tilde{\mu}_8 = \mu_8$.

Within our mean field approximation such a state would be energetically less favored than a state with the same total density, but $\mu_8 = 0$. This is shown in the right panel of Fig. 4.4. The energy density ϵ of the system is given by

$$\epsilon(T = 0, n, n_8) = \Omega(T = 0, \mu, \tilde{\mu}_8) + \mu n + \mu_8 n_8 \ . \tag{4.71}$$

As usual, we take the pressure (and thus the energy density) of the (non-trivial) vacuum to be zero, $\Omega(0, 0, 0) = 0$. In the right panel of Fig. 4.4 the energy per baryon, E/A, is displayed as a function of the total baryon number density ρ_B. The solid line is the result for $\mu_8 = 0$, i.e., it corresponds to the unequal red and blue quark densities as shown in the left panel. The dashed line corresponds to the result for equal red and blue quark densities. As one can see in the figure, the energy of this solution is always higher than the energy of the solution with unequal densities. This means, according to this result, a large homogeneous system of equally many red, green and blue quarks is unstable against decay into several domains in which the density of the gapped quarks is larger than the density of the ungapped quarks. On the other hand, the energy difference is not very large, less than 3 MeV per baryon. Therefore it seems likely, that the homogeneous solution with equal densities would be favored, once color-electric and surface energies are taken into account.

For comparison we also show the result for the calculation without the Hartree contribution (dash–dotted line). In this case E/A is slightly lower. Thus, the "gluon tadpole" acts like an external color chemical potential, as obvious from Eq. (4.70). In particular, if the "gluon tadpole" had indeed been strong enough to neutralize the color charge it would have shifted the solid line on top of the dashed one.

Finally, we show the energy per baryon without diquark pairing, i.e., $\Delta = \Delta_0 = 0$ (dotted line). As one can see the pairing energy is about 60 MeV per baryon. From this point of view, the energy needed to neutralize color is a minor effect. We will come back to this in more details in Chapter 6, where we construct color and *electrically* neutral matter for applications to neutron stars.

The small values for Δ_0 we found in Fig. 4.4 seem to justify the common practice to neglect this condensate completely. To get some idea about to what extent this result depends on the coupling H_0 in the δ_0 channel we now turn to a purely magnetic interaction, $g_E = 0$. In order to keep the vacuum properties fixed we chose $g_M = \frac{4}{3}g = 3.67\Lambda^{-2}$, where g is the common electric and magnetic coupling constant used before. With this choice the effective coupling constant $G_s^{(0)}$, but also $G_s^{(8)}$ and the scalar diquark coupling constant H remain unchanged. On the other hand the δ_0 channel becomes more repulsive: We now obtain $H_0 = -H$, whereas we had $H_0 = -H/2$ for the Lorentz-invariant interaction. Similarly, we

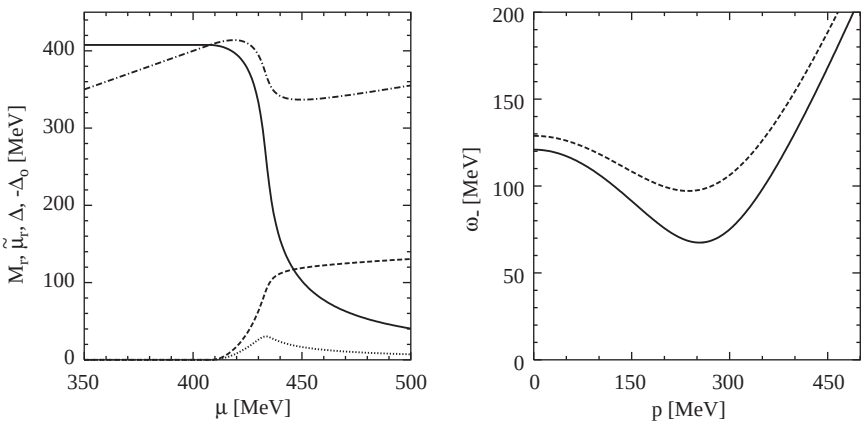

Fig. 4.5. Various quantities obtained with the purely magnetic interaction, $g_{\rm E}=0$ and $g_{\rm M}=3.67/\Lambda^2$. Left panel: M_r (solid), Δ (dashed), $-\Delta_0$ dotted, and $\tilde{\mu}_r$ (dash–dotted) as functions of the quark chemical potential μ. Right panel: Dispersion law $\omega_-(\vec{p})$ at $\mu=433.4$ MeV. The dashed line was calculated neglecting Δ_0 in the gap equations, whereas the solid line corresponds to the exact solution. A similar figure is shown in Ref. [212] for slightly different parameters.

get a strong vector repulsion, $G_v^{(0)}=-G_s^{(0)}$ instead of $G_v^{(0)}=-G_s^{(0)}/2$ which we had before. Finally, $G_v^{(8)}$ becomes attractive but is strongly reduced.

Our results are displayed in Fig. 4.5. In the left panel we show the behavior of M_r, Δ, $-\Delta_0$, and $\tilde{\mu}_r$ as functions of μ. The most striking difference to our previous example (Fig. 4.3) is the fact that we now find a smooth crossover instead of a first-order phase transition. In the chiral limit the phase transition becomes second order. This is obviously due to the strong vector repulsion, similar to the examples we have discussed in Section 2.3.2. The new aspect of the present result is that it was obtained including diquark condensates. The fact, that there are two competing condensates, ϕ and δ, was one of the main arguments supporting the belief that the chiral phase transition at zero temperature and large μ should be first order [12]. Here we found a counter example to this argument.[35]

Because of the larger value of the coupling constant $|H_0|$, the absolute value of the induced diquark gap $|\Delta_0|$ is now larger than in the previous example, although it remains well below the value of Δ. This can be understood from the fact that a large δ_0 requires both, color and chiral symmetry, to be broken strongly (see Table 4.2). i.e., large values of Δ and large constituent quark masses at the same time. This also explains why $|\Delta_0|$ has a maximum in the transition region, where both, Δ and M, are not small.

[35] It is clear, however, that this particular result should not be taken literally, because it would imply the existence of a color superconducting quark gas at arbitrarily low densities. The same words of caution are in order for the so-called "coexistence phase" which has recently been discussed in Refs. [220,221]. Based on NJL model calculations, it was claimed in these references that even in the chiral limit, ϕ and δ could coexist in one phase. (Such a phase has also been observed in Ref. [177].) The reason for this behavior is that in these examples the chiral phase transition takes place at a chemical potential which is larger than the vacuum quark mass (i.e., it does not correspond to "case (a)", according to the classification of Section 2.3.2). Therefore, there is a regime, $M_{\rm vac}<\mu<\mu_{\rm c}$ which corresponds to a phase with $\phi\neq 0$, but with a non-zero density of quarks. Then, according to the Cooper theorem, δ must be non-zero, too, if there is an attractive interaction in the scalar diquark channel. From this point of view, the existence of a color superconducting low-density constituent quark gas in the model is not very surprising, although unphysical.

At the maximum, located at $\mu = 433.4\,\mathrm{MeV}$, we find $\Delta_0 = -30.4\,\mathrm{MeV}$, while $\Delta = 89.4\,\mathrm{MeV}$, $M_r = 264.3\,\mathrm{MeV}$, and $\tilde{\mu}_r = 369.9\,\mathrm{MeV}$. In terms of Eqs. (4.59) and (4.60) this corresponds to $\mu_{\mathrm{eff}} = 371.1\,\mathrm{MeV}$, $M_{\mathrm{eff}} = 270.7\,\mathrm{MeV}$, and $|\Delta_{\mathrm{eff}}| = 67.5\,\mathrm{MeV}$. The resulting dispersion law $\omega_-(\vec{p})$ is shown in the right panel of Fig. 4.5 (solid line). At $|\vec{p}| = \sqrt{\mu_{\mathrm{eff}}^2 - M_{\mathrm{eff}}^2} = 253.8\,\mathrm{MeV}$ it has a minimum with $\omega_- = |\Delta_{\mathrm{eff}}| = 67.5\,\mathrm{MeV}$. On the other hand, if we neglect Δ_0 in the gap equation, we get $M_{\mathrm{eff}} = M_r = 286.5\,\mathrm{MeV}$, $\mu_{\mathrm{eff}} = \tilde{\mu}_r = 372.5\,\mathrm{MeV}$, and $\Delta_{\mathrm{eff}} = \Delta = 97.6\,\mathrm{MeV}$. Consequently, the minimum value of ω_- is now 97.6 MeV, almost 50% more as without neglecting Δ_0. The corresponding dispersion law is indicated by the dashed line in the right panel of Fig. 4.5. As one can see, the entire function $\omega_-(\vec{p})$ is shifted to higher energies as compared with the solid curve and the minimum is more shallow.

Finally, we would like to come back to the question of possible gapless solutions. Obviously, none of our numerical examples presented so far came close to condition (4.61). For instance, if we take $M_r = 264.3\,\mathrm{MeV}$, $\tilde{\mu}_r = 369.9\,\mathrm{MeV}$, and $\Delta = 89.4\,\mathrm{MeV}$, as found for the purely magnetic interaction at $\mu = 433.4\,\mathrm{MeV}$, one would need $\Delta_0 = -125.1\,\mathrm{MeV}$, about four times as large as the actual value. The situation was even worse for the Lorentz-invariant interaction where the discrepancy was about a factor 50 at $\mu = \mu_{\mathrm{crit}}$ and became larger with increasing chemical potential. In fact, none of our numerical examples fulfilled $|\Delta_0| \geqslant |\Delta|$, which we identified as a necessary condition for gapless color superconducting states.

To get some insight on what an interaction which yields such a state could look like, we invert the problem and employ the gap equations to calculate the effective coupling constants which are consistent with a given set of gap parameters. For instance, Eq. (4.61) is obviously fulfilled if we choose $M_r = \Delta = 100\,\mathrm{MeV}$ and $\tilde{\mu}_r = -\Delta_0 = 350\,\mathrm{MeV}$. For simplicity we might assume $M_b = M_r$ and $\tilde{\mu}_b = \tilde{\mu}_r$. Except of Δ_0 this is within the typical range of these quantities in the earlier examples. If we now take $m = 5\,\mathrm{MeV}$ and a cut-off $\Lambda = 600\,\mathrm{MeV}$, as before, and $\mu = 450\,\mathrm{MeV}$, the gap equations yield $G_s^{(0)}\Lambda^2 = 3.36$, $G_v^{(0)}\Lambda^2 = -1.41$, $H\Lambda^2 = 6.80$, $H_0\Lambda^2 = 6.18$, and $G_s^{(8)}\Lambda^2 = G_v^{(8)}\Lambda^2 = 0$. Here the essential difference to our earlier examples is the need of an *attractive* interaction in the H_0 channel. Furthermore, the interaction is relatively strong in both diquark channels. However, for these parameters there is another solution with $M_r = M_b = 58.1\,\mathrm{MeV}$, $\tilde{\mu}_r = \tilde{\mu}_b = 362.8\,\mathrm{MeV}$, $\Delta = 966.6\,\mathrm{MeV}$, and $\Delta_0 = 16.1\,\mathrm{MeV}$. It turns out that for the gapless solution the value of the thermodynamic potential Ω is about $900\,\mathrm{MeV/fm^3}$ higher than for the other solution.

Hence, similar to what we found in the schematic example of Section 4.3.3, the gapless state does not correspond to a stable solution. In fact, we did not succeed to construct any stable gapless color superconducting solution. A similar observation was made in Ref. [222] for gapless states in the color–flavor locked phase. This suggests that gapless color superconductors might in general be unstable. Although a rigorous proof is still missing, this could be understood as follows: For a single gap parameter, e.g., ϕ or δ, it is easy to see, that the effect of the gap is to lower the kinetic part of the thermodynamic potential, i.e., to make the first term in Eq. (4.49) more negative to the expense of a positive condensation energy V, see Eq. (4.44). However, in the case of a gapless color superconductor the various gap parameters conspire in such a way, that the advantage in the kinetic term gets lost (at least partially), but we still have to pay the price of a positive V. The instability of the gapless solutions is therefore quite reasonable.

More recently, it has been shown that the standard scalar diquark condensate δ can have a gapless excitation spectrum if the chemical potentials for up and down quarks are very different [223,224]. (Similar case for three flavors have been discussed in Refs. [225,226].) In this case, the mechanism is rather different from ours, since the gapless solutions do not come about through the interplay of several condensates, but as a consequence of the stress imposed by the unequal chemical potentials (or masses). In the sense of the above discussion, these gapless solutions are unstable as well. However, as shown in

Refs. [223,224], the decay of these solutions could be forbidden by additional constraints, like charge neutrality. We will come back to this scenario in Section 6.4.

4.4. Spin-1 pairing of the "blue" quarks

The diquark condensates we have discussed so far, i.e., the scalar condensates δ and δ_0, only involved two colors ("red" and "green") while the quarks of the third color ("blue") were left unpaired. Of course, these quarks will also be subject to a Cooper instability if there is an attractive channel in which they can pair. Since only a single color is involved, the pairing must take place in a channel which is symmetric in color. Assuming *s*-wave condensation in an isospin-singlet channel, a possible candidate is a spin-1 condensate. This had already been suggested in Ref. [10]. Although in that reference the size of the corresponding gap was estimated to be much smaller than the gap in the scalar channel, its existence could have interesting astrophysical consequences [12]:

Suppose a new-born neutron star contains a quark core consisting of up and down quarks. Within the first few minutes the temperature of the star drops below 1 MeV [227] and hence well below the critical temperature $T_c \simeq 0.57\Delta(T=0)$ for forming a scalar condensate, if Δ is of the order of several tens of MeV, as estimated above. This means, practically all red and green quarks are gapped and the specific heat of the quark core is completely determined by the blue quarks. As long as these remain unpaired, they can radiate neutrinos via the direct URCA process and dominantly contribute to the cooling of the star. A possible pairing of the blue quarks could thus change the cooling behavior dramatically, once the temperature drops below the corresponding critical temperature. Another interesting point is the emergence of an electromagnetic Meissner effect, which would of course strongly affect the magnetic field of the neutron star.

In this context a more detailed knowledge about the properties of a possible spin-1 condensate, in particular its size, and its thermal properties would be desirable. This will be the subject of the following discussion.

4.4.1. Condensation pattern and symmetries

We consider the complex vector order parameter

$$\zeta_n = \langle q^{\mathrm{T}} C \sigma^{0n} \tau_2 \hat{P}_3^{(c)} q \rangle \ , \tag{4.72}$$

where $\sigma^{\mu\nu} = \mathrm{i}/2[\gamma^\mu, \gamma^\nu]$ and $\hat{P}_3^{(c)} = \frac{1}{3} - \frac{1}{\sqrt{3}}\lambda_8$ is the projector on color 3, i.e., the blue quarks. ζ_n describes the spin-1 pairing of two quarks in a relative s-state. (Other forms of spin-1 condensates are discussed, e.g., in Refs. [9,15,228–230].)

An interesting feature of ζ_n is that it is not neutral with respect to the "rotated" electric charge $\tilde{Q}$, defined in Eq. (4.9). For the transformations given in Eqs. (4.7) and (4.8) we find

$$\begin{aligned} q \to \mathrm{e}^{\mathrm{i}\alpha Q} q \quad &\Rightarrow \quad \zeta_n \to \mathrm{e}^{\mathrm{i}\alpha/3} \zeta_n \\ q \to \mathrm{e}^{\mathrm{i}\alpha' \lambda_8} q \quad &\Rightarrow \quad \zeta_n \to \mathrm{e}^{-4\mathrm{i}\alpha'/\sqrt{3}} \zeta_n \end{aligned} \tag{4.73}$$

and hence

$$q \to \mathrm{e}^{\mathrm{i}\alpha \tilde{Q}} q \quad \Rightarrow \quad \zeta_n \to \mathrm{e}^{\mathrm{i}\alpha} \zeta_n \ . \tag{4.74}$$

We can find a different linear combination,

$$\tilde{Q}' = Q + \tfrac{1}{4\sqrt{3}}\,\lambda_8 \ , \tag{4.75}$$

under which ζ_n remains invariant. However, there is no generalized electric charge for which both, δ and ζ_n, are neutral. This means, if both, δ and ζ_n, are present in a neutron star, there will be an electromagnetic Meissner effect, which would strongly influence the magnetic field. Recently, similar effects have been discussed in Refs. [230–232]. The detailed evaluation of the Meissner masses for our case (two flavors, one color) remains to be done.

It is obvious, that a non-vanishing vector $\vec{\zeta}$, pointing in some direction in space, also breaks the $O(3)$ rotational symmetry of the system spontaneously. There are well-known examples for spin-1 pairing in condensed matter physics, e.g., superfluid ^{3}He, where some phases are also anisotropic [233]. In relativistic systems this is certainly not a very frequent phenomenon. It is possible only at finite chemical potential, which itself breaks Lorentz invariance explicitly. Since $O(3)$ is a global symmetry of QCD, there should be collective Nambu–Goldstone excitations in the spectrum. However, in Lorentz non-invariant systems, there are subtleties which can spoil the standard proof of the Goldstone theorem, leading to peculiarities, like excitations with quadratic dispersion laws or an unusual number of Goldstone bosons [234–240].

In Refs. [238,239], this problem has been analyzed within an effective Ginzburg–Landau type potential for the complex order parameter $\vec{\zeta}$.[36] The potential consists of a mass term with the "wrong sign" in order to get a non-trivial solution and two different fourth-order terms,

$$V(\vec{\zeta}) = -a^2\zeta_n^\dagger\zeta_n + \tfrac{1}{2}\,\lambda_1(\zeta_n^\dagger\zeta_n)^2 + \tfrac{1}{2}\,\lambda_2\zeta_m^\dagger\zeta_m^\dagger\zeta_n\zeta_n \tag{4.76}$$

with $\lambda_1+\lambda_2>0$ for stability. In fact, the λ_2-term explicitly breaks the $O(3)$ invariance, but its introduction is conceptionally useful because it lifts the degeneracy between the $M_J=0$ and the $M_J=\pm1$ states:

For $\lambda_2<0$ the potential is minimized by a $(J=1,\,M_J=0)$-state,

$$\vec{\zeta}(M_J=0) = \zeta\begin{pmatrix}0\\0\\1\end{pmatrix} \tag{4.77}$$

with $|\zeta| = a/\sqrt{\lambda_1+\lambda_2}$. This solution corresponds to an anti-ferromagnet. The spectrum of small oscillations above this ground state consists of 1+2 Nambu–Goldstone bosons, all with linear dispersion law: one zero-sound phonon and two spin waves [238,239]. Implying a finite Landau critical velocity, this fact is crucial for a macroscopic superfluid behavior of the system [240].

On the other hand, for $\lambda_2>0$ the potential is minimized by $(J=1,\,M_J=\pm1)$-states,

$$\vec{\zeta}(M_J=\pm1) = \mp\frac{\zeta}{\sqrt{2}}\begin{pmatrix}1\\ \pm\mathrm{i}\\0\end{pmatrix} \tag{4.78}$$

with $|\zeta| = a/\sqrt{\lambda_1}$. This corresponds to ferromagnetic solutions. In this case the Nambu–Goldstone spectrum above this ground state consists of one phonon with linear dispersion law and one spin wave whose energy tends to zero with momentum squared [238,239].

[36] This has been done in the context of Bose–Einstein condensation in ultra-cold alkali atoms.

As mentioned above, if the underlying Hamiltonian is exactly rotational invariant, the last term in Eq. (4.76) must vanish, i.e., $\lambda_2 = 0$. The $M_J = 0$-solutions are then degenerate with the $M_J = \pm 1$-solutions [229]. In real systems, it will therefore depend on details of the surrounding which solution is realized (if any).

In the following, we will mostly concentrate on the $M_J = 0$ case which has been discussed in Ref. [241]. The case $M_J = \pm 1$ is more complicated and has so far only been investigated at zero temperature [229]. This will briefly be discussed afterwards.

4.4.2. Gap equation

In order to analyze the spin-1 condensate more quantitatively, we employ again an NJL-type model. As mentioned above, we will first restrict ourselves to the case $M_J = 0$, Eq. (4.77), i.e., we consider a non-vanishing expectation value

$$\zeta = \langle q^{\mathrm{T}} C \sigma^{03} \tau_2 \hat{P}_3^{(c)} q \rangle \ . \tag{4.79}$$

We also keep the dominant condensation channels at high and at low density, i.e., the scalar color-antitriplet diquark condensate δ, Eq. (4.5), and the quark–antiquark condensate ϕ, Eq. (4.24). However, for simplicity, we neglect the other condensates discussed in Section 4.3 and all other condensates possibly induced by a non-vanishing ζ.

To allow for condensation in the ζ-channel in Hartree approximation, we need an attractive quark–quark interaction with the quantum numbers of a Lorentz-tensor, flavor-singlet and color-sextet.[37] Guided by the structure of instanton-induced interactions (see Appendix A.3) we consider a quark–antiquark term

$$\mathscr{L}_{q\bar{q}} = G\{(\bar{q}q)^2 - (\bar{q}\vec{\tau}q)^2 - (\bar{q}\mathrm{i}\gamma_5 q)^2 + (\bar{q}\mathrm{i}\gamma_5\vec{\tau}q)^2\} \tag{4.80}$$

and a quark–quark term

$$\begin{aligned}\mathscr{L}_{qq} = {} & H_{\mathrm{s}}\{(\bar{q}\mathrm{i}\gamma_5 C\tau_2\lambda_A\bar{q}^{\mathrm{T}})(q^{\mathrm{T}}C\mathrm{i}\gamma_5\tau_2\lambda_A q) - (\bar{q}C\tau_2\lambda_A\bar{q}^{\mathrm{T}})(q^{\mathrm{T}}C\tau_2\lambda_A q)\} \\ & - H_{\mathrm{t}}(\bar{q}\sigma^{\mu\nu}C\tau_2\lambda_S\bar{q}^{\mathrm{T}})(q^{\mathrm{T}}C\sigma_{\mu\nu}\tau_2\lambda_S q) \ ,\end{aligned} \tag{4.81}$$

where λ_A and λ_S are again the antisymmetric and symmetric color generators, respectively. For instanton-induced interactions the coupling constants fulfill the relation $G : H_{\mathrm{s}} : H_{\mathrm{t}} = 1 : \frac{3}{4} : \frac{3}{16}$, but for the moment we will treat them as arbitrary parameters. As long as they stay positive, the interaction is attractive in the channels giving rise to δ, ζ, and ϕ.

Applying the same techniques as in Section 4.3.2 it is straightforward to calculate the mean-field thermodynamic potential $\Omega(T, \mu)$ in the presence of these condensates. One finds

$$\begin{aligned}\Omega(T,\mu) = {} & -4\sum_{i=1}^{3}\int\frac{\mathrm{d}^3p}{(2\pi)^3}\left[\frac{\omega_i^- + \omega_i^+}{2} + T\ln(1+\mathrm{e}^{-\omega_i^-/T}) + T\ln(1+\mathrm{e}^{-\omega_i^+/T})\right] \\ & + \frac{1}{4G}(M-m)^2 + \frac{1}{4H_{\mathrm{s}}}|\Delta|^2 + \frac{1}{16H_{\mathrm{t}}}|\Delta'|^2 \ ,\end{aligned} \tag{4.82}$$

[37] Again, we may in principle allow for Lorentz non-invariant Lagrangians, where the time-space components (the σ^{0i}-terms) and the space–space components (the σ^{ij}-terms) of the interaction enter with different coupling constants. However, since only the time-space components are relevant for our condensation pattern, this would not make any difference in the results.

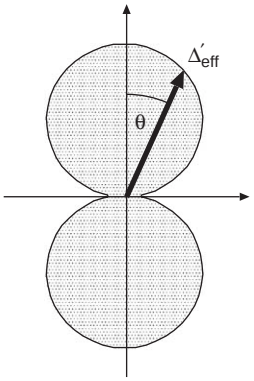

Fig. 4.6. Schematic illustration of the angle dependence of $\Delta'_{\rm eff}$.

where again m is the bare quark mass, $M = m - 2G\phi$, $\Delta = -2H_{\rm s}\delta$, and

$$\Delta' = 4H_{\rm t}\zeta \ . \tag{4.83}$$

The dispersion laws for the red and green quarks are the "standard" ones, i.e.,

$$\omega^{\mp}_{1,2}(\vec{p}) = \sqrt{(\sqrt{\vec{p}^2 + M^2} \mp \mu)^2 + |\Delta|^2} \ , \tag{4.84}$$

whereas the dispersion laws for the blue quarks now read

$$\omega^{\mp}_{3}(\vec{p}) = \sqrt{(\sqrt{M^2_{\rm eff} + \vec{p}^2} \mp \mu_{\rm eff})^2 + |\Delta'_{\rm eff}|^2} \ , \tag{4.85}$$

where the effective chemical potential, the effective mass, and the effective gap are angle-dependent quantities,

$$\mu^2_{\rm eff} = \mu^2 + |\Delta'|^2 \sin^2\theta, \quad M_{\rm eff} = M\mu/\mu_{\rm eff}, \quad |\Delta'_{\rm eff}|^2 = |\Delta'|^2 \left(\cos^2\theta + \frac{M^2}{\mu^2_{\rm eff}} \sin^2\theta\right) \ . \tag{4.86}$$

Here $\cos\theta = p_3/|\vec{p}|$. Thus, as expected, for $\Delta' \neq 0$, $\omega^{\mp}_3(\vec{p})$ is an anisotropic function of $\vec{p}$, reflecting the spontaneous breakdown of rotational invariance. The dependence of the effective gap $\Delta'_{\rm eff}$ on the polar angle θ is illustrated in Fig. 4.6. For $M = 0$, it vanishes at $\theta = \pi/2$. In general, its minimal value is given by

$$\Delta'_{\rm min} = \Delta'_{\rm eff}\left(\theta = \frac{\pi}{2}\right) = \frac{M|\Delta'|}{\sqrt{\mu^2 + |\Delta'|^2}} \ . \tag{4.87}$$

For our later analysis of the specific heat we will need the density of states,

$$N(E) = \int \frac{{\rm d}^3 p}{(2\pi)^3}\, \delta(\omega^-_3(\vec{p}) - E) \tag{4.88}$$

for the low-lying quasiparticle spectrum. To that end we expand ω_3^- about its minimum. One obtains

$$\omega_3^-(\vec{p}) \approx \sqrt{\Delta'^2_{\min} + v_\perp^2 (p_\perp - p_0)^2 + v_3^2 p_3^2}\ , \tag{4.89}$$

where $p_\perp^2 = p_1^2 + p_2^2$, and

$$v_\perp = \sqrt{1 - \left(\frac{\mu M}{\mu^2 + |\Delta'|^2}\right)^2}, \quad v_3 = \frac{\Delta'_{\min}}{M}, \quad p_0 = \frac{v_\perp}{v_3}\,|\Delta'|\ . \tag{4.90}$$

Inserting this into Eq. (4.88), we find that the density of states is linear in energy,

$$N(E) = \frac{1}{2\pi}\,\frac{\mu^2 + |\Delta'|^2}{|\Delta'|}\,E\theta(E - \Delta'_{\min})\ . \tag{4.91}$$

This linear dependence is typical for effectively two-dimensional systems: The angular structure of the gap restricts the low-lying excitations to stay in the "equator plane", i.e., $\theta = \pi/2$.

The gap equations for Δ, Δ' and M are again derived by minimizing Ω with respect to these variables. Imposing $\partial\Omega/\partial\Delta'^* = 0$, we get

$$\Delta' = 16\,H_t\Delta' \sum_{-+}\int \frac{\mathrm{d}^3p}{(2\pi)^3}\left(1 \mp \frac{\vec{p}_\perp^{\,2}}{\mu_{\rm eff}\sqrt{\vec{p}^2 + M_{\rm eff}^2}}\right)\frac{1}{\omega_3^\mp}\,\tanh\frac{\omega_3^\mp}{2T}\ . \tag{4.92}$$

Note that Δ does not explicitly enter this equation. In turn, the gap equation for Δ, resulting from $\partial\Omega/\partial\Delta^* = 0$, takes the standard form (Eq. (4.57) with $H \to H_s$ and $\omega_\mp \to \omega_1^\mp$) and does not explicitly depend on Δ'. On the other hand, both, Δ and Δ', enter the gap equation for M,

$$M = m + 4GM\sum_{-+}\int \frac{\mathrm{d}^3p}{(2\pi)^3}\left\{2\,\frac{E_p \mp \mu}{E_p\omega_1^\mp}\,\tanh\frac{\omega_1^\mp}{2T} + \left(1 \mp \frac{\mu^2}{\mu_{\rm eff}\sqrt{\vec{p}^2 + M_{\rm eff}^2}}\right) \times \frac{1}{\omega_3^\mp}\,\tanh\frac{\omega_3^\mp}{2T}\right\}\ , \tag{4.93}$$

which follows from the requirement $\partial\Omega/\partial M = 0$. We thus have a set of three equations, where the equations for Δ and Δ' are not directly coupled, but only through their dependence on M. In particular, for $M = 0$ they decouple.

Numerical solutions of the gap equations are presented in Fig. 4.7. We have chosen a sharp 3-momentum cut-off $\Lambda = 600\,\mathrm{MeV}$, a current quark mass $m = 5\,\mathrm{MeV}$, and $G\Lambda^2 = 2.4$ for the coupling constant in the quark–antiquark part [241]. Obviously, these parameters are close to the region fixed by fitting f_π and m_π (see Table 2.2) as well as those employed in Section 4.3.4 and lead to reasonable vacuum properties ($M = 393\,\mathrm{MeV}$, $f_\pi = 93.6\,\mathrm{MeV}$, $m_\pi = 129\,\mathrm{MeV}$, $\langle\bar{u}u\rangle = (-244\,\mathrm{MeV})^3$). In order to fix the coupling constants H_s and H_t we have employed the instanton relation, $G : H_s : H_t = 1 : \frac{3}{4} : \frac{3}{16}$. The resulting values of M, Δ, and Δ' as functions of μ at $T = 0$ are displayed in the figure. The chemical potentials correspond to baryon densities of about 4–7 times nuclear matter density. In agreement with the earlier expectations of Ref. [10] Δ' is relatively small, about two to three orders of magnitude smaller than Δ in

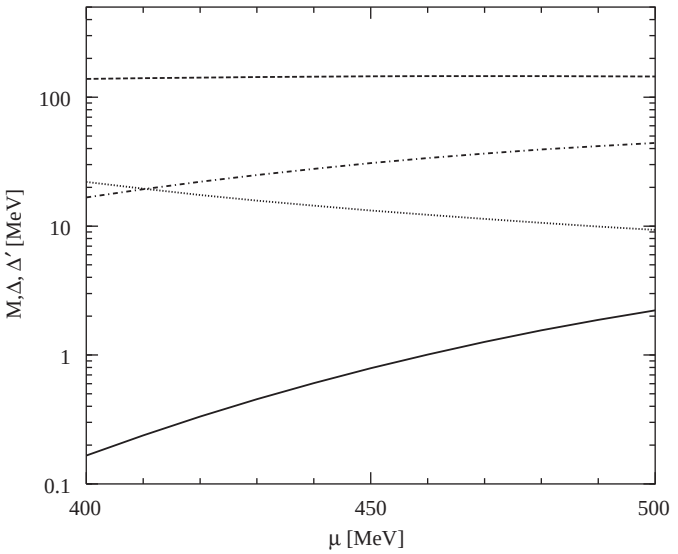

Fig. 4.7. M (dotted), Δ (dashed), and Δ' (solid) at $T=0$ as functions of the quark chemical potential μ using $\Lambda=600\,\mathrm{MeV}$, $m=5\,\mathrm{MeV}$, and $G\Lambda^2=2.4$. The coupling constants H_s and H_t are fixed by the instanton relation $G:H_\mathrm{s}:H_\mathrm{t}=1:\frac{3}{4}:\frac{3}{16}$. The dash–dotted line indicates the result for Δ' if the value of H_t is doubled. Reprinted with permission from Ref. [241]. Copyright (2003) by the American Physical Society.

this regime. However, it is strongly μ-dependent and rises by more than a factor of 10 between $\mu=400$ and 500 MeV. Being a solution of a self-consistencyproblem, Δ' is also extremely sensitive to the coupling constant H_t. If we double the value of H_t, we arrive at the dash–dotted line for Δ', which is then almost comparable to Δ (see also Fig. 4.10). We also find that Δ' is very sensitive to the cut-off. This can be traced back to the factor $(1-\vec{p}_\perp^{\,2}/s)$ in the gap equation (4.92) which can become negative for large momenta. It is quite obvious then, that also the form of the regularization, i.e., sharp cut-off, form factor, etc., will have a strong impact on the results.

4.4.3. Thermal behavior

With increasing temperature both condensates, δ and ζ, are reduced and eventually vanish in second-order phase transitions at critical temperatures T_c and T_c', respectively. It has been shown [172] that T_c is approximately given by the well-known BCS relation

$$T_\mathrm{c}\approx 0.57\Delta(T=0)\ . \tag{4.94}$$

In order to derive a similar relation for T_c' we inspect the gap equation (4.92) at $T=0$ and in the limit $T\to T_\mathrm{c}'$. Neglecting M (since $M\ll\mu$ this is valid up to higher orders in M^2/μ^2) and antiparticle contributions one gets

$$\int\frac{\mathrm{d}^3p}{(2\pi)^3}\left\{\left[\left(1-\frac{\vec{p}_\perp^{\,2}}{s}\right)\frac{1}{\omega_3^-(\vec{p})}\right]_{\Delta'(T=0)}-\left(1-\frac{\vec{p}_\perp^{\,2}}{\mu|\vec{p}|}\right)\frac{1}{|\mu-|\vec{p}||}\tanh\frac{|\mu-|\vec{p}||}{2T_\mathrm{c}'}\right\}\approx 0\ . \tag{4.95}$$

Since the integrand is strongly peaked near the Fermi surface, the $|\vec{p}|$-integrand must approximately vanish at $|\vec{p}|=\mu$, after the angular integration has been performed. From this condition one finds to

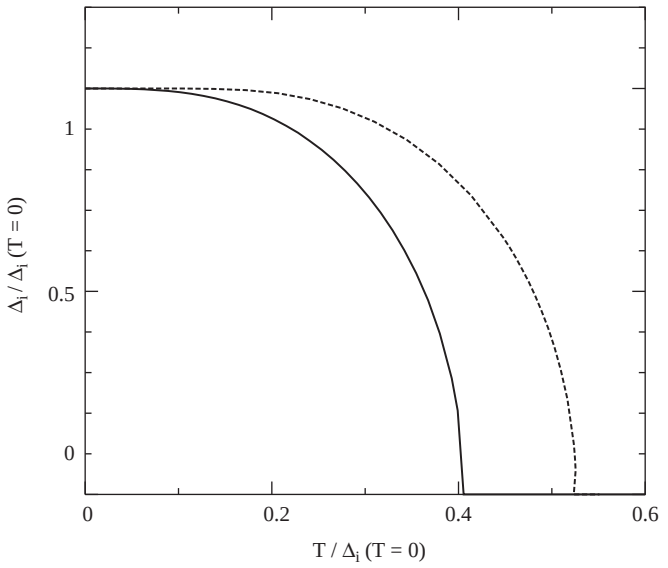

Fig. 4.8. $\Delta_i/\Delta_i(T=0)$ as function of $T/\Delta_i(T=0)$. Dashed: $\Delta_i=\Delta$. Solid: $\Delta_i=\Delta'$. The calculations have been performed at $\mu=450$ MeV for the same parameters as employed in Fig. 4.7. Reprinted with permission from Ref. [241]. Copyright (2003) by the American Physical Society.

lowest order in Δ'/μ

$$T_c' \approx \tfrac{1}{3}\,\Delta'(T=0)\ . \tag{4.96}$$

For the scalar condensate, the analogous steps would lead to $T_c/\Delta(T=0)\approx\frac{1}{2}$ instead of Eq. (4.94). This gives a rough idea about the quality of the approximation. Note that there are other examples of diquark condensates, where $T_c\neq 0.57\Delta(T=0)$ [242]. This is also the case for crystalline superconductors [243].

Numerical results for $\Delta(T)$ and $\Delta'(T)$ are shown in Fig. 4.8. The quantities have been rescaled in order to facilitate a comparison with the above relations for T_c and T_c'. The results are in reasonable agreement with our estimates. These findings turn out to be quite insensitive to the actual choice of parameters.

The specific heat is given by[38]

$$c_v = -T\,\frac{\partial^2\Omega}{\partial T^2}\ . \tag{4.98}$$

[38] Although standard, this formula is not quite correct (I thank Igor Shovkovy for having pointed out this problem to me.): Strictly, c_v is defined as the temperature dependence of the internal energy ϵ at fixed volume and at fixed *particle number*, i.e., $c_v=(\partial\epsilon/\partial T)|_{V,N}=(T/V)(\partial S/\partial T)|_{V,N}$. If we were allowed to evaluate the derivative at fixed chemical potential we would get Eq. (4.98). Keeping the particle number fixed, the correct expression is

$$c_v = -T\left\{\frac{\partial^2\Omega}{\partial T^2}-\left(\frac{\partial^2\Omega}{\partial\mu^2}\right)^{-1}\left(\frac{\partial^2\Omega}{\partial T\partial\mu}\right)^2\right\}\ . \tag{4.97}$$

However, we have checked numerically that the correction term is negligible (see also Ref. [171]).

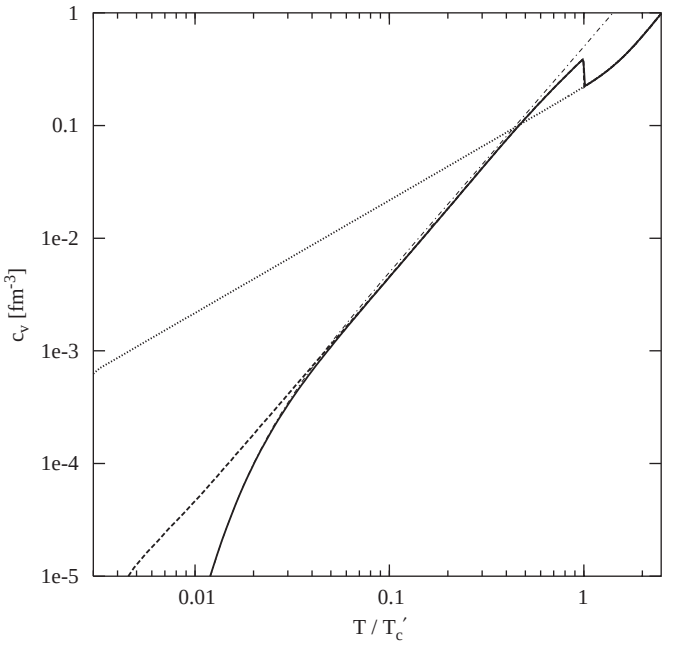

Fig. 4.9. Specific heat as function of T/T_c'. The calculations have been performed at $\mu = 450\,\mathrm{MeV}$ for the same parameters as employed in Fig. 4.7, however, for numerical convenience with the doubled value of H_t. Solid: full calculation, dashed: result for $M = 0$, dotted: without spin-1 condensate. The dash–dotted line indicates the result of Eq. (4.100). Reprinted with permission from Ref. [241]. Copyright (2003) by the American Physical Society.

For $T \ll T_c$ it is completely dominated by the blue quarks, since the contribution of the red and green ones is suppressed by a factor $e^{-\Delta/T}$. Thus, keeping the ω_3^--part only and neglecting the T-dependence of M and Δ', one gets from Eq. (4.82)

$$c_v \approx \int \frac{d^3p}{(2\pi)^3}\left(\frac{\omega_3^-}{T}\right)^2 \frac{1}{\cosh^2(\omega_3^-/2T)} \ . \tag{4.99}$$

At low temperatures we can replace the cosh by an exponential. Employing the density of states, Eq. (4.91), the integral is then readily turned out. One finds

$$c_v \approx \frac{12}{\pi}\,\frac{\mu^2 + |\Delta'|^2}{|\Delta'|}\,T^2 e^{-\Delta'_{\min}/T} \sum_{n=0}^{3} \frac{1}{n!}\left(\frac{\Delta'_{\min}}{T}\right)^n \ . \tag{4.100}$$

According to the approximations made, this expression should be valid for $T \ll T_c'$. In this regime c_v depends quadratically on T for $T \gtrsim \Delta'_{\min}$, and is exponentially suppressed at lower temperatures.

To test this relation we evaluate $c_v(T)$ numerically using Eq. (4.82) and (4.98). The results for fixed $\mu = 450\,\mathrm{MeV}$ are displayed in Fig. 4.9. For numerical convenience we have doubled the value of H_t,

leading to a relatively large $\Delta'(T=0)=30.8\,\mathrm{MeV}$. The critical temperature is $T_c'\simeq 0.40\Delta'(T=0)$. For the energy gap we find $\Delta'_{\min}=0.074T_c'$. It turns out that Eq. (4.100), evaluated with constant values of Δ' and M, (dash–dotted line) is in almost perfect agreement with the numerical result (solid line) up to $T\approx T_c'/2$. The phase transition, causing the discontinuity of c_v at $T=T_c'$, is of course outside the range of validity of Eq. (4.100). We also display c_v for $M=0$ (dashed line). Since $\Delta'_{\min}$ vanishes in this case, there is no exponential suppression, and c_v is proportional to T^2 down to arbitrarily low temperatures. However, even when M is included, the exponential suppression is partially canceled by the sum on the r.h.s. of Eq. (4.100). For comparison, we also show c_v for a system with $\Delta'=0$, which exhibits a linear T dependence at low temperatures (dotted line).

Our results show that, even though the magnitude of the gap parameter Δ' is strongly model dependent, its relations to the critical temperature and the specific heat are quite robust. Thus, if we had empirical data, e.g., for the specific heat of dense quark matter, they could be used to extract information about the existence and the size of Δ'. In this context neutron stars and their cooling properties are the natural candidates to look at.

As already mentioned, in Ref. [12] it was suggested that the spin-1 pairing of the blue quarks might have observable consequences for the cooling of a neutron star. (The relevance of c_v and the possible effect of diquark condensates on neutron star cooling was also discussed in Refs. [244–246].) According to the original idea, quite soon after the temperature has dropped below the critical temperature for the spin-1 pairing, the contribution of the blue quarks to the specific heat will be exponentially suppressed. Obviously, this argument has to be somewhat refined since, as seen above, $c_v(T)$ first behaves as T^2 and the exponential suppression sets in only at $T<\Delta'_{\min}$.

On the other hand, we should admit that there are good reasons to doubt that a spin-1 isospin-singlet condensate is stable in a neutron star, where we have to impose neutrality constraints. In order to pair, the up and down quarks should have similar Fermi momenta, whereas for charge neutrality one needs roughly twice as many down quarks as up quarks. In fact, it has been argued that these constraints could completely prohibit the existence of two-flavor color superconducting matter in neutron stars [247]. In that case, there is the possibility that up and down quarks are separately paired in single-*flavor* spin-one condensates [15,228–230].) However, as we will see in Chapter 6, it is possible that the standard spin-0 condensate δ is not destroyed by the neutrality conditions. For ζ, this question has not yet been investigated, but, given that Δ' is presumably small, ζ should be much more fragile and will probably not survive. In this case, the fate of the blue quarks is rather unclear.

4.4.4. Spin-1 pairing in the red–green sector

As we have discussed earlier, the coupling strengths in the various channels are poorly known and the choice of the instanton relation, to fix their ratios is not at all stringent. At least in principle, this implies the possibility that the red and green quarks are also paired in a spin-1 state if the ratio $H_t:H_s$ is large enough. To investigate this scenario, we extend the formalism of Section 4.4.2 to include a condensate of the form

$$\zeta_{rg}=\langle q^{\mathrm{T}}C\sigma^{03}\tau_2\hat{P}_{12}^{(c)}q\rangle \tag{4.101}$$

together with the other condensates. $\hat{P}_{12}^{(c)}=\frac{2}{3}+\frac{1}{\sqrt{3}}\lambda_8$ is the projector on the first two colors, i.e., the red and the green quarks. Denoting the corresponding gap parameter by Δ'_{rg}, the thermodynamic potential,

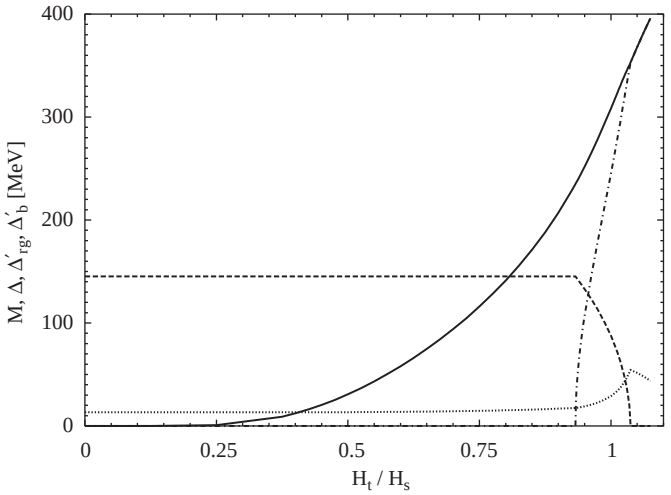

Fig. 4.10. Gap parameters as functions of the ratio between tensor and scalar coupling constant H_t and H_s: constituent quark mass M (dotted), scalar diquark gap Δ (dashed), and spin-1 gap parameters Δ'_{rg} (dash–dotted) and Δ'_b (solid). The calculations have been performed at $\mu = 450$ MeV. Except of H_t, which is varied, the parameters are the same as in Fig. 4.7.

Eq. (4.82) gets an additional term $|\Delta'_{rg}|^2/(8H_t)$, and the dispersion laws for the red and green quarks are now given by an expression analogous to Eqs. (4.85) and (4.86), but with an effective gap

$$|\Delta^{rg}_{\text{eff}}|^2 = |\Delta|^2 + |\Delta'_{rg}|^2 \left(\cos^2\theta + \frac{M^2}{\mu^{rg\,2}_{\text{eff}}} \sin^2\theta \right) . \tag{4.102}$$

Numerical results are presented in Fig. 4.10 where the various gap parameters are displayed as functions of the tensor coupling H_t at fixed chemical potential μ. For the other parameters we have taken the same values as in Sections 4.4.2 and 4.4.3. For the sake of clarity, we now call the spin-1 gap parameter of the blue quarks Δ'_b, instead of Δ'.

We find three different regimes: For $H_t < 0.93 H_s$, we have the "standard situation" that the red and green quarks are paired in a scalar condensate, i.e., $\Delta \neq 0$ (dashed line), whereas $\Delta'_{rg} = 0$. Then, in some intermediate regime, $0.93 < H_t/H_s < 1.04$, both, Δ and Δ'_{rg}, are non-zero. Here one can nicely see that both condensates compete for the same quarks and, hence, Δ decreases while Δ'_{rg} (dash–dotted line) rises steeply. Finally, for $H_t > 1.04 H_s$, $\Delta = 0$ and all quarks are paired in a spin-1 condensate. As a consequence, Δ'_{rg} is equal to Δ'_b (solid line) in this regime. It is quite remarkable that the transition from spin-0 to spin-1 pairing in the red/green sector is smooth, i.e., there are two second-order phase transitions, instead of a single first-order transition. This demonstrates again that the presence of two competing condensates does not automatically guarantee a first-order phase transition (see Section 4.3.4).

The properties of the two "new" phases have not yet been investigated in detail. In fact, it might be difficult to motivate such an analysis, since "typical" interactions, like instantons ($H_t : H_s = 1 : 4$) or single gluon exchange ($H_t = 0$), do by far not provide enough strength in the tensor channel.

4.4.5. $M_J = \pm 1$

As discussed in Section 4.4.1, the condensation could also take place in the $(J=1,\ M_J=\pm 1)$-channel. According to Eq. (4.78), this means that we have a condensate of the form

$$\mp\langle q^{\mathrm{T}} C\sigma^{01}\tau_2 \hat{P}_3^{(c)} q\rangle = \mathrm{i}\langle q^{\mathrm{T}} C\sigma^{02}\tau_2 \hat{P}_3^{(c)} q\rangle = \frac{\zeta}{\sqrt{2}}\ , \tag{4.103}$$

where we have assumed that only the blue quarks condense in this channel. With this ansatz we can again apply the techniques of Section 4.3.2 to calculate the thermodynamic potential. In practice, however, this turns out to be more difficult than for $M_J = 0$. The dispersion laws $\omega(\vec{p})$ of the quasiquark excitations generally correspond to the eigenvalues of the inverse Nambu–Gorkov propagator. In the present case, this leads to the following secular equation in the blue quark sector

$$\begin{aligned} f(\omega^2) = {} & [(\omega^2 - E_-^2)(\omega^2 - E_+^2) - |\Delta'|^2(\omega^2 + \vec{p}^2\cos^2(\theta) - \mu^2 - M^2)]^2 \\ & - 4|\Delta'|^4((\omega^2 - M^2)\vec{p}^2\cos^2(\theta) + M^2\mu^2) \\ & = 0\ , \end{aligned} \tag{4.104}$$

where $E_\mp = \sqrt{\vec{p}^2 + M^2} \mp \mu$, as before, while the gap parameter is given by $\Delta' = 4\sqrt{2}H_{\mathrm{t}}\zeta$. This equation is of fourth order in ω^2. Hence, instead of two, there are four different dispersion laws for the blue quasiquarks, and their explicit expressions are in general rather complicated. In this context it is instructive to inspect the case $\theta = 0$ (or $\theta = \pi$), where the solutions take relatively simple forms. One finds

$$\begin{aligned} &\omega_{-,1}^2(|\vec{p}|, \theta = 0) = E_-^2, \quad \omega_{-,2}^2(|\vec{p}|, \theta = 0) = E_p^2 + \mu^2 + |\Delta'|^2 - 2\sqrt{E_p^2\mu^2 + \vec{p}^2|\Delta'|^2}\ , \\ &\omega_{+,1}^2(|\vec{p}|, \theta = 0) = E_+^2, \quad \omega_{+,2}^2(|\vec{p}|, \theta = 0) = E_p^2 + \mu^2 + |\Delta'|^2 + 2\sqrt{E_p^2\mu^2 + \vec{p}^2|\Delta'|^2}\ . \end{aligned} \tag{4.105}$$

Hence, only two of the solutions are affected by the gap, while the other two are not. In fact, from a non-relativistic point of view one would expect that only quarks with spin up (down) can participate in an $M_J = +1$ ($M_J = -1$) condensate and, thus, the spin down (up) quarks are "blind" to this condensate. Relativistically, this remains true for quarks moving parallel or antiparallel to the z-direction, because

$$C(\mp\sigma^{01} + \mathrm{i}\sigma^{02}) = 2\mathrm{i}\begin{pmatrix} \mathbb{1} \pm \sigma_3 & 0 \\ 0 & \mathbb{1} \pm \sigma_3 \end{pmatrix}\ . \tag{4.106}$$

Here σ_3 is a Pauli matrix in spin space. This observation trivially implies that there is always one gapless mode, $\omega_{-,1}^2 = 0$ at $\theta = 0$ and $\vec{p}^2 = \mu^2 - M^2$.

The two other solutions at $\theta = 0$ turn out to be identical to the $M_J = 0$-dispersion laws at $\theta = \pi/2$,

$$\omega_{\mp,2}(|\vec{p}|, \theta = 0) = \omega_3^{\mp}\left(|\vec{p}|, \theta = \frac{\pi}{2}\right) \tag{4.107}$$

with $\omega_3^{\mp}$ as given in Eq. (4.85). Hence, for massless quarks, there is a second gapless mode at $\theta = 0$, which corresponds to the $\omega_{-,2}$ branch at $\vec{p}^2 = \mu^2 + |\Delta'|^2$. In general, $\omega_{-,2}$ has a minimal value which is given by Eq. (4.87).

For arbitrary polar angles, the solutions of Eq. (4.104) are quite complicated. Therefore Alford et al. [229] have determined the dispersion laws numerically. In addition they have also derived an approximate expression, valid for $M = 0$ and ω, $||\vec{p}| - \mu| \ll \mu$. In this case, they find that there are not only gapless modes at the "poles", i.e., $\theta = 0, \pi$, but in a finite regime of order Δ'/μ around them. When they introduce

finite quark masses $M \gtrsim \Delta'$, this effect goes away and there remains a single gapless solution at the poles. It would be interesting to analyze the corresponding thermal and transport properties of the system, but this has not yet been done.

As pointed out in Section 4.4.1, the ground state energy of the system must be the same for $M_J = 0$ and for $M_J = \pm 1$ if rotational invariance is not broken explicitly, i.e., if the Hamiltonian commutes with the total angular momentum $\vec{J}$. This has been confirmed in Ref. [229] by explicit calculation. This result, although expected on general grounds, is quite remarkable in view of the rather different properties of the dispersion laws.

5. Three-flavor color superconductors

In this chapter our analysis is extended to three quark flavors. The additional flavor degree of freedom allows for new condensation patterns, most important the "color–flavor locking" (CFL) where both color and flavor $SU(3)$ are broken, leaving a residual unbroken $SU(3)$ symmetry under a certain combination of color and flavor rotations [16]. The main features of this phase are briefly summarized in Section 5.1 for the idealized case of three degenerate flavors. After that we discuss the influence of explicit symmetry breaking due to a realistic strange quark mass. We will show that the self-consistent treatment of the quark masses has important effects.

5.1. Three degenerate flavors

5.1.1. Condensation patterns

In Eq. (4.4) we have introduced the scalar diquark condensate,

$$s_{AA'} = \langle q^{\mathrm{T}} C \gamma_5 \tau_A \lambda_{A'} q \rangle \ , \tag{5.1}$$

where τ_A and $\lambda_{A'}$ are the antisymmetric generators of $SU(N_f)$ and $SU(N_c)$, acting in flavor space and in color space, respectively. Hence, in general $s_{AA'}$ is a matrix with a flavor index A and a color index A'. As before, we restrict ourselves to the physical number of colors, $N_c = 3$. Then $\lambda_{A'}$ denotes the three antisymmetric Gell–Mann matrices, λ_2, λ_5, and λ_7.

In the two-flavor case, which we have discussed in the previous chapter, there is only one anti-symmetric generator in flavor space, $\tau_A = \tau_2$, and the condensates $s_{2A'}$ form a vector with three color components A'. Since we can always rotate this vector into the $A' = 2$-direction by a global $SU(3)$ color transformation, it was sufficient to restrict the discussion of two-flavor color superconductors to a non-vanishing s_{22}. (The only exception was in Section 4.3.4 where we remarked that *global* color neutrality could be achieved by the formation of domains where the vector $s_{2A'}$ points into different directions.)

For three flavors, the flavor operators τ_A also denote the three antisymmetric Gell–Mann matrices, i.e., $s \equiv (s_{AA'})$ is a 3×3 matrix, $A, A' \in \{2, 5, 7\}$. Since the rows and columns of this matrix are in general three linearly independent vectors in color or flavor space, respectively, it is obvious that it usually cannot be reduced to a matrix with a single non-vanishing element by color or flavor rotations. In general, the best we can do is to bring the matrix in triangular form, e.g.,

$$s = \begin{pmatrix} s_{22} & 0 & 0 \\ s_{52} & s_{55} & 0 \\ s_{72} & s_{75} & s_{77} \end{pmatrix} \ , \tag{5.2}$$

where five of the six non-vanishing components can be chosen to be real. To this end we only need to perform general $SU(3)$ transformations in color space and diagonal $U(3)$ transformations in flavor space, i.e., a transformation to this form is still possible if the flavor $SU(3)$ is explicitly broken by unequal masses.

In the following we assume that we have three degenerate flavors, i.e., the Lagrangian is symmetric under $SU(3)$ transformations, both, in color and in flavor space. In this case we can perform a Ginzburg–Landau analysis. Similar to Eqs. (4.76)–(4.78) the effective potential reads

$$V(s) = -a^2 \operatorname{tr} s^\dagger s + \tfrac{1}{2}\lambda_1 (\operatorname{tr} s^\dagger s)^2 + \tfrac{1}{2}\lambda_2 \operatorname{tr}(s^\dagger s)^2 \tag{5.3}$$

with two invariant quartic terms. For $\lambda_2 < 0$ the ground state is of the form [62,248,249]

$$s_{22} \neq 0 \quad \text{and} \quad s_{AA'} = 0 \text{ if } (A, A') \neq (2, 2)\ . \tag{5.4}$$

Obviously, this is identical to the two-flavor condensate, embedded into the enlarged flavor space. A phase with this characteristics is therefore called "2SC phase" (i.e., "two-flavor color superconducting phase"). Most properties of this phase are of course identical to the real two-flavor case and do not need to be discussed again. The main difference is that in the enlarged flavor group the condensate is no longer a singlet but transforms as an antitriplet. As a consequence also chiral $SU(3)_L \times SU(3)_R$ is broken down to $SU(2)_L \times SU(2)_R$.

For $\lambda_2 > 0$ the ground state takes the form of a unit matrix [62,248,249],

$$s_{22} = s_{55} = s_{77} \neq 0 \quad \text{and} \quad s_{AA'} = 0 \text{ if } A \neq A'\ . \tag{5.5}$$

This is the so-called "color–flavor locked" (CFL) phase because the color index is locked to the flavor index (a better explanation of this name will be given in Section 5.1.2). A similar condensation pattern is well known from the B-phase of liquid ^{3}He where the components of the spin and the orbital angular momentum of the pair are locked in the same way (see, e.g., Ref. [233]). In the context of color superconductors it was suggested first in Ref. [16]. These authors considered a slightly more general ansatz with a totally symmetric color–flavor wave function. Besides combining a color antitriplet with a flavor antitriplet, as in Eq. (5.1), this can also be achieved with two sextets (see Table 4.1). In fact, in the CFL phase, the antitriplet terms are in general accompanied by induced sextet terms, which, in an obvious generalization of our notation, are of the form $s_{00} = s_{11} = s_{33} = s_{44} = s_{66} = s_{88}$ [16,62,250,251]. However, at least for interactions with the quantum numbers of a single gluon exchange, where the color-sextet channel is repulsive, these terms have been found to be small [16,251]. Therefore we will neglect them in the following.

For three-flavor QCD at asymptotic densities it can be shown that the CFL phase is the correct ground state [62,63]. The same is true for NJL-type models with three degenerate flavors. The main features of this condensation pattern will be summarized below (also see Ref. [12]).

5.1.2. Properties of the CFL phase

The three non-vanishing diquark condensates which form the CFL phase (Eq. (5.5)) are listed in Table 5.1. Separately, each of them looks like a two-flavor color superconductor, being a color and flavor antitriplet in the scalar channel. The first condensate is identical to the "standard" two-flavor scalar condensate and consists of paired red and green u and d quarks (cf. Eq. (4.6)). The two other condensates have the same structure but rotated in color and flavor space, i.e., $(r, g, b) \to (g, b, r) \to (b, r, g)$

Table 5.1
Color-flavor structure of the diquark pairs involved in the CFL phase

Condensate	$s_{22} = \langle q^{\mathrm{T}} C\gamma_5\tau_2\lambda_2 q\rangle$	$s_{55} = \langle q^{\mathrm{T}} C\gamma_5\tau_5\lambda_5 q\rangle$	$s_{77} = \langle q^{\mathrm{T}} C\gamma_5\tau_7\lambda_7 q\rangle$
Diquark pairs	(u_r, d_g), (u_g, d_r)	(d_g, s_b), (d_b, s_g)	(s_b, u_r), (s_r, u_b)

and $(u, d, s) \to (d, s, u) \to (s, u, d)$. Hence, all of the nine color–flavor combinations participate in a condensate,[39] and therefore all fermionic excitations are "gapped". In general, one finds an octet with $\Delta_{\mathrm{oct}} = \Delta_{\bar{3}} - \Delta_6$ and a singlet with $\Delta_{\mathrm{sing}} = 2\Delta_{\bar{3}} + 4\Delta_6$, where $\bar{3}$ and 6 refer to pairing in the color-antitriplet and color-sextet channel, respectively [16,228,251].Thus, $\Delta_{\mathrm{sing}} = 2\Delta_{\mathrm{oct}}$ if the color-sextet contribution is neglected. Moreover, for QCD at asymptotic densities it can be shown that $\Delta_{\mathrm{oct}} = 2^{-1/3}\Delta_{\mathrm{2SC}}$, where Δ_{2SC} is the gap of the corresponding 2SC solution [62]. For NJL-type interactions, further details of the dispersion laws and the gap equations will be presented in Section 5.2.1 within a more general framework.

In the CFL phase, unlike the 2SC phase, color and flavor $SU(3)$ as well as chiral symmetry are broken completely: The $SU(2)$ subgroups which are left unbroken, e.g., by s_{22} are broken by s_{55} and s_{77}. However, the CFL ground state is invariant under certain combinations of color and flavor rotations. This is more or less evident from the color–flavor structure of the condensates (see Table 5.1). For instance, if we declare the up quarks to be down quarks and vice versa, and at the same time interchange the meaning of red and green, the pairing pattern remains unchanged. Formally, one can easily check that

$$q^{\mathrm{T}} C\gamma_5(\tau_2\lambda_2 + \tau_5\lambda_5 + \tau_7\lambda_7)q \text{ is invariant under } q \to \mathrm{e}^{\mathrm{i}\theta_a(\tau_a - \lambda_a^{\mathrm{T}})} q \ , \tag{5.6}$$

where a runs from 1 to 8: Color and flavor transformations are locked to a common $SU(3)_{c+V}$ which explains the name "color–flavor locking". Note that this mechanism is not new. We already mentioned that an analogous pairing pattern and thus similar symmetry properties exist in liquid ^{3}He where the orbital angular momentum of the pair is locked to the spin. But also in the case of chiral symmetry breaking in vacuum the left- and right-handed $SU(N_f)$ transformations are locked to a common $SU(N_f)_V$ (see also Ref. [250]). In the CFL phase, both left- and right-handed flavor rotations, are locked to the color rotations and thereby indirectly to each other.

As before, the standard $U(1)$ symmetry, related to baryon number conservation, is broken down to Z_2. However, in contrast to the two-flavor case (cf. Section 4.1.2) it is not possible to define an unbroken "rotated" baryon number. Similarly, if we assume that the non-superconducting state is symmetric under $U_A(1)$ (which should be the case at very high densities), this is also broken down to Z_2. Thus, the pattern of symmetry breaking in the CFL phase reads

$$SU(3)_c \times SU(3)_L \times SU(3)_R \times U(1)(\times U_A(1)) \longrightarrow SU(3)_{c+V} \times Z_2(\times Z_{2A}) \ . \tag{5.7}$$

As a consequence of the complete breaking of $SU(3)_c$, all eight gluons acquire a mass in the CFL phase. The corresponding Meissner masses at asymptotic densities have been calculated in Ref. [252]. In contrast to the two-flavor case, Eq. (5.7) contains also spontaneously broken *global* symmetries of QCD. Hence, there are Goldstone bosons, namely a pseudoscalar octet related to the broken chiral symmetry,

[39] As one can see in Table 5.1, six species are paired with a fixed partner, whereas the remaining three (u_r, d_g, s_b) form a "triangle". Formally, this is related to the fact that the 9×9 matrix $a\tau_2\lambda_2 + b\tau_5\lambda_5 + c\tau_7\lambda_7$ can be decomposed into three 2×2 blocks and one 3×3 block [213]. This will become important later on.

and a scalar singlet related to the breaking of $U(1)$. In addition there could be a massless pseudoscalar singlet which corresponds to the breaking of $U_A(1)$.

Gauging a diagonal subgroup of the unbroken vector symmetry we can again define a "rotated" electromagnetic charge,

$$\tilde{Q} = Q - \tfrac{1}{2}\lambda_3 - \tfrac{1}{2\sqrt{3}}\lambda_8 \equiv Q - \mathrm{diag}_c(\tfrac{2}{3}, -\tfrac{1}{3}, -\tfrac{1}{3}) \ . \tag{5.8}$$

This definition differs from that in the two-flavor case, Eq. (4.9), by the λ_3-term. Since the 2SC ground state is invariant under $\exp(\mathrm{i}\alpha\lambda_3)$, we could have added this term in that case, too, but there was no need to do so. One can easily check that all diquark pairs listed in Table 5.1 have vanishing net $\tilde{Q}$-charge, i.e., the CFL ground state is a perfect insulator for $\tilde{Q}$-photons.

Another interesting result is that the $\tilde{Q}$-charges of all excitations, including the quarks, are integers (in units of the rotated charge of the electron). This is exactly what we expect from a confining theory! This observation has led Schäfer and Wilczek to the hypothesis of "quark–hadron continuity" [253]: It turns out that the CFL phase has the same symmetries and the same low-lying excitation spectrum as confined hypernuclear matter at low densities, i.e., there is a one-to-one correspondence between the quarks, gluons, and Goldstone bosons in the CFL phase, and the baryons, vector mesons, and Goldstone bosons in superfluid hypernuclear matter. This would imply that no phase transition is needed between the low-density and the high-density regime, and it is just a matter of convenience to describe the former in the language of hadronic degrees of freedom and the latter referring to quarks and gluons.[40]

Of course, all this only holds in the idealized case of an exact flavor $SU(3)$ symmetry. In reality we know that the ground state at low densities is "ordinary", i.e., non-strange, nuclear matter (unless the strange quark matter hypothesis turns out to be correct). Still there could be some modified quark–hadron continuity if the nuclear matter phase is followed by (almost symmetric) hypernuclear matter. On the other hand, coming from high densities, the CFL phase could be followed by a 2SC phase at lower densities, before matter turns into the hadronic phase (cf. upper right panel of Fig. 1.1 in the Introduction). In this case the transition would not be continuous. This so-called "color–flavor unlocking" transition from the CFL to the 2SC phase in the presence of realistic strange quark masses will be studied in great detail in the next section.

5.2. *Realistic strange quark masses*

The situations discussed so far are idealizations of the real world, where the strange quark mass M_s is neither infinite, such that strange quarks can be neglected completely (as we did in Chapter 4), nor degenerate with the masses of the up and down quarks (as assumed in Section 5.1). This leads to the question, whether quark matter at moderate densities behaves more like a two-flavor color superconductor or like a color–flavor locked state or like something else.

Since standard BCS pairing involves fermions with opposite momenta, $\vec{p}_a = -\vec{p}_b$, near their respective Fermi surface, pairing is only possible, if the two Fermi momenta are not too far apart, or, equivalently,

[40] There are interesting, although controversial, attempts to explain the structure of the vacuum in an analogous way, assuming that the vacuum is a Higgs phase with color–flavor locked octets of quark–antiquark condensates, $\langle \bar{q}\tau_a^{\mathrm{T}}\lambda_a q\rangle$ [254] (also see Ref. [255] how this could be tested on the lattice). Basically, this would lead to the same spectrum, i.e., integer charged quarks, massive gluons and massless pseudoscalar Goldstone bosons. Possible consequences of CFL diquark condensates at zero density have been discussed much earlier [256].

if the attraction is sufficiently strong. (Note that for unequal Fermi momenta a Cooper instability is no longer guaranteed for arbitrarily weak attractions, since in the non-interacting case the creation of a BCS pair would always enhance the free energy.) A rough estimate for the pairing condition is given by

$$|p_{\mathrm{F}}^a - p_{\mathrm{F}}^b| = \lesssim \sqrt{2}\Delta_{ab} \ , \tag{5.9}$$

where $p_{\mathrm{F}}^i = \theta(\mu_i - M_i)\sqrt{\mu_i^2 - M_i^2}$ are the nominal Fermi momenta and Δ_{ab} is the corresponding pairing gap.[41] In this section we will assume exact isospin symmetry ($m_u = m_d$) and that the chemical potentials for all quarks are equal. (Unequal chemical potentials will be discussed in Chapter 6.) The above criterion is then always fulfilled for the pairing of up and down quarks.

Obviously, for sufficiently large quark chemical potentials $\mu \gg M_s$, the strange quark mass (and thus its difference to the light quark masses) is negligible in Eq. (5.9) and *us*- and *ds*-pairing becomes possible as well. Hence, we expect a phase similar to the CFL phase, i.e., with non-vanishing values for s_{22}, s_{55}, and s_{77}. However, as a consequence of the mass difference, $M_s > M_u = M_d$, this phase will be less symmetric than in the idealized case discussed above. In particular we expect the condensates which contain one strange and one non-strange quark, i.e., s_{55} and s_{77}, to be smaller than s_{22} which contains only non-strange quarks. This corresponds to an $SU(2)_{\mathrm{color}+V}$ subgroup of the original symmetry, where isospin rotations are locked to certain $SU(2)$ rotations in color space. Later, when we also consider isospin breaking by non-equal chemical potentials (Chapter 6), all condensates will in general be different from each other. Following common practice, we will nevertheless call this phase "CFL phase" whenever s_{22}, s_{55}, and s_{77} do not vanish.

At small chemical potentials, the strange quark mass cannot be neglected against μ and a phase with $s_{55} = s_{77} \neq 0$ is no longer favored. From this we would conclude, that quark matter at low chemical potentials, $\mu \simeq M_s$, is a two-flavor color superconductor ("2SC"), where only up and down quarks participate in a diquark condensate. In addition, there also could be unpaired strange quarks.[42] In this case, the phase is often called "2SC+s" phase, but we will usually not make this distinction.

On the other hand, below a certain value of μ, one should finally reach the hadronic phase. This brings us back to the discussion in the end of the previous section. If we start in the CFL phase and keep lowering the chemical potential, the question is whether we first observe a transition to a 2SC phase followed by a transition to the hadronic phase at lower μ or whether the CFL phase is directly connected to the hadronic phase without an intermediate 2SC phase. The latter would be particularly interesting, since it would again imply the possibility of a quark–hadron continuity scenario. In this case, however, there must be at least one phase transition, e.g., from ordinary (non-strange) nuclear matter to superfluid hypernuclear matter

[41] This approximate relation has been derived in Ref. [257] for a simplified model with two quark species, requiring that the paired state is more favored than an unpaired state. For quark matter with three colors and three flavors the authors of Ref. [258] find a similar relation with $\sqrt{2}$ on the r.h.s. replaced by 2 for CFL pairing being more favored than no pairing at all and by a number not less than $\sqrt{3}$ for CFL pairing being more favored than 2SC pairing. For most of our purposes these details do not really matter. In particular we will never employ Eq. (5.9) to determine the stability of a given phase, but mostly for qualitative arguments. We should also mention that in certain physical situations the formally stable solutions are forbidden by additional constraints and the "unstable" solution is the only allowed one. In these cases Eq. (5.9) can be violated strongly (see Section 6.4).

[42] Similar to the blue up and down quarks (see Section 4.4), the strange quarks could pair in a spin-1 [229,228] or in a color-sextet [259] channel.

which then can continuously evolve to the CFL phase. (For a systematic discussion of the symmetry properties of the various quark and hadron phases, see Ref. [260].)

It is obvious from the discussion above that the answer to this question depends on the strange quark mass. If M_s is large, the CFL phase is disfavored already at large values of μ, possibly above the critical μ for the transition to the hadronic phase, whereas small values of M_s would favor a quark–hadron continuity scenario. More quantitative investigations have been performed first in Refs. [177,213,260]. The authors of Ref. [213] have studied the color–flavor unlocking phase transition in a model calculation with different values of M_s. Assuming that the region below $\mu \simeq 400$ MeV belongs to the hadronic phase, these authors came to the conclusion that a 2SC-phase exists if $M_s \gtrsim 250$ MeV. Here M_s is the constituent mass of the strange quark, which was treated as a free parameter in Ref. [213]. A similar analysis has been performed in Ref. [177] employing an instanton mediated interaction.

We have already seen, however, that constituent quark masses, if treated self-consistently, are T- and μ-dependent quantities, which in general depend on the presence of quark–antiquark and diquark condensates and which can even change discontinuously at a first-order phase boundary. This means, not only the phase structure depends on the effective quark mass, but also the quark mass depends on the phase. This interdependence has not been taken into account in Refs. [177,213]. In this situation the natural next step is to generalize the analysis of the previous chapter to three flavors and to study the interplay between diquark condensates and quark–antiquark condensates within an NJL-type model. In fact, the early analysis of Ref. [260] went already in this direction, although the authors made some simplifying assumptions about the quark dispersion laws. Below, we present a detailed discussion of these issues, mainly following Refs. [261,262].

5.2.1. Formalism

To get started, we supply the three-flavor NJL-type Lagrangian discussed in Chapter 3 with a quark–quark interaction term, i.e.,

$$\mathscr{L}_{\text{eff}} = \bar{q}(\mathrm{i}\partial\!\!\!/ - \hat{m})q + \mathscr{L}_{q\bar{q}} + \mathscr{L}_{qq} \ , \tag{5.10}$$

where

$$\mathscr{L}_{q\bar{q}} = G \sum_{a=0}^{8} [(\bar{q}\tau_a q)^2 + (\bar{q}\mathrm{i}\gamma_5\tau_a q)^2] - K[\det{}_f(\bar{q}(1+\gamma_5)q) + \det{}_f(\bar{q}(1-\gamma_5)q)] \tag{5.11}$$

as before, and

$$\mathscr{L}_{qq} = H \sum_{A=2,5,7} \sum_{A'=2,5,7} (\bar{q}\mathrm{i}\gamma_5\tau_A\lambda_{A'}C\bar{q}^{\mathrm{T}})(q^{\mathrm{T}}C\mathrm{i}\gamma_5\tau_A\lambda_{A'}q) \ . \tag{5.12}$$

Again, these effective interactions might arise via Fierz rearrangement from some underlying more microscopic theory and are understood to be used at mean-field level in Hartree approximation.

Note that $\mathscr{L}_{\text{eff}}$ is only the simplest Lagrangian which combines the phenomenologically constrained quark–antiquark interaction of Chapter 3 with a term which allows for diquark condensation in the scalar color-antitriplet channels. For instance, we neglect the interesting possibility of a combined quark–quark and quark–antiquark six-point interaction which naturally arises from a Fierz transformation of the instanton interaction [177]. We also neglect further condensates, like induced condensates or possible spin-1 pairing of so-far unpaired species.

Starting from $\mathscr{L}_{\rm eff}$ we proceed in the usual way. In order to calculate the mean-field thermodynamic potential at temperature T and quark chemical potential μ, we linearize the interaction in the presence of the diquark condensates s_{AA} and the quark–antiquark condensates ϕ_i. Introducing the constituent quark masses as in Eq. (3.5),

$$M_i = m_i - 4G\phi_i + 2K\phi_j\phi_k, \quad (i,j,k) = \text{any permutation of } (u,d,s)\ , \tag{5.13}$$

and the diquark gaps

$$\Delta_A = -2Hs_{AA}\ , \tag{5.14}$$

and employing Nambu–Gorkov formalism one gets

$$\begin{aligned}\Omega(T,\mu) = &-T\sum_n\int\frac{\mathrm{d}^3p}{(2\pi)^3}\,\frac{1}{2}\,\mathrm{Tr}\,\ln\left(\frac{1}{T}\,S^{-1}(\mathrm{i}\omega_n,\vec{p})\right)\\ &+2G(\phi_u^2+\phi_d^2+\phi_s^2)-4K\phi_u\phi_d\phi_s+H(|s_{22}|^2+|s_{55}|^2+|s_{77}|^2)\ .\end{aligned} \tag{5.15}$$

Here

$$S^{-1}(p) = \begin{pmatrix} \not{p}-\hat{M}+\mu\gamma^0 & \sum_A \Delta_A\gamma_5\tau_A\lambda_A \\ -\sum_A\Delta_A^*\gamma_5\tau_a\lambda_A & \not{p}-\hat{M}-\mu\gamma^0\end{pmatrix} \tag{5.16}$$

is the inverse fermion propagator, where $\hat{M}=\mathrm{diag}(M_u,M_d,M_s)$. Taking into account the Dirac structure, color, flavor, and the Nambu–Gorkov components, S^{-1} is a 72×72 matrix, and the trace in Eq. (5.15) has to be evaluated in this 72-dimensional space.

Since we are only dealing with one common chemical potential, there is some simplification due to isospin symmetry, $m_u=m_d$, which implies

$$\phi_u=\phi_d \quad\text{and}\quad s_{55}=s_{77}\ , \tag{5.17}$$

and thus $M_u=M_d$ and $\Delta_5=\Delta_7$. In this case a tedious but straightforward calculation yields

$$\begin{aligned}&\frac{1}{2}\,\mathrm{Tr}\,\ln\left(\frac{1}{T}\,S^{-1}(\mathrm{i}\omega_n,\vec{p})\right)\\ &\quad=3\ln\left(\frac{1}{T^4}(x_{uu}^+x_{uu}^- + 2|\Delta_2|^2y_{uu}+|\Delta_2|^4)\right)\\ &\qquad+2\ln\left(\frac{1}{T^4}(x_{uu}^+x_{ss}^- + 2|\Delta_5|^2y_{us}+|\Delta_5|^4)\right)+2\ln\left(\frac{1}{T^4}\,(x_{ss}^+x_{uu}^- + 2|\Delta_5|^2y_{us}+|\Delta_5|^4)\right)\\ &\qquad+\ln\left(\frac{1}{T^8}\left[x_{uu}^+x_{uu}^-x_{ss}^+x_{ss}^- + 2|\Delta_2|^2x_{ss}^+x_{ss}^-y_{uu}+4|\Delta_5|^2(x_{uu}^+x_{ss}^- + x_{ss}^+x_{uu}^-)y_{us}\right.\right.\\ &\qquad+|\Delta_2|^4x_{ss}^+x_{ss}^- + 4|\Delta_2|^2|\Delta_5|^2(x_{ss}^+x_{us}^- + x_{us}^+x_{ss}^-)+4|\Delta_5|^4(x_{uu}^+x_{ss}^- + x_{ss}^+x_{uu}^- + 4y_{us}^2)\\ &\qquad\left.\left.+8|\Delta_2|^2|\Delta_5|^4y_{ss}+32|\Delta_5|^6y_{us}+16|\Delta_5|^8\right]\right)\end{aligned} \tag{5.18}$$

where we have introduced the abbreviations

$$x_{ff'}^{\pm} = (\omega_n\pm\mathrm{i}\mu)^2+\vec{p}^{\,2}+M_fM_{f'} \quad\text{and}\quad y_{ff'}=\omega_n^2+\mu^2+\vec{p}^{\,2}+M_fM_{f'}\ . \tag{5.19}$$

With these definitions one finds for the argument of the first logarithm on the r.h.s. of Eq. (5.18)

$$x_{uu}^{+}x_{uu}^{-} + 2|\Delta_2|^2 y_{uu} + |\Delta_2|^4 = (\omega_n^2 + \omega_u^{-2})(\omega_n^2 + \omega_u^{+2}) \tag{5.20}$$

with

$$\omega_u^{\mp} = \sqrt{(\sqrt{\vec{p}^2 + M_u^2} \mp \mu)^2 + |\Delta_2|^2}\ . \tag{5.21}$$

Obviously, these are exactly the dispersion laws of the paired quarks in a two-flavor color superconductor, Eq. (4.56). The corresponding Matsubara sums are readily turned out using Eq. (2.49).

The other terms in Eq. (5.18) are in general more complicated. There are, however, two simplifying limits. The first one corresponds to a two-flavor color superconductor, together with unpaired strange quarks. In this case Δ_5 vanishes and Eq. (5.18) becomes

$$\begin{aligned}
&\frac{1}{2}\,\mathrm{Tr}\,\ln\left(\frac{1}{T}\,S^{-1}(\mathrm{i}\omega_n, \vec{p})\right)\Big|_{\Delta_5=0} \\
&\quad = 4\left[\ln\left(\frac{\omega_n^2 + \omega_u^{-2}}{T^2}\right) + \ln\left(\frac{\omega_n^2 + \omega_u^{+2}}{T^2}\right)\right] + 2\left[\ln\left(\frac{\omega_n^2 + E_u^{-2}}{T^2}\right) + \left(\frac{\omega_n^2 + E_u^{+2}}{T^2}\right)\right] \\
&\qquad + 3\left[\ln\left(\frac{\omega_n^2 + E_s^{-2}}{T^2}\right) + \ln\left(\frac{\omega_n^2 + E_s^{+2}}{T^2}\right)\right]
\end{aligned} \tag{5.22}$$

with $E_f^{\mp} = \sqrt{\vec{p}^2 + M_f^2} \mp \mu$. Here we recover the fact, that only four of the six light quarks (two colors) participate in the 2SC condensate, while the two remaining ones and all strange quarks fulfill the dispersion laws of free particles with effective masses M_f.

We can also reproduce the structure of the dispersion laws of the idealized three-flavor symmetric CFL-state. To this end we evaluate Eq. (5.18) for $M_u = M_s$ and $\Delta_2 = \Delta_5$. One finds

$$\begin{aligned}
&\frac{1}{2}\,\mathrm{Tr}\,\ln\left(\frac{1}{T}\,S^{-1}(\mathrm{i}\omega_n, \vec{p})\right)\Big|_{M_u=M_s,\ \Delta_2=\Delta_5} \\
&\quad = \left[\ln\left(\frac{\omega_n^2 + \omega_{\mathrm{oct}}^{-2}}{T^2}\right) + \ln\left(\frac{\omega_n^2 + \omega_{\mathrm{oct}}^{+2}}{T^2}\right)\right] + \left[\ln\left(\frac{\omega_n^2 + \omega_{\mathrm{sing}}^{-2}}{T^2}\right) + \ln\left(\frac{\omega_n^2 + \omega_{\mathrm{sing}}^{+2}}{T^2}\right)\right]
\end{aligned} \tag{5.23}$$

with $\omega_{\mathrm{oct}}^{\mp} = \omega_u^{\mp}$ and $\omega_{\mathrm{sing}}^{\mp} = \sqrt{(\sqrt{\vec{p}^{\,2} + M_u^2} \mp \mu)^2 + |2\Delta_2|^2}$. Thus $\Delta_{\mathrm{sing}} = 2\Delta_{\mathrm{oct}}$, as already mentioned in Section 5.1.2.

The Matsubara sums over Eqs. (5.22) and (5.23) can again be turned out with the help of Eq. (2.49). In general, i.e., for Eq. (5.18) with arbitrary values of the condensates, this cannot be done so easily. If one combines the second with the third logarithm on the r.h.s., the argument becomes a polynomial of fourth order in ω_n^2. The same is true for the argument of the fourth logarithm. The corresponding dispersion laws are related to the zeros of these polynomials. Although, in principle, the zeros of a polynomial of fourth order can be determined analytically, the resulting expressions are usually difficult to handle. Therefore, in practice one has to determine the dispersion laws numerically. After that, one can again employ Eq. (2.49) to calculate the Matsubara sum. Alternatively, one can turn out the Matsubara sum numerically

without previous determination of the dispersion laws. To that end, in order to get a convergent result, one should subtract and add a properly chosen term, $\sum_n A_n = \sum_n (A_n - B_n) + \sum_n B_n$, where A_n stands for Eq. (5.18), $\sum_n B_n$ can be turned out analytically and $A_n - B_n$ is well-behaved. This is the method we have used.[43]

Because of the isospin relations, Eq. (5.17), the thermodynamic potential depends on four different condensates, ϕ_u, ϕ_s, s_{22}, and s_{55}. The self-consistent solutions are again given by the stationary points of the potential,

$$\frac{\delta\Omega}{\delta\phi_u} = \frac{\delta\Omega}{\delta\phi_s} = \frac{\delta\Omega}{\delta s_{22}^*} = \frac{\delta\Omega}{\delta s_{55}^*} = 0 \ . \tag{5.24}$$

The explicit evaluation of these derivatives is trivial, but leads to rather lengthy and not very illuminating expressions, which we do not present. However, since the thermodynamic potential is a function of the squared diquark gaps, $|\Delta_A|^2$, it is obvious that there are always trivial solutions $\Delta_A = 0$, independent of the values of the other gap parameters. For the non-trivial solutions the four equations are coupled and have to be solved simultaneously. The stable solution is again the one which corresponds to the lowest value of Ω.

5.2.2. Numerical results without 't Hooft interaction

To fix the parameters for the numerical analysis we begin again with a color current interaction (cf. Eq. (4.67)),

$$\mathscr{L}_{\rm int} = -g \sum_{a=1}^{8} (\bar{q}\gamma^\mu \lambda_a q)^2 \ . \tag{5.25}$$

This interaction was also the starting point of the model calculations in Refs. [16,213,260]. Performing Fierz transformations we find that the effective coupling constants which enter Eqs. (5.11) and (5.12) are related to each other as (see Appendix A.3)

$$G : K : H = 1 : 0 : \tfrac{3}{4} \ . \tag{5.26}$$

In addition, there are again various other channels, which in principle should be taken into account to be fully self-consistent.[44] This is, however, not the goal of the present calculation. At this point, Eq. (5.25) should only be viewed as a "typical" interaction, used to relate the coupling constant in the diquark channel to the quark–antiquark coupling constant.

Perhaps the most severe limitation of this choice is the fact that the six-point interaction completely vanishes, i.e., $K = 0$. Similar to what we have discussed in Section 2.4, this means that there is no

[43] Some authors use simplified dispersion laws to circumvent this problem. The authors of Ref. [260] assume that, even in the presence of a symmetry breaking dynamical strange quark mass, the dispersion laws in the CFL phase are of the standard form, Eq. (4.56), with an octet gap attributed to the six non-strange and two strange quarks, and a singlet gap attributed to the third strange quark. The authors of Ref. [263] make the assumption that the particle part and the antiparticle part of the Hamiltonian separate. This enables them to derive an analytical expression for the quasiparticle energies. It turns out that the numerical results obtained in this approximate way are very similar to our exact solutions.

[44] As discussed in Section 4.3, already for two flavors, a self-consistent treatment requires the simultaneous consideration of possible expectation values in six different channels. Here we should have at least twice as many, because of the broken flavor symmetry. Moreover, as mentioned earlier, even in the idealized case of three massless flavors, there is an induced color-sextet diquark condensates in the CFL-phase [16,62,251].

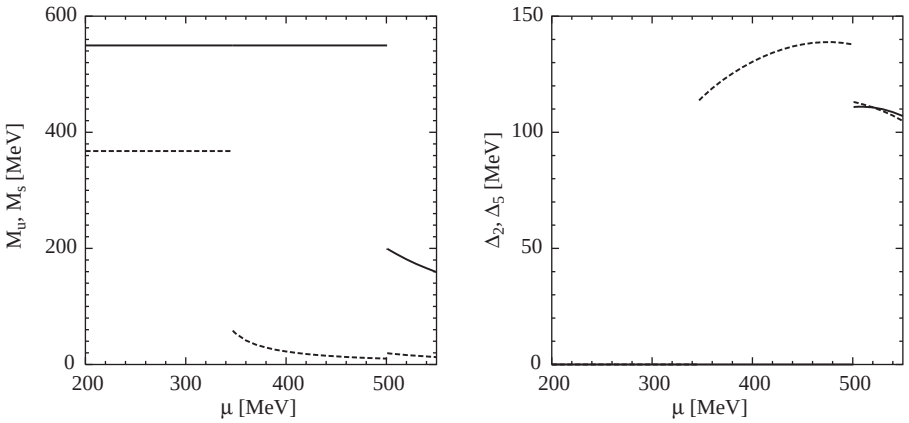

Fig. 5.1. Gap parameters at $T = 0$ as functions of the quark chemical potential μ for $K = 0$. Left: Constituent masses of up and down quarks (dashed), and of strange quarks (solid). Right: Diquark gaps Δ_2 (dashed) and Δ_5 (solid). Adapted with permission from Ref. [261] with slightly different parameters.

flavor mixing in the quark–antiquark channel. There is of course flavor mixing in the (flavor-antitriplet) diquark condensates, where always quarks of two different flavors are paired. Hence, the strange quarks decouple from the non-strange quarks in all but the CFL phase. The consequences of this limitation will be investigated in Section 5.2.3 where we introduce non-vanishing values of K.

Employing Eq. (5.26), there remain four parameters: the coupling constant G, the cut-off Λ, and the two current quark masses, m_u and m_d. We take $\Lambda = 602.3\,\text{MeV}$ and $m_u = 5.5\,\text{MeV}$ as in parameter set RKH [145] of Table 3.1, and tune the two remaining parameters, G and m_s, to reproduce the vacuum constituent quark masses $M_u = 367.6\,\text{MeV}$ and $M_s = 549.5\,\text{MeV}$ of that set. In this way we find $G\Lambda^2 = 2.319$ and $m_s = 112.0\,\text{MeV}$.

We begin with the discussion of the results at zero temperature. The behavior of the four gap parameters as functions of the quark chemical potential μ is displayed in Fig. 5.1. In the left panel we show the constituent quark masses M_u and M_s, in the right panel the diquark gaps Δ_2 and Δ_5. One can clearly distinguish between three phases. At low chemical potentials $\mu < \mu_1 = 346.9\,\text{MeV}$, the system remains in the vacuum phase, i.e., the diquark gaps vanish and the constituent quark masses stay at their vacuum values. For the condensates this means $s_{22} = s_{55} = s_{77} = 0$, while ϕ_u and ϕ_s are large. Hence, in a schematic sense, we can identify this phase with the "hadronic phase", keeping in mind the limitations of this picture we have discussed earlier.

At $\mu = \mu_1$ a first-order phase transition takes place and the system becomes a two-flavor color superconductor: The diquark condensate s_{22} has now a non-vanishing expectation value, related to a non-vanishing diquark gap Δ_2, whereas Δ_5 remains zero. Just above the phase boundary we find $\Delta_2 = 113.7\,\text{MeV}$. At the same time the mass of the up quark drops from the vacuum value to $M_u = 58.3\,\text{MeV}$. With increasing μ, M_u decreases further, while Δ_2 increases until it reaches a maximum at $\mu \simeq 475\,\text{MeV}$. Just below the next phase boundary at $\mu = \mu_2 = 500.8\,\text{MeV}$ we find $\Delta_2 = 137.8\,\text{MeV}$ and $M_u = 10.0\,\text{MeV}$.

In the 2SC phase the baryon number density is of course no longer zero and increases from about 2.5 times nuclear matter density at $\mu = \mu_1$ to about 6.5 times nuclear matter density at $\mu = \mu_2$. The density of strange quarks remains zero up to $\mu = \mu_2$.

At $\mu = \mu_2$ the system undergoes a second phase transition, now from the 2SC phase into the CFL phase, which is characterized by a non-vanishing diquark gap Δ_5 (together with a non-vanishing Δ_2). The phase transition is again of first order: At the transition point Δ_5 jumps from zero to 110.9 MeV, while M_s drops from 549.5 to 199.6 MeV. The non-strange quantities are also discontinuous and change in the opposite direction: M_u jumps from 10.9 to 19.4 MeV, and Δ_2 drops from 137.8 to 113.1 MeV, in rather good agreement with the asymptotic relation $\Delta_{\rm oct} = 2^{-1/3}\Delta_{\rm 2SC}$ [62]. The density jumps from 6.5 to 9.3 times nuclear matter density.

As anticipated, unlike the ideal $SU(3)$-flavor symmetric case, the sizes of the gaps Δ_2 and Δ_5 are no longer equal. In fact, as we are quite far away from an exact $SU(3)$ symmetry, it is remarkable that the diquark gaps Δ_2 and Δ_5 are so similar at the transition point. At least partially, this may be attributed to the cut-off. Obviously, when the Fermi momentum comes close to Λ important parts of the gap equation are cut off, and the gap becomes smaller with increasing chemical potentials. For the up and down quarks this situation is reached somewhat earlier than for the strange quarks because of their higher Fermi momenta, related to their lower mass. This also explains why we find $\Delta_5 > \Delta_2$ above $\mu \simeq 520$ MeV. Here we certainly approach the limits of the model.

The most important point of our analysis is the discontinuous behavior of the strange quark mass at the phase boundary. As we have argued in the introductory part of this section, we expect the CFL phase to be stable if μ is considerably larger than M_s and that it becomes unstable when $\mu \lesssim M_s$. Clearly, this kind of reasoning can only be used to estimate the critical μ if M_s is more or less constant. Obviously this is not the case. Just above the phase boundary we have $\Delta_5^{\rm crit} := |p_{\rm F}^u - p_{\rm F}^s|/\sqrt{2} = 29\,{\rm MeV} < \Delta_5 = 111\,{\rm MeV}$, which means that the approximate stability condition, Eq. (5.9), is well satisfied and far away from its limit. In fact, the reason for the phase transition at $\mu = \mu_2$ is not that u and s quarks can no longer pair below that value. We still find a CFL solution down to much lower values of μ. However, for $\mu < \mu_2$, this solution is only metastable, and there is a more favored solution with a much higher strange quark mass which cannot support a pairing of u and s quarks. In this sense we may say that the 2SC–CFL phase transition is driven by the chiral phase transition in the strange sector, although of course all condensates mutually influence each other.

Relations like Eq. (5.9) have been used to argue, that the color–flavor-unlocking transition at $T = 0$ must be first order, because the mismatch of the Fermi surfaces of strange and non-strange quarks prevents the gap parameter Δ_5 from becoming arbitrarily small [213,257,258]. Qualitatively, our results support these arguments, even though the quantitative values for the minimal gap derived in these references cannot be applied to cases with density-dependent masses: We find that there is indeed a non-vanishing lowest possible value of Δ_5 for metastable CFL solutions and the minimal value of Δ_5 in an absolutely stable CFL phase is even larger.

We now extend our analysis to non-vanishing temperatures. For an easier interpretation, let us first neglect the diquark condensates. The resulting phase diagram in the μ–T plane is shown in the left panel of Fig. 5.2. Since for $K = 0$ the different quark flavors decouple, there are two separate phase boundaries, corresponding to the chiral phase transition of the non-strange quarks at lower chemical potentials and of the strange quarks at higher chemical potentials. Thus, at low temperatures, we have three different regimes. When the temperature is increased, both phase boundaries end in a second-order endpoint.

When diquark condensates are included (right panel) these first-order phase boundaries are partially shifted to lower chemical potentials, but remain qualitatively unchanged. As discussed for zero temperature, at low temperatures the disappearance of one type of quark–antiquark condensate is always accompanied by the appearance of a new diquark condensate. We have the "hadronic" (better: normally

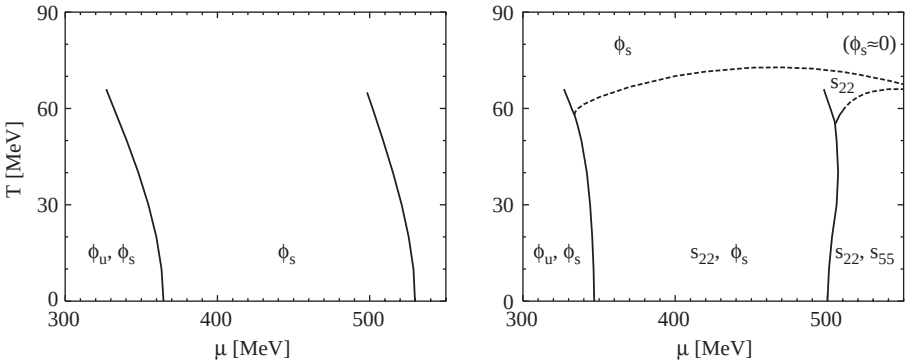

Fig. 5.2. Phase diagram for $K = 0$ in the μ–T plane without (left) and with (right) diquark condensates taken into account. The solid lines indicate phase boundaries with a first-order phase transition, the dashed lines correspond to second-order phase transitions. The different phases can be distinguished by different values for the various condensates. Within the figure we have indicated only those condensates which are significantly different from zero. (Note that because of isospin symmetry, $\phi_d = \phi_u$ and $s_{77} = s_{55}$.) The right figure has been adapted from Ref. [261] for slightly different parameters.

conducting) phase with $\phi_u, \phi_s \neq 0$ and vanishing diquark condensates, the 2SC phase with $\phi_s, s_{22} \neq 0$, but $\phi_u \approx 0$ and $s_{55} \neq 0$, and the CFL phase with $s_{22}, s_{55} \neq 0$, but $\phi_u, \phi_s \approx 0$. On the other hand, at high temperatures all condensates vanish. This leads to two additional phase boundaries. The first one corresponds to the melting of the diquark condensate in the 2SC phase. As we have seen before, this is a second-order phase transition with a transition temperature approximately given by the standard BCS relation, Eq. (4.94). For instance, at $\mu = 400\,\text{MeV}$ we find $\Delta_2(T = 0) = 130.3\,\text{MeV}$, and $T_c = 70.1\,\text{MeV}$, whereas from Eq. (4.94) we would expect $T_c = 74.3\,\text{MeV}$.

Starting from the CFL phase and increasing the temperature, one first observes a melting of the diquark gap Δ_5, before at somewhat higher temperatures Δ_2 vanishes as well. The intermediate 2SC phase "above" the CFL-phase is partially separated from the 2SC regime "left" to the CFL-phase by the upper part of the chiral phase boundary of the strange quark. Note that this part of the phase boundary is not affected at all by the diquark condensate, since the strange quarks are completely decoupled from the non-strange sector. In particular, the critical endpoint is at the same place as in the left figure. (The same is of course true for the endpoint of the non-strange chiral phase boundary which is located in a regime where the diquark condensates vanish.)

Based on the assumption that Δ_5 is always smaller than Δ_2 (which is not really true at $T = 0$, as we have seen), the earlier disappearance of Δ_5 and hence the existence of a 2SC phase "above" the CFL phase was already anticipated in Ref. [12]. Applying similar arguments as at zero temperature (cf. Refs. [213,257,258]) it was also predicted in that reference, that the corresponding color–flavor unlocking transition should stay first order. This was corroborated by a second argument, claiming that the phase transition corresponds to a finite-temperature chiral restoration phase transition in a three-flavor theory. In this case the universality arguments of Ref. [48] should apply, stating that the phase transition should be of first order.

Indeed, following the phase boundary from the left, we find that the transition continues to be first order. However, above a critical point at $\mu \simeq 511\,\text{MeV}$ and $T \simeq 60\,\text{MeV}$ the phase transition becomes second order. This is illustrated in Fig. 5.3, where the constituent masses (left panel) and the diquark gaps

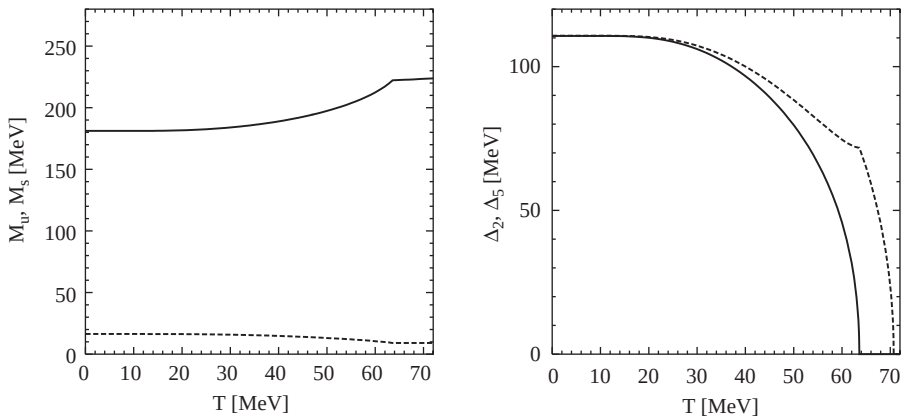

Fig. 5.3. Gap parameters at $\mu = 520\,\mathrm{MeV}$ as functions of the temperature. Left: Constituent masses of up and down quarks (dashed), and of strange quarks (solid). Right: Diquark gaps Δ_2 (dashed) and Δ_5 (solid). Adapted from Ref. [261] for slightly different parameters.

(right panel) are displayed as functions of the temperature for fixed $\mu = 520\,\mathrm{MeV}$. As one can see, both condensates smoothly go to zero at $T = 63.5$ and $70.7\,\mathrm{MeV}$, respectively. Of course, it is possible that the second-order phase transitions are artifacts of the mean-field approximation and become first order if fluctuations are included [264,265]. In any case, the arguments of Refs. [213,257,258] in favor of a first-order color–flavor unlocking phase transition are much less stringent at finite temperature, where even for vanishing condensates the Fermi surfaces are smeared due to thermal effects. The applicability of the universality argument is also questionable in the present situation because the 2SC phase is not a three-flavor chirally restored phase, but only $SU(2) \times SU(2)$ symmetric. Recall that even $SU(3)_V$ is broken spontaneously by the flavor-antitriplet diquark condensates, and explicitly by the unequal current quark masses. Therefore a rigorous prediction of the true order of the phase transition is rather difficult.

Finally, we should repeat that our results at $\mu \gtrsim 500\,\mathrm{MeV}$ are sensitive to the cut-off. This is somewhat disturbing, since the entire CFL phase belongs to this region. As we will see below, the situation improves when a flavor mixing interaction is included, which shifts the 2SC–CFL phase boundary to lower chemical potentials.

5.2.3. Influence of the 't Hooft interaction

We now study the effect of a non-vanishing 't Hooft interaction on the results of the previous section [262]. To this end we replace the color current interaction, Eqs. (5.25) and (5.26), by a set of parameters with $K \neq 0$. For a better comparison with our previous results we leave the cut-off Λ and the light current mass m_u unchanged, but vary the coupling constant G and the strange current mass m_s in such a way that the vacuum masses M_u and M_s remain constant. We also keep the quark–quark coupling constant H at a fixed value. This means that instead of $H : G = 3 : 4$ we now have $H : G_{\mathrm{eff}} = 3 : 4$, where $G_{\mathrm{eff}} = G - \frac{1}{2} K \phi_s^{\mathrm{vac}}$ is the effective four-point coupling which determines the light quark constituent mass in vacuum (cf. Eq. (2.86)).

Four sets of parameters obtained in this way (including the $K = 0$ parameters of the previous section) are listed in Table 5.2. Set III is of particular interest because, apart from the quark–quark coupling constant, it is identical to parameter set RKH of Table 3.1 (i.e., the empirical fit of Ref. [145]). This was

Table 5.2
Model parameters employed in the numerical studies of this section

Set	Λ (Mev)	m_u (Mev)	m_s (Mev)	$G\Lambda^2$	$K\Lambda^5$	$H\Lambda^2$	$H:G$
I	602.3	5.5	112.0	2.319	0.00	1.739	0.75
II	602.3	5.5	123.6	2.123	5.00	1.739	0.82
III	602.3	5.5	140.7	1.835	12.36	1.739	0.95
IV	602.3	5.5	158.5	1.536	20.00	1.739	1.13

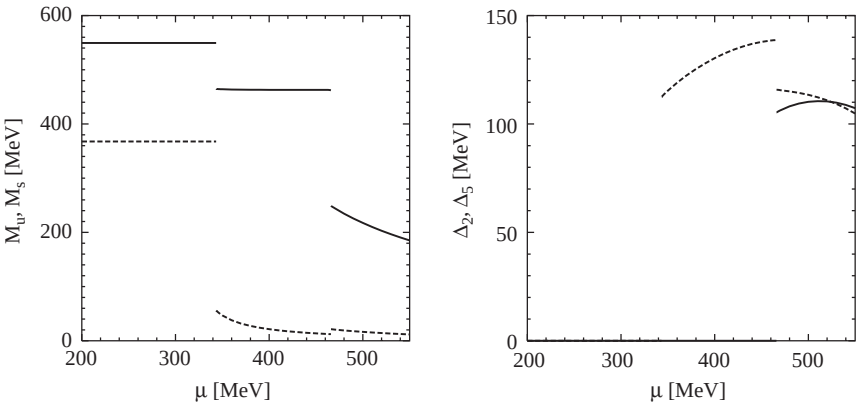

Fig. 5.4. The same as Fig. 5.1, but for $K\Lambda^5 = 12.36$ (Table 5.2, parameter set III).

our standard parameter set for the numerical studies in Chapter 3, e.g., for investigating the strange matter hypothesis in Section 3.3. Therefore let us begin with these parameters.

In Fig. 5.4, the constituent masses and the diquark gaps at $T = 0$ are displayed as functions of the chemical potential. When we compare this figure with Fig. 5.1, the analogous figure for $K = 0$, we see that the essential features remain unchanged: There are three distinct phases, i.e., vacuum with spontaneously broken chiral symmetry, 2SC, and CFL, separated by first-order phase boundaries at which the constituent quark masses change discontinuously. Of course, as pointed out several times before, due to the flavor mixing at $K \neq 0$ the strange quark mass stays no longer constant across the first phase boundary, such that $M_s < M_s^{\text{vac}}$ in the 2SC phase. This has the consequence that the 2SC phase is less stable against transitions to the CFL phase and thus the critical chemical potential μ_2 for the 2SC–CFL phase transition is shifted to lower values. (The critical chemical potential μ_1 corresponding to the vacuum-2SC phase transition is only slightly reduced.) In turn, since the CFL phase starts at lower chemical potentials, the value of M_s just above μ_2 is larger than for $K = 0$ and this causes a larger difference between the diquark condensates Δ_2 and Δ_5 in this regime. Roughly speaking, we may say that the CFL solutions are not very sensitive to K, but solutions which have only been metastable for $K = 0$ become absolutely stable down to lower values of μ when K is increased.

For $K = 0$ we found that the density of strange quarks is zero in the entire 2SC phase. One could have expected that this is changed by a flavor mixing interaction which reduces M_s in the 2SC phase and in this way the threshold for populating strange quark states. We see, however, that the situation is more

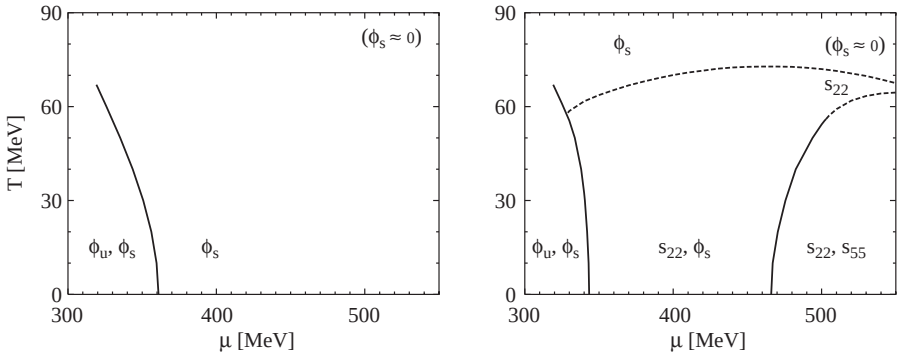

Fig. 5.5. The same as Fig. 5.2, but for $K\Lambda^5 = 12.36$ (Table 5.2, parameter set III).

complicated because at the same time the 2SC–CFL phase boundary is lowered as well. Nevertheless, for parameter set III there is indeed a small regime (about 3 MeV below μ_2) where the density of strange quarks is non-zero.

We now turn to non-vanishing temperature. The μ–T phase diagram for parameter set III is displayed in the right panel of Fig. 5.5. In order to understand the main differences to the $K = 0$ case (Fig. 5.2) it is again instructive, first to neglect the influence of the diquark condensates. The corresponding phase diagrams are displayed in the left panels of both figures. As one can see, the main effect of the flavor mixing is that the second phase boundary, i.e., the one which for $K = 0$ was related to the chiral phase transition of the strange quark has completely disappeared for $K\Lambda^5 = 12.36$. This difference has important consequences for the phase diagrams with diquark condensates included (right panels): For $K = 0$ (Fig. 5.2) the phase boundary between 2SC and CFL phase at low temperatures has two origins: the chiral phase transition of the strange quark and the color–flavor locking transition. Whereas the former tends to turn the phase boundary to the left (the strange quark condensate ϕ_s is more stable at lower μ) the latter tends to turn the boundary to the right (the diquark condensates s_{55} and s_{77} are more stable at higher μ). As a consequence of this competition the phase boundary goes up more or less vertically and finally splits into two branches. This is quite different for $K\Lambda^5 = 12.36$ (Fig. 5.5). Since without diquark condensates (left) there is no second phase transition, the behavior of the phase boundary is basically dictated by the diquark condensates. Consequently, it turns to the right and there is no splitting into two branches. As for $K = 0$, the phase transition is first order at lower T but becomes second order above $T \simeq 56$ MeV. (We repeat that it must be first order at low temperature because of the mismatch of the strange and the non-strange Fermi surfaces.)

A more general overview about the K dependence of the phase structure is given in Fig. 5.6 where the phase boundaries are displayed for the four parameter sets of Table 5.2. For the sake of clarity, we do not distinguish between first- and second-order phase transitions in this diagram. Obviously, except of the 2SC–CFL boundary, all other phase boundaries are rather insensitive to K, once the vacuum masses and the value of the quark–quark coupling constant H are fixed. As discussed above, the 2SC–CFL phase boundary is shifted to lower chemical potentials when K is increased. However, even for the relatively large value $K\Lambda^5 = 20$, there is still a large region where the 2SC phase is the most dominant quark phase.

In this context we should note that the above analysis of flavor mixing effects is not complete, since some terms which could arise from the instanton interaction are missed in our starting point, Eqs. (5.10)–(5.12).

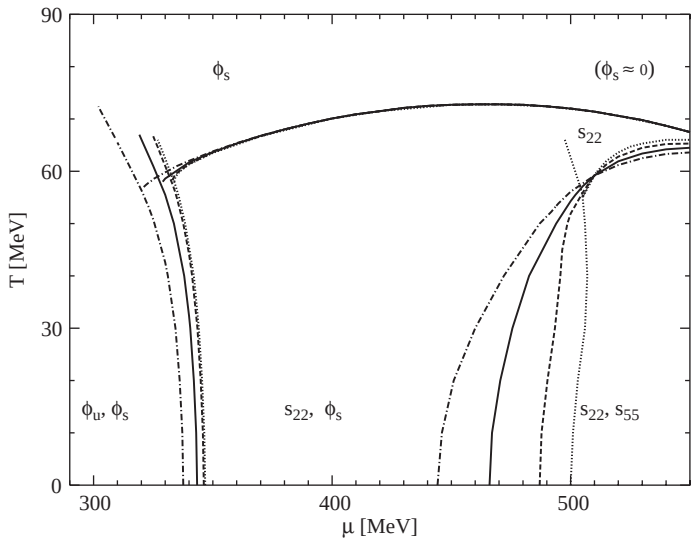

Fig. 5.6. Phase diagrams in the μ–T plane for parameter set I ($K = 0$, dotted), II ($K\Lambda^5 = 5$, dashed), III ($K\Lambda^5 = 12.36$, solid), and IV ($K\Lambda^5 = 20$, dash–dotted).

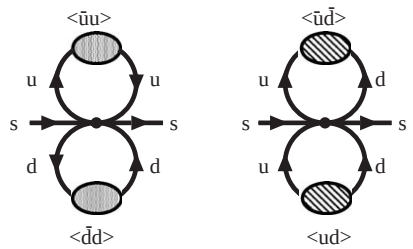

Fig. 5.7. Two contributions to the constituent mass of the strange quark. Left: self-energy proportional to $\phi_u \phi_d$. Right: self-energy proportional to $|s_{22}|^2$.

To see this, consider a six-point vertex as shown in Fig. 3.1. We have seen earlier that this vertex can contribute to the constituent quark mass if we close two quark loops (Fig. 3.2). Thus the self-energy of the strange quark (for instance) contains a term proportional to the non-strange condensates ϕ_u and ϕ_d, as depicted in the left diagram of Fig. 5.7. This term has been taken into account in our model (see Eq. (5.13)). However, in the presence of diquark condensates there is also a term proportional to $|s_{22}|^2$ due to the fact, that a diquark pair can be created or destroyed in the condensate (right diagram of Fig. 5.7). This contribution has not been taken into account in our calculations. Similarly, if one closes a single quark loop and Fierz transforms the resulting four-point vertex one obtains flavor and density-dependent contributions to the quark–quark interaction which are not contained in Eq. (5.12). Instanton effects of this type have partially been discussed in Ref. [177], but not self-consistently including constituent quark masses away from the chiral limit. An extension of our model in this direction would certainly be very interesting.

Our calculations suggest that the 2SC phase is favored in a relatively large regime, even for rather large values of K. However, before drawing early conclusions we should recall that our model is lacking a realistic description of the hadronic phase. Hence, it is still possible that the 2SC phase is excluded if the hadron–quark phase transition takes place at a relatively large chemical potential. Examples for this scenario will be discussed in Section 7.1. We should also mention that the stress imposed to the Cooper pairs by unequal masses could result in new phases, like crystalline color superconductors [20,21] or a CFL phase with condensed kaons [17–19]. These phases will briefly be discussed in Section 6.4. Before, we will introduce another source of stress which comes about by the requirement of electric and color neutrality. As a consequence, the chemical potentials and, thus, the Fermi momenta of up and down quarks become unequal, thereby disfavoring the 2SC phase. This will be investigated in more detail in the next chapter.

6. Neutral quark matter

In the previous chapter we have restricted ourselves to the thermodynamics of quark matter depending on temperature and one common quark chemical potential. However, for the description of a possible quark core of a neutron star we must consider neutral quark matter in beta equilibrium. As in our discussion of strange quark matter in Section 3.3, this means that we have to deal with more than one independent chemical potential. In the present case the situation is even more involved. In addition to electric neutrality, we also have to impose color neutrality, which is not automatically realized in color superconducting phases with color-independent chemical potentials (see Section 4.3.4).[45] In fact, strictly speaking, the matter has to be in a color singlet state. However, as shown in Ref. [266], the energy related to projecting color neutral systems onto color singlets becomes negligible in the thermodynamic limit. It is thus sufficient to require electric and color neutrality.

It has been pointed out by Alford and Rajagopal that these constraints strongly disfavor the 2SC phase, such that this phase might not be present in compact stars [247]. The basic arguments can be understood in the following way. Suppose we have a system of up, down, and strange quarks together with leptons. As we have seen in Section 4.3.4, imposing color neutrality in 2SC matter does not cost much energy and we may concentrate on electric neutrality. Moreover, as discussed in Section 3.3, the lepton fraction is very small in beta equilibrated matter, such that their contribution to the electric charge can be neglected. The quark densities must then satisfy the relation (cf. Fig. 3.9)

$$2n_u - n_d - n_s \approx 0 \ . \tag{6.1}$$

Obviously, for equal quark masses this relation is realized by equal densities $n_u = n_d = n_s$ and quark matter is in the CFL phase. The arguments of Alford and Rajagopal are based on an expansion in the strange quark mass, which they assumed to be small compared with the chemical potential. In this case the densities and thus the Fermi momenta are still similar to each other and we may write $p_{\mathrm{F}}^i = \bar{p}_{\mathrm{F}} + \delta p_{\mathrm{F}}^i$ with $\delta p_{\mathrm{F}}^i \ll \bar{p}_{\mathrm{F}}$. Hence

$$n_i = \frac{1}{\pi^2}\, {p_{\mathrm{F}}^i}^3 \approx \frac{1}{\pi^2}\,(\bar{p}_{\mathrm{F}}^3 + 3\bar{p}_{\mathrm{F}}^2 \delta p_{\mathrm{F}}^i) \ . \tag{6.2}$$

[45] This applies at least to NJL-type models. As mentioned earlier, there are arguments that color superconducting phases in QCD are automatically color neutral [217–219]. This would be one more reason to correct the NJL model for color neutrality.

Inserting this into Eq. (6.1) we find

$$p_{\mathrm{F}}^{d} - p_{\mathrm{F}}^{u} \approx p_{\mathrm{F}}^{u} - p_{\mathrm{F}}^{s} \ , \tag{6.3}$$

i.e., the Fermi momenta of up and down quarks differ approximately by the same amount as the Fermi momenta of up and strange quarks. This implies that *us* pairing is as likely as *ud* pairing. Indeed, within their expansion scheme Alford and Rajagopal found that, whenever *ud* pairing is more favored than no pairing at all, the CFL phase is even more favored, and there is thus no room left for the 2SC phase. Assuming that the strange quark mass is smaller in the CFL phase than in the 2SC phase, as motivated by our previous results, the argument becomes even stronger [247].

On the other hand, the assumption of a small strange quark mass which was the basis of the expansion in Ref. [247] might not be justified in the 2SC phase. Instead, as we have seen in Section 5.2, it might be more realistic to assume that there are no strange quarks at all. In this case Eq. (6.1) implies $p_{\mathrm{F}}^{d} \approx 2^{1/3} p_{\mathrm{F}}^{u}$. For instance, for $p_{\mathrm{F}}^{u} = 400\,\mathrm{MeV}$ this means that the Fermi momenta of *u* and *d* differ by about 100 MeV and hence, according to Eq. (5.9), the gap should be larger than about 70 MeV for the 2SC phase to be stable. From this point of view a stable neutral 2SC phase seems not to be excluded.

In this situation it is obviously worthwhile to extend the NJL-model analysis to include unequal chemical potentials. This has been done first by Steiner et al. [267], and shortly afterwards by Neumann et al. [270], focusing on somewhat different issues. The crucial point is again, that NJL model calculations allow to study the effects of density and phase-dependent quark masses, which have not been included self-consistently in the estimates of Ref. [247]. In this chapter we discuss the results of these investigations.

6.1. Formalism

6.1.1. Conserved charges and chemical potentials

We consider a system of quarks and leptons described by the thermodynamic potential

$$\Omega(T, \{\mu_{f,c}\}, \{\mu_{\ell_i}\}) = \Omega_q(T, \{\mu_{f,c}\}) + \Omega_\ell(T, \{\mu_{\ell_i}\}) \ , \tag{6.4}$$

where $\mu_{f,c}$ is the chemical potential of a quark with flavor f and color c, while μ_{ℓ_i} refers to a lepton of type $\ell_i \in \{e, \mu, \ldots\}$. For Ω_ℓ we simply take a gas of non-interacting leptons, while the quark part is derived from the NJL model and will be discussed in more detail in Section 6.1.2.

The various particle densities can be derived from Ω in the standard way,

$$n_{f,c} = -\frac{\partial \Omega}{\partial \mu_{f,c}}, \quad n_{\ell_i} = -\frac{\partial \Omega}{\partial \mu_{\ell_i}} \ . \tag{6.5}$$

The total flavor and color densities are then given by

$$n_f = \sum_c n_{f,c}, \qquad n_c = \sum_f n_{f,c} \ . \tag{6.6}$$

We are mainly interested in describing the conditions present in compact stars older than a few minutes, when neutrinos can freely leave the system. In this case lepton number is not conserved and we have four independent conserved charges, namely the total electric charge n_Q and the three color charges. Neglecting the τ-lepton, which is too heavy to play a role in neutron stars, the total electric charge is given by

$$n_Q = \tfrac{2}{3} n_u - \tfrac{1}{3} n_d - \tfrac{1}{3} n_s - n_e - n_\mu \ . \tag{6.7}$$

For the color charges, instead of n_r, n_g, and n_b, we will often use the linear combinations

$$n = n_r + n_g + n_b, \quad n_3 = n_r - n_g, \quad n_8 = \frac{1}{\sqrt{3}}(n_r + n_g - 2n_b) \ . \tag{6.8}$$

Here n corresponds to the total quark number density. Since $n = 3\rho_B$, it is also related to the conserved baryon number. n_3 and n_8 describe color asymmetries. Note that in contrast to Eq. (4.28) we do not assume $n_r = n_g$.

The four conserved charges $\{n_i\} = \{n, n_3, n_8, n_Q\}$ are related to four independent chemical potentials $\{\mu_i\} = \{\mu, \mu_3, \mu_8, \mu_Q\}$, such that

$$n_i = -\frac{\partial\Omega}{\partial\mu_i} \ . \tag{6.9}$$

The individual quark chemical potentials $\mu_{f,c}$ are then given by

$$\mu_{f,c} = \mu + \mu_Q(\tfrac{1}{2}(\tau_3)_{ff} + \frac{1}{2\sqrt{3}}(\tau_8)_{ff}) + \mu_3(\lambda_3)_{cc} + \mu_8(\lambda_8)_{cc} \ . \tag{6.10}$$

Here, as before, τ_i and λ_j are Gell–Mann matrices corresponding to flavor and color, respectively. The electron and muon chemical potentials are simply

$$\mu_e = \mu_\mu = -\mu_Q \ . \tag{6.11}$$

Eqs. (6.10) and (6.11) imply

$$\mu_{d,c} = \mu_{s,c} = \mu_{u,c} + \mu_e \quad \text{for all } c \ , \tag{6.12}$$

which is usually referred to as beta equilibrium.

We are mostly interested in electrically and color neutral matter, which is characterized by

$$n_Q = n_3 = n_8 = 0 \ . \tag{6.13}$$

Since we have four conserved charges and three neutrality conditions the neutral solutions can be characterized by one independent variable, namely the quark number density n. In the four-dimensional space spanned by the chemical potentials $\{\mu_i\}$ these solutions form one or several one-dimensional lines. This is a straightforward generalization of the situation in Section 3.3. Since for normal conducting quark matter n_3 and n_8 automatically vanish for $\mu_3 = \mu_8 = 0$, these chemical potentials did not play any role in that context and effectively we only had to deal with two chemical potentials and one neutrality condition. (Similarly, many cases to be discussed below are restricted to $\mu_3 = 0$.)

On the other hand, the above situation can be generalized further. For instance, in a proto-neutron star a few seconds after the collapse of the progenitor, neutrinos are trapped, and we get an additional chemical potential related to the conserved lepton number. At the same time, however, we get another constraint from the fact that the lepton fraction, i.e., the total lepton number divided by the total baryon number, is fixed to the value present in the progenitor star. Although we will mostly refer to the above case of four conserved charges, the formalism we develop in this part is straightforwardly generalized to other cases.

6.1.2. Thermodynamic potential for non-uniform quark chemical potentials

In order to attack the problems discussed above we need to extend the NJL model of Section 5.2.1 to non-uniform chemical potentials for different flavors and colors. This amounts to replacing the chemical

potential μ in the inverse fermion propagator Eq. (5.16) by a diagonal matrix $\hat{\mu}$ with flavor and color-dependent components $\mu_{f,c}$. Although not all of these components are independent if we impose beta equilibrium (see Eq. (6.10)) we keep them as arbitrary inputs at this point. The essential difference to the situation in Section 5.2.1 is the fact that unequal chemical potentials for up and down quarks violate isospin symmetry. Hence Eq. (5.17) does no longer hold, and we have to deal with six different condensates, i.e., the three constituent masses M_u, M_d and M_s, and the three diquark condensates s_{22}, s_{55} and s_{77}. Because of this lower degree of symmetry the explicit evaluation of the integrand in Eq. (5.15) becomes of course much more involved.

As we have discussed in Section 5.1.2, even though quarks of all colors and flavors participate in a condensate in the CFL phase, not every quark species is paired with all others, but there are certain combinations (see Table 5.1). In particular, six of the nine color–flavor species have only one fixed partner species, while the remaining three form a triangle. As a consequence, S^{-1} can be decomposed into several independent blocks [213,247,267], and Tr ln $S^{-1}(p)$ can be written as a sum,

$$\begin{aligned}\text{Tr ln } S^{-1}(p) = &(\text{Tr ln } \mathscr{M}_{ug,dr} + \text{Tr ln } \mathscr{M}_{dr,ug}) + (\text{Tr ln } \mathscr{M}_{ub,sr} + \text{Tr ln } \mathscr{M}_{sr,ub}) \\ &+ (\text{Tr ln } \mathscr{M}_{db,sg} + \text{Tr ln } \mathscr{M}_{sg,db}) + \text{Tr ln } \mathscr{M}_{ur,dg,sb}\ ,\end{aligned} \tag{6.14}$$

where the matrices $\mathscr{M}$ correspond to the different independent blocks of S^{-1}. Six of them have a 2×2 structure in the 18-dimensional space spanned by color, flavor and Nambu–Gorkov degrees of freedom,

$$\mathscr{M}_{f_1c_1,f_2c_2} = \begin{pmatrix} \not{p}^{+}_{f_1,c_1} - M_{f_1} & \Delta_{f_1,f_2}\gamma_5 \\ -\Delta^{*}_{f_1,f_2}\gamma_5 & \not{p}^{-}_{f_2,c_2} - M_{f_2} \end{pmatrix}\ , \tag{6.15}$$

where $\not{p}^{\pm}_{f,c} = \not{p} \pm \mu_{f,c}\gamma_0$. These blocks describe the pairing of two species of quarks with flavors f_1 and f_2 and colors c_1 and c_2, respectively. Δ_{f_1,f_2} is the corresponding diquark gap, i.e., $\Delta_{ud} \equiv \Delta_{du} \equiv \Delta_2$, $\Delta_{us} \equiv \Delta_{su} \equiv \Delta_5$, and $\Delta_{ds} \equiv \Delta_{sd} \equiv \Delta_7$.

The remaining block involves three quark species and is a 6×6 matrix in color–flavor Nambu–Gorkov space,

$$\mathscr{M}_{ur,dg,sb} = \begin{pmatrix} \not{p}^{+}_{u,r} - M_u & 0 & 0 & 0 & -\Delta_2\gamma_5 & -\Delta_5\gamma_5 \\ 0 & \not{p}^{+}_{d,g} - M_d & 0 & -\Delta_2\gamma_5 & 0 & -\Delta_7\gamma_5 \\ 0 & 0 & \not{p}^{+}_{s,b} - M_s & -\Delta_5\gamma_5 & -\Delta_7\gamma_5 & 0 \\ 0 & \Delta^{*}_2\gamma_5 & \Delta^{*}_5\gamma_5 & \not{p}^{-}_{u,r} - M_u & 0 & 0 \\ \Delta^{*}_2\gamma_5 & 0 & \Delta^{*}_7\gamma_5 & 0 & \not{p}^{-}_{d,g} - M_d & 0 \\ \Delta^{*}_5\gamma_5 & \Delta^{*}_7\gamma_5 & 0 & 0 & 0 & \not{p}^{-}_{s,b} - M_s \end{pmatrix}. \tag{6.16}$$

(Including the Dirac components, this is of course a 24×24 matrix, while Eq. (6.15) describes 8×8 matrices.)

This block structure has interesting consequences: It is known from ordinary superconductors, where electrons with spin up are paired with electrons with spin down, that the respective number densities, $n_\uparrow$ and $n_\downarrow$, are always equal to each other. This is true even in the presence of a magnetic field, as long as the superconducting state remains intact [268]. Some time ago it has been shown that the analogous statement holds for color superconductors, if one considers two species with unequal chemical potentials

[143] or masses [257].[46] From this it was originally concluded that in the CFL phase where all quarks participate in a condensate, the densities $n_{f,c}$ are equal for all flavors and colors. This would mean that the CFL phase is always electrically and color neutral, even for unequal quark masses [257]. However, as pointed out by Steiner et al. [267], only those quarks which are paired in the same 2×2 block have the same density,whereas the densities could differ for different blocks. Furthermore, the argument does not apply to the 6×6 block. According to the color–flavor structure discussed above this means for the CFL phase

$$n_{u,g} = n_{d,r}, \quad n_{u,b} = n_{s,r}, \quad n_{d,b} = n_{s,g} \quad \text{(CFL)} \ , \tag{6.17}$$

leading to the remarkable identities

$$n_u = n_r, \quad n_d = n_g, \quad n_s = n_b \quad \text{(CFL)} \ . \tag{6.18}$$

These relations guarantee neutrality of CFL matter under the rotated electromagnetism $\tilde{Q}$, Eq. (5.8), but in general they do not preclude the presence of ordinary electric or color charges [267]. Note, however, that color neutral CFL matter is automatically electrically neutral as long as no leptons are present.

In the 2SC phase, where $\Delta_5 = \Delta_7 = 0$, Eq. (6.16) can be decomposed further, and we obtain a new 2×2 block involving red *u*-quarks and green *d*-quarks. Together with the other 2×2 block which contains Δ_2 this leads to the relations

$$n_{u,r} = n_{d,g}, \quad n_{u,g} = n_{d,r} \quad \text{(2SC)} \ . \tag{6.19}$$

The corresponding relations for other possible phases, e.g., with two non-vanishing diquark condensates, can be obtained analogously.

The further elaboration of the thermodynamic potential contains only straightforward manipulations, but the result is extremely lengthy and will not be presented here. The self-consistent solutions for the condensates ϕ_f and s_{AA}, i.e., the stationary points of Ω_q are determined numerically [269].

6.2. Numerical results

In this section we first explore the phase structure at $T = 0$ in the space of the different chemical potentials μ_i and determine the electric and color charge densities in the various regimes [270]. Based on these results, we then construct solutions of homogeneous electrically and color neutral quark matter and analyze the corresponding equation of state [267].

6.2.1. Equal chemical potentials

To have a well-defined starting point we begin with the "standard case" of a uniform, color and flavor independent, chemical potential for all quarks, i.e., $\mu_3 = \mu_8 = \mu_Q = 0$. This implies that no leptons are present. As model parameters we adopt again parameter set RKH of Table 3.1 [145], for the bare quark

[46] In Ref. [143] it was shown for a system of two massless flavors that $n_u = n_d$ for $|\mu_u - \mu_d| < 2\Delta$, but the densities become unequal for $|\mu_u - \mu_d| > 2\Delta$. Without further constraints, the latter belongs to the regime where the diquark condensate is unstable, confirming the statement that the densities in the stable regime are equal. However, under certain conditions there could be stable color superconducting solutions with $|\mu_u - \mu_d| > 2\Delta$ if their decay is prohibited by the requirement of local charge neutrality [223,224]. This situation is never realized in the numerical examples to be discussed below. In principle, however, this possibility should be kept in mind and will briefly be discussed in Section 6.4.

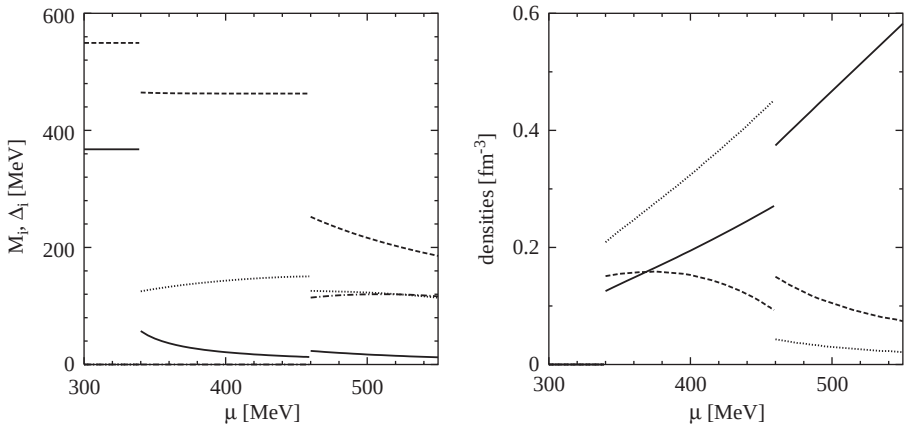

Fig. 6.1. Gap parameters and densities at $T = \mu_3 = \mu_8 = \mu_Q = 0$ as functions of μ. Left: $M_u = M_d$ (solid), M_s (dashed), Δ_2 (dotted), and $\Delta_5 = \Delta_7$ (dash–dotted). Right: $n/10$ (solid), n_8 (dashed), and n_Q (dotted). Adapted with permission from Ref. [270].

masses, the cut-off, and the coupling constants G and K. For the diquark coupling we take $G = H$. This is the value we have chosen in Ref. [270], following the choice of parameters in the first version of Ref. [267].[47] Obviously, this is very similar to parameter set III in Table 5.2, where we had $H = 0.95G$.

With these parameters we obtain the results which are displayed in Fig. 6.1. In the left panel we show once again the constituent masses and diquark gaps as functions of μ. Since isospin symmetry is still preserved, we still have $M_u = M_d$ and $\Delta_5 = \Delta_7$, as in Section 5.2. Since the parameters are almost the same, the results are of course very similar to those presented in Fig. 5.4: We find three phases: a normal conducting phase at low chemical potentials, followed by a 2SC phase and, finally, a CFL phase. At the first-order phase boundaries we observe again strong discontinuities in the quark masses.

In the right panel we show the corresponding densities. Note that the quark number density n (solid line) has been divided by 10 to fit to the scale. The dotted line corresponds to the electric charge density n_Q, the dashed line to the color density n_8. The color density n_3 is identically zero. We find again that all densities vanish in the "normal phase", i.e., this phase corresponds to the vacuum. As discussed earlier it has to be like this: As soon as up and down quarks are present, their Fermi surfaces are subject to a Cooper instability leading to the formation of the diquark condensate s_{22}. This argument will no longer go through, once we have switched on one of the other chemical potentials which lift the degeneracy of the Fermi surfaces of all up and down quarks.

The two other phases carry both, electric and color charges. The electric charge of the 2SC phase is easily understood. Since $\mu_Q = 0$, there are no leptons and the densities of up and down quarks are equal. Moreover, in this example there are no strange quarks, which are too heavy to be populated in this regime. Hence the total electric charge density is given by $n_Q = n/6$. The non-vanishing color density n_8 is the same effect we have already encountered in Section 4.3.4 and reflects the fact that for equal chemical potentials the densities of the paired (red and green) quarks are larger than the density of the unpaired (blue) quarks. Numerically, we find $(n_r - n_b)/n = 10\%$ at the lower boundary and $(n_r - n_b)/n = 3\%$ at the upper boundary of the 2SC phase.

[47] In their final version these authors have taken $H : G = 3 : 4$.

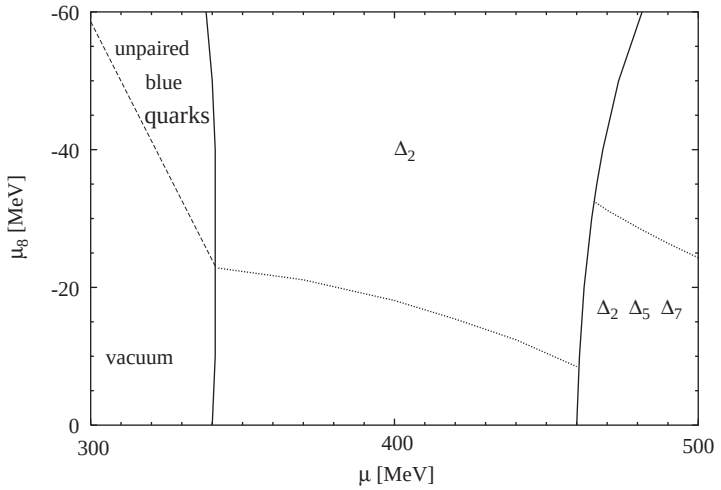

Fig. 6.2. Phase diagram in the μ–μ_8 plane for $T=\mu_3=\mu_Q=0$. The various phases separated by the solid lines are characterized by different non-vanishing diquark gaps Δ_i as indicated in the figure. In the non-superconducting phase quarks are present only above the dashed line. The dotted lines are the lines of color neutral matter. In the CFL phase this also corresponds to electrically neutral matter. Taken with permission from Ref. [270].

Just above the transition to the CFL phase this ratio does not change very much, whereas the electric charge density drops significantly due to a strong increase of the density of strange quarks. To a large extent, this is caused by a sudden drop of the strange quark mass, but this is only part of the story. For instance, at $\mu=500$ MeV we have $M_u=M_d=17.2$ MeV and $M_s=216.5$ MeV. Using these numbers in a free gas approximation we would expect $n_Q=0.049\,\mathrm{fm}^{-3}$, whereas numerically we find $n_Q=0.030\,\mathrm{fm}^{-3}$. This difference is caused by the diquark pairing, which links the flavor densities in the CFL phase directly to the color densities, as discussed in Eq. (6.18). For $n_3=0$ one finds $n_Q=1/(2\sqrt{3})\,n_8$, in agreement with our numerical results.

6.2.2. Phase structure

Aiming the construction of electrically and color neutral quark matter we have in general to introduce non-vanishing chemical potentials μ_8 and μ_Q to remove the charge densities n_8 and n_Q we have found above. In order to see how these additional chemical potentials influence the phase boundaries, we first study them separately.

In Fig. 6.2 we show the phase diagram in the μ–μ_8 plane for $\mu_Q=\mu_3=0$. The (first-order) phase boundaries are indicated by solid lines. We find again the three phases discussed before, i.e., the normal phase, the 2SC phase, and the CFL phase. For $\mu_8=0$ we have seen that the "normal phase" actually corresponds to the vacuum. However, when $\mu_b=\mu-\frac{2}{\sqrt{3}}\mu_8$ becomes larger than the vacuum masses of the light quarks (the region above the dashed line), blue up and down quark states can be populated forming a gas of unpaired blue quarks. Here we have neglected that in principle these quarks could pair in a different channel as discussed in Section 4.4. Moreover, we should repeatedly note that our model is not suited for a realistic description of the low-density regime, where confinement and hadronic degrees of freedom have to be taken into account.

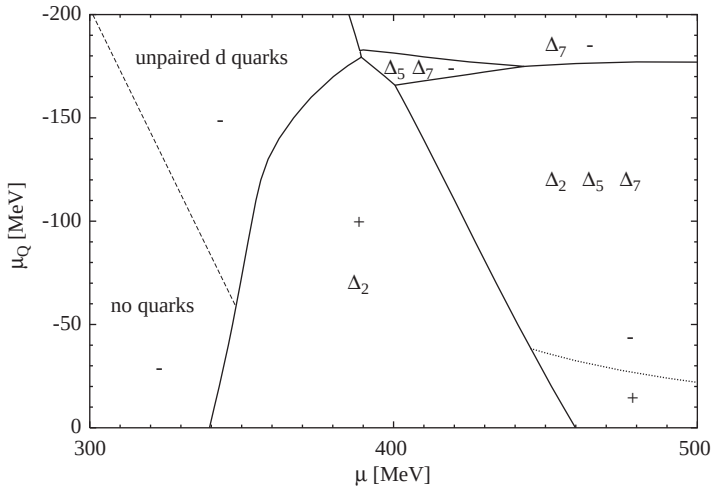

Fig. 6.3. Phase diagram in the μ–μ_Q plane for $T = \mu_3 = \mu_8 = 0$. The various phases separated by the solid lines are characterized by different non-vanishing diquark gaps Δ_i as indicated in the figure. In the non-superconducting phase quarks are present only above the dashed line. The "+" and "−" signs indicate the sign of the electric charge density in the corresponding region. The dotted line corresponds to electrically (but not color) neutral matter in the CFL phase. Taken with permission from Ref. [270].

In the color superconducting phases we have indicated the lines of color neutral matter (dotted). In the CFL phase, as discussed below Eq. (6.18), color neutral quark matter is automatically electrically neutral as well, i.e., in the CFL phase the dotted line already corresponds to a neutral matter solution, we are looking for. It meets the phase boundary to the 2SC phase at $\mu = 465.7\,\text{MeV}$ and $\mu_8 = -32.5\,\text{MeV}$. The 2SC matter which is in chemical and mechanical equilibrium with the neutral CFL matter at this point carries both, electric and color charge, $n_Q = 0.464\ \text{fm}^{-3}$ and $n_8 = -0.329\ \text{fm}^{-3}$. In Section 6.3, this point will be our starting point to construct neutral mixed phases. Unlike color neutral CFL matter, color neutral 2SC matter is not electrically neutral but positively charged. In fact, a non-vanishing μ_8 does not change the ratio of up and down quarks and hence, as long as no strange quarks are present, $n_Q/n = \frac{1}{6}$, as before.

In Fig. 6.3 we show the phase diagram in the μ–μ_Q plane for $\mu_8 = \mu_3 = 0$. Since we are interested in neutralizing the electrically positive 2SC phase, we choose μ_Q to be negative. As long as this is not too large, we find again the normal phase at lower values of μ, the 2SC phase in the intermediate region and the CFL phase for large μ. This changes dramatically around $\mu_Q \simeq -180\,\text{MeV}$ where both, the 2SC phase and the CFL phase disappear and a new phase emerges. This phase is analogous to the 2SC phase but with *ds* pairing, instead of *ud* pairing ("2SC$_{ds}$"). In a small intermediate regime there is yet another phase which contains *us* and *ds* but no *ud* pairs ("SC$_{us+ds}$").

Qualitatively, the existence of these phases is quite plausible: At low values of $|\mu_Q|$, the Fermi momenta of the up and down quarks are relatively similar to each other, whereas the strange quarks are suppressed because of their larger mass. With increasing negative μ_Q, however, the up quarks become more and more disfavored and eventually the Fermi momenta are ordered as $p_F^u < p_F^s < p_F^d$. It is then easy to imagine that only *ds* pairing or—in some intermediate regime—only *us* and *ds* pairing is possible.

Following this argument, one might expect that there is always a value of μ_Q, where the Fermi momenta of up and strange quarks are equal and hence the 2SC phase should either be followed by the CFL phase or

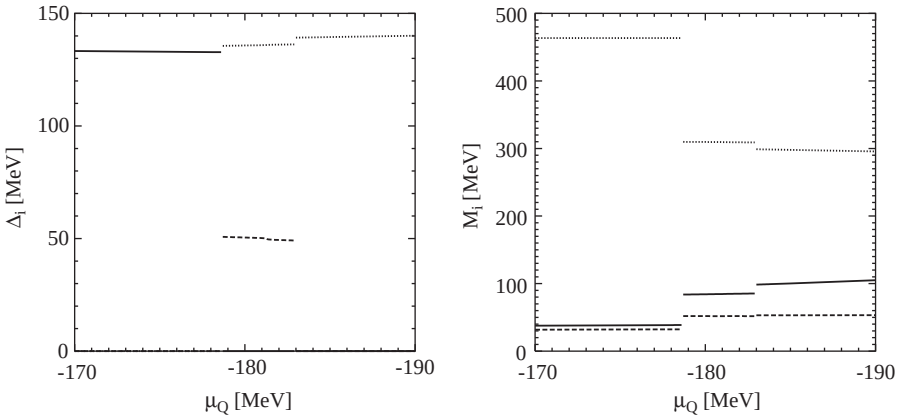

Fig. 6.4. Diquark gaps and quark masses for $T=\mu_3=\mu_8=0$, and $\mu=390$ MeV as functions of μ_Q. Left: Δ_2 (solid), Δ_5 (dashed), and Δ_7 (dotted). Right: M_u (solid), M_d (dashed), and M_s (dotted). Adapted with permission from Ref. [270].

by a phase with *us*-pairing only. However, this is not the case because of the discontinuous behavior of the quark masses. This is illustrated in Fig. 6.4 where the diquark gaps and constituent quark masses are shown as functions of μ_Q for fixed $\mu=390$ MeV and $\mu_3=\mu_8=0$. The 2SC–SC$_{us+ds}$ phase transition takes place at $\mu_Q=-178.6$ MeV, corresponding to $\mu_u=\mu+\frac{2}{3}\mu_Q\simeq 270$ MeV and $\mu_d=\mu_s=\mu-\frac{1}{3}\mu_Q\simeq 450$ MeV. Below the transition point the strange quark mass is larger than 460 MeV and, consequently, no strange quarks are present. At the transition point the strange quark mass drops to 310 MeV and the nominal Fermi momentum $p_{\mathrm{F}}^s=\sqrt{\mu_s^2-M_s^2}$ is immediately larger than p_{F}^u.

It turns out that the stability of the various condensates is rather well described by the criterion given in Eq. (5.9). In the 2SC phase, just below the phase boundary, we have $\Delta_2=132.8$ MeV, slightly larger than $\Delta_2^{\mathrm{crit}}:=|p_{\mathrm{F}}^d-p_{\mathrm{F}}^u|/\sqrt{2}=127.4$ MeV. At the phase boundary the latter rises to 133.6 MeV due to a sudden increase of the up quark mass by more than 40 MeV. Taking the earlier value of Δ_2, the above criterion is no longer fulfilled, which is consistent with our numerical result that the *ud*-pairs break up. This level of agreement is certainly better than one should expect (see footnote 41). In fact, in the SC$_{us+ds}$ phase we find Δ_5 continuously decreasing from 50.8 to 49.1 MeV whereas $\Delta_5^{\mathrm{crit}}=|p_{\mathrm{F}}^s-p_{\mathrm{F}}^u|/\sqrt{2}$ increases from 48.2 to 52.6 MeV, slightly violating Eq. (5.9). Nevertheless, qualitatively, one can understand the break-up of the *us* pairs, which occurs at $\mu_Q=-183.0$ MeV, from the fact that at this point Δ_5^{crit} jumps to 62.6 MeV due to a further increase of M_u and a further decrease of M_s. Moreover, the fact that we always find $\Delta_5\approx|p_{\mathrm{F}}^s-p_{\mathrm{F}}^u|/\sqrt{2}$, at least in this example, indicates that the SC$_{us+ds}$ phase is rather fragile and might disappear upon small variations of the model parameters.

In the phase diagram, Fig. 6.3, we also indicate the sign of the electric charge density for the various regions, and the line of electrically neutral matter in the CFL phase (dotted line). Note that there is no other electrically neutral regime in this diagram (apart from the vacuum at small μ and $\mu_Q=0$). In the normal phase, there are again no quarks below the dashed line, corresponding to the line $\mu-\frac{1}{3}\mu_Q=M_d$. This region is nevertheless negatively charged due to the leptons which are present for any $\mu_Q<0$. Above the dashed line there are also down quarks rendering the matter even more negative. (In the right corner of this phase there is also a tiny fraction of up quarks.)

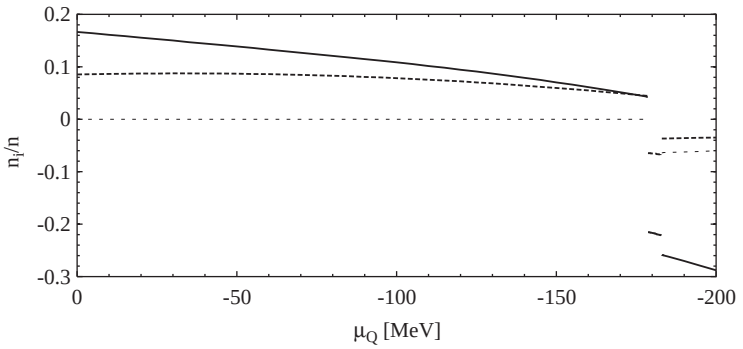

Fig. 6.5. Relative densities for $T = \mu_3 = \mu_8 = 0$, and $\mu = 390\,\mathrm{MeV}$ as functions of μ_Q: n_Q/n (solid), n_8/n (dashed), and n_3/n (dotted). Adapted with permission from Ref. [270].

The "new" phases, $2\mathrm{SC}_{ds}$ and SC_{us+ds}, are negatively charged as well. On the contrary, the entire 2SC phase is positively charged, even at the largest values of $|\mu_Q|$. This is illustrated in Fig. 6.5 where the various charge densities n_i divided by the total quark number density n are plotted as functions of μ_Q, again for fixed $\mu = 390\,\mathrm{MeV}$ and $\mu_3 = \mu_8 = 0$. As expected, n_Q/n (solid line) decreases with increasing negative μ_Q. However, in the 2SC phase ($0 \geqslant \mu_Q > -178.6\,\mathrm{MeV}$) it stays positive and before the point of neutrality is reached the phase transition to the SC_{us+ds} phase takes place.

The difficulty to obtain electrically neutral 2SC matter can be traced back to the fact that, according to Eq. (6.19), the sum of red and green *u* quarks is equal to the sum of red and green *d* quarks. As long as no strange quarks are present, the related positive net charge can only be compensated by the blue quarks and the leptons. This requires a very large negative μ_Q. However, before this point is reached it becomes more favored to form a different phase with a relatively large fraction of strange quarks which then also participate in a diquark condensate.[48] Again, the self-consistent treatment, which leads to a sudden drop of the strange quark mass and hence to a sudden increase of the strange Fermi momentum, is crucial in this context.

So far we have not considered the effect of a non-vanishing chemical potential μ_8 on top of a non-vanishing μ_Q. Since the blue quarks are the main carriers of negative electric charge in the 2SC phase, one could hope that increasing the number of blue quarks, as necessary for color neutrality, could also help to electrically neutralize 2SC matter. It turns out, however, that the rather small values of μ_8 which are needed for color neutrality (see Fig. 6.2) do not change the above results qualitatively.

At this point we should note that the non-existence of *stable* neutral 2SC solutions in the present grand canonical treatment does not mean that neutral 2SC matter does not exist at all. At large negative values of μ_Q there are neutral 2SC solutions which are metastable. This means, there are other solutions, e.g., in the $2SC_{ds}$ phase, which have a larger pressure for the same chemical potentials. However, these other solutions are not neutral but in general colored and negatively charged. Therefore a finite piece of neutral 2SC matter cannot simply decay into a different phase. Instead, there are basically two possibilities. The first one is a phase separation, leading to a globally neutral mixed phase of two or more charged components in chemical and mechanical equilibrium. This scenario will be discussed in more detail in

[48] This is very similar to the arguments of Alford and Rajagopal [247] discussed in the introductory part to the present chapter. The main difference is that we do not compare different *neutral* phases with each other, but phases in chemical equilibrium.

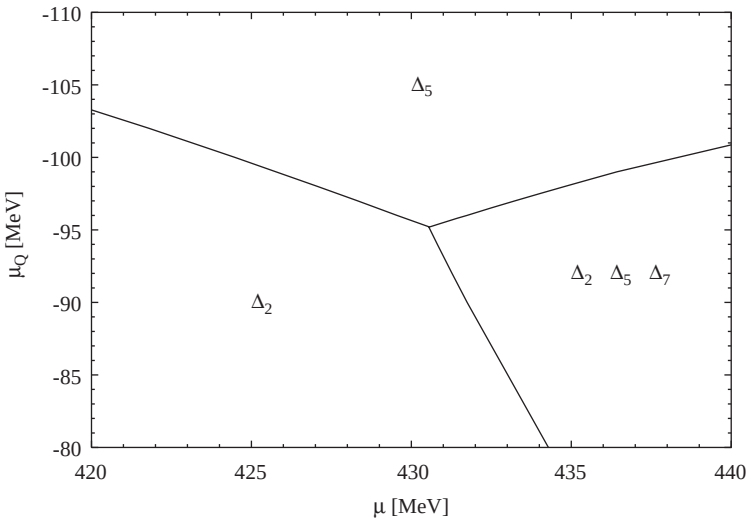

Fig. 6.6. Phase diagram in a plane defined by μ and μ_Q as independent variables and $\mu_3 = -\mu_Q/2$ and $\mu_8 = -\mu_Q/7 - 30\,\mathrm{MeV}$. The various phases separated by the solid lines are characterized by different non-vanishing diquark gaps Δ_i as indicated in the figure. Taken with permission from Ref. [270].

Section 6.3. On the other hand, if the corresponding Coulomb and surface energies are too large, this phase separation is not favored. In this case the "metastable" solutions could be stable, if there is no other homogeneous neutral solution with a higher pressure at the same value of μ. These solutions, which have been constructed first in Ref. [267] will be discussed in Section 6.2.3.

To conclude this section, we consider an example where $\mu_3 \neq 0$. At first sight, there seems to be no motivation for this. In fact, there is no need to vary μ_3, as long as we are only interested in finding electrically and color neutral solutions of homogeneous normal, 2SC, or CFL matter. For normal and 2SC matter, this follows from the fact that both phases have an unbroken $SU(2)_c$ symmetry, and thus $n_3 = 0$ for $\mu_3 = 0$. The situation is more complicated for the CFL phase, but we have seen already that CFL matter can be neutralized by applying a non-vanishing chemical potential μ_8 and $\mu_3 = \mu_Q = 0$. Nevertheless, as we will see in Section 6.3.2, the construction of neutral mixed phases requires also non-vanishing values of μ_3. In this context we will encounter another phase, which is not present in Figs. 6.2 and 6.3. For illustration we consider a plane in the four-dimensional $\{\mu_i\}$-space where μ and μ_Q are taken as independent variables and μ_3 and μ_8 are given by $\mu_3 = -\mu_Q/2$ and $\mu_8 = -\mu_Q/7 - 30\,\mathrm{MeV}$. The relevance of this particular choice will become more clear in Section 6.3.2. Here we just note that $\mu_3 = -\mu_Q/2$ means that $\mu_{u,r} = \mu_{d,g}$. Also the sum $\mu_{s,r} + \mu_{u,b}$, corresponding to the chemical potential related to a pair of a red strange quark and a blue up quark, equals the sum$\mu_{s,g} + \mu_{d,b}$, corresponding to the chemical potential related to a pair of green strange quarks and blue down quarks. Together with the relations given in Eq. (6.17) and the isospin symmetry of the original Lagrangian this implies for the CFL phase that $n_u = n_d$ or, according to Eq. (6.18), $n_r = n_g$ and thus $n_3 = 0$.

In Fig. 6.6 we show a small part of the resulting phase diagram. Here, in addition to the standard 2SC and CFL phases, we find a phase where only u and s quarks are paired ("2SC$_{us}$"). We have thus found examples for all three Δ_A, $A = 2, 5, 7$, being the only non-vanishing scalar diquark gaps in some regime. Taking all possible combinations of no, one, two, or three of these condensates (see Table 6.1),

Table 6.1
Phases and corresponding non-vanishing diquark gaps

Phase	N	2SC	2SC$_{us}$	2SC$_{ds}$	SC$_{ud+us}$	SC$_{ud+ds}$	SC$_{us+ds}$	CFL
Diquark gaps	—	Δ_2	Δ_5	Δ_7	Δ_2, Δ_5	Δ_2, Δ_7	Δ_5, Δ_7	Δ_2, Δ_5, Δ_7

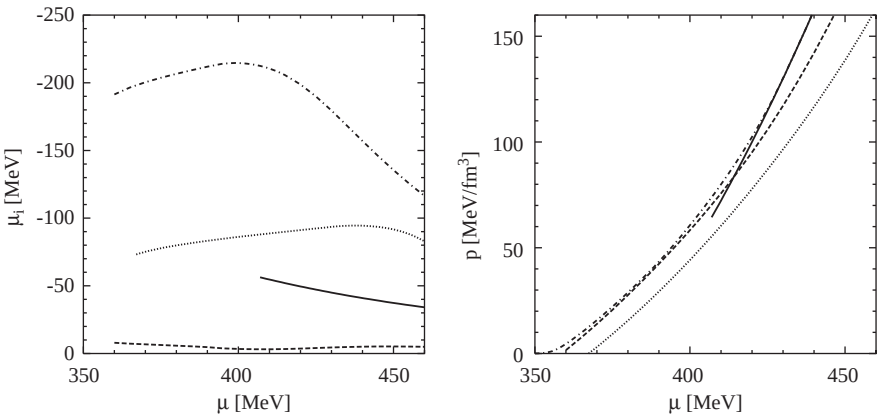

Fig. 6.7. Quantities related to electrically and color neutral homogeneous CFL, 2SC, and normal quark matter as functions of the quark number chemical potential μ. Left: chemical potentials $\mu_8^{(\mathrm{CFL})}$ (solid), $\mu_8^{(\mathrm{2SC})}$ (dashed), $\mu_Q^{(\mathrm{2SC})}$ (dash–dotted), $\mu_Q^{(\mathrm{normal})}$ (dotted). Note that $\mu_Q^{(\mathrm{CFL})} = \mu_8^{(\mathrm{normal})} = 0$. Right: pressure in the CFL phase (solid), 2SC (dashed), and normal quark matter (dotted). Also shown is the pressure of the mixed phase solution constructed in Section 6.3.2 (dash–dotted).

the phases SC$_{ud+us}$ and SC$_{ud+ds}$, i.e., the combinations $\Delta_2 + \Delta_5$ and $\Delta_2 + \Delta_7$ are the only ones we have not encountered. These phases might exist as well, but we have not searched for them systematically.

6.2.3. Homogeneous neutral solutions

Solutions of homogeneous electrically and color neutral quark matter obtained within our model are presented in Fig. 6.7. In the left panel we show the chemical potentials μ_8 and μ_Q, needed to neutralize the matter in a given phase. As pointed out above, the fact that we did not find regions of absolutely stable solutions of neutral normal or 2SC quark matter in the phase diagram does not exclude the existence of metastable solutions. These might finally turn out to be stable if mixed phases are suppressed due to surface and Coulomb effects and if there is no other neutral solution with a higher pressure at the same value of μ.

The latter is analyzed in the right panel of Fig. 6.7. We find that the CFL phase (solid line) is the phase with the highest pressure for $\mu > 414\,\mathrm{MeV}$. Below this point the 2SC phase (dashed) is most favored, whereas the pressure of normal quark matter (dotted) is always lower. This means, we do not confirm the predictions of Alford and Rajagopal according to which the 2SC phase is always disfavored against CFL or normal quark matter [247]. The reason for this is the fact that the arguments of Alford and Rajagopal are based on an expansion in the strange quark mass, which fails if M_s is large. As one can see in Fig. 6.8, where the constituent masses and diquark gaps are displayed for the various solutions, this is obviously

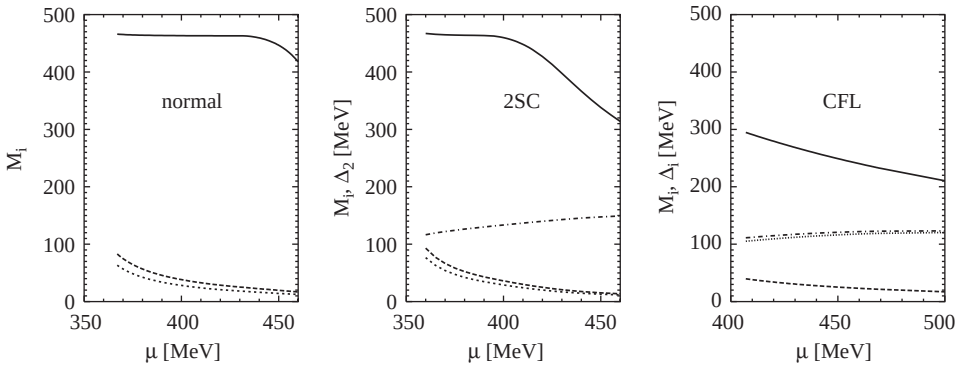

Fig. 6.8. Constituent masses and diquark gaps for homogeneous electrically and color neutral quark matter. Left: M_u (dashed), M_d (dotted), and M_s (solid) in the normal phase. Center: M_u (dashed), M_d (dotted), M_s (solid), and Δ_2 (dash–dotted) in the 2SC phase. Right: $M_u = M_d$ (dashed), M_s (solid), Δ_2 (dash–dotted), and $\Delta_5 = \Delta_7$ in the CFL phase.

the case. In fact, the fraction of strange quarks in the 2SC phase is only 5% at $\mu = 414\,\mathrm{MeV}$ and vanishes below $\mu = 395\,\mathrm{MeV}$.

In this context it is interesting to revisit the arguments for the limit of large strange quark masses which we gave in the Introduction to this chapter. There we estimated the difference of the up and down Fermi momenta for neutral matter in the normal phase to be about 100 MeV, which agrees well with the value we find for $|\mu_Q|$ in this phase (see Fig. 6.7). From this value, applying Eq. (5.9) we concluded that there will be a stable 2SC solution if $\Delta_2 \gtrsim 70\,\mathrm{MeV}$. Since we find gaps of more than 100 MeV this is consistent with our results. (Note, that $|\mu_Q|$ in the 2SC phase, which is greater than 200 MeV at $\mu \simeq 400\,\mathrm{MeV}$, is not the relevant quantity to compare with, because we first have to prepare *neutral* quark matter in the normal phase and than check whether the mismatch of the corresponding Fermi surfaces can be overcome by the gap.)

Our results are in qualitative agreement with Ref. [267] where a similar NJL model calculation has been presented first. The main difference is that the authors of Ref. [267] used a smaller diquark coupling ($H = 0.75G$ instead of $H = G$) and therefore find smaller gaps. This could be the reason why the neutral 2SC solutions presented in that reference cease to exist for $\mu \lesssim 440\,\mathrm{MeV}$. Therefore, in contrast to our results, neutral normal quark matter is favored below this value, simply because there is no other solution. On the other hand, whenever there is a neutral 2SC solution, it is more favored than neutral normal quark matter, in agreement with our findings.

We should recall that we have only considered the case of zero temperature and non-conserved lepton number, appropriate for neutron stars older than a few minutes. Steiner et al. [267] have also analyzed the case of finite temperature and conserved lepton number, which is relevant during the evolution from a proto-neutron star, where neutrinos are trapped, to a cold compact star, where the neutrinos can freely leave the system. The authors showed that in this case the 2SC phase is favored because neutral CFL matter excludes electrons (at least at $T = 0$ and still disfavors them at $T >= 0$) and can therefore not easily accommodate a finite lepton number.

Finally, we come back to the hypothesis of absolutely stable strange quark matter [39,40]. In our earlier analysis in Section 3.3 the effects of color superconductivity have not been taken into account. Since the formation of diquark condensates gives rise to extra binding energy, it is in principle possible

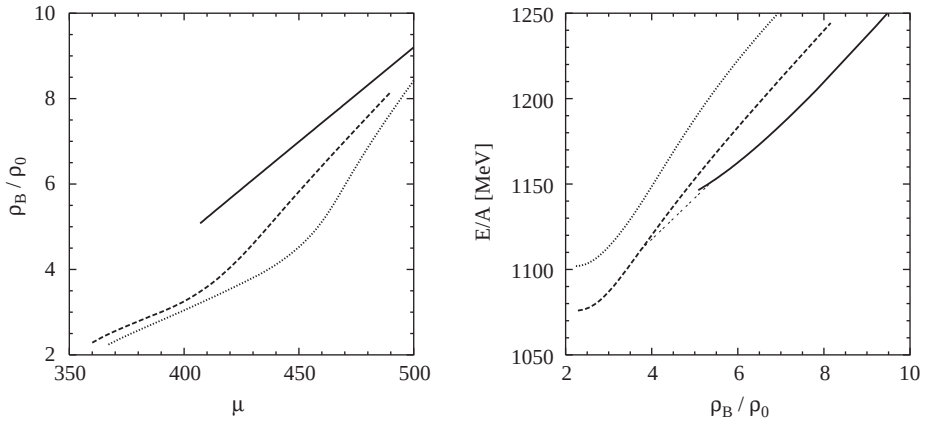

Fig. 6.9. Baryon number density ρ_B as function of the quark number chemical potential μ (left), and energy per baryon number E/A as function of ρ_B (right) for homogeneous electrically and color neutral quark matter: CFL (solid), 2SC (dashed), and normal quark matter (dotted). The thin double-dashed line indicates E/A in a 2SC–CFL mixed phase obtained in a Maxwell construction with two separately neutral components.

that SQM which would be unstable in the normal quark phase becomes absolutely stable in the CFL phase [271,272]. To analyze this question, we calculate the energy per baryon number E/A as function of the baryon number density ρ_B for our solutions of neutral quark matter. The results are displayed in the right panel of Fig. 6.9. For clarity, we also show the relation between ρ_B and μ (left panel). In both figures the dotted line corresponds to normal quark matter, i.e., to the equation of state used in Section 3.3. The solid and the dashed lines correspond to CFL and 2SC matter, respectively.

We see that the diquark condensates indeed lead to an appreciable reduction of E/A. Although this effect is stronger in the CFL phase than in the 2SC phase, it is not strong enough to produce a minimum in the CFL phase. In fact, this could have been anticipated from Fig. 6.7 since we did not find a CFL solution with zero pressure.[49] Thus if we prepare a large but finite piece of CFL matter and then slowly decrease the external pressure, the matter will expand. Eventually, when the pressure reaches the critical value (corresponding to the crossing of the 2SC and CFL lines in Fig. 6.7), the system will follow the thin double-dashed line in Fig. 6.9 and make a transition into the 2SC phase.

We also see that the minimal values of E/A, both in the CFL phase and in the 2SC phase are still considerably larger as 930 MeV, the value in ^{56}Fe. Thus, although a more systematic study of the parameter dependence remains to be done, our results suggest, that including diquark condensates will not alter the main conclusions drawn in Section 3.3.

[49] In our numerical analysis, we did not succeed to find a neutral CFL solution for $\mu \lesssim 407$ MeV. Since the neutral 2SC solution is favored already for $\mu \leqslant 414$ MeV, this is of no relevance for the present discussion. Nevertheless, we should note that the fate of the CFL solution below $\mu \simeq 407$ MeV is not clear. Since solutions of the gap equation correspond to stationary points of the thermodynamic potential they cannot simply "end" at some point, but only "turn around". Hence, if there is no neutral CFL solution below a certain value of μ, there must be two solutions above this point. Of course, this second solution would be unstable.

6.3. Mixed phases

As one can see in Fig. 6.7, the values of the chemical potentials μ_8 and μ_3 needed to neutralize matter for a given value of μ depend on the phase. Hence, neutral matter in one phase is never in chemical equilibrium with neutral matter in a different phase, even if their quark number chemical potentials μ are the same. In particular, the points of equal pressure do not fulfill the Gibbs condition for a phase transition, stating that the pressure and *all* chemical potentials should be the same in coexisting phases.

To see what this means, suppose two volumes of neutral quark matter in different phases, but with equal pressure and equal quark number chemical potential, are brought in contact with each other. According to the above, the two phases must differ in at least one chemical potential μ_i. Hence the total free energy of the system can be lowered by transferring a part of the corresponding charge Q_i from the phase with the higher μ_i to the phase with the lower μ_i, keeping the two volumes and the total number of quarks in each phase constant. If not prevented by the emerging Coulomb forces, this process will go on until the chemical potentials in both phases are equal. Obviously, in this state the two phases are no longer separately neutral but oppositely charged.

These considerations suggest that instead of requiring locally neutral matter it might be energetically more favored to form mixed phases of several components in chemical equilibrium which are only neutral in total. This scenario has been pushed forward by Glendenning about a decade ago [273]. Although formulated in a quite general way for systems with more than one conserved charge, Glendenning mainly applied his results to the quark–hadron phase transition in neutron stars where he only had to care about electric neutrality. In this case a neutral mixed phase can obviously be constructed in those regions of the phase boundary where the charge densities of the two components have opposite signs. Below we generalize this procedure to the more complex case of constructing electrically and color neutral mixed phases.

6.3.1. Formalism

We consider a mixed phase consisting of two components, 1 and 2, in thermal, chemical, and mechanical equilibrium. In terms of the thermodynamic potential the phase equilibrium can be expressed as the equality

$$\Omega(T, \{\mu_i\}; \chi^{(1)}) = \Omega(T, \{\mu_i\}; \chi^{(2)}) \ , \tag{6.20}$$

where $\chi^{(1)}$ and $\chi^{(2)}$ are two different sets of condensates which solve the coupled gap equations at temperature T and chemical potentials $\{\mu_i\} = \{\mu, \mu_3, \mu_8, \mu_Q\}$. At fixed temperature, Eq. (6.20) defines a three-dimensional first-order phase boundary in the four-dimensional space spanned by the chemical potentials $\{\mu_i\}$.

Since $\chi^{(1)} \neq \chi^{(2)}$, the densities

$$n_i^{(\alpha)} = -\frac{\partial\Omega(T, \{\mu_i\}; \chi^{(\alpha)})}{\partial\mu_i} \tag{6.21}$$

are in general different in the two coexisting phases. In particular, the neutrality condition, Eq. (6.13), is in general not fulfilled simultaneously for both components. However, as indicated above it is sufficient to demand that the *average* charge and color densities of the mixed phase vanish [273]. If the two components

occupy the volume fractions $x^{(1)}$ and $x^{(2)} = 1 - x^{(1)}$, respectively, the average densities are given by

$$n_i = x^{(1)}\, n_i^{(1)} + (1 - x^{(1)})\, n_i^{(2)} \ . \tag{6.22}$$

This is zero for

$$x^{(1)} = \frac{n_i^{(2)}}{n_i^{(2)} - n_i^{(1)}} \ . \tag{6.23}$$

To be meaningful the solution must be in the interval $0 < x^{(1)} < 1$. This is fulfilled when the charge densities $n_i^{(1)}$ and $n_i^{(2)}$ have opposite signs, which is an obvious prerequisite for a charge neutral mixture. For a single charge, e.g., n_Q, it is the only one. However, in order to get simultaneous neutrality for three charges, Eq. (6.13), we have to require that the result of Eq. (6.23) is the same for $i = Q$, 3, and 8. This is the case when

$$n_Q^{(1)} : n_Q^{(2)} = n_3^{(1)} : n_3^{(2)} = n_8^{(1)} : n_8^{(2)} \ . \tag{6.24}$$

In our numerical calculations we will restrict ourselves to $T = 0$. Then, as already mentioned, the phase boundaries, Eq. (6.20), are three-dimensional surfaces in the four-dimensional space of chemical potentials. Since Eq. (6.24) imposes two additional constraints, electrically and color neutral mixed phases can be constructed along a one-dimensional line. In the simplest case this line starts at a point where the neutrality line of phase 1 ($n_Q^{(1)} = n_3^{(1)} = n_8^{(1)} = 0$), meets the phase boundary and it ends where the neutrality line of phase 2 meets the phase boundary. Between these two points $x^{(1)}$ changes continuously from 1 to 0.

However, in our system there are also two-dimensional manifolds with three coexisting phases

$$\Omega(T, \{\mu_i\}; \chi_1) = \Omega(T, \{\mu_i\}; \chi_2) = \Omega(T, \{\mu_i\}; \chi_3) \ . \tag{6.25}$$

It is thus possible that the neutrality line in a two-component mixed phase meets a third phase boundary before the fraction of one of the two components has become zero. In this case we can construct a neutral mixed phase consisting of three components. The corresponding neutrality condition reads

$$\hat{N}\,\vec{x} \equiv \begin{pmatrix} n_Q^{(1)} & n_Q^{(2)} & n_Q^{(3)} \\ n_3^{(1)} & n_3^{(2)} & n_3^{(3)} \\ n_8^{(1)} & n_8^{(2)} & n_8^{(3)} \end{pmatrix} \begin{pmatrix} x^{(1)} \\ x^{(2)} \\ x^{(3)} \end{pmatrix} = 0 \ . \tag{6.26}$$

In order to find a non-trivial solution for $\vec{x}$, we must have $\det \hat{N} = 0$. Together with Eq. (6.25), this again restricts the possible solutions to a one-dimensional subspace. Moreover, since the fractions $x^{(\alpha)}$ should be non-negative, for each $i = Q$, 3, 8 the densities $n_i^{(\alpha)}$ must not have the same sign for all $\alpha = 1, 2, 3$. (The correct normalization $\sum_\alpha x^{(\alpha)} = 1$ can always be achieved and does not lead to further constraints.)

Finally, there even could be a mixed phase, consisting of four components. The corresponding phase boundary is one-dimensional and again the region of possible neutral mixed phases is further restricted by the requirement that the various fractions x_i should not be negative.

6.3.2. Numerical results

Following Ref. [270], we now apply the formalism developed above to the model of Section 6.2 to construct electrically and color neutral mixed phases. Starting point is $\mu = 465.7\,\text{MeV}$, $\mu_8 = -32.5\,\text{MeV}$,

Table 6.2
Composition of electrically and color neutral mixed phases, corresponding quark number chemical potentials and average baryon number densities. The various components are defined in Table 6.1

Components	μ (MeV)	ρ_B/ρ_0
N, 2SC	340.9–388.6	0.00–2.94
N, 2SC, SC_{us+ds}	388.6–388.7	2.94–2.94
N, 2SC, SC_{us+ds}, $2\mathrm{SC}_{us}$	388.7–388.8	2.94–3.06
2SC, SC_{us+ds}, $2\mathrm{SC}_{us}$	388.8–395.4	3.06–3.40
2SC, SC_{us+ds}	395.4–407.7	3.40–3.86
2SC, SC_{us+ds}, CFL	407.7–426.5	3.86–5.69
2SC, SC_{us+ds}, CFL, $2\mathrm{SC}_{us}$	426.5–427.1	5.69–5.75
2SC, CFL, $2\mathrm{SC}_{us}$	427.1–430.6	5.75–6.10
2SC, CFL	430.6–465.7	6.10–7.69

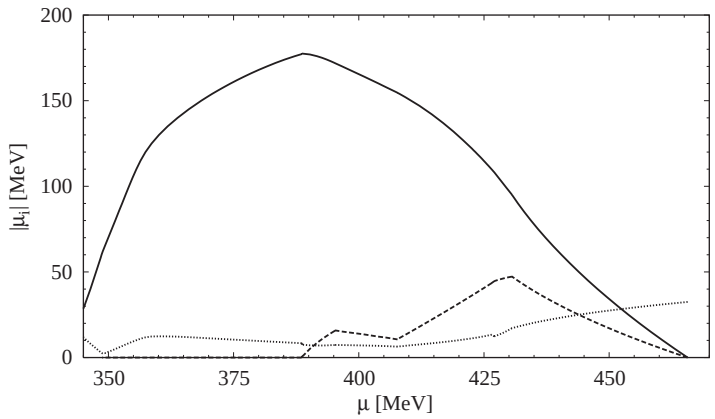

Fig. 6.10. Chemical potentials μ_i corresponding to the electrically and color neutral mixed phases, listed in Table 6.2: $-\mu_Q$ (solid), μ_3 (dashed), and $-\mu_8$ (dotted). Adapted with permission from Ref. [270].

and $\mu_3 = \mu_Q = 0$ where the line of neutral CFL matter meets the boundary to the 2SC phase (see Fig. 6.2). At lower values of μ, mixed phases become possible and are energetically favored as long as Coulomb and surface effects are neglected. Altogether we find nine mixed phase regimes characterized by different compositions of coexisting phases (see Table 6.2). The corresponding chemical potentials μ_i as functions of μ are displayed in Fig. 6.10. In Table 6.2 we also list the corresponding minimal and maximal quark number densities, averaged over the components of the respective mixed phase.

In the regime closest to the region of homogeneous neutral CFL matter ($430.6\,\mathrm{MeV} < \mu < 465.7\,\mathrm{MeV}$), we find a mixed phase consisting of a CFL component and a 2SC component. The volume fraction $x^{(2\mathrm{SC})}$ of the 2SC component is displayed in the left panel of Fig. 6.11. In the higher-μ part of this region it is completely negligible, but even at the lower end it remains below 2%. Consequently, the CFL component must stay almost neutral by itself. Indeed, the relative charge densities n_i/n, $i = 3, 8, Q$ (right panel of Fig. 6.11) are very small. As we have discussed in Section 6.2.2, n_3-neutrality of the CFL phase is maintained by the relation $\mu_3 = -\mu_Q/2$. For the actual values of μ_3 and $\mu_Q/2$ in the 2SC–CFL mixed

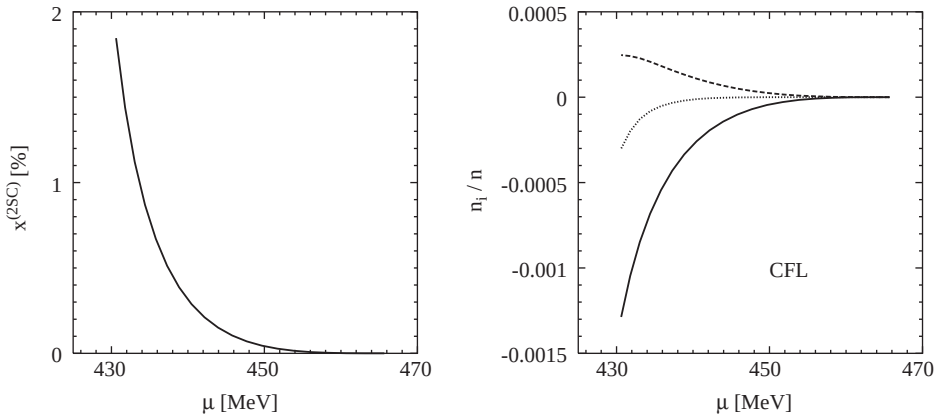

Fig. 6.11. Quantities related to the neutral 2SC–CFL mixed phase as functions of the quark number chemical potential μ. Left: Volume fraction $x^{(2SC)}$ of the 2SC component. Right: Relative densities in the CFL component: n_Q/n (solid), n_8/n (dashed), and n_3/n (dotted). Adapted with permission from Ref. [270].

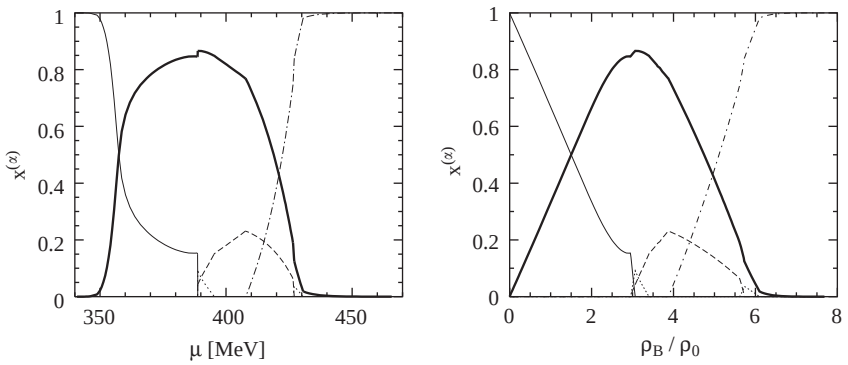

Fig. 6.12. Volume fractions $x^{(\alpha)}$ of the various components α in the mixed phase region as functions of the quark number chemical potential μ (left) and as functions of the averaged baryon number density $\rho_B = n/3$ in units of $\rho_0 = 0.17$ fm^{-3} (right): normal (thin solid), 2SC (bold solid), CFL (dash–dotted), SC$_{us+ds}$ (dashed), 2SC$_{us}$ (dotted). Left figure adapted with permission from Ref. [270].

phase we find a deviation of less than 1% from this relation, while μ_8 can approximately be fitted by $\mu_8 = -\mu_Q/7 - 30$ MeV. This is the reason why we have calculated the phase diagram shown in Fig. 6.6 with these constraints.

In that figure it can be seen that the 2SC–CFL phase boundary meets the boundary to the 2SC$_{us}$ phase at $\mu = 430.6$ MeV. Below that point we get a three-component neutral mixed phase, consisting of 2SC, CFL and 2SC$_{us}$. Then, on a short interval in μ, we even find a four-component neutral mixed phase (2SC, CFL, 2SC$_{us}$, and SC$_{us+ds}$) before upon further decreasing μ the system goes over into a neutral 2SC–CFL–SC$_{us+ds}$ mixed phase.

In the left panel of Fig. 6.12 the volume fractions of the various components of the mixed phases are plotted as functions of μ. To get some idea about the corresponding densities, we also show the volume

fractions as functions of the average baryon number density ρ_B (right panel). Whereas the 2SC–CFL mixed phase (Fig. 6.11) is completely dominated by the CFL component, thereafter the CFL fraction becomes quickly smaller with decreasing μ, while in particular the 2SC component, becomes more and more important. Below $\mu = 407.7\,\text{MeV}$ ($\rho_B \simeq 3.9\rho_0$) the CFL component disappears completely.

An admixture of normal quark matter is found below $\mu = 388.8\,\text{MeV}$ ($\rho_B \simeq 3.1\rho_0$). The fractions of the superconducting phases other than the 2SC phase then rapidly become smaller and vanish at $\mu = 388.6\,\text{MeV}$ ($\rho_B \simeq 3.0\rho_0$), while the fraction of normal matter strongly increases.[50] Nevertheless the 2SC phase stays the dominant component for $\mu \gtrsim 360\,\text{MeV}$ ($\rho_B \approx 1.5\rho_0$).

As discussed in Section 6.2.2, apart from the vacuum there is no solution of stable neutral non-superconducting quark matter in our model. Therefore the normal-2SC mixed phase cannot end in normal homogeneous quark matter but only in the vacuum. Hence, the chemical potential μ_Q must finally go to zero. Eventually, at $\mu = 348.6\,\text{MeV}$ ($\rho_B \simeq 0.02\rho_0$), $|\mu_Q|$ drops below 60 MeV and we enter the regime where the normal phase only consists of electrons without quarks (cf. Fig. 6.3). This means, the corresponding mixed phase consists of (electrically positive) 2SC-droplets surrounded by regions without quarks and neutralized by a homogeneous background of electrons.[51] Since the electrons are color neutral, the 2SC component must be color neutral by itself. This is maintained by an increase of $|\mu_8|$ in this regime. At $\mu = 340.9\,\text{MeV}$ we finally reach the vacuum.

6.3.3. Surface and Coulomb effects

When we compare the mixed phase results with the results obtained in Section 6.2.3 for homogeneous phases we see that the regions where the mixed phases are dominated by the CFL phase or by the 2SC phase, roughly correspond to those regions where we found homogeneous CFL or 2SC matter, respectively, to be favored. There are of course differences in details. In order to decide which of the two scenarios is the more realistic one we should recall that so far we have neglected the surface energy and the energies of the electric and color-electric fields in the mixed phases. Without these terms the mixed phases would be favored, which follows already from the general arguments given in the beginning of Section 6.3. Quantitatively this is shown in the left panel of Fig. 6.13 where the difference in bulk free energy, $\delta\Omega = \Omega^{(\text{mix})} - \Omega^{(\text{hom})}$ between the mixed phase solution and the most favored homogeneous neutral solution is plotted. $\delta\Omega$ is negative, as expected, and has a minimum of about $-5\,\text{MeV/fm}^3$ at the chemical potential which corresponds to the 2SC–CFL phase transition point in the homogeneous case. (The second rise of $|\delta\Omega|$ below $\mu \simeq 490\,\text{MeV}$ is do to the appearance of a normal quark matter component in the mixed phase.)

Of course, the mixed phases are only stable if this gain in bulk free energy is larger than the neglected surface and (electric and color-electric) Coulomb contributions. For the two-component mixed phases these can, in principle, be estimated adapting the techniques which have been developed by Ravenhall et al. [274] in the context of nuclear matter at sub-saturation densities and which have been applied, among others, in Refs. [258,275,276] to analyze possible quark–hadron mixed phases in neutron stars.

---

[50] Note, however, that by construction all volume fractions $x^{(\alpha)}$ are continuous functions of both, μ and ρ_B in the entire mixed phase region. Therefore the pretended steps in the figure only correspond to very rapid changes, but not to discontinuities.

[51] In the spirit of the schematic picture discussed in Section 2.3.3 where the solutions of dense quark matter in equilibrium with the vacuum were identified with "nucleons", one might be tempted to view this mixed phase as a gas or plasma of "atoms". However, even on a very schematic level, this would not make sense. Clearly, there is no 2SC phase inside nucleons or nuclei. Thus, although it is interesting to see how our procedure brings itself to an end by finally reaching the vacuum in a consistent way, the results should not be trusted in the low-density regime.

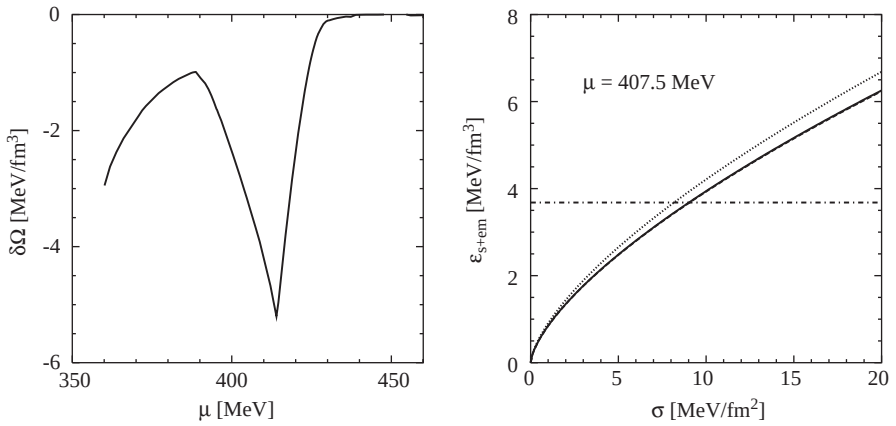

Fig. 6.13. Left: Difference in bulk free energy, $\delta\Omega = \Omega^{(\mathrm{mix})} - \Omega^{(\mathrm{hom})}$ between the mixed phase solution and the most favored homogeneous neutral solution (CFL matter for $\mu > 414$ MeV, 2SC matter for $\mu < 414$ MeV, see Fig. 6.7). Right: Surface and Coulomb energy per volume for the 2SC + SC_{us+ds} mixed phase at $\mu = 407.5$ MeV as a function of the surface tension σ: slabs (dotted), SC_{us+ds} rods (dashed), and SC_{us+ds} drops (solid). (The results for rods and drops are almost indistinguishable.) The dash–dotted line indicates the value of $-\delta\Omega$ at this point. Note that the color-electric Coulomb energy has not been included.

According to these references, the surface and the electromagnetic Coulomb contribution to the energy density are given by

$$\epsilon_s = \frac{\mathrm{d}x\sigma}{r_0}, \quad \epsilon_{\mathrm{em}} = 2\pi\alpha_{\mathrm{em}} f_d(x)(\delta n_Q)^2 r_0^2 \ , \tag{6.27}$$

where σ is the surface tension, x the volume fraction of the rarer phase, and δn_Q the difference of the electric charge density in the two phases. The result depends on the geometry which is controlled by the dimension d, corresponding to slabs ("lasagna phase", $d = 1$), rods ("spaghetti phase", $d = 2$), and drops ($d = 3$), and the parameter r_0, which denotes the radius of the rods or drops, or the half-thickness of the slabs of the rarer phase. The geometrical factor $f_d(x)$ is given by

$$f_d(x) = \frac{1}{d+2}\left(\frac{2 - dx^{1-2/d}}{d-2} + x\right) \ . \tag{6.28}$$

For $d = 2$ one must interprete f_d as a continuous function of d and take the appropriate limit.

In principle, the surface plus Coulomb contribution to the energy is now easily obtained, minimizing the sum of ϵ_s and ϵ_{em} with respect to r_0. This gives

$$\epsilon_{s+\mathrm{em}} = \tfrac{3}{2}\,(4\pi\alpha_{\mathrm{em}} d^2 f_d(x) x^2 (\delta n_Q)^2 \sigma^2)^{1/3} \ . \tag{6.29}$$

In practice, however, one generally has to deal with the problem that the surface tension is poorly known. For the quark–hadron case, typical estimates range from 10 to 100 MeV fm^{-2} [275] or even 300 MeV/fm^2 [258], whereas until very recently practically nothing was known for quark–quark mixed phases. In this situation, the best one can do is to determine the maximal surface tension which is compatible with the existence of a mixed phase and to compare this value with "plausible" estimates. This is similar to what has been done in Ref. [258] for the interface between nuclear and CFL matter.

As an example we consider the 2SC–SC$_{us+ds}$ phase at $\mu = 407.5\,\mathrm{MeV}$ where we have found a gain in bulk free energy of $3.7\,\mathrm{MeV/fm^3}$. (The maximum of $|\delta\Omega|$ is located in a three-component mixed phase which cannot be addressed by the formulae of Ref. [274].) At this point we have $x \equiv x^{(\mathrm{SC}_{us+ds})} = 0.23$ and $\delta n_Q = 0.52\,\mathrm{fm}^{-3}$. The resulting surface plus Coulomb energy density as a function of σ is displayed in the right panel of Fig. 6.13. It turns out that the $d = 1$ solution (dotted) is somewhat higher in energy, whereas the solutions for $d = 2$ (dashed) and $d = 3$ (solid) are practically identical. (The "spaghetti phase", $d = 2$ is slightly favored, but this is hardly seen in the plot.) For these solutions the gain in bulk energy (indicated by the dash–dotted line) is already weight out for a surface tension $\sigma \simeq 10\,\mathrm{MeV/fm^2}$.

This sounds like a rather small number, which has originally been taken as an indication against the mixed-phase scenario [270]. Very recently, however, Reddy and Rupak have *calculated* the surface tension between normal and 2SC phase in a two-flavor model [277], employing Landau–Ginzburg theory to determine the gradient contribution to the free energy at the interface [9]. The result was a surprisingly small surface tension of only a few MeV, which led the authors to the conclusion that in their case the mixed phase was in fact favored [277]. It would be certainly very interesting to redo this kind of calculation for the three-flavor case as well.

In the considerations above we have not yet included the color-electric energy. As an order-of-magnitude estimate we note that the corresponding contribution is of similar form as ϵ_{em} with α_{em} replaced by α_s, and δn_Q replaced by the difference of excess blue quarks $\delta n_8/\sqrt{3}$. In our example, the latter is about one order of magnitude smaller than δn_Q and has to be squared, whereas α_s should be about two orders of magnitude larger than α_{em}. We thus expect the color-electric energy to be of the same order as the electromagnetic one. (Note that, because of the power $\frac{1}{3}$ in Eq. (6.29), we are not very sensitive to details.) Anyway, it is clear that the color-electric energy will further lower the maximum value of σ compatible with a mixed phase.

On the other hand, if σ is small, but color forces are strong, there could be a third scenario where color neutrality is realized locally whereas electric neutrality is realized only globally, leading to mixed phases of color neutral but electrically charged components [278]. In this case, we would be left with the more standard situation of only two independent chemical potentials, μ and μ_Q, and only mixed phases with two components would be possible.

Finally, we should note that we have restricted our analysis to diquark condensates $s_{AA'}$ with $A = A'$. For homogeneous phases this was motivated by the fact, that the two most important condensation patterns, 2SC and CFL, can always be brought into this form without loss of generality (see Section 5.1.1). For mixed phases, this is in principle different. Here the color rotations are additional degrees of freedom which could be exploited to reduce the bulk energy of the mixed phase. For instance, as discussed in Section 4.3.4 we could construct a color neutral mixed phase without applying color chemical potentials by combining several components of the same condensate, but rotated into different color directions. However, as we have seen in Fig. 4.4 the related gain in bulk free energy is small. Therefore it is unlikely that including color rotated condensates would strongly change the equation of state.

6.4. Discussion: alternative pairing patterns

The results of the previous section suggest that, in spite of the arguments given in Ref. [247], the 2SC phase could play an important role under compact star conditions—either as a homogeneous phase or as the dominant component in a mixed phase. However, our analysis is still rather incomplete:

First, we need a better description of the hadronic phase, which so far is represented at best by a vacuum phase with spontaneously broken chiral symmetry. It is thus possible that a realistic hadronic phase is much more stable and the deconfinement phase transition takes place at much higher densities where the 2SC phase plays no role. In the next chapter, we will therefore use an alternative approach and construct a hybrid equation of state with the hadronic part taken from other models.

In addition, there are other pairing patterns which we have not yet considered:

6.4.1. CFL+Goldstone phase

So far, we have neglected the role of the Goldstone bosons in the CFL phase. It is obvious that the charged Goldstone bosons ($\pi^\pm$, $K^\pm$) are sensitive to μ_Q. Moreover, the stress imposed by unequal quark masses acts as an additional effective chemical potential. For instance, the reduced Fermi momentum $p_{\rm F}^s = \sqrt{\mu^2 - m_s^2} \simeq \mu - m_s^2/(2\mu)$ could be interpreted as a result of an effective strangeness chemical potential $m_s^2/(2\mu)$. Combining μ_Q and mass effects, one finds the effective chemical potentials [19]

$$\tilde{\mu}_{\pi^+} = \mu_Q + \frac{m_d^2 - m_u^2}{2\mu}, \quad \tilde{\mu}_{K^+} = \mu_Q + \frac{m_s^2 - m_u^2}{2\mu}, \quad \tilde{\mu}_{K^0} = \frac{m_s^2 - m_d^2}{2\mu}\ , \tag{6.30}$$

and the same with the opposite sign for π^-, K^-, and $\bar{K}^0$. Hence, if one of these effective chemical potentials exceeds the mass of the corresponding Goldstone boson, these mesons condense.

These processes can systematically be studied within high-density effective field theory [279,280]. (For a recent overview, see Ref. [14].) Roughly speaking, this corresponds to χPT in the CFL phase, but with the essential difference that at high densities all coefficients can be calculated within high-density QCD, instead of being determined empirically. Assuming that $U_A(1)$-breaking effects can be neglected, this leads to rather small Goldstone masses of the order $m_q\Delta/\mu$ [280]. For instance, when the asymptotic results are extrapolated down to 400 MeV, one finds kaon masses of about 5–20 MeV [12]. As a consequence, meson condensation is expected to occur already for rather small values of $m_s \sim m_d^{1/3}\Delta^{2/3}$ or $|\mu_Q| \sim \sqrt{m_d m_s}\Delta/p_{\rm F}$ [18]. A phase diagram in the $m_s^2/(2\mu)$–μ_Q plane is presented in Ref. [19]. Further CFL phases containing η condensates have recently been discussed in Ref. [281].

For $\mu_Q = 0$ and large enough m_s, the K^0 condense. Because of the condensation energy, the pressure in the CFL+K^0 phase is higher than in the CFL phase (otherwise the kaons would not condense) and therefore the CFL+K^0 phase could be favored against neutral 2SC matter in regions where the CFL phase is not. This effect has been estimated in Ref. [267]. The authors found that the kaon condensate lowers the critical quark chemical potential of the 2SC–CFL phase transition by about 16 MeV. This is not dramatic but could make a difference if, for instance, the transition point to the hadronic phase turns out to be in the same region.

In principle, the CFL+Goldstone phases can also be studied within NJL-type models. In fact, since the applicability of the high-density effective Lagrangian method becomes questionable at moderate densities, it would be interesting to have alternative approaches to compare with. In particular, it would be interesting to investigate the role of non-vanishing quark–antiquark condensates and $U_A(1)$-breaking terms. As mentioned in Section 2.4, NJL models have already been employed to study pion condensation at non-zero isospin chemical potential [142] (see also Ref. [138]). An extension to the CFL phase is straightforward but technically involved.

6.4.2. Crystalline color superconductors

Another possibility is the formation of so-called crystalline color superconductors or "LOFF phases", named after Larkin, Ovchinnikov, Fulde, and Ferrell who suggested this kind of pairing for electromagnetic superconductors [282,283]. In the QCD context this has been discussed first in Ref. [20]. The essential feature of LOFF pairing is that the total momentum of a pair does not vanish, i.e., the momenta of the paired fermions are not opposite to each other. This has the advantage that both fermions can stay in the vicinity of their respective Fermi surfaces, even for rather different Fermi momenta, i.e., the pair can be formed without cost of free energy. On the other hand, LOFF pairing is in general disfavored against BCS pairing by phase space.

As an example, consider two quarks of type a and b with momenta

$$\vec{k}_a = \vec{q} + \vec{p} \quad \text{and} \quad \vec{k}_b = \vec{q} - \vec{p} \ , \tag{6.31}$$

forming a diquark pair with total momentum $2\vec{q}$. In the most simple case $\vec{q}$ is constant and the same for all pairs in the condensate. If we now restrict both quarks to their Fermi surfaces, $|\vec{k}_a| = k_a^{\mathrm{F}}$ and $|\vec{k}_b| = k_b^{\mathrm{F}}$, it follows that the possible vectors $\vec{p}$ lie on a circle which corresponds to the crossing of two spherical shells with radii k_a^{F} and k_b^{F} whose centers are displaced by $2\vec{q}$. Hence, in contrast to the standard BCS case where pairing takes place in the vicinity of the two-dimensional Fermi surface, it is now restricted to the region close to this one-dimensional circle. This explains why for equal Fermi momenta BCS pairing is favored. Moreover, because of the lower dimensionality of the regime where non-interacting LOFF pairs can be created (or destroyed) without cost of free energy, there is no divergence in the gap equation which guarantees the existence of a non-vanishing gap parameter for arbitrarily weak attractive interactions.

Nevertheless, for certain values of the chemical potential difference, LOFF pairing can be more favored than BCS pairing or no pairing at all. If the analysis is restricted to condensates with a single fixed value $2\vec{q}$ of the pair momentum (but $|\vec{q}|$ being a parameter which is varied to minimize the free energy for given chemical potentials), this regime turns out to be very small [20]. Note that in this case, rather than forming a real crystal, the gap function takes the form of a plane wave,

$$\langle q(\vec{x})^{\mathrm{T}} \mathcal{O} q(\vec{x}) \rangle \sim \Delta \mathrm{e}^{2\mathrm{i}\vec{q}\cdot\vec{x}} \ . \tag{6.32}$$

It is obvious that allowing for more complex structures could enlarge the available phase space, rendering LOFF phases more favorable. This has been analyzed by Bowers and Rajagopal [21] within a Ginzburg–Landau approach. In this analysis, the authors considered superpositions of various plane waves, still with a single value of $|\vec{q}|$ but different directions. It was found that crystalline phases can compete with BCS pairing over a wide range of chemical potentials, with a face-centered cubic structure being most favored. These findings led the authors to speculate that for neutral matter the regime between hadronic and CFL phase could completely be occupied by a crystalline phase, with no 2SC phase at all [284]. The lower left phase diagram in Fig. 1.1 was inspired by this idea.

It should be noted, however, that, in spite of being rather involved, the analysis of Ref. [21] has only been performed within a simple toy model with two massless flavors. This leaves room for further investigations, in particular about mass effects and the role of the strange quarks. Certainly, an NJL-model analysis of these questions would be very interesting, although rather complicated. In this context our analysis of mixed phases could be instructive. Since mixed phases are necessarily related to non-uniform structures in space and sometimes even to certain geometries, like rods or slabs, they might be viewed as some form of "crystals" as well. Similar to the large number of different mixed phases which we have

found in Section 6.3 we could thus imagine that the phase diagram contains a series of different crystal structures if masses and strange quarks are taken into account.

Of course, the mixed phases in Section 6.3 have been constructed under the simplifying assumption that each component is homogeneous and infinitely extended. Obviously, this is only justified if the structures are much larger than the average distance between the quarks. Unfortunately, we can not say much about the structure sizes in the mixed phases as long as we do not know the surface tension. To get a rough idea we inspect the "lasagna" solution ($d = 1$) of the example discussed in the right panel (dotted line) and take $\sigma = 10\,\mathrm{MeV/fm^2}$. For this case we find $r_0 = 0.8\,\mathrm{fm}$, meaning that the thickness of the SC_{us+ds} slabs is 1.6 fm, while that of the 2SC slabs is 5.4 fm. (For $d = 2$ or $d = 3$ we get somewhat larger structures, $r_0 = 1.8$ and 2.6 fm, respectively.) On the other hand, the average distance between the quarks is 0.7 fm in the SC_{us+ds} component and 0.8 fm in the 2SC component. This means, the geometric sizes are only a few times larger than the inter-quark distances and our treatment of the mixed phases as consisting of infinite homogeneous components seems to be inappropriate.

It is interesting that the sizes in the above example are almost the same as in the LOFF phases. Taking again the $d = 1$ solution with $\sigma = 10\,\mathrm{MeV/fm^2}$ we have a period of 7.0 fm. For a LOFF phase described by a single plane wave, the authors of Refs. [20,21] find $|\vec{q}| \approx 1.2\delta\mu$, where $\delta\mu = \mu_Q/2$ (cf. Eq. (2.73)). For the actual value $\mu_Q \approx 155\,\mathrm{MeV}$, this translates into a periodicity $L = \pi/(0.6\mu_Q) = 6.7\,\mathrm{fm}$, i.e., almost the same as in the mixed phase. Since the latter depends on our (rather arbitrary) choice of the string tension, this coincidence might be completely accidental. On the other hand, it could also be taken as an indication that a small string tension of $10\,\mathrm{MeV/fm^2}$ is not too unrealistic.

Before proceeding to the next point, we would like to mention that some authors have also investigated the possibility of particle–hole pairing with non-vanishing total momentum ("Overhauser pairing") [285–288]. In weak coupling, it was found that this pairing scheme can compete with BCS only for an extremely large number of colors ($N_c \gtrsim 1000$) [286,287], but it could become competitive in the non-perturbative regime [288].

6.4.3. Gapless color superconductors

We have already mentioned the gapless color superconducting phases. Partially following an old idea of Sarma [289], this has first been discussed by Shovkovy and Huang [223,224] in the context of two massless quark flavors. This phase does not correspond to an entirely new pairing pattern, but rather to the fact that in a certain interval of μ_Q the 2SC gap equation has two branches of solutions. The first branch is the continuation of the standard BCS solution at $\mu_Q = 0$. Here $\Delta > |\mu_Q|/2$ and the quasiparticle spectrum contains four gapped modes. At $T = 0$ the densities of the paired quark species are equal, as given in Eq. (6.19). For $\mu_Q \neq 0$, the four gapped modes are no longer completely degenerate, but they split into pairs of two with gaps $\Delta_\pm := \Delta \pm |\mu_Q|/2$. In the second branch of solutions $\Delta < |\mu_Q|/2$. Although, as before, four quark species participate in the condensate, only two of the corresponding dispersion laws are gapped, whereas the other two are not. This is the reason why this phase is called "gapless 2SC" (g2SC) phase.[52] Here the number densities of the paired quarks are not equal.

Obviously, the g2SC solutions do not satisfy the stability criterion, Eq. (5.9). In fact, at fixed chemical potentials this branch corresponds to local maxima of the thermodynamic potential and is indeed unstable. The important result of Refs. [223,224] is that this can change if local neutrality constraints $n_Q = n_8 = 0$

[52] However, it is possible that the gapless modes experience another Cooper instability and, e.g., form a secondary spin-1 condensate [224].

are imposed, instead of keeping μ_Q and μ_8 at fixed values. In this case it depends on the coupling strength in the scalar diquark channel whether the standard 2SC solution (strong coupling), the g2SC solution (intermediate) or the normal conducting solution (weak) is favored at given quark number chemical potential. In their model calculation, the authors of Refs. [223,224] find that the g2SC solution is favored at $\mu = 400\,\mathrm{MeV}$ if (in our language) $0.7 \lesssim H : G \lesssim 0.8$. Although this is a relatively small interval, it is just centered by the "standard" value $H : 0G = 0.75$ and could therefore be quite relevant. A similar pairing pattern for the CFL phase with massive strange quarks has been discussed in Ref. [226].

Very recently, Huang and Shovkovy have calculated the Meissner masses of the gluons in the g2SC phase [290]. It turned out that some of them become imaginary. While this seems to signal some kind of instability, the final interpretation is not yet clear.

6.4.4. Breached color superconductors

A similar mechanism has also been suggested for pairing one light and one heavy flavor with different Fermi momenta [225,291]. For example, consider a system of ultra-relativistic up quarks and non-relativistic strange quarks with Fermi momenta $p_{\mathrm{F}}^u > p_{\mathrm{F}}^s$ and linearize the dispersion laws of the non-interacting particles near their Fermi surfaces,

$$E_-^i(p) \simeq V^i(p - p_{\mathrm{F}}^i), \quad V^i = \frac{p_{\mathrm{F}}^i}{\sqrt{{p_{\mathrm{F}}^i}^2 + {M_{\mathrm{F}}^i}^2}}\,. \tag{6.33}$$

Obviously, $V^s \ll V^u \simeq 1$, which means that increasing the momentum of a strange quark is relatively inexpensive. In the presence of attractive interactions it could therefore be favorable to promote the strange quarks to pair with the up quarks around the up-quark Fermi surface, rather than deforming both Fermi surfaces. The result is also a gapless ("breached") color superconductor with a similar characteristics as discussed above [225]. Again, this scenario was found to be unstable for fixed chemical potentials, but it could be stable for fixed total or relative particle densities [225]. Of course, in the thermodynamic limit this apparent difference between canonical and grand canonical treatment can only hold if a phase separation is again inhibited by long-range forces. (See also Ref. [292] for a recent discussion of the stability problem.)

The "interior gap" which has been discussed in Ref. [291] is basically the same mechanism for the opposite case where the Fermi momentum of the heavier species is larger than that of the lighter. Although this case is rather unlikely to play a role in quark matter, we have seen in the context of the "exotic" phase SC_{us+ds} that unusual orderings of the Fermi momenta should not be excluded completely.

6.4.5. Deformed Fermi spheres

Yet another possibility to support the pairing of two quark species with different Fermi momenta is to deform their Fermi surfaces in an anisotropic way. Recently, this has been studied in Ref. [293]. To that end, the authors considered a two-flavor system with an excess of down quarks. In this case the overlap of the two Fermi surfaces can be enhanced if the up- and down-quark Fermi spheres are deformed into oblate and prolate ellipsoids, respectively. While favoring the pairing near the equators of the ellipsoids, the deformation costs of course kinetic energy. Nevertheless, the authors of Ref. [293] found that the BCS state becomes unstable with respect to spontaneous quadrupole deformations already at small asymmetries.

7. Application: neutron stars with color superconducting quark cores

In this chapter we apply our NJL quark matter equation of state to investigate the possible existence of deconfined quark matter in compact stars.

We have already seen in Section 6.2.3 that absolutely stable strange quark matter is unlikely to exist within this model, even in the presence of color–flavor locking diquark condensates. This rules out the existence of pure quark stars ("strange stars"), but hybrid stars, consisting of hadronic matter in the outer parts and a quark matter core, are not a priori excluded.

For a quantitative examination of this possibility we need a realistic equation of state for the hadronic phase. Since this cannot be obtained within an NJL mean-field calculation we adopt hadronic equations of state from other models (Section 7.1.1). Comparing these with the NJL equation of state for the quark phase, we construct the phase transitions and finally employ the resulting hybrid equations of state to calculate the structure of compact stars.

Whereas most models of hybrid stars are based on bag-model descriptions of the quark matter phase, two early investigations which employed the NJL model have been performed in Refs. [294,295]. It was found by both groups that quarks exist at most in a small mixed phase regime but not in a pure quark core. Similar to our findings in the context with SQM this could be traced back to the relatively large values for the effective bag constant and the effective strange quark mass.

However, these calculations did not include diquark condensates. As we have seen in Section 6.2.3 these give an extra contribution to the pressure and therefore work in favor of a quark phase. Recently, it was shown within a bag model [296] that this could have sizeable consequences for the hadron–quark phase transition and for the properties of compact stars. On the other hand, as pointed out before, bag-model calculations miss possible effects of the density and phase dependence of quark masses and bag constants. It is therefore interesting to perform a similar investigation based on an NJL model equation of state where these effects can be studied. This has been done in Refs. [297,298]. Below, we discuss the results.

7.1. Hadron–quark phase transition

7.1.1. Hadronic equations of state

To put our analysis on a relatively broad basis, we employ four different hadronic equations of state.

Two of them, taken from Refs. [299,300], are microscopic equations of state based on the non-relativistic Brueckner–Bethe–Goldstone (BBG) many-body theory, treated in Brueckner–Hartree–Fock (BHF) approximation. It has been shown that the non-relativistic BBG expansion is well convergent [301,302], and the BHF level of approximation is accurate in the density range relevant for neutron stars.

The first equation of state, "BHF(N,l)" contains only nucleons and non-interacting leptons and has been derived in Ref. [299] using the Paris potential [303] as two-nucleon interaction and the Urbana model as three-body force [304,305]. The resulting nuclear matter equation of state fulfills several requirements [299], namely (i) it reproduces the correct nuclear matter saturation point ρ_0, (ii) the incompressibility is compatible with the values extracted from phenomenology, (iii) the symmetry energy is compatible with nuclear phenomenology, (iv) the causality condition is always fulfilled.

The second equation of state, "BHF(N,H,l)", is a recent extension of the first one which contains also hyperon (Σ^- and Λ) degrees of freedom [300]. This is physically motivated by the fact that the baryon chemical potentials reached in the interiors of neutron stars are likely to be large enough that these particle

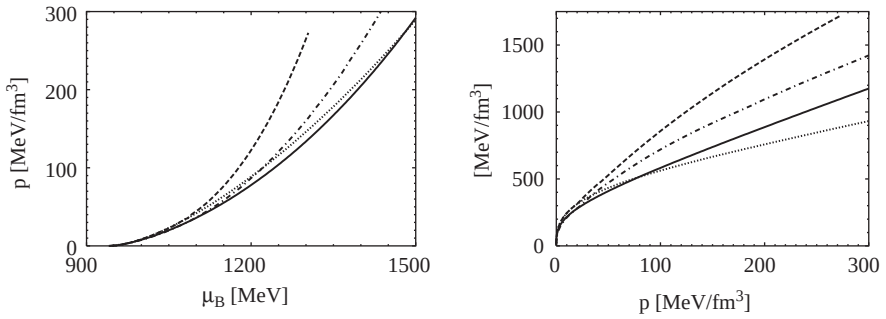

Fig. 7.1. Properties of the hadronic equations of state employed in our analysis: pressure as function of baryon chemical potential (left) and energy density as function of pressure (right). The different lines correspond to the following equations of state (see text): BHF(N,l) [299] (dotted), BHF(N,H,l) [300] (dashed), χSU(3) [307] (solid), and RMF240 [155] (dash–dotted).

states are populated. Obviously, to include these additional degrees of freedom, the bare nucleon–hyperon and hyperon–hyperon interactions are needed. For the nucleon–hyperon interaction the Nijmegen soft-core model [306] has been adopted in Ref. [300]. Unfortunately, because of lacking experimental data, the hyperon–hyperon interaction is practically unknown. Therefore, as a first approximation, the authors of Ref. [300] have decided to neglect this interaction completely.

In order to estimate the level of uncertainty caused by this neglect we employ two other hadronic equations of state which also contain hyperons but which are not based on microscopic interactions. One of them, "RMF240", has been derived within relativistic mean-field theory and is tabulated in Ref. [155]. It also reproduces the correct nuclear matter saturation point and yields reasonable values for the symmetry energy and the incompressibility K. Here we adopt the parameter set with $K = 240\,\mathrm{MeV}$.

Finally, we take an equation of state of Ref. [307] (hereafter "χSU(3)") which has been derived within a QCD motivated hadronic model with a non-linear realization of chiral $SU(3)$.

The key properties of the four hadronic equations of state are plotted in Fig. 7.1. In the left panel, the pressure is displayed as a function of the baryon chemical potential. The corresponding energy densities as functions of the pressure are displayed in the right panel. The curves correspond to neutral matter in beta equilibrium. They agree fairly well at the lower end where the equations of state are partially constrained by empirical data. However, there are quite some differences if one moves up to higher densities, which may mainly reflect the uncertainties in the hyperon sector.

The two microscopic equations of state, (BHF(N,l) and BHF(N,H,l)), are indicated by the dotted and the dashed lines, respectively. They are of course identical below the hyperon threshold, but then the presence of hyperons softens the equation of state considerably, which results in a steeper increase of pressure as a function of baryon chemical potential [300]. It is therefore quite remarkable that the pressure predicted by the chiral model χSU(3) (solid) remains even below the BHF(N,l) result up to $\mu_B \simeq 1480\,\mathrm{MeV}$, although hyperons included. Finally, the relativistic mean-field equation of state RMF240 (dash–dotted) plays some intermediate role, being softer than BHF(N,l) but still considerably stiffer than BHF(N,H,l).

7.1.2. Hadron–quark hybrid equation of state

Having selected the hadronic equations of state we can now construct the corresponding phase transitions to NJL quark matter. Motivated by the conclusion of Ref. [258] that a quark–hadron mixed phase is

Table 7.1
Various quantities related to the phase transitions identified in Fig. 7.2 (10 hadron–quark phase transitions and the 2SC–CFL phase transition for parameter set HK): critical baryon chemical potential, and baryon and energy densities below (1) and above (2) the phase transition

Transition		μ_B (MeV)	$\rho_B^{(1)}/\rho_0$	$\rho_B^{(2)}/\rho_0$	$\epsilon^{(1)}$ (MeV/fm^3)	$\epsilon^{(2)}$ (MeV/fm^3)
BHF(N,l) →	RKH(N)	1478	4.6	7.9	884	1707
	RKH(CFL)	1312	3.7	6.4	672	1282
	HK(N)	1454	4.5	6.9	852	1446
	HK(CFL)	1280	3.6	6.1	634	1186
RMF240 →	RKH(CFL)	1397	6.5	7.7	1279	1567
	HK(CFL)	1326	5.4	6.8	1039	1345
χSU(3) →	RKH(N)	1477	5.4	7.9	1092	1701
	RKH(CFL)	1284	3.6	6.0	657	1188
	HK(N)	1441	5.1	6.5	1000	1353
	HK(2SC)	1216	3.0	3.4	536	627
HK(2SC) → H	K(CFL)	1260	4.0	5.7	746	1117

unlikely to be stable for reasonable values of the surface tension, and by the original conclusion of Ref. [270] that this is also the case for quark–quark mixed phases (see Section 6.3.2), we restrict ourselves to analyze sharp phase transitions from neutral hadronic matter to homogeneous neutral quark matter.

In order to study the influence of color superconductivity we consider both, the equation of state without diquark condensates developed in Section 3.3 and the equation of state with diquark condensates developed in Section 6.2. Since the quark–quark coupling constant employed there, $H = G$, is likely to be an upper limit, this could be considered as two extreme cases.

In Fig. 7.2 the pressure of the various hadronic and quark matter equations of state is displayed as a function of the baryon chemical potential. The dash–dotted lines correspond to the hadronic equations of state. These are the same curves as shown in Fig. 7.1. The other lines correspond to NJL quark matter in the normal phase (dotted), or in a color superconducting phase. Here we have indicated the part which belongs to the 2SC phase by a dashed line and the part which belongs to the CFL phase by a solid line. Since the two solutions cross each other at the 2SC–CFL transition point, the slope of the pressure increases discontinuously at this point. Physically, this is related to a sudden increase of the baryon number density due to the fact that the number of strange quarks jumps from almost zero in the 2SC phase to $\frac{1}{3}$ of the total quark number in the CFL phase. In contrast, there is no such behavior in the normal quark matter phase where the strange quarks come in smoothly. (As we have seen earlier, this can be different if the flavor mixing is weak.)

For given hadronic and quark equations of state, the hadron–quark phase transition point is now easily read off as the point of equal pressure, i.e., the point where the lines $p(\mu_B)$ cross. The results are summarized in Table 7.1. We begin our discussion with the four left panels of Fig. 7.2 where the quark equations of state are based on our "standard" parameter set RKH [145] which we have employed in most

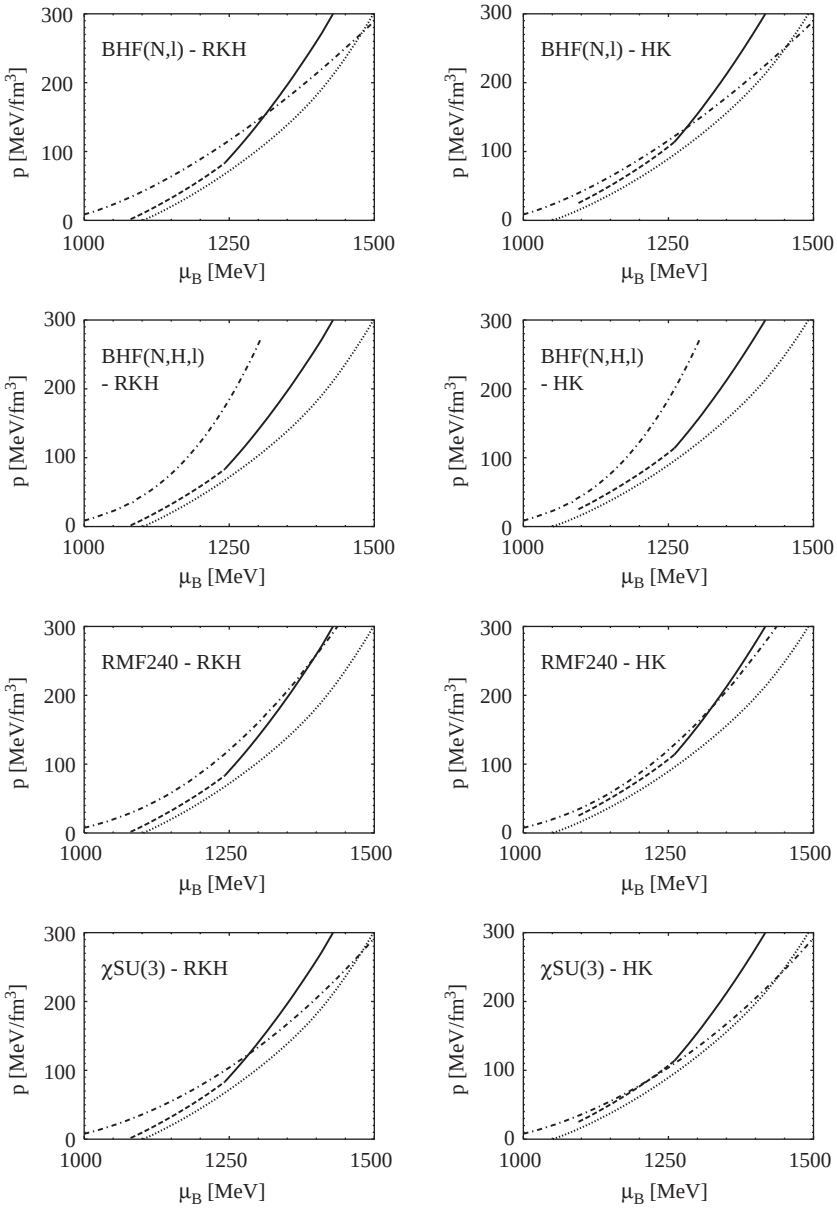

Fig. 7.2. Pressure of neutral matter in beta equilibrium as a function of baryon chemical potential. Dash–dotted lines: hadronic matter (BHF(N,l) [299], BHF(N,H,l) [300], RMF240 [155], χSU(3) [307]). The other lines correspond to NJL quark matter in the normal (dotted), 2SC (dashed) or CFL phase (solid), obtained with the parameter sets RKH [145] (left panels) or HK [71] (right panels). The quark–quark coupling constant was taken to be $H = G$. The results of the upper three figures on the left have been presented in a different form in Ref. [297], the two figures at the bottom have been adapted with permission from Ref. [298].

calculations presented in this work. In fact, the solid, dashed, and dotted lines are the same as the solid, dashed, and dotted lines in Fig. 6.7, although displayed on different scales. (Note that $\mu_B = 3\mu$.)

Depending on the hadronic equation of state, we find three different cases: For the BHF calculation without hyperons (BHF(N,l)) and for the χSU(3) model we find a hadron–quark phase transition for both, normal and color superconducting quark matter. Clearly, the presence of diquark condensates can lower the critical chemical potential substantially. On the other hand, the BHF calculation which includes hyperons (BHF(N,H,l)) does not cross with the quark matter equation of state up to large density, even if color superconducting phases are included. In that case there would be no phase transition to quark matter at all, at least at densities relevant for neutron stars. Finally, for the relativistic mean-field equation of state (RMF240), we find an intermediate situation where a phase transition only takes place if diquark pairing is taken into account.

In spite of these differences, the above results lead to the general observation that a hadron–quark phase transition only takes place if strange quarks play a non-negligible role in the quark–matter phase. In the normal conducting phase it only happens (if it happens at all) at relatively large chemical potentials, well above the strange quark threshold, $\mu_B^{\rm th} \simeq 1300\,\text{MeV}$. At the respective critical potentials we find about 25% strange quarks. For color superconducting quark matter we find no phase transition to the 2SC phase but only to the CFL phase. Obviously, this is related to the kink at the 2SC–CFL transition point which strongly accelerates—or even enables—the phase transition from the hadronic phase. As discussed above, this increased slope corresponds to a higher density which is mainly due to the sudden appearance of a large amount of strange quarks in the CFL phase. On the contrary, in the 2SC phase the introduction of color superconductivity practically does not change the slope of the pressure curve, but only leads to a moderate shift which can be attributed to some additional binding caused by the formation of Cooper pairs. Thus, looking at the four left panels of Fig. 7.2 there seems to be little chance for the presence of a 2SC phase in neutral strongly interacting matter. This was also our conclusion in Ref. [297].

It turns out, however, that this statement depends strongly on the vacuum constituent mass of the non-strange quarks. This is quite obvious if we neglect the binding energy. In this case, the point of zero pressure is just given by $\mu_B = 3M_u^{\rm vac}$. Hence, a reduction of $M_u^{\rm vac}$ by, say, 50 MeV would approximately shift the quark matter curves in Fig. 7.2 by 150 MeV to the left, and quark matter would become competitive to hadronic matter. (Note that the shift due to the formation of Cooper pairs in the 2SC phase is only about 25 MeV.) In fact, the authors of Ref. [278] have been able to construct a hadron–quark phase transition within a color superconducting two-flavor NJL model using a parametrization with $M^{\rm vac} = 314\,\text{MeV}$ [308]. (In that calculation the hadronic phase was described by the χSU(3) equation of state.) However, since they did not include any strange quarks in their model, it was not clear whether there still would be a window for a stable 2SC phase if one allows for a CFL phase as well.

In Ref. [298], we have studied the role of the non-strange quark mass in this context, employing—besides the parameters used above—the NJL-model parameters of Hatsuda and Kunihiro, i.e., parameter set HK of Table 3.1 [71]. With these parameters one finds $M_u^{\rm vac} = 335.5\,\text{MeV}$, instead of 367.7 MeV we had before, i.e., the reduction is rather moderate. For the quark–quark coupling constant we take again $H = G$.

The resulting pressure curves are displayed in the right panels of Fig. 7.2. As expected, the quark matter curves are shifted to lower chemical potentials, but in most cases this does not lead to a qualitative change of the behavior. The only exception is found for the χSU(3) equation of state. In this case we indeed get a phase transition into the 2SC phase before that is replaced by the CFL phase at a somewhat higher chemical potential (see Table 7.1 for details). Although the window is rather small, it could make a qualitative difference for compact stars, as we will discuss below.

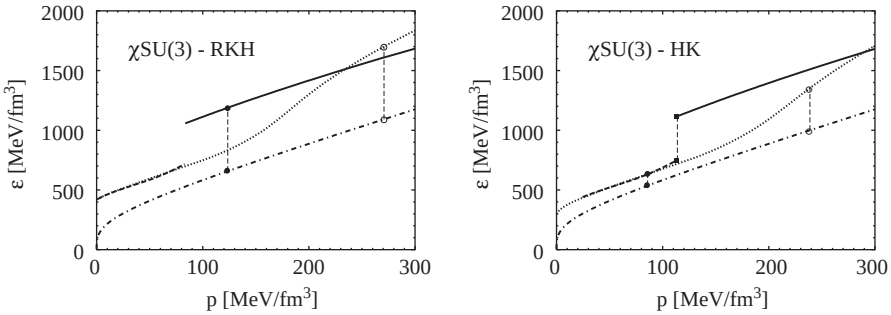

Fig. 7.3. Energy density as a function of pressure for the hadronic equation of state χSU(3) [307] (dash–dotted lines) and NJL quark matter obtained with parameter sets RKH [145] (left panel) and HK [71] (right panel) and $H = G$: normal phase (dotted), 2SC (dashed), CFL (solid). The points with the thin vertical lines indicate the positions of the phase transitions. Adapted with permission from Ref. [298].

To prepare for that discussion, let us have a look at the energy densities in the various phases. At the first-order phase boundaries the density and, hence, the energy density increase discontinuously. The corresponding values are listed in Table 7.1. As one can see there, in most cases the discontinuity is rather large. The only exception is the χSU(3)-2SC transition where the energy density is only moderately increased. This is further illustrated in Fig. 7.3 where the energy density is plotted as a function of pressure for the hadronic equation of state χSU(3) and the various quark matter phases obtained with parameter set RKH (left) and HK (right). The hadronic equation of state is again indicated by the dash–dotted lines, while the dotted, dashed, and solid lines correspond to the normal, 2SC, and CFL phase, respectively. We have also indicated the positions of the phase transitions. The open and closed circles mark the phase transition from the hadronic phase to normal or color superconducting quark matter, respectively, while the 2SC–CFL phase transition in the right panel is indicated by the squares. In the left panel, the 2SC–CFL phase transition is only "virtually" present because the hadronic phase is still favored in that region. It is nevertheless an important effect, because it pushes the energy density in the quark phase to higher values at low pressure. As a consequence, including color superconducting phases in the NJL model is qualitatively different from the behavior in a bag model. This will be discussed below.

7.1.3. Comparison with bag model studies

The effect of color superconductivity on the hadron–quark phase transition and the structure of compact stars has been discussed in Ref. [296] where the authors applied a bag model equation of state to describe the quark phase. The corresponding contribution to the pressure is given by [296]

$$p_{\mathrm{BM}}^{(\mathrm{CFL})}(\mu) = -\frac{6}{\pi^2}\int_0^{\nu} \mathrm{d}p\, p^2(p-\mu) - \frac{3}{\pi^2}\int_0^{\nu} \mathrm{d}p\, p^2(\sqrt{p^2+m_s^2}-\mu) + \frac{3\Delta^2\mu^2}{\pi^2} - B\ , \tag{7.1}$$

where

$$\nu = 2\mu - \sqrt{\mu^2 + \frac{m_s^2}{3}} \tag{7.2}$$

is the common Fermi momentum which is related to the equal number densities of the u, d, and s quarks in the CFL phase, $n_u = n_d = n_s = (\nu^3 + 2\Delta^2\mu)/\pi^2$. These expressions are based on an expansion in Δ/μ, and the masses of the up and down quarks have been neglected. Like the bag constant B, the diquark gap Δ is treated as a free parameter and is kept constant with varying μ.

Comparing Eq. (7.1) with the analogous expression for normal quark matter in a bag model, Eq. (2.12), one sees that the main effect of the gap is the extra term $3\Delta^2\mu^2/\pi^2$. It has been pointed out in Ref. [296] that, although this correction, being of order $\Delta^2\mu^2$, is formally small in comparison with the total pressure (order μ^4), it could have a strong impact on the phase transition point. This is in agreement with our NJL model results.

In the bag model the effect of the Δ^2-term may be interpreted as an effective reduction of the bag constant, $B \to B - 3\Delta^2\mu^2/\pi^2$, enhancing the pressure and reducing the energy density for a given chemical potential. In other words, the function $\epsilon(p)$ is basically shifted downwards and to the right by the diquark condensate, which both leads to a reduction of ϵ for a given p. Obviously, this is quite different in the NJL model, as one can see in Fig. 7.3. If we compare the solid line with the dotted line we see that color superconductivity *enhances* the energy density in a certain regime of pressure. The reason is again the fact that the CFL phase always contains a large amount of (relatively heavy) strange quarks which strongly contribute to the energy density, whereas normal NJL quark matter contains no or very few strange quarks up to much larger values of p.

In this context it is again useful to introduce an effective bag model parametrization of the NJL model equation of state. To that end we insert the μ dependent values of the constituent strange quark mass M_s and the average diquark gap $\Delta = \sqrt{(\Delta_2^2 + \Delta_5^2 + \Delta_7^2)/3}$ (see Fig. 6.8) into Eq. (7.1) and define an effective bag constant B_{eff} by equating the result with the pressure obtained in the NJL model. Alternatively, we may define an effective bag constant B'_{eff} in the analogous way, but using the current quark mass m_s instead of M_s.[53]

B_{eff} and B'_{eff} are displayed as function of μ_B in Fig. 7.4 (solid and dash–dotted lines, respectively). For comparison we also show the results for the normal quark phase (dotted and dashed). In all cases the effective bag constants grow with μ_B, and they are always larger in the CFL phase than in normal quark matter. Thus, although in the CFL phase the pressure is larger than in the normal phase (see Fig. 6.7), the enhancement is smaller than one would naively expect from Eq. (7.1) if B is kept constant.

For the chemical potentials corresponding to the phase transitions M_s, B_{eff} and B'_{eff} are listed in Table 7.2. These values are relatively large compared with "typical" bag model parameters which are used in the context of neutron stars, e.g., Ref. [296]. As a consequence, the energy densities are quite large as well. As we will see below, this has important implications for the structure of compact stars.

[53] As pointed out in Section 2.3.3, there is some arbitrariness in defining effective bag constants. The above definitions of B_{eff} and B'_{eff} differ from those given in Eqs. (2.68) and (2.70) by the fact that we now start from the pressure as a function of the chemical potential instead of the energy density as a function of density. This is only a matter of convenience but should not change the general picture. We repeat that we introduce effective bag constants only for the *interpretation* of our results, which are obtained in a well-defined way within the NJL model.

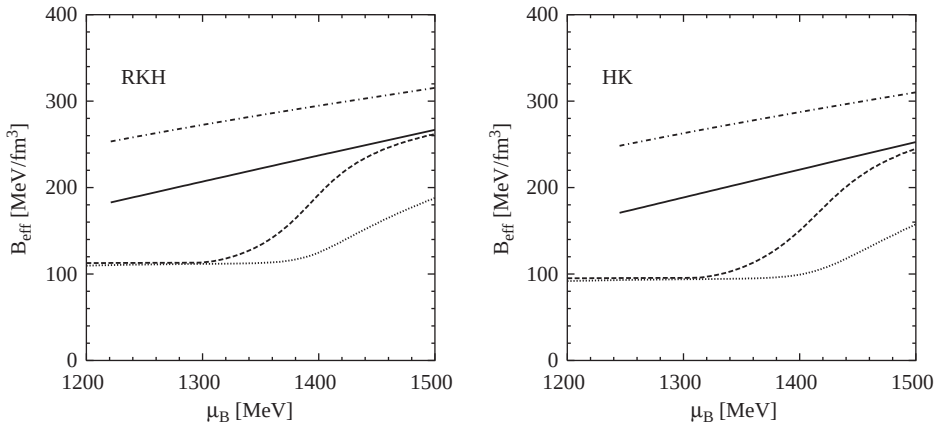

Fig. 7.4. Effective bag constants as functions of the baryon number chemical potential μ_B: $B_{\rm eff}$ (solid) and $B'_{\rm eff}$ (dash–dotted) for homogeneous neutral CFL matter, and $B_{\rm eff}$ (dotted) and $B'_{\rm eff}$ (dashed) for homogeneous neutral normal quark matter (dotted). Left: Parameter set RKH [145] with $H = G$. Right: Parameter set HK [71] with $H = G$.

Table 7.2
Average diquark gap $\Delta = \sqrt{(\Delta_2^2 + \Delta_5^2 + \Delta_7^2)/3}$, constituent strange quark mass, and effective bag constants in the strange quark matter phase at the phase transition points

Transition		Δ (MeV)	M_s (MeV)	$B_{\rm eff}$ (MeV/fm^3)	$B'_{\rm eff}$ (MeV/fm^3)
BHF(N,l) →	RKH(N)	—	283	176	254
	RKH(CFL)	115	261	211	275
	HK(N)	—	346	127	215
	HK(CFL)	114	284	182	258
RMF240 →	RKH(CFL)	120	236	236	294
	HK(CFL)	118	267	197	269
χSU(3) →	RKH(N)	—	284	175	254
	RKH(CFL)	113	271	202	269
	HK(N)	—	365	118	202
HK(2SC) →	HK(CFL)	111	292	175	252

7.2. Neutron star structure

The mass of a static compact star as a function of its radius can be obtained by solving the Tolman–Oppenheimer–Volkoff equation [309] which reads

$$\frac{\mathrm{d}p}{\mathrm{d}r} = -\frac{[p(r) + \epsilon(r)][M(r) + 4\pi r^3 p(r)]}{r[r - 2M(r)]} \,. \tag{7.3}$$

Here p and ϵ are pressure and energy density, as before, and

$$M(r) = 4\pi \int_0^r r'^2 \, \mathrm{d}r' \epsilon(r') \tag{7.4}$$

is the integrated energy inside a "sphere" of radius r (in Schwarzschild metric). We have used gravitational units, $G = c = 1$ (G gravitational constant).

The radius R and the gravitational mass M_G of the star are given by the value of r for which the pressure vanishes and the corresponding value of $M(r)$, i.e.,

$$p(R) = 0, \quad M_G = M(R) \ . \tag{7.5}$$

For a given equation of state, $\epsilon = \epsilon(p)$, Eq. (7.3) can easily be integrated numerically, starting from the center of the star and moving outwards. In this way, if one continuously varies the central pressure $p_c := p(0)$, one obtains a curve $M_G(R)$ which relates masses and radii for that equation of state. Note that stable branches of these curves have to fulfill the condition $\mathrm{d}M_G/\mathrm{d}p_c > 0$. Otherwise the solutions are unstable against small radial oscillations and collapse.

Since we are mostly interested in quark–hadron hybrid stars we restrict our analysis to those hadronic equations of state for which we have found a transition to a quark phase in Section 7.1.2. This was not the case for the microscopic equation of state with hyperons, BHF(N,H,l). Neutron star properties for this equation of state have been discussed in Ref. [300]. The authors have found a very low maximum mass, $M_G^{\max} = 1.25 M_\odot$. Hence, since neutron star masses of $1.44 M_\odot$ have been observed [310,312], it is clear that this equation of state cannot describe the whole interior of neutron stars correctly, i.e., it is probably too soft at high densities.[54]

The curves $M_G(R)$ resulting for the three other hadronic and the related hybrid equations of state are displayed in Fig. 7.5. The dash–dotted lines indicate the results for a purely hadronic star (upper line: BHF(N,l), central line: RMF240, lower line: χSU(3)). For a more realistic description of the crust, i.e., the region of subnuclear matter densities, we have employed the equations of state of Baym et al. [313] for $\rho_B < 0.001\,\mathrm{fm}^{-3}$ and of Negele and Vautherin [314] for $0.001\,\mathrm{fm}^{-3} < \rho_B < 0.08\,\mathrm{fm}^{-3}$. As typical for non-self-bound objects, large radii correspond to small gravitational masses and thus small central pressures. Therefore with increasing central pressure we have to follow the dash–dotted lines from right to left. Eventually, the central pressure is large enough that a phase transition to a quark phase takes place. The resulting $M_G(R)$ above this point are indicated by dotted lines for a transition to normal quark matter and by a solid line for a transition to quark matter in the CFL phase. As we have seen in Section 7.1.2, for the χSU(3) equation of state in combination with the HK quark equation of state (lower right panel), there is a phase transition from hadronic matter to the 2SC phase, followed by a second phase transition to the CFL phase. Here we have indicated the part of the curve which corresponds to a 2SC phase (but not yet a CFL phase) in the center of the star by a dashed line. This part of the figure is also presented in an enlarged form in Fig. 7.6.

The onset of a quark matter phase in the center of the star implies of course a deviation from the corresponding hadronic matter curve. Because of the discontinuous energy density at the phase transition point (see Table 7.1 and Fig. 7.3) this is always related to a cusp in the mass-radius relation. These cusps are clearly visible in Figs. 7.5 and 7.6. It turns out, however, that for all transitions to normal or

[54] Alternatively, this problem could in principle be cured if a phase transition to quark matter takes place before the star becomes unstable, provided the corresponding hybrid equation of state supports higher masses [118,311].

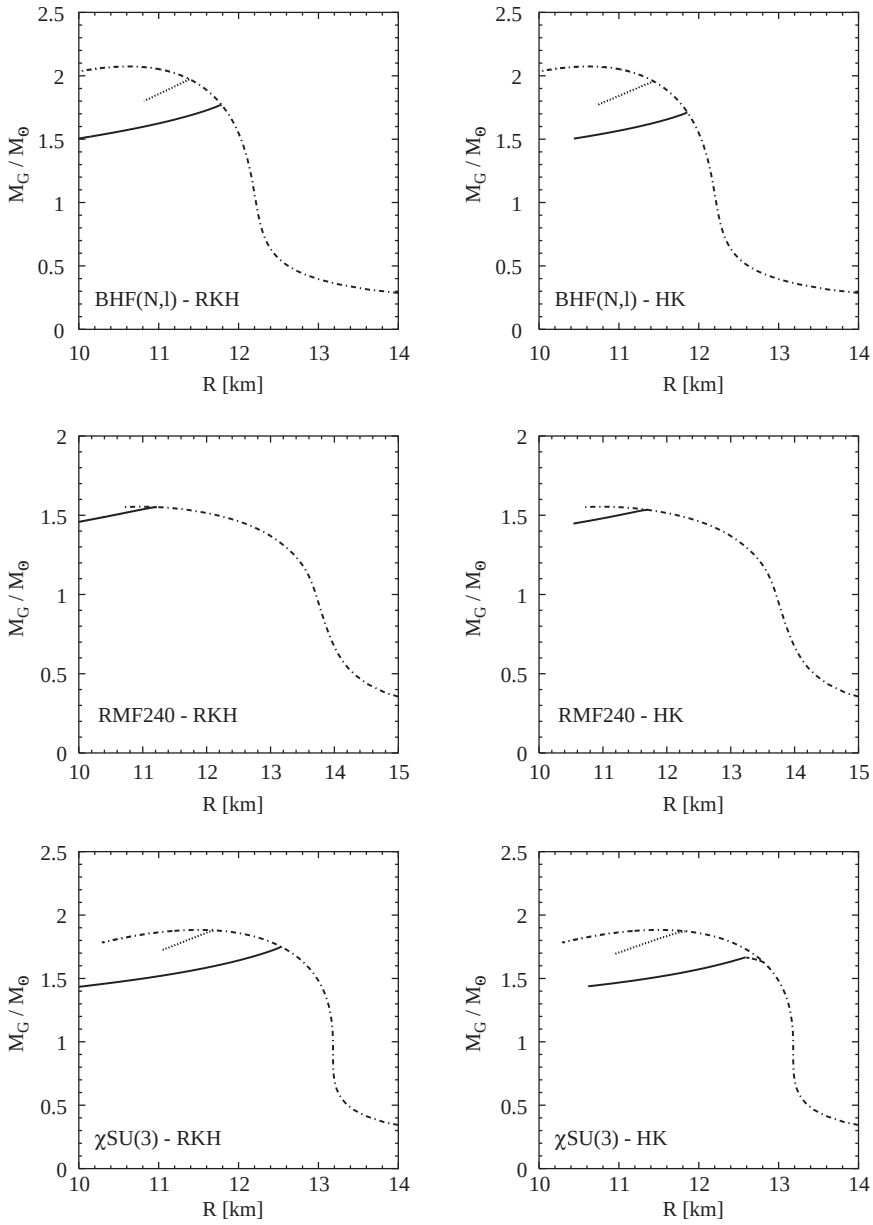

Fig. 7.5. Gravitational masses of static compact stars as functions of the radius for the different equations of state. The dash–dotted lines indicate the results for a purely hadronic star: BHF(N,l) (upper line), RMF240 (central line), χSU(3) (lower line). The other lines indicate the presence of a quark phase in the center: normal phase (dotted), 2SC dashed, CFL (solid). The quark phases in the three left panels have been calculated with parameter set RKH with $H = G$, those in the right panels with parameter set HK with $H = G$. The results of the upper two figures on the left have been presented in a different form in Ref. [297], the two figures at the bottom have been adapted with permission from Ref. [298].

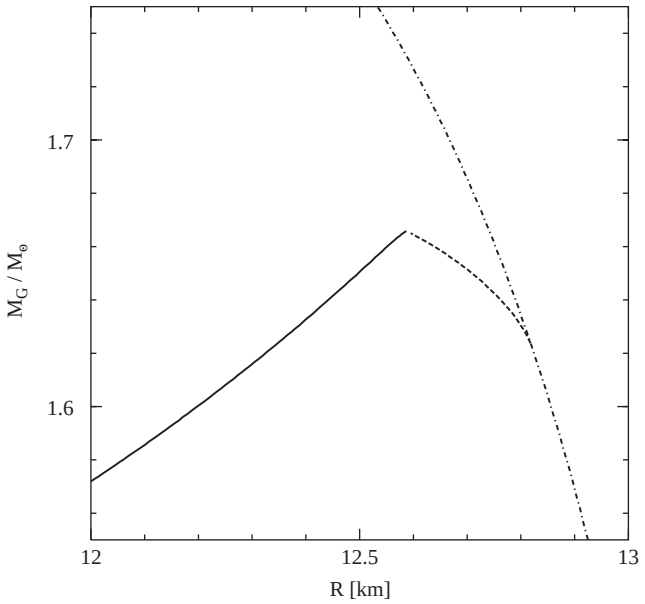

Fig. 7.6. Enlarged detail of the lower right panel of Fig. 7.5, showing the emergence of a color superconducting quark core in a compact star calculated with a χSU(3)-HK hybrid equation of state. The meaning of the various line types is the same as in Fig. 7.5. Taken with permission from Ref. [298].

to CFL quark matter the effect is so strong that the star is rendered unstable. Only in the hadron-2SC phase transition (Fig. 7.6) the star remains stable but becomes unstable at the subsequent 2SC–CFL phase transition. Hence, if the correct equation of state lies in the range covered by our model equations of state, hybrid stars, if they exist, should have a quark core in the 2SC phase and contain only a small fraction of strange quarks: There is no stable star with a CFL or a normal quark matter core. This is at amusing variance with Ref. [247] who argued that there is no 2SC phase in compact stars.

The essential question is thus, whether or not the equation of state contains an interval where the 2SC phase is favored. As we have demonstrated, the answer to this question can depend rather sensitively on the value of the non-strange constituent quark mass in vacuum. However, the overall picture which emerges from our results is that a stable 2SC phase and, hence, a stable hybrid star appear to be rather unlikely to exist. In all but one case we either found no hadron–quark phase transition at all or a transition to normal or CFL matter, and the star becomes unstable as soon as the phase transition occurs. Only if we combine the very stiff χSU(3) equation of state with the HK NJL model equation of state, hybrid stars can exist in a small mass window between 1.62 and $1.66 M_\odot$. Here we should also recall that we have chosen a relatively large quark–quark coupling constant $H = G$. With a smaller coupling, there would be less binding in the 2SC phase and eventually the window will shut. On the other hand, if we further decrease the constituent mass of the non-strange quarks, the window could become wider. Similarly, a larger constituent mass of the strange quarks would render the CFL phase less favored and thereby help stabilizing the 2SC phase. A systematic study in all these directions still remains to be done. This should also include the consideration of other color superconducting phases which have not been taken into account here (see Section 6.4).

We should also note that we cannot exclude the existence of so-called third family solutions of compact stars [315] with pure quark matter cores. This would be the case if the unstable branch "recovers" at some higher density and rises again. Looking at our solutions, there seems to be some tendency which points into this direction. Unfortunately, the densities which are necessary to decide on this interesting point cannot be reached in our model, since we would have to choose quark number chemical potentials larger than the cut-off.

In the above analysis we have assumed sharp phase transitions between homogeneous neutral phases. In the case of a mixed phase the energy density would not jump, but continuously interpolate between the hadronic and the quark solution. As a consequence, the cusps in Fig. 7.3 would be smoothed out and the instability would not occur immediately at the onset of the mixed phase. We expect, however, that in this case the star would become unstable before the mixed phase goes over into a pure quark phase if this is CFL or normal quark matter. Considering non-superconducting quark matter we thus confirm the results of Ref. [294]. Including color superconductivity in the CFL phase does not change these findings.

Since this result is relatively insensitive to the choice of the hadronic equation of state, it must mainly be attributed to the NJL-type quark equation of state. In the bag-model investigation of Ref. [296], the authors have employed a hadronic equation of state which is comparable to the BHF equation of state without hyperons. For a bag constant $B = 137\,\mathrm{MeV/fm^3}$ and a strange quark mass $M_s = 200\,\mathrm{MeV}$ they found that a star with a pure quark core is unstable without color superconductivity, but stable if a (CFL) diquark gap of 100 MeV is chosen. If we compare the above numbers with the effective quantities listed in Table 7.2, we see that the essential differences are again the relatively large values of the strange quark mass and of the effective bag constant in the NJL model. Therefore the energy densities just above the phase transition are considerably larger in the NJL model than in the bag model, and this is finally responsible for the instability.[55]

As pointed out many times before, our results rely on the assumption that the NJL model parameters which have been fitted in vacuum can be applied to dense matter. It is of course possible that this is not the case. Thus our arguments could also be turned around: If there were strong hints, e.g. for the existence of a pure CFL quark core in compact stars, this would indicate a considerable modification of the effective NJL-type quark interactions in dense matter. This observation could then be used to constrain the parameters (provided the hadronic part is sufficiently well under control).

But even if there are no quark cores in compact stars and hence no natural laboratories for color superconducting phases, the properties of these phases can nevertheless influence the maximum mass of neutron stars, as evident from Fig. 7.5. The corresponding maximum masses are also listed in Table 7.3. Since the quark effects are larger if the phase transition occurs long before the would-be maximum mass of a purely hadronic equation of state is reached, the results become less sensitive to the hadronic equation of state if quarks and in particular the effects of color superconductivity are included: Whereas for the purely hadronic equations of state, we find $M_G^{\max}$ between 1.55 and 2.07 solar masses, our results scatter only between 1.53 and 1.77 solar masses if color superconducting quark matter is included. In particular, the inclusion of color superconducting quark matter keeps the neutron star maximum mass well below two solar masses, independently of details of the hadronic equation of state. Hence, the observation of

[55] The authors of Ref. [296] have also taken into account contributions of the "pseudo"-Goldstone bosons of the broken chiral symmetry to the thermodynamic potential in the CFL phase. However, since in neutral CFL matter the electric charge chemical potential vanishes, no charged bosons are excited, while the contributions of a possible K_0-condensate are small [296].

Table 7.3
Maximum gravitational mass $M_G^{\max}$ (in terms of solar masses $M_\odot$) for a purely hadronic equation of state and for hybrid equations of state with phase transitions to normal or color superconducting (cs) quark matter

Equations of state	Hadronic	hadr. + normal	hadr. + cs
BHF(N,l), RKH	2.07	1.97	1.77
BHF(N,l), HK		1.96	1.71
RMF240, RKH	1.55	—	1.55
RMF240, HK		—	1.53
χSU(3), RKH	1.88	1.88	1.75
χSU(3), HK		1.87	1.66

a neutron star with a mass well above two solar masses would seriously question our NJL-type description of the quark matter phase, using parameters which are fixed in vacuum.

8. Summary and discussion

In this report we have explored the properties of deconfined quark matter, focusing on the regime of low temperatures and "moderate" densities, which cannot be accessed by perturbative or present-day lattice calculations. Main issue was the investigation of color-superconducting phases and the influence of dynamically generated effective quark masses on these phases. To that end we employed NJL-type models, where both, diquark pairing and dynamical mass generation, can be treated on the same footing. This turned out to be crucial, in particular for the understanding of the transition from two-flavor (2SC) to three-flavor (CFL) color superconductors. We found that this transition is basically triggered by a strong discontinuous drop of the effective strange quark mass which has its roots in the corresponding chiral phase transition.

To work this out more clearly, we started with a detailed study of the chiral phase transition for color non-superconducting quark matter. A central point was the comparison of the NJL model with the MIT bag model, which is the most commonly used model to describe the equation of state of deconfined quark matter. In the NJL model, the bag constant arises dynamically as a consequence of spontaneous chiral symmetry breaking. Whereas for vanishing quark masses (and zero temperature) the two models behave almost identically, differences arise when finite current quark masses are introduced. Naturally, these effects become more pronounced in the three-flavor case. Here we found that both, the effective strange quark mass and the effective bag constant, are density dependent quantities which are large compared with "typical" bag model parameters. One important consequence is that the model does not support the hypothesis of absolutely stable strange quark matter, as long as the model parameters do not differ drastically from a vacuum fit.

As pointed out above, the consideration of dynamical quark masses remains crucial when we turn to color superconducting phases. We also analyzed a spin-1 diquark condensate as a possible pairing channel for those quarks which are left over from the standard spin-0 condensate in the 2SC phase. Another important question was the effect of neutrality constraints, which must be imposed, e.g., to

describe possible quark matter cores of neutron stars. Generally, these constraints tend to disfavor the 2SC phase. Nevertheless, whereas estimates based on the assumption of small strange quark masses predict that the 2SC phase is never the most favored neutral phase, NJL model calculations reveal that large values of M_s could again stabilize the 2SC solution. In this context we have also investigated the possibility of electrically and color neutral mixed phases. Neglecting Coulomb and surface effects we found a rich structure of mixed phases with up to four components. The gain in bulk free energy is, however, quite small. It is therefore unclear whether the mixed phases survive if surface and Coulomb effects are included.

Finally, we applied the NJL model to study the possibility of color superconducting quark matter cores in neutron stars. To that end, we combined different hadronic equations of state with the NJL model ones to construct a sharp hadron–quark phase transition. The resulting hybrid equations of state have then been employed in a Tolman–Oppenheimer–Volkoff equation. In most cases we found a phase transition from hadronic matter to the CFL phase. It turned out that in these cases the energy density in the quark phase is too large to support a stable star with a quark matter core. This result could again be traced back to the large effective strange quark masses. So far we found a single example where the hadron–quark phase transition went to the 2SC phase. In this case a stable quark matter core was possible. However, a more systematic investigation of the parameter dependence of these results still needs to be done.

In fact, for all topics we discussed in this work, there are details which deserve further investigation. Many of them have been discussed in the corresponding sections and will not be repeated here. In the following we concentrate on the major questions.

Presumably, the most severe limitation of our analysis is the problem of parameter fixing, which has been addressed in Section 4.2 and several other places. At present, there is practically no other way than relying on vacuum fits, which could be a rather bad assumption at large densities. Therefore, most of our analysis must primarily be taken as qualitative hints, e.g., about the role of the strange quark mass or the effect of neutrality constraints. In this situation, further improvements on the more fundamental side, allowing to evolve the weak-coupling approaches down to lower densities, are highly desirable. To some extent we may also hope to learn something about the interaction by comparing our predictions with observational facts. Unfortunately, since so far most of the predictions are negative ones, e.g., the non-existence of strange quark matter or CFL matter cores in neutron stars, this can at best be a falsification. This underlines ones more the necessity to work out more phenomenological details. For instance data on neutron star cooling could provide severe constraints on the minimal pairing gaps in a possible quark–matter core [316].

Returning to Fig. 1.1 in the Introduction, we note that we have mostly elaborated on the phases shown in the upper right diagram (plus some extra phases which might appear if we add further axes to the diagram, see Fig. 6.3). On the other hand, phases like the CFL+K phase or crystalline phases, suggested in the two lower phase diagrams of Fig. 1.1, have not yet been studied in the framework of NJL-type models. As pointed out in Section 6.4, this could be interesting, since μ-dependent quark masses could have important effects on these phases as well. The description of crystalline phases is probably more difficult, whereas in order to study CFL+K (or more general CFL+Goldstone) phases one only has to add further condensates with the corresponding quantum numbers.

In general, the role and the properties of Goldstone bosons in the various color superconducting phases should be worked out in more detail. On the RPA-level, the Goldstone bosons can be constructed generalizing the Bethe–Salpeter equation shown in Fig. 2.4 to Nambu–Gorkov space. Because of baryon

number non-conservation, mesons and diquarks can mix. This is formally described by the presence of off-diagonal Nambu–Gorkov components.[56]

A theoretically interesting case is the anisotropic spin-1 condensate discussed in Section 4.4. Since general arguments predict rather different Goldstone spectra for $M_J = 0$ and for $M_J = \pm 1$ [238,239] it would be instructive to see how this comes about by explicit calculation. In this context it is interesting to note that quite recently, an abnormal number of Goldstone modes has also been reported for the case of the usual scalar diquark condensate in a two-flavor NJL model [318]. Although an academic example (since these modes correspond to the spontaneously broken *global* $SU(3)_c$ of the NJL model whereas in QCD, they are "eaten" by the gluons), it nicely illustrates that the counting of Goldstone bosons becomes highly non-trivial in Lorentz-non-invariant systems [234].

The Goldstone spectrum arising from chiral symmetry breaking in the CFL phase has been determined in leading-order QCD at asymptotic densities [280,319]. The most interesting features are that the excitations have reversed mass ordering (i.e., $m_K < m_\pi$) and are very light. For instance, if one extrapolates the resulting expressions down to "moderate" chemical potentials, $\mu \sim 500\,\mathrm{MeV}$, one typically finds $m_K \sim 15\,\mathrm{MeV}$. These small masses are a consequence of the fact that the symmetry breaking terms in the corresponding effective Lagrangian must be quadratic, rather than linear, in the quark masses in order to be consistent with the Z_{2A} symmetry of the CFL phase [16]. As discussed in Eq. (5.7) the latter is a residual part of the $U_A(1)$ symmetry which is not explicitly broken at asymptotic energies where instanton effects vanish. It would be interesting to compare these results with an NJL-model calculation with "realistic" parameters. In particular, the effects of non-vanishing $\langle\bar{q}q\rangle$ condensates and of $U_A(1)$ breaking terms ('t Hooft interaction) should be analyzed.

A partially related problem is the question whether the BCS mean-field approach we have used throughout this work is appropriate to describe quark matter at "moderate" densities. It is well known that BCS theory is a weak-coupling theory which works best if the correlation length ξ_c is much larger than the average distance d between the fermions. In this case many Cooper pairs—which are only temporary correlations between changing partners—overlap each other and phase fluctuations average away. On the other hand, for $\xi_c/d \ll 1$, the system is better described as a Bose–Einstein condensate, consisting of strongly coupled pairs with fixed partners.[57] The transition region is more difficult to describe. However, it is known from metallic superconductors that deviations from BCS behavior, e.g., in the relation between T_c and the gap at $T = 0$ (Eq. (4.94)), are visible already if ξ_c/d becomes smaller than about 100.

In Ref. [320], ξ_c/d has been studied for a two-flavor color superconductor within a QCD-like model. This model basically corresponds to solving a Dyson–Schwinger equation of the weak-coupling type, Eq. (4.14), but with a running coupling constant which has been modified to regulate the low-momentum behavior. Keeping the momentum dependence of the gap, the authors analyzed the spatial structure of the Cooper pairs via a Fourier transform and calculated the coherence length. The result was that ξ_c/d

[56] A similar but technically simpler issue are possible precursor effects of color superconductivity at temperatures *above* T_c, which have been described in Ref. [317]. Employing an NJL-type model, the authors calculated the spectral function in the scalar color-antitriplet diquark channel and monitored its behavior when the temperature approaches T_c from above. At T_c both, mass and width, of this mode go to zero but already at $T \simeq 1.2T_c$ the authors find a relatively sharp low-lying peak which indicates precritical fluctuations. The authors suggest that this could have observable effects in heavy-ion collisions.

[57] We are in not necessarily restricted to pair correlations. For instance, one might think of superfluid nuclear matter as three quarks strongly coupled to a nucleon, which is then Cooper paired with a second three-quark cluster. It is possible that similar correlations still exist above the deconfinement phase transition. From this point of view it might be worthwhile to revisit the idea of a six-quark condensate which has been suggested long ago by Barrois [7].

drops below 10 for $\mu < 1\,\mathrm{GeV}$. Since in our NJL-model approach the gaps are momentum independent we cannot perform the same kind of analysis. However, as a rule of thumb we may identify the coherence length with the inverse of the gap, $\xi_c \sim 1/\Delta$. Inserting typical numbers one finds ξ_c/d of the order 2 to 3 at $\mu = 500\,\mathrm{MeV}$, which clearly calls into question the applicability of the BCS treatment.

It should be noted that the analogous estimate applied to the vacuum gap equation looks even more worrisome. If we identify the constituent quark mass with $1/\xi_c$ and the quark condensate with a density, we get $\xi_c/d \sim |\langle\bar{q}q\rangle|^{1/3}/M \lesssim 1$. In fact, it has been argued some time ago that chiral symmetry is *not* broken in the NJL model because of strong phase fluctuations due to pionic modes [321]. This point has subsequently been studied by various authors, explicitly taking into account meson loops, e.g., via a $1/N_c$ expansion. It was found that meson-loop effects could be large but do not necessarily restore chiral symmetry [129,322,323]. (Similar conclusions have been drawn in Refs. [324–326] within different approaches.) However, as discussed in Section 2.3.5, the importance of the meson loops is in general controlled by a new cut-off parameter which has to be introduced because of the non-renormalizability of the NJL model. Therefore no definite statement can be made without fixing this parameter [322].

This analogy tells us that fluctuation effects could be, but do not need to be dangerous for the phases we have discussed in this report. In this context it is interesting to see that recent lattice studies of the NJL model at finite chemical potential find non-vanishing diquark condensates which are in rather good agreement with the corresponding large-N_c limit [327]. Also, NJL-model results seem to be in good agreement with lattice QCD for $N_c = 2$ [328], which is accessible by standard methods even at $\mu \neq 0$. On the other hand, an explicit investigation of fluctuation effects within the (continuum) NJL model does not seem to be a rewarding effort.

Here we have more or less reached the limits of the model. After all, NJL-type models are schematic models which are motivated to major extent by their simplicity. They become questionable when the merits of the simplified interaction get lost by using highly complicated approximation schemes. In that case one should think about other approaches. To study fluctuation effects, Lagrangians with bosonic degrees of freedom, like the effective Lagrangians mentioned in Section 6.4, are probably more appropriate. Of course, final answers must come from QCD or—if available—from empirical observations, but model calculations may help to bring the ideas on the right track.

Acknowledgements

Most of the work reported here has been performed at the Institut für Kernphysik at the TU Darmstadt. I would like to thank the entire theory group for a stimulating atmosphere and in particular Jochen Wambach for constant support and encouragement. I also acknowledge financial support by GSI Darmstadt between 2001 and 2003. Early roots go back to my time at the State University of New York in Stony Brook, and I would like to thank Gerry Brown and the Alexander von Humboldt Foundation for support. The final write-up of the report has been completed while I was participating in the INT program on “QCD and Dense Matter: From Lattices to Stars” (INT-04-1) in Seattle.

I am most indebted to my long-term collaborator Micaela Oertel who has actively contributed to most topics discussed in this work. I am also grateful to her and to Bernd-Jochen Schaefer for carefully reading the manuscript.

It was a great pleasure for me to collaborate with Jiří Hošek who taught me the basics of color superconductivity and always opened my mind for new ideas. I also thank him for his repeated hospitality in Prague.

Work related to neutron stars has been performed in collaboration with Marcello Baldo, Fiorella Burgio, and Hans-Josef Schulze. I thank them for their repeated hospitality in Catania and for providing me with the data of their equations of state [299,300]. I also thank Matthias Hanauske and Detlev Zschiesche for supplying me with the data of their equation of state [307].

I also would like to thank Martin Frank and especially Frederik Neumann for fruitful collaborations. Part of the present work has overlap with their diploma theses.

I have benefitted a lot from various workshops, where I had illuminating discussions with Mark Alford, Burkhard Kämpfer, Daniel Litim, Maria-Paola Lombardo, Krishna Rajagopal, Georges Ripka, Dirk Rischke, Sanjay Reddy, Thomas Schäfer, Jürgen Schaffner-Bielich, Igor Shovkovy, and Edward Shuryak. In this context I would like to thank ECT* in Trento, INT in Seattle, and KITP in Santa Barbara for financial support. I also acknowledge stimulating discussions during the weekly meetings of the Frankfurt-Darmstadt Color Superconductivity Group of the Virtual Institute for Dense Hadronic Matter and QCD Phase Transitions by the Helmholtz Association.

Special thanks go to David Blaschke for many stimulating discussions and his hospitality at various places.

Useful discussions with Zoheir Aouissat, Peter Braun-Munzinger, Bengt Friman, Axel Maas, Ralf Rapp, Robert Roth, Bernd-Jochen Schaefer, Michael Urban, Jochen Wambach, Verena Werth, and Andreas Wirzba are also gratefully acknowledged.

I also would like to thank Norbert Grewe for illuminating discussions and for providing me with his lecture notes on superconductivity.

Finally, I thank Carsten Isselhorst, Alexander Mai, and especially Thomas Roth for their help with computer related problems.

Appendix A. Fierz transformations

A.1. General aim

We consider a local four-point interaction of the form

$$\mathscr{L}_{\rm int} = g_I(\bar{q}\hat{\Gamma}^{(I)}q)^2 = g_I\Gamma^{(I)}_{ij}\Gamma^{(I)}_{kl}\bar{q}_i q_j \bar{q}_k q_l \ . \tag{A.1}$$

Taking into account the anticommutation rules for fermions, this leads to the identities

$$\mathscr{L}_{\rm int} = -g_I\Gamma^{(I)}_{ij}\Gamma^{(I)}_{kl}\bar{q}_i q_l \bar{q}_k q_j =: \mathscr{L}_{\rm ex} \tag{A.2}$$

and

$$\mathscr{L}_{\rm int} = g_I\Gamma^{(I)}_{ij}\Gamma^{(I)}_{kl}\bar{q}_i \bar{q}_k q_l q_j =: \mathscr{L}_{qq} \ . \tag{A.3}$$

So far, $\mathscr{L}_{\rm int} = \mathscr{L}_{\rm ex} = \mathscr{L}_{qq}$. However, if we restrict ourselves to Hartree-type approximations where the first field is contracted with the second, and the third one with the fourth, $\mathscr{L}_{\rm ex}$ yields the exchange diagrams (Fock terms) of $\mathscr{L}_{\rm int}$ while $\mathscr{L}_{qq}$ yields the particle-particle and antiparticle–antiparticle contributions. To that end we wish to rewrite the operators as

$$\Gamma^{(I)}_{ij}\Gamma^{(I)}_{kl} = \sum_M c^I_M \Gamma^{(M)}_{il}\Gamma^{(M)}_{kj} \tag{A.4}$$

to get

$$\mathscr{L}_{\rm ex} = -g_I \sum_M c_M^I (\bar{q}\hat{\Gamma}^{(M)} q)^2 \ . \tag{A.5}$$

Combining this with the Hartree Lagrangian $\mathscr{L}_{\rm dir} \equiv \mathscr{L}_{\rm int}$ we get for the total effective quark–antiquark interaction

$$\mathscr{L}_{q\bar{q}} = \mathscr{L}_{\rm dir} + \mathscr{L}_{\rm ex} = \sum_M G_M (\bar{q}\hat{\Gamma}^{(M)} q)^2 \tag{A.6}$$

with $G_M = c_M^I g_I$ for $M \neq I$ and $G_I = (1 - c_I^I) g_I$.

In the same way one can employ

$$\Gamma_{ij}^{(I)} \Gamma_{kl}^{(I)} = \sum_D {\rm d}_D^I (\hat{\Gamma}^{(D)} C)_{ik} (C\hat{\Gamma}^{(D)})_{lj} \ , \tag{A.7}$$

to write the quark–quark interaction as

$$\mathscr{L}_{qq} = \sum_D H_D (\bar{q}\hat{\Gamma}^{(D)} C \bar{q}^{\rm T})(q^{\rm T} C \hat{\Gamma}^{(D)} q) \tag{A.8}$$

with $H_D = {\rm d}_D^I g_I$.

By construction, $\mathscr{L}_{q\bar{q}}$ and $\mathscr{L}_{qq}$ are to be used in Hartree approximation only, to avoid double counting.

A.2. Fierz identities for local four-point operators

In this section we list the coefficients c_M^I and d_D^I defined in Eqs. (A.4) and (A.7) for various operators.

A.2.1. Operators in Dirac space

(a) *Quark–antiquark channel (exchange diagrams)*:

$$\begin{pmatrix} (\mathbb{1})_{ij}(\mathbb{1})_{kl} \\ ({\rm i}\gamma_5)_{ij}({\rm i}\gamma_5)_{kl} \\ (\gamma^\mu)_{ij}(\gamma_\mu)_{kl} \\ (\gamma^\mu\gamma_5)_{ij}(\gamma_\mu\gamma_5)_{kl} \\ (\sigma^{\mu\nu})_{ij}(\sigma_{\mu\nu})_{kl} \end{pmatrix} = \begin{pmatrix} \frac{1}{4} & -\frac{1}{4} & \frac{1}{4} & -\frac{1}{4} & \frac{1}{8} \\ -\frac{1}{4} & \frac{1}{4} & \frac{1}{4} & -\frac{1}{4} & -\frac{1}{8} \\ 1 & 1 & -\frac{1}{2} & -\frac{1}{2} & 0 \\ -1 & -1 & -\frac{1}{2} & -\frac{1}{2} & 0 \\ 3 & -3 & 0 & 0 & -\frac{1}{2} \end{pmatrix} \begin{pmatrix} (\mathbb{1})_{il}(\mathbb{1})_{kj} \\ ({\rm i}\gamma_5)_{il}({\rm i}\gamma_5)_{kj} \\ (\gamma^\mu)_{il}(\gamma_\mu)_{kj} \\ (\gamma^\mu\gamma_5)_{il}(\gamma_\mu\gamma_5)_{kj} \\ (\sigma^{\mu\nu})_{il}(\sigma_{\mu\nu})_{kj} \end{pmatrix} \ , \tag{A.9}$$

$$\begin{aligned} (\gamma^0)_{ij}(\gamma^0)_{kl} = \tfrac{1}{4}\{ & (\mathbb{1})_{il}(\mathbb{1})_{kj} + ({\rm i}\gamma_5)_{il}({\rm i}\gamma_5)_{kj} \\ & + (\gamma^0)_{il}(\gamma^0)_{kj} - (\gamma^m)_{il}(\gamma_m)_{kj} + (\gamma^0\gamma_5)_{il}(\gamma^0\gamma_5)_{kj} - (\gamma^m\gamma_5)_{il}(\gamma_m\gamma_5)_{kj} \\ & - (\sigma^{0n})_{il}(\sigma_{0n})_{kj} + \tfrac{1}{2}(\sigma^{mn})_{il}(\sigma_{mn})_{kj}\} \ . \end{aligned} \tag{A.10}$$

(b) *Quark–quark channel*

$$\begin{pmatrix} (\mathbb{1})_{ij}(\mathbb{1})_{kl} \\ (\mathrm{i}\gamma_5)_{ij}(\mathrm{i}\gamma_5)_{kl} \\ (\gamma^\mu)_{ij}(\gamma_\mu)_{kl} \\ (\gamma^\mu\gamma_5)_{ij}(\gamma_\mu\gamma_5)_{kl} \\ (\sigma^{\mu\nu})_{ij}(\sigma_{\mu\nu})_{kl} \end{pmatrix} = \begin{pmatrix} \frac{1}{4} & -\frac{1}{4} & \frac{1}{4} & -\frac{1}{4} & -\frac{1}{8} \\ -\frac{1}{4} & \frac{1}{4} & \frac{1}{4} & -\frac{1}{4} & \frac{1}{8} \\ 1 & 1 & -\frac{1}{2} & -\frac{1}{2} & 0 \\ 1 & 1 & \frac{1}{2} & \frac{1}{2} & 0 \\ -3 & 3 & 0 & 0 & -\frac{1}{2} \end{pmatrix} \begin{pmatrix} (\mathrm{i}\gamma_5 C)_{ik}(C\mathrm{i}\gamma_5)_{lj} \\ (C)_{ik}(C)_{lj} \\ (\gamma^\mu\gamma_5 C)_{ik}(C\gamma_\mu\gamma_5)_{lj} \\ (\gamma^\mu C)_{ik}(C\gamma_\mu)_{lj} \\ (\sigma^{\mu\nu}C)_{ik}(C\sigma_{\mu\nu})_{lj} \end{pmatrix} , \tag{A.11}$$

$$\begin{aligned} (\gamma^0)_{ij}(\gamma^0)_{kl} = \tfrac{1}{4}\{&(\mathrm{i}\gamma_5 C)_{ik}(C\mathrm{i}\gamma_5)_{lj} + (C)_{ik}(C)_{lj} \\ &+ (\gamma^0\gamma_5 C)_{ik}(C\gamma^0\gamma_5)_{lj} - (\gamma^m\gamma_5 C)_{ik}(C\gamma_m\gamma_5)_{lj} \\ &+ (\gamma^0 C)_{ik}(C\gamma^0)_{lj} - (\gamma^m C)_{ik}(C\gamma_m)_{lj} \\ &- (\sigma^{0n}C)_{ik}(C\sigma_{0n})_{lj} + \tfrac{1}{2}(\sigma^{mn}C)_{ik}(C\sigma_{mn})_{lj}\} . \end{aligned} \tag{A.12}$$

A.2.2. Generators of $U(N)$

We use the following notation:
τ_a, $a = 1, \ldots, N^2-1$: generators of $SU(N)$, normalized as $\mathrm{Tr}[\tau_a\tau_b] = 2\delta_{ab}$,
$\mathbb{1}$: $N \times N$ unit matrix, $\tau_0 = \sqrt{2/N}\mathbb{1}$,
τ_S: symmetric generators (including τ_0), τ_A: antisymmetric generators.
(a) *Quark–antiquark channel (exchange diagrams)*:

$$\begin{pmatrix} (\mathbb{1})_{ij}(\mathbb{1})_{kl} \\ (\tau_a)_{ij}(\tau_a)_{kl} \end{pmatrix} = \begin{pmatrix} \dfrac{1}{N} & \dfrac{1}{2} \\ 2\dfrac{N^2-1}{N^2} & -\dfrac{1}{N} \end{pmatrix} \begin{pmatrix} (\mathbb{1})_{il}(\mathbb{1})_{kj} \\ (\tau_a)_{il}(\tau_a)_{kj} \end{pmatrix} . \tag{A.13}$$

(b) *Quark–quark channel*:

$$\begin{pmatrix} (\mathbb{1})_{ij}(\mathbb{1})_{kl} \\ (\tau_a)_{ij}(\tau_a)_{kl} \end{pmatrix} = \begin{pmatrix} \dfrac{1}{2} & \dfrac{1}{2} \\ \dfrac{N-1}{N} & -\dfrac{N+1}{N} \end{pmatrix} \begin{pmatrix} (\tau_S)_{ik}(\tau_S)_{lj} \\ (\tau_A)_{ik}(\tau_A)_{lj} \end{pmatrix} . \tag{A.14}$$

A.3. Specific examples

In the following, τ_a and λ_a denote operators in $SU(N_f)$ flavor space or $SU(N_c)$ color space, respectively. Repeated indices are summed over. Flavor or color indices run from 1 to $N_{f,c}^2 - 1$, unless explicitly stated otherwise. For Dirac indices $(a^\mu)^2 \equiv a^\mu a_\mu$, etc.

A.3.1. Color current interaction

(a) Lorentz-invariant interaction:

$$\mathscr{L}_{\mathrm{int}} = -g(\bar{q}\gamma^\mu\lambda_a q)^2 , \tag{A.15}$$

$$
\begin{aligned}
\Rightarrow \mathscr{L}_{\rm ex} = {} & \frac{2(N_c^2-1)}{N_f N_c^2}\, g \left[(\bar{q}q)^2 + (\bar{q}\mathrm{i}\gamma_5 q)^2 - \frac{1}{2}(\bar{q}\gamma^\mu q)^2 - \frac{1}{2}(\bar{q}\gamma^\mu\gamma_5 q)^2 \right] \\
& + \frac{(N_c^2-1)}{N_c^2}\, g \left[(\bar{q}\tau_a q)^2 + (\bar{q}\mathrm{i}\gamma_5\tau_a q)^2 - \frac{1}{2}(\bar{q}\gamma^\mu\tau_a q)^2 - \frac{1}{2}(\bar{q}\gamma^\mu\gamma_5\tau_a q)^2 \right] \\
& - \frac{1}{N_f N_c}\, g \left[(\bar{q}\lambda_a q)^2 + (\bar{q}\mathrm{i}\gamma_5\lambda_a q)^2 - \frac{1}{2}(\bar{q}\gamma^\mu\lambda_a q)^2 - \frac{1}{2}(\bar{q}\gamma^\mu\gamma_5\lambda_a q)^2 \right] \\
& - \frac{1}{2N_c}\, g \left[(\bar{q}\tau_a\lambda_{a'} q)^2 + (\bar{q}\mathrm{i}\gamma_5\tau_a\lambda_{a'} q)^2 - \frac{1}{2}(\bar{q}\gamma^\mu\tau_a\lambda_{a'} q)^2 - \frac{1}{2}(\bar{q}\gamma^\mu\gamma_5\tau_a\lambda_{a'} q)^2 \right] \\
= {} & \frac{(N_c^2-1)}{N_c^2}\, g \sum_{a=0}^{N_f^2-1} \left[(\bar{q}\tau_a q)^2 + (\bar{q}\mathrm{i}\gamma_5\tau_a q)^2 - \frac{1}{2}(\bar{q}\gamma^\mu\tau_a q)^2 - \frac{1}{2}(\bar{q}\gamma^\mu\gamma_5\tau_a q)^2 \right] \\
& - \frac{1}{2N_c}\, g \sum_{a=0}^{N_f^2-1} \left[(\bar{q}\tau_a\lambda_{a'} q)^2 + (\bar{q}\mathrm{i}\gamma_5\tau_a\lambda_{a'} q)^2 - \frac{1}{2}(\bar{q}\gamma^\mu\tau_a\lambda_{a'} q)^2 - \frac{1}{2}(\bar{q}\gamma^\mu\gamma_5\tau_a\lambda_{a'} q)^2 \right] ,
\end{aligned}
\tag{A.16}
$$

$$
\begin{aligned}
\mathscr{L}_{qq} = {} & \frac{N_c+1}{2N_c}\, g \Big[(\bar{q}\mathrm{i}\gamma_5 C\tau_A\lambda_{A'}\bar{q}^{\rm T})(q^{\rm T}C\mathrm{i}\gamma_5\tau_A\lambda_{A'}q) + (\bar{q}C\tau_A\lambda_{A'}\bar{q}^{\rm T})(q^{\rm T}C\tau_A\lambda_{A'}q) \\
& - \frac{1}{2}(\bar{q}\gamma^\mu\gamma_5 C\tau_A\lambda_{A'}\bar{q}^{\rm T})(q^{\rm T}C\gamma_\mu\gamma_5\tau_A\lambda_{A'}q) - \frac{1}{2}(\bar{q}\gamma^\mu C\tau_S\lambda_{A'}\bar{q}^{\rm T})(q^{\rm T}C\gamma_\mu\tau_S\lambda_{A'}q) \Big] \\
& - \frac{N_c-1}{2N_c}\, g \Big[(\bar{q}\mathrm{i}\gamma_5 C\tau_S\lambda_{S'}\bar{q}^{\rm T})(q^{\rm T}C\mathrm{i}\gamma_5\tau_S\lambda_{S'}q) + (\bar{q}C\tau_S\lambda_{S'}\bar{q}^{\rm T})(q^{\rm T}C\tau_S\lambda_{S'}q) \\
& - \frac{1}{2}(\bar{q}\gamma^\mu\gamma_5 C\tau_S\lambda_{S'}\bar{q}^{\rm T})(q^{\rm T}C\gamma_\mu\gamma_5\tau_S\lambda_{S'}q) - \frac{1}{2}(\bar{q}\gamma^\mu C\tau_A\lambda_{S'}\bar{q}^{\rm T})(q^{\rm T}C\gamma_\mu\tau_A\lambda_{S'}q) \Big] .
\end{aligned}
\tag{A.17}
$$

In particular, we have

$$
G := \mathrm{coeff}((\bar{q}\tau_a q)^2) = \frac{(N_c^2-1)}{N_c^2}\, g , \tag{A.18}
$$

$$
H := \mathrm{coeff}((\bar{q}\mathrm{i}\gamma_5 C\tau_A\lambda_{A'}\bar{q}^{\rm T})(q^{\rm T}C\mathrm{i}\gamma_5\tau_A\lambda_{A'}q)) = \frac{N_c+1}{2N_c}\, g \tag{A.19}
$$

and thus

$$
H : G = \frac{N_c}{2(N_c-1)} = \frac{3}{4} , \tag{A.20}
$$

where the last equality holds for $N_c = 3$.

(b) Electric and magnetic gluon exchange:

$$
\mathscr{L}_{\rm int} = -g_{\rm E}(\bar{q}\gamma^0\lambda_a q)^2 + g_{\rm M}(\bar{q}\vec{\gamma}\lambda_a q)^2 . \tag{A.21}
$$

We want to derive to derive the six effective coupling constants of Eq. (4.68).

To this end, we first consider electric gluons only:

$$\mathscr{L}_{\rm int}^{\rm (E)} = -g_{\rm E}(\bar{q}\hat{\gamma}^0\lambda_a q)^2 \tag{A.22}$$

$$\Rightarrow \quad \mathscr{L}_{\rm ex}^{\rm (E)} = \frac{2(N_c^2-1)}{N_f N_c^2}\, g_{\rm E}\left[\frac{1}{4}(\bar{q}q)^2 + \frac{1}{4}(\bar{q}\gamma^0 q)^2 + \cdots\right] - \frac{1}{N_f N_c}\, g_{\rm E}\left[\frac{1}{4}(\bar{q}\lambda_a q)^2 + \frac{1}{4}(\bar{q}\gamma^0\lambda_a q)^2 + \cdots\right] + \cdots\,, \tag{A.23}$$

$$\mathscr{L}_{qq}^{\rm (E)} = \frac{N_c+1}{2N_c}\, g_{\rm E}\left[\frac{1}{4}(\bar{q}\mathrm{i}\gamma_5 C\tau_A\lambda_{A'}\bar{q}^{\rm T})(q^{\rm T}C\mathrm{i}\gamma_5\tau_A\lambda_{A'}q) + \frac{1}{4}(\bar{q}\gamma^0\gamma_5 C\tau_A\lambda_{A'}\bar{q}^{\rm T})(q^{\rm T}C\gamma_0\gamma_5\tau_A\lambda_{A'}q) + \cdots\right] + \cdots\,, \tag{A.24}$$

where only those terms have been listed explicitly which are relevant for Eq. (4.68).

Now we rewrite Eq. (A.21) as

$$\mathscr{L}_{\rm int} = -(g_{\rm E}-g_{\rm M})(\bar{q}\gamma^0\lambda_a q)^2 - g_{\rm M}(\bar{q}\gamma^\mu\lambda_a q)^2 \tag{A.25}$$

and combine the results of Eq. (A.16) with Eq. (A.23), and of Eq. (A.17) with Eq. (A.24).

$$\Rightarrow \quad \mathscr{L}_{\rm ex} = \frac{N_c^2-1}{2N_f N_c^2}[(g_{\rm E}+3g_{\rm M})(\bar{q}q)^2 + (g_{\rm E}-g_{\rm M})(\bar{q}\gamma^0 q)^2 + \cdots] - \frac{1}{4N_f N_c}[(g_{\rm E}+3g_{\rm M})(\bar{q}\lambda_a q)^2 + (g_{\rm E}-g_{\rm M})(\bar{q}\gamma^0\lambda_a q)^2 + \cdots] + \cdots\,, \tag{A.26}$$

$$\mathscr{L}_{qq} = \frac{N_c+1}{8N_c}[(g_{\rm E}+3g_{\rm M})(\bar{q}\mathrm{i}\gamma_5 C\tau_A\lambda_{A'}\bar{q}^{\rm T})(q^{\rm T}C\mathrm{i}\gamma_5\tau_A\lambda_{A'}q) + (g_{\rm E}-g_{\rm M})(\bar{q}\gamma^0\gamma_5 C\tau_A\lambda_{A'}\bar{q}^{\rm T})(q^{\rm T}C\gamma_0\gamma_5\tau_A\lambda_{A'}q) + \cdots] + \cdots\,. \tag{A.27}$$

Adding the Hartree term $\mathscr{L}_{\rm dir}$, and taking $N_f = 2$ and $N_c = 3$ we reproduce the coefficient given in Eq. (4.68).

A.3.2. Two-flavor instanton-induced interaction

The two-flavor instanton-induced interaction reads [37,177]

$$\mathscr{L}_{\rm int} = \frac{g}{4(N_c^2-1)}\left\{\frac{2N_c-1}{2N_c}[(\bar{q}q)^2 - (\bar{q}\mathrm{i}\gamma_5 q)^2 - (\bar{q}\tau_a q)^2 + (\bar{q}\mathrm{i}\gamma_5\tau_a q)^2] - \frac{1}{4N_c}[(\bar{q}\sigma^{\mu\nu}q)^2 - (\bar{q}\sigma^{\mu\nu}\tau_a q)^2]\right\}\,, \tag{A.28}$$

$$\Rightarrow \mathscr{L}_{\bar{q}q} = g\left\{\frac{1}{4N_c^2}[(\bar{q}q)^2 - (\bar{q}\mathrm{i}\gamma_5 q)^2 - (\bar{q}\tau_a q)^2 + (\bar{q}\mathrm{i}\gamma_5\tau_a q)^2] + \frac{N_c-2}{16N_c(N_c^2-1)}[(\bar{q}\lambda_{a'}q)^2 - (\bar{q}\mathrm{i}\gamma_5\lambda_{a'}q)^2 - (\bar{q}\tau_a\lambda_{a'}q)^2 + (\bar{q}\mathrm{i}\gamma_5\tau_a\lambda_{a'}q)^2] + \frac{1}{32(N_c^2-1)}[(\bar{q}\sigma^{\mu\nu}\lambda_{a'}q)^2 - (\bar{q}\sigma^{\mu\nu}\tau_a\lambda_{a'}q)^2]\right\}\,, \tag{A.29}$$

$$\mathscr{L}_{\rm qq} = g\left\{\frac{1}{8N_c(N_c-1)}\left[(\bar{q}\mathrm{i}\gamma_5 C\tau_2\lambda_A\bar{q}^{\rm T})(q^{\rm T}C\mathrm{i}\gamma_5\tau_2\lambda_A q)-(\bar{q}C\tau_2\lambda_A\bar{q}^{\rm T})(q^{\rm T}C\tau_2\lambda_A q)\right]\right.$$
$$\left.-\frac{1}{16N_c(N_c+1)}(\bar{q}\sigma^{\mu\nu}C\tau_2\lambda_S\bar{q}^{\rm T})(q^{\rm T}C\sigma_{\mu\nu}\tau_2\lambda_S q)\right\}\ . \tag{A.30}$$

Comparing the coefficients with Eqs. (4.80) and (4.81) we can identify

$$G=\frac{1}{4N_c^2},\quad H_{\rm s}=\frac{1}{8N_c(N_c-1)},\quad H_{\rm t}=\frac{1}{16N_c(N_c+1)}\ , \tag{A.31}$$

and thus

$$G:H_{\rm s}:H_{\rm t}=1:\frac{N_c}{2(N_c-1)}:\frac{N_c}{4(N_c+1)}=1:\frac{3}{4}:\frac{3}{16}\ , \tag{A.32}$$

where the last equality holds for $N_c=3$.

Appendix B. Two-flavor Nambu–Gorkov propagator

In this appendix we sketch the derivation of the two-flavor Nambu–Gorkov propagator $S(p)$ which corresponds to the inverse propagator

$$S^{-1}(p)=\begin{pmatrix}\not{p}+\hat{\mu}\gamma^0-\hat{M} & (\Delta+\Delta_0\gamma^0)\gamma_5\tau_2\lambda_2\\ (-\Delta^*+\Delta_0^*\gamma^0)\gamma_5\tau_2\lambda_2 & \not{p}-\hat{\mu}\gamma^0-\hat{M}\end{pmatrix}\ , \tag{B.1}$$

given in Section 4.3.1, Eq. (4.35). The inverse is defined by

$$S^{-1}(p)S(p)=\mathbb{1}\ . \tag{B.2}$$

Writing the Nambu–Gorkov components of $S(p)$ explicitly,

$$S(p)=\begin{pmatrix}S_{11}(p) & S_{12}(p)\\ S_{21}(p) & S_{22}(p)\end{pmatrix}\ , \tag{B.3}$$

this yields

$$(\not{p}+\hat{\mu}\gamma^0-\hat{M})S_{11}(p)+(\Delta+\Delta_0\gamma^0)\gamma_5\tau_2\lambda_2 S_{21}(p)=1\ , \tag{B.4}$$

$$(-\Delta^*+\Delta_0^*\gamma^0)\gamma_5\tau_2\lambda_2 S_{11}(p)+(\not{p}-\hat{\mu}\gamma^0-\hat{M})S_{21}(p)=0\ , \tag{B.5}$$

and two analogous equations which result from the above ones if one replaces

$$S_{11}\to S_{22},\quad S_{21}\to S_{12},\quad \hat{\mu}\to-\hat{\mu},\quad \Delta\to-\Delta^*,\quad \Delta_0\to\Delta_0^*\ . \tag{B.6}$$

Employing Eq. (B.5), we can eliminate S_{21},

$$S_{21}(p)=\frac{\not{p}_r^-+M_r}{p_r^{-2}-M_r^2}(\Delta^*-\Delta_0\gamma^0)\gamma_5\tau_2\lambda_2 S_{11}(p)\ , \tag{B.7}$$

where we have defined

$$p^\pm=\begin{pmatrix}p^0\pm\hat{\mu}\\ \vec{p}\end{pmatrix}\ , \tag{B.8}$$

and the indices r and b denote the red and blue color components, respectively. Then Eq. (B.4) becomes

$$\left[\left(\not{p}_r^+ - M_r - |\Delta|^2\frac{\not{p}_r^- - M_r}{p_r^{-2} - M_r^2} - \Delta\Delta_0^*\frac{\not{p}_r^- - M_r}{p_r^{-2} - M_r^2}\gamma^0 \right.\right.$$
$$\left.\left. -\Delta^*\Delta_0\gamma^0\,\frac{\not{p}_r^- - M_r}{p_r^{-2} - M_r^2} - |\Delta_0|^2\gamma^0\,\frac{\not{p}_r^- - M_r}{p_r^{-2} - M_r^2}\,\gamma^0\right)\hat{P}_{12}^{(c)} + (\not{p}_b^+ - M_b)\hat{P}_3^{(c)}\right] S_{11}(p) = 1\ . \quad \text{(B.9)}$$

Here $P_3^{(c)} = \frac{1}{3} - \frac{1}{\sqrt{3}}\lambda_8$ and $P_{12}^{(c)} = 1 - P_3^{(c)}$ are the projectors on the blue and the red/green sector in color space, respectively.

The important observation is that the operator in front of S_{11} is diagonal in color space and does not depend on flavor. Moreover, the "blue" part, i.e., the term proportional to $\hat{P}_3^{(c)}$, takes the standard form and can easily be inverted. The problem has thus been reduced to inverting an, admittedly complicated, expression in Dirac space for the "red" part of the propagator.

The final result reads

$$\begin{aligned} S_{11}(p) = {} & \frac{1}{(p_0^2 - \omega_-^2)(p_0^2 - \omega_+^2)} \\ & \times [(p_r^{-2} - M_r^2)(\not{p}_r^+ + M_r) - |\Delta|^2(\not{p}_r^- + M_r) \\ & + \Delta\Delta_0^*\gamma^0(\not{p}_r^- + M_r) + \Delta^*\Delta_0(\not{p}_r^- + M_r)\gamma^0 - |\Delta_0|^2\gamma^0(\not{p}_r^- + M_r)\gamma^0]\hat{P}_{12}^{(c)} \\ & + \frac{\not{p}_b^+ + M_b}{(p_0 - E_-)(p_0 + E_+)}\hat{P}_3^{(c)}\ , \end{aligned} \quad \text{(B.10)}$$

where $\omega_\mp$ and $E_\mp$ are the dispersion laws given in Eqs. (4.52) and (4.51), respectively. Inserting this into Eq. (B.7), one finds

$$\begin{aligned} S_{21}(p) = {} & \frac{1}{(p_0^2 - \omega_-^2)(p_0^2 - \omega_+^2)} \\ & \times [-\Delta^*((\not{p}_r^- + M_r)(\not{p}_r^+ - M_r) - |\Delta|^2 - \Delta^*\Delta_0\gamma^0) \\ & + \Delta_0^*((\not{p}_r^- + M_r)\gamma^0(\not{p}_r^+ - M_r) - \Delta\Delta_0^* - |\Delta_0|^2\gamma^0)]\gamma_5\tau_2\lambda_2\ . \end{aligned} \quad \text{(B.11)}$$

The two remaining Nambu–Gorkov components are easily obtained by the symmetry relations Eq. (B.6).

Note that in all expressions given above, p^0 has to be interpreted as a short-hand notation for a Matsubara frequency $\mathrm{i}\omega_n$.

References

[1] J.C. Collins, M.J. Perry, Phys. Rev. Lett. 34 (1975) 1353.
[2] N. Cabibbo, G. Parisi, Phys. Lett. 59B (1975) 67.
[3] J. Cleymans, R.V. Gavai, E. Suhonen, Phys. Rep. 130 (1986) 217.
[4] H. Meyer-Ortmanns, Rev. Mod. Phys. 68 (1996) 473.
[5] U. Heinz, M. Jacob, nucl-th/0002042.
[6] Brookhaven National Laboratory, press release 03-49, http://www.bnl.gov/bnlweb/pubaf/pr/2003/bnlpr061103.htm.
[7] B. Barrois, Nucl. Phys. B 129 (1977) 390.

[8] S.C. Frautschi, Asymptotic freedom and color superconductivity in dense quark matter, in: N. Cabibbo (Ed.), Proceedings of the Workshop on Hadronic Matter at Extreme Energy Density, Erice, 1978.
[9] D. Bailin, A. Love, Phys. Rep. 107 (1984) 325.
[10] M. Alford, K. Rajagopal, F. Wilczek, Phys. Lett. B 422 (1998) 247.
[11] R. Rapp, T. Schäfer, E.V. Shuryak, M. Velkovsky, Phys. Rev. Lett. 81 (1998) 53.
[12] K. Rajagopal, F. Wilczek, The condensed matter physics of QCD, in: M. Shifman (Ed.), B.L. Ioffe Festschrift At the Frontier of Particle Physics/Handbook of QCD, vol. 3, World Scientific, Singapore, 2001, pp. 2061–2151.
[13] M. Alford, Ann. Rev. Nucl. Part. Sci. 51 (2001) 131.
[14] T. Schäfer, Quark matter, in: A.B. Santra, et al. (Eds.), Quarks and Mesons, Proc. of the BARC workshop on Quarks and Mesons, Bhabha Atomic Research Center, Mumbai, India, 2003, Narosa Publishing House, New Delhi, 2004; hep-ph/0304281.
[15] D.H. Rischke, Prog. Part. Nucl. Phys. 52 (2004) 197.
[16] M. Alford, K. Rajagopal, F. Wilczek, Nucl. Phys. B 537 (1999) 443.
[16a] K. Rajagopal, Nucl. Phys. A 661 (1999) 150c.
[17] T. Schäfer, Phys. Rev. Lett. 85 (2000) 5531.
[18] P.F. Bedaque, T. Schäfer, Nucl. Phys. A 697 (2002) 802.
[19] D.B. Kaplan, S. Reddy, Phys. Rev. D 65 (2002) 054042.
[20] M. Alford, J. Bowers, K. Rajagopal, Phys. Rev. D 63 (2001) 074016.
[21] J. Bowers, K. Rajagopal, Phys. Rev. D 66 (2002) 065002.
[22] M.G. Alford, Nucl. Phys. Proc. Suppl. 117 (2003) 65.
[23] S. Weinberg, Phys. Rev. Lett. 31 (1973) 494.
[24] H. Fritzsch, M. Gell–Mann, H. Leutwyler, Phys. Lett. 47B (1973) 365.
[25] D.J. Gross, F. Wilczek, Phys. Rev. Lett. 30 (1973) 1343.
[26] H.D. Politzer, Phys. Rev. Lett. 30 (1973) 1346.
[27] S. Bethge, hep-ex/0211012.
[28] J. Greensite, Prog. Part. Nucl. Phys. 51 (2003) 1.
[29] G. Ripka, Lecture Notes in Physics, vol. 639, Springer, Berlin, 2004.
[30] J. Gasser, H. Leutwyler, Phys. Rep. 87 (1982) 77.
[31] G. Ecker, Prog. Part. Nucl. Phys. 35 (1995) 1.
[32] V. Bernard, N. Kaiser, U.-G. Meißner, Int. J. Mod. Phys. E 4 (1995) 193.
[33] P. Gerber, H. Leutwyler, Nucl. Phys. B 321 (1989) 387.
[34] T.D. Cohen, R.J. Furnstahl, D.K. Griegel, Phys. Rev. C 45 (1992) 1881.
[35] G. 't Hooft, Phys. Rev. D 14 (1976) 3432;
G. 't Hooft, Phys. Rep. 142 (1986) 357.
[36] E.V. Shuryak, Nucl. Phys. B 198 (1982) 83.
[37] T. Schäfer, E.V. Shuryak, Rev. Mod. Phys. 70 (1998) 323.
[38] R. Brockmann, R. Machleidt, Phys. Rev. C 42 (1990) 1965.
[39] A.R. Bodmer, Phys. Rev. D 4 (1971) 1601.
[40] E. Witten, Phys. Rev. D 30 (1984) 272.
[41] M.A. Halasz, A.D. Jackson, R.E. Shrock, M.A. Stephanov, J.J.M. Verbaarschot, Phys. Rev. D 58 (1998) 096007.
[42] J.B. Natowitz, et al., Phys. Rev. C 65 (2002) 034618.
[43] P. Braun-Munzinger, J. Stachel, C. Wetterich, Phys. Lett. B 596 (2004) 61.
[44] P. Braun-Munzinger, I. Heppe, J. Stachel, Phys. Lett. B 465 (1999) 15.
[45] Conceptional Design Report, GSI 2002, http://www.gsi.de/GSI-Future/cdr.
[46] E. Laermann, O. Philipsen, Ann. Rev. Nucl. Part. Sci. 53 (2003) 163.
[47] F. Karsch, E. Laermann, hep-lat/0305025.
[48] R.D. Pisarski, F. Wilczek, Phys. Rev. D 29 (1984) 338.
[49] F. Karsch, E. Laermann, A. Peikert, Nucl. Phys. B 605 (2001) 579.
[50] C.R. Allton, S. Ejiri, S.J. Hands, O. Kaczmarek, F. Karsch, E. Laermann, C. Schmidt, Phys. Rev. D 68 (2003) 014507.
[51] S. Ejiri, C.R. Allton, S.J. Hands, O. Kaczmarek, F. Karsch, E. Laermann, C. Schmidt, Prog. Theor. Phys. Suppl. 153 (2004) 118.
[52] Z. Fodor, S.D. Katz, Phys. Lett. B 534 (2002) 87.

[53] Z. Fodor, S.D. Katz, JHEP 0203 (2002) 014.
[54] Z. Fodor, S.D. Katz, JHEP 0404 (2004) 050.
[55] A. Hart, M. Laine, O. Philipsen, Phys. Lett. B 505 (2001) 141.
[56] Ph. de Forcrand, O. Philipsen, Nucl. Phys. B 642 (2002) 290.
[57] M. D'Elia, M.P. Lombardo, Phys. Rev. D 67 (2003) 014505.
[58] R. Casalbuoni, S. De Curtis, R. Gatto, G. Pettini, Phys. Lett. B 231 (1989) 463;
R. Casalbuoni, S. De Curtis, R. Gatto, G. Pettini, Phys. Rev. D 41 (1990) 1610.
[59] M. Asakawa, K. Yazaki, Nucl. Phys. A 504 (1989) 668.
[60] M. Stephanov, K. Rajagopal, E. Shuryak, Phys. Rev. Lett. 81 (1998) 4816.
[61] M. Stephanov, K. Rajagopal, E. Shuryak, Phys. Rev. D 60 (1999) 114028.
[62] T. Schäfer, Nucl. Phys. B 575 (2000) 269.
[63] N. Evans, J. Hormuzdiar, S.D. Hsu, M. Schwetz, Nucl. Phys. B 581 (2000) 391.
[64] K. Rajagopal, E. Shuster, Phys. Rev. D 62 (2000) 085007.
[65] Y. Nambu, G. Jona-Lasinio, Phys. Rev. 122 (1961) 345.
[66] Y. Nambu, G. Jona-Lasinio, Phys. Rev. 124 (1961) 246.
[67] J. Bardeen, L.N. Cooper, J.R. Schrieffer, Phys. Rev. 106 (1957) 162.
[68] J. Berges, K. Rajagopal, Nucl. Phys. B 538 (1999) 215.
[69] U. Vogl, W. Weise, Progr. Part. Nucl. Phys. 27 (1991) 195.
[70] S.P. Klevansky, Rev. Mod. Phys. 64 (1992) 3.
[71] T. Hatsuda, T. Kunihiro, Phys. Rep. 247 (1994) 221.
[72] G. Ripka, Quarks Bound by Chiral Fields, Clarendon Press, Oxford, 1997.
[73] A. Chodos, R.L. Jaffe, K. Johnson, C.B. Thorn, V.F. Weisskopf, Phys. Rev. D 9 (1974) 3471.
[74] A. Chodos, R.L. Jaffe, K. Johnson, C.B. Thorn, Phys. Rev. D 10 (1974) 2599.
[75] T. DeGrand, R.L. Jaffe, K. Johnson, J. Kiskis, Phys. Rev. D 12 (1975) 2060.
[76] A.I. Vainshtein, V.I. Zakharov, M.A. Shifman, JETP Lett. 27 (1978) 60.
[77] E.V. Shuryak, Phys. Lett. 79B (1978) 135.
[78] C.M. Bender, P. Hays, Phys. Rev. D 14 (1976) 2622.
[79] R.L. Jaffe, hep-th/0307014.
[80] A. Chodos, C.B. Thorn, Phys. Rev. D 12 (1975) 2733.
[81] G.E. Brown, M. Rho, Phys. Lett. 82B (1979) 177.
[82] A.W. Thomas, S. Théberge, G.A. Miller, Phys. Rev. D 24 (1981) 216.
[83] M. Rho, Phys. Rep. 240 (1994) 1; corrected and updated version: hep-ph/0206003.
[84] D. Izatt, C. DeTar, M. Stephenson, Nucl. Phys. B 199 (1982) 269.
[85] J.-L. Dethier, R. Goldflam, E.M. Henley, L. Wilets, Phys. Rev. D 27 (1983) 2191.
[86] C.E. Carlson, T.H. Hansson, C. Peterson, Phys. Rev. D 27 (1983) 1556.
[87] K. Saito, A.W. Thomas, Phys. Rev. C 51 (1995) 2757.
[88] P.A.M. Guichon, Phys. Lett. B 200 (1988) 325.
[89] K. Saito, A.W. Thomas, Phys. Lett. B 327 (1994) 9.
[90] K. Saito, K. Tsushima, A.W. Thomas, Nucl. Phys. A 609 (1996) 339.
[91] G.E. Brown, A.D. Jackson, H.A. Bethe, P. Pizzochero, Nucl. Phys. A 560 (1993) 1035.
[92] E. Farhi, R.L. Jaffe, Phys. Rev. D 30 (1984) 2379.
[93] J. Goldstone, Nuovo Cimento 19 (1961) 154;
J. Goldstone, A. Salam, S. Weinberg, Phys. Rev. 127 (1962) 965.
[94] H. Kleinert, On the hadronization of quark theories, Lectures presented at the Erice Summer Institute 1976; in: A. Zichichi (Ed.), Understanding the Fundamental Constituents of Matter, Plenum Press, New York, 1978, p. 289.
[95] M.K. Volkov, Ann. Phys. (NY) 157 (1984) 282.
[96] T. Hatsuda, T. Kunihiro, Phys. Lett. B 145 (1984) 7.
[97] M.L. Goldberger, S.B. Treiman, Phys. Rev. 110 (1958) 1178.
[98] M. Gell–Mann, R.J. Oakes, B. Renner, Phys. Rev. 175 (1968) 2195.
[99] K. Hagiwara, et al., Review of particle physics, Phys. Rev. D 66 (2002) 010001.
[100] R. Dashen, Phys. Rev. 183 (1969) 1245.
[101] V. Dmitrašinović, R.H. Lemmer, R. Tegen, Phys. Lett. B 284 (1992) 201.

[102] B. Holstein, Phys. Lett. B 244 (1990) 83.
[103] H.G. Dosch, S. Narison, Phys. Lett. B 417 (1998) 173.
[104] L. Giusti, F. Rapuano, M. Talevi, A. Vladikas, Nucl. Phys. B 538 (1999) 249.
[105] V. Bernard, U.-G. Meißner, I. Zahed, Phys. Rev. D 36 (1987) 819.
[106] T. Hatsuda, T. Kunihiro, Phys. Lett. B 185 (1987) 304.
[107] J.I. Kapusta, Finite Temperature Field Theory, Cambridge University Press, Cambridge, 1989.
[108] T.M. Schwarz, S.P. Klevansky, G. Papp, Phys. Rev. C 60 (1999) 055205.
[109] J.D. Walecka, Ann. of Phys. 83 (1974) 491;
B.D. Serot, J.D. Walecka, Adv. Nucl. Phys. 16 (1986) 1.
[110] A. Blotz, private communication; A. Blotz, Diplomarbeit, Bochum, 1990, unpublished.
[111] M. Buballa, Nucl. Phys. A 611 (1996) 393.
[112] M. Buballa, M. Oertel, Nucl. Phys. A 642 (1998) 39c.
[113] B.-J. Schaefer, J. Wambach, nucl-th/0403039.
[114] D. Ebert, K.G. Klimenko, Nucl. Phys. A 728 (2003) 203.
[115] M. Jaminon, B. Van den Bossche, Nucl. Phys. A 582 (1995) 517;
J. Cugnon, M. Jaminon, B. Van den Bossche, Nucl. Phys. A 598 (1996) 515; B. Van den Bossche, nucl-th/9807010.
[116] M. Jaminon, B. Van den Bossche, Nucl. Phys. A 686 (2001) 341.
[117] X. Jin, B.K. Jennings, Phys. Lett. B 374 (1996) 13.
[118] G.F. Burgio, M. Baldo, P.K. Sahu, H.-J. Schulze, Phys. Rev. C 66 (2002) 025802.
[119] R. Aguirre, Phys. Lett. B 559 (2003) 207.
[120] J. Gasser, H. Leutwyler, M.E. Sainio, Phys. Lett. B 253 (1991) 252.
[121] P. Büttiker, U.-G. Meißner, Nucl. Phys. A 668 (2000) 97.
[122] M. Lutz, S. Klimt, W. Weise, Nucl. Phys. A 542 (1992) 521.
[123] C.V. Christov, et al., Prog. Part. Nucl. Phys. 37 (1996) 91.
[124] R. Alkofer, H. Reinhardt, H. Weigel, Phys. Rep. 265 (1996) 139.
[125] N. Ishii, W. Bentz, K. Yazaki, Phys. Lett. B 318 (1993) 26.
[126] C. Hanhart, S. Krewald, Phys. Lett. B 344 (1995) 55.
[127] M. Oertel, M. Buballa, J. Wambach, Yad. Fiz. 64 (2001) 757.
[128] M. Oertel, Doctoral Thesis, TU Darmstadt, 2000, hep-ph/0012224.
[129] M. Oertel, M. Buballa, J. Wambach, Nucl. Phys. A 676 (2000) 247.
[130] V. Dmitrašinović, H.-J. Schulze, R. Tegen, R.H. Lemmer, Ann. Phys. (NY) 238 (1995) 332.
[131] E.N. Nikolov, W. Broniowski, C.V. Christov, G. Ripka, K. Goeke, Nucl. Phys. A 608 (1996) 411.
[132] W. Florkowski, W. Broniowski, Phys. Lett. B 386 (1996) 62.
[133] W. Bentz, A.W. Thomas, Nucl. Phys. A 696 (2001) 138.
[134] W. Bentz, T. Horikawa, N. Ishii, A.W. Thomas, Nucl. Phys. A 720 (2003) 95.
[135] D.T. Son, M. Stephanov, Phys. Rev. Lett. 86 (2001) 592.
[136] J.B. Kogut, D.K. Sinclair, Phys. Rev. D 66 (2002) 014508; ibid. 034505.
[137] B. Klein, D. Toublan, J.J.M. Verbaarschot, Phys. Rev. D 68 (2003) 014009.
[138] D. Toublan, J.B. Kogut, Phys. Lett. B 564 (2003) 212.
[139] A. Barducci, R. Casalbuoni, G. Pettini, L. Ravagli, Phys. Rev. D 69 (2004) 096004.
[140] A. Barducci, R. Casalbuoni, G. Pettini, L. Ravagli, Phys. Lett. B 564 (2003) 217.
[141] M. Frank, M. Buballa, M. Oertel, Phys. Lett. B 562 (2003) 221.
[142] M. Frank, Diploma Thesis, TU Darmstadt, 2003, unpublished.
[143] P.F. Bedaque, Nucl. Phys. A 697 (2002) 569.
[144] O. Kiriyama, S. Yasui, H. Toki, Int. J. Mod. Phys. E 10 (2001) 501.
[145] P. Rehberg, S.P. Klevansky, J. Hüfner, Phys. Rev. C 53 (1996) 410.
[146] I. Heppe, Diploma Thesis, Universität Heidelberg, 1998, unpublished.
[147] D. Ebert, H. Reinhardt, Nucl. Phys. B 271 (1986) 188.
[148] V. Bernard, R.L. Jaffe, U.-G. Meßiner, Phys. Lett. B 198 (1987) 92.
[149] T. Hatsuda, T. Kunihiro, Phys. Lett. B 198 (1987) 126.
[150] T. Kunihiro, Phys. Lett. B 219 (1989) 363.

[151] S. Klimt, M. Lutz, U. Vogl, W. Weise, Nucl. Phys. A 516 (1990) 429;
U. Vogl, M. Lutz, S. Klimt, W. Weise, Nucl. Phys. A 516 (1990) 469.
[152] G.A. Miller, B.M. Nefkens, I. Šlaus, Phys. Rep. 194 (1990).
[153] P. Costa, private communication.
[154] C. Alcock, E. Farhi, Phys. Rev. D 32 (1985) 1273;
C. Alcock, A.V. Olinto, Ann. Rev. Nucl. Part. Sci. 38 (1988) 161.
[155] N.K. Glendenning, Compact Stars, Springer, New York, 1996.
[156] J.M. Lattimer, M. Prakash, Phys. Rep. 333 (2000) 121.
[157] J.J. Drake, et al., Astrophys. J. 572 (2002) 996.
[158] F.M. Walter, J. Lattimer, Astrophys. J. 576 (2002) L145.
[159] R.L. Jaffe, W. Busza, J. Sandweiss, F. Wilczek, Rev. Mod. Phys. 72 (2000) 1125.
[160] M. Buballa, M. Oertel, Phys. Lett. B 457 (1999) 261.
[161] S. Chakrabarty, Phys. Rev. D 43 (1991) 627.
[162] O.G. Benvenuto, G. Lugones, Phys. Rev. D 51 (1995) 1989.
[163] M. Dey, I. Bombaci, J. Dey, S. Ray, B.C. Samanta, Phys. Lett. B 438 (1998) 123;
M. Dey, I. Bombaci, J. Dey, S. Ray, B.C. Samanta, Phys. Lett. B 447 (1999) 352 (erratum ibid. 467 (1999) 303).
[164] K. Langfeld, H. Reinhardt, M. Rho, Nucl. Phys. A 622 (1997) 620.
[165] K. Langfeld, M. Rho, Nucl. Phys. A 660 (1999) 475.
[166] I.N. Mishustin, L.M. Satarov, H. Stöcker, W. Greiner, Phys. Atom. Nucl. 64 (2001) 802.
[167] C. Ratti, Europhys. Lett. 61 (2003) 314.
[168] L.N. Cooper, Phys. Rev. 104 (1956) 1189.
[169] H. Fröhlich, Phys. Rev. 79 (1950) 845.
[170] J. Polchinski, Lectures presented at TASI, 1992, hep-th/9210046.
[171] A.L. Fetter, J.D. Walecka, Quantum Theory of Many-Particle Systems, Mc Graw-Hill, New York, 1971.
[172] R.D. Pisarski, D.H. Rischke, Phys. Rev. D 60 (1999) 094013.
[173] F. Weber, Acta Phys. Polon. B 30 (1999) 3149.
[174] D. Blaschke, N. Glendenning, A. Sedrakian (Eds.), Physics of Neutron Star Interiors, Lectures Notes in Physics, vol. 578, Springer, Berlin, 2001.
[175] R.D. Pisarski, D.H. Rischke, Phys. Rev. D 61 (2000) 051501, 074017.
[176] G.W. Carter, D. Diakonov, Phys. Rev. D 60 (1999) 016004.
[177] R. Rapp, T. Schäfer, E.V. Shuryak, M. Velkovsky, Ann. Phys. (NY) 280 (2000) 35.
[178] D.T. Son, Phys. Rev. D 59 (1999) 094019.
[179] T. Schäfer, F. Wilczek, Phys. Rev. D 60 (1999) 114033.
[180] Q. Wang, D.H. Rischke, Phys. Rev. D 65 (2002) 054005.
[181] S. Elitzur, Phys. Rev. D 12 (1975) 3978.
[182] K. Splittorff, Phys. Rev. D 68 (2003) 054504.
[183] D.H. Rischke, Phys. Rev. D 62 (2000) 034007.
[184] G.W. Carter, D. Diakonov, Nucl. Phys. B 582 (2000) 571.
[185] D. Diakonov, H. Forkel, M. Lutz, Phys. Lett. B 373 (1996) 147.
[186] B. Vanderheyden, A.D. Jackson, Phys. Rev. D 62 (2000) 094010.
[187] S.B. Rüster, D.H. Rischke, Phys. Rev. D 69 (2004) 045011.
[188] D.K. Hong, V.A. Miransky, I.A. Shovkovy, L.C.R. Wijewardhana, Phys. Rev. D 61 (2000) 056001 (erratum ibid. D 62 (2000) 059903).
[189] G.M. Eliashberg, Sov. Phys. JETP 11 (1960) 696;
G.M. Eliashberg, Sov. Phys. JETP 12 (1961) 1000.
[190] S.R. Beane, P.F. Bedaque, M.J. Savage, Nucl. Phys. A 688 (2001) 931;
S.R. Beane, P.F. Bedaque, Phys. Rev. D 62 (2000) 117502.
[191] W.E. Brown, J.T. Liu, H.-c. Ren, Phys. Rev. D 61 (2000) 114012; W.E. Brown, J.T. Liu, H.-c. Ren, Phys. Rev. D 62 (2000) 054013, 054016.
[192] C.A. De Carvalho, Nucl. Phys. B 183 (1980) 182.
[193] A.A. Abrikosov Jr., Sov. J. Nucl. Phys. 37 (1983) 459.
[194] T. Schäfer, E.V. Shuryak, J.J.M. Verbaarschot, Phys. Rev. D 51 (1995) 1267.

[195] T. Schäfer, Phys. Rev. D 57 (1998) 3950.
[196] [LEPS Collaboration], T. Nakano, et al., Phys. Rev. Lett. 91 (2003) 012002.
[197] [DIANA Collaboration], V.V. Barmin, et al., Yad. Fiz. 66 (2003) 1763.
[198] [CLAS Collaboration], S. Stepanyan, Phys. Rev. Lett. 91 (2003) 252001.
[199] [SAPHIR Collaboration], J. Barth, et al., Phys. Lett. B 572 (2003) 127.
[200] [HERMES Collaboration], A. Airapetian, et al., Phys. Lett. B 585 (2004) 213.
[201] M. Praszalowicz, in: M. Jezabeck, M. Praszalowicz (Eds.), Skyrmions and Anomalies, World Scientific, Singapore, 1987, p. 112.
[202] D. Diakonov, V. Petrov, M.V. Polyakov, Z. Phys. A 359 (1997) 305.
[203] T.D. Cohen, hep-ph/0312191.
[204] R.L. Jaffe, hep-ph/0405268 and references therein.
[205] R.L. Jaffe, F. Wilczek, Phys. Rev. Lett. 91 (2003) 232003.
[206] E.V. Shuryak, I. Zahed, Phys. Lett. B 589 (2004) 21.
[207] N. Evans, S.D.H. Hsu, M. Schwetz, Nucl. Phys. B 551 (1999) 275;
N. Evans, S.D.H. Hsu, M. Schwetz, Phys. Lett. B 449 (1999) 281.
[208] T. Schäfer, F. Wilczek, Phys. Lett. B 450 (1999) 325.
[209] D. Boyanowski, H.J. de Vega, Phys. Rev. D 63 (2001) 114028.
[210] T. Schäfer, K. Schwenzer, Phys. Rev. D 70 (2004) 054007.
[211] A. Gerhold, A. Ipp, A. Rebhan, Phys. Rev. D 70 (2004) 105015.
[212] M. Buballa, J. Hošek, M. Oertel, Phys. Rev. D 65 (2002) 014018.
[213] M. Alford, J. Berges, K. Rajagopal, Nucl. Phys. B 558 (1999) 219.
[214] A. Mishra, H. Mishra, Phys. Rev. D 69 (2004) 014014.
[215] Y. Nambu, Phys. Rev. 117 (1960) 648;
L.P. Gorkov, JETP 7 (1958) 993.
[216] J. Hošek, hep-ph/9812516.
[217] D.D. Dietrich, D.H. Rischke, Prog. Part. Nucl. Phys. 53 (2004) 305.
[218] A. Gerhold, A. Rebhan, Phys. Rev. D 68 (2003) 011502.
[219] A. Kryjevski, Phys. Rev. D 68 (2003) 074008.
[220] M. Kitazawa, T. Koide, T. Kunihiro, Y. Nemoto, Prog. Theor. Phys. 108 (2002) 929.
[221] D. Blaschke, M.K. Volkov, V.L. Yudichev, Eur. Phys. J. A 17 (2003) 103.
[222] M. Alford, J. Berges, K. Rajagopal, Phys. Rev. Lett. 84 (2000) 598.
[223] I. Shovkovy, M. Huang, Phys. Lett. B 564 (2003) 205.
[224] M. Huang, I. Shovkovy, Nucl. Phys. A 729 (2003) 835.
[225] E. Gubankova, W.V. Liu, F. Wilczek, Phys. Rev. Lett. 91 (2003) 032001.
[226] M. Alford, C. Kouvaris, K. Rajagopal, Phys. Rev. Lett. 92 (2004) 222001; hep-ph/0406137.
[227] A. Burrows, James M. Lattimer, Astrophys. J. 307 (1986) 178.
[228] T. Schäfer, Phys. Rev. D 62 (2000) 094007.
[229] M.G. Alford, J.A. Bowers, J.M. Cheyne, G.A. Cowan, Phys. Rev. D 67 (2003) 054018.
[230] A. Schmitt, Doctoral Thesis, Universität Frankfurt/Main, nucl-th/0405076.
[231] A. Schmitt, Q. Wang, D.H. Rischke, Phys. Rev. Lett. 91 (2003) 242301.
[232] A. Schmitt, Q. Wang, D.H. Rischke, Phys. Rev. D 69 (2004) 094017.
[233] D. Vollhardt, P. Wölfe, The Superfluid Phases of Helium, vol. 3, Taylor and Francis, London, 1990.
[234] H. Nielsen, S. Chadha, Nucl. Phys. B 105 (1976) 445.
[235] H. Leutwyler, Phys. Rev. D 49 (1994) 3033.
[236] T. Schäfer, D.T. Son, M.A. Stephanov, D. Toublan, J.J. Verbaarschot, Phys. Lett. B 522 (2001) 67.
[237] F. Sannino, W. Schäfer, Phys. Lett. B 527 (2002) 142.
[238] T.-L. Ho, Phys. Rev. Lett. 81 (1998) 742.
[239] T. Ohmi, K. Machida, J. Phys. Soc. Japan 67 (1998) 1822.
[240] V.A. Miransky, I.A. Shovkovy, Phys. Rev. Lett. 88 (2002) 111601.
[241] M. Buballa, J. Hošek, M. Oertel, Phys. Rev. Lett. 90 (2003) 182002.
[242] A. Schmitt, Q. Wang, D.H. Rischke, Phys. Rev. D 66 (2002) 114010.
[243] J.A. Bowers, J. Kundu, K. Rajagopal, E. Shuster, Phys. Rev. D 64 (2001) 014024.

[244] G.W. Carter, S. Reddy, Phys. Rev. D 62 (2000) 103002.
[245] P. Jaikumar, M. Prakash, T. Schäfer, Phys. Rev. D 66 (2002) 063003.
[246] I.A. Shovkovy, P.J. Ellis, Phys. Rev. C 66 (2002) 015802.
[247] M. Alford, K. Rajagopal, JHEP 0206 (2002) 031.
[248] R.D. Pisarski, D.H. Rischke, Phys. Rev. Lett. 83 (1999) 37.
[249] A.J. Paterson, Nucl. Phys. B 190 (1981) 188;
D. Pisarski, D.L. Stein, J. Phys. A 14 (1981) 3341.
[250] R.D. Pisarski, D.H. Rischke, Proceedings of the Judah Eisenberg Memorial Symposium, Nuclear Matter, Hot and Cold, Tel Aviv, 1999, nucl-th/9907094.
[251] I.A. Shovkovy, L.C.R. Wijewardhana, Phys. Lett. B 470 (1999) 189.
[252] D.H. Rischke, Phys. Rev. D 62 (2000) 034007.
[253] T. Schäfer, F. Wilczek, Phys. Rev. Lett. 82 (1999) 3956.
[254] C. Wetterich, Phys. Lett. B 462 (1999) 164;
C. Wetterich, Phys. Rev. D 64 (2001) 036003;
C. Wetterich, Phys. Lett. B 525 (2002) .
[255] T. Schäfer, Phys. Rev. D 64 (2001) 037501.
[256] M. Srednicki, L. Susskind, Nucl. Phys. B 187 (1981) 93.
[257] K. Rajagopal, F. Wilczek, Phys. Rev. Lett. 86 (2001) 3492.
[258] M. Alford, K. Rajagopal, S. Reddy, F. Wilczek, Phys. Rev. D 64 (2001) 074017.
[259] T. Brauner, J. Hošek, R. Sýkora, Phys. Rev. D 68 (2003) 094004.
[260] T. Schäfer, F. Wilczek, Phys. Rev. D 60 (1999) 074014.
[261] M. Buballa, M. Oertel, Nucl. Phys. A 703 (2002) 770.
[262] M. Oertel, M. Buballa, in: M. Buballa, W. Nörenberg, B.-J. Schaefer, J. Wambach (Eds.), Ultrarelativistic Heavy-Ion Collisions, Proceedings of the XXX International Workshop on Gross Properties of Nuclei and Nuclear Excitations, Hirschegg, Austria, January 13–19, 2002, GSI Darmstadt, 2002, pp. 110–115.
[263] F. Gastineau, R. Nebauer, J. Aichelin, Phys. Rev. C 65 (2002) 045204.
[264] D.N. Voskresensky, nucl-th/0306077.
[265] I. Giannakis, D. Hou, H.-c. Ren, D.H. Rischke, Phys. Rev. Lett. 93 (2004) 232301.
[266] P. Amore, M.C. Birse, J.A. McGovern, N.R. Walet, Phys. Rev. D 65 (2002) 074005.
[267] A. Steiner, S. Reddy, M. Prakash, Phys. Rev. D 66 (2002) 094007.
[268] A.M. Clogston, Phys. Rev. Lett. 9 (1962) 266;
B.S. Chandrasekhar, App. Phys. Lett. 1 (1962) 7.
[269] F. Neumann, Diploma Thesis, TU Darmstadt, 2003, unpublished.
[270] F. Neumann, M. Buballa, M. Oertel, Nucl. Phys. A 714 (2003) 481.
[271] J. Madsen, Phys. Rev. Lett. 87 (2001) 172003.
[272] G. Lugones, J.E. Horvath, Phys. Rev. D 66 (2002) 074017.
[273] N.K. Glendenning, Phys. Rev. D 46 (1992) 1274.
[274] D.G. Ravenhall, C.J. Pethick, J.R. Wilson, Phys. Rev. Lett. 50 (1983) 2066.
[275] H. Heiselberg, C.J. Pethick, E.F. Staubo, Phys. Rev. Lett. 70 (1993) 1355.
[276] N.K. Glendenning, S. Pei, Phys. Rev. C 52 (1995) 2250.
[277] S. Reddy, G. Rupak, nucl-th/0405054.
[278] I. Shovkovy, M. Hanauske, M. Huang, Phys. Rev. D 67 (2003) 103004.
[279] R. Casalbuoni, R. Gatto, Phys. Lett. B 464 (1999) 111.
[280] D.T. Son, M.A. Stephanov, Phys. Rev. D 61 (2000) 074012 (erratum ibid. D 62 (2000) 059902).
[281] A. Kryjevski, D.B. Kaplan, T. Schäfer, hep-ph/0404290.
[282] A.I. Larkin, Yu.N. Ovchinnikov, Zh. Eksp. Teor. Fiz. 47 (1964) 1136;
A.I. Larkin, Yu.N. Ovchinnikov, Sov. Phys. JETP 20 (1965) 762.
[283] P. Fulde, R.A. Ferrell, Phys. Rev. 135 (1964) A550.
[284] J. Bowers, K. Rajagopal, Nucl. Phys. A 715 (2003) 867c.
[285] A.W. Overhauser, Adv. Phys. 27 (1978) 343.
[286] E. Shuster, D.T. Son, Nucl. Phys. B 573 (2000) 434.
[287] B. Park, M. Rho, A. Wirzba, I. Zahed, Phys. Rev. D 62 (2000) 034015.

[288] R. Rapp, E. Shuryak, I. Zahed, Phys. Rev. D 63 (2001) 034008.
[289] G. Sarma, J. Phys. Chem. Solids 24 (1963) 1029.
[290] M. Huang, I. Shovkovy, Phys. Rev. D 70 (2004) 051501 (R).
[291] W.V. Liu, F. Wilczek, Phys. Rev. Lett. 90 (2003) 047002.
[292] M.M. Forbes, E. Gubankova, W.V. Liu, F. Wilczek, hep-ph/0405059.
[293] H. Müther, A. Sedrakian, Phys. Rev. D 67 (2003) 085024.
[294] K. Schertler, S. Leupold, J. Schaffner-Bielich, Phys. Rev. C 60 (1999) 025801.
[295] A. Steiner, M. Prakash, J.M. Lattimer, Phys. Lett. B 486 (2000) 239.
[296] M. Alford, S. Reddy, Phys. Rev. D 67 (2003) 074024.
[297] M. Baldo, M. Buballa, G.F. Burgio, F. Neumann, M. Oertel, H.-J. Schulze, Phys. Lett. B 562 (2003) 153.
[298] M. Buballa, F. Neumann, M. Oertel, I. Shovkovy, Phys. Lett. B 595 (2004) 36.
[299] M. Baldo, I. Bombaci, G.F. Burgio, Astron. Astrophys. 328 (1997) 274.
[300] M. Baldo, G.F. Burgio, H.-J. Schulze, Phys. Rev. C 58 (1998) 3688;
M. Baldo, G.F. Burgio, H.-J. Schulze, Phys. Rev. C 61 (2000) 055801.
[301] H.Q. Song, M. Baldo, G. Giansiracusa, U. Lombardo, Phys. Rev. Lett. 81 (1998) 1584;
H.Q. Song, M. Baldo, G. Giansiracusa, U. Lombardo, Phys. Lett. B 473 (2000) 1.
[302] M. Baldo, G.F. Burgio, in: D. Blaschke, N. Glendenning, A. Sedrakian (Eds.), Physics of Neutron Star Interiors, Lectures Notes in Physics, vol. 578, Springer, Berlin, 2001, p. 1.
[303] M. Lacombe, B. Loiseau, J.M. Richard, R. Vinh Mau, J. Côté, P. Pirès, R. de Tourreil, Phys. Rev. C 21 (1980) 861.
[304] J. Carlson, V.R. Pandharipande, R.B. Wiringa, Nucl. Phys. A 401 (1983) 59.
[305] R. Schiavilla, V.R. Pandharipande, R.B. Wiringa, Nucl. Phys. A 449 (1986) 219.
[306] P. Maessen, Th. Rijken, J. de Swart, Phys. Rev. C 40 (1989) 2226.
[307] P. Papazoglou, S. Schramm, J. Schaffner-Bielich, H. Stöcker, W. Greiner, Phys. Rev. C 57 (1998) 2576;
P. Papazoglou, D. Zschiesche, S. Schramm, J. Schaffner-Bielich, H. Stöcker, W. Greiner, Phys. Rev. C 59 (1999) 411;
M. Hanauske, D. Zschiesche, S. Pal, S. Schramm, H. Stöcker, W. Greiner, Astrophys. J. 537 (2000) 50329.
[308] M. Huang, P.F. Zhuang, W.Q. Chao, Phys. Rev. D 67 (2003) 065015.
[309] R.C. Tolman, Phys. Rev. 55 (1939) 364;
J.R. Oppenheimer, G. Volkoff, Phys. Rev. 55 (1939) 374.
[310] R.A. Hulse, J.H. Taylor, Astrophys. J. 195 (1975) L51.
[311] C. Maieron, M. Baldo, G.F. Burgio, H.-J. Schulze, Phys. Rev. D 70 (2004) 043010.
[312] S.E. Thorsett, D. Chakrabarty, Astrophys. J. 512 (1999) 288.
[313] G. Baym, C. Pethick, P. Sutherland, Astrophys. J. 170 (1971) 299.
[314] J. Negele, D. Vautherin, Nucl. Phys. A 207 (1973) 298.
[315] U.H. Gerlach, Phys. Rev. 172 (1968) 1325.
[316] D. Blaschke, D.N. Voskresensky, H. Grigorian, astro-ph/0403171.
[317] M. Kitazawa, T. Koide, T. Kunihiro, Y. Nemoto, Phys. Rev. D 65 (2002) 091504.
[318] D. Blaschke, D. Ebert, K.G. Klimenko, M.K. Volkov, V.L. Yudichev, Phys. Rev. D 70 (2004) 014006.
[319] M. Rho, A. Wirzba, I. Zahed, Phys. Lett. B 473 (2000) 126.
[320] H. Abuki, T. Hatsuda, K. Itakura, Phys. Rev. D 65 (2002) 074014.
[321] H. Kleinert, B. Van den Bossche, Phys. Lett. B 474 (2000) 336.
[322] M. Oertel, M. Buballa, J. Wambach, Phys. Lett. B 477 (2000) 77.
[323] G. Ripka, Nucl. Phys. A 683 (2001) 463.
[324] E. Babaev, Phys. Rev. D 62 (2000) 074020.
[325] E. Babaev, Int. J. Mod. Phys. A 16 (2001) 1175.
[326] T. Lee, Y. Oh, nucl-th/9909078.
[327] S. Hands, D.N. Walters, Phys. Lett. B 548 (2002) 196;
S. Hands, D.N. Walters, Phys. Rev. D 69 (2004) 076011.
[328] C. Ratti, W. Weise, Phys. Rev. D 70 (2004) 054013.